Defining glucocorticoid signalling in inflammation and cancer

Fiona Marie Leslie

Submitted in accordance with the requirements for the degree of Doctor of Philosophy

University of Leeds

Faculty of Medicine and Health

March 2022

Intellectual Property and Publication Statement

The candidate confirms that the work submitted is their own and that appropriate credit has been given where reference has been made to the work of others.

Chapter 3

The SILAC phosphoproteomic work, sample preparation was performed by Dr Stephen Kershaw and the University of Manchester Proteomics department (University of Manchester School of Medical Sciences).

Chapter 4

Library preparation, bulk mRNA sequencing and initial bioinformatics: read alignment and differential expression was performed by Novogene Ltd, Cambridge.

Two figures in Chapter 2: Methods, and Chapter 4 were provided by Novogene

Figure 1.1 Chromosome alignment distribution for each sample

Figure 1.2 Gene density distribution

Figure 4.9 Correlation and Principle component analysis.

Acknowledgements

Abstract

Glucocorticoids (Gc) represent a mainstay treatment to limit the damaging effects of inflammation resulting from inflammatory disease and as an aid to cancer therapy. The purpose of this study was to evaluate factors which modify Gc signalling, in an attempt to further define the complex mechanism of action. The glucocorticoid receptor (GR) is a ubiquitous, ligand-activated transcription factor and mediates Gc-regulated activation and repression of gene expression. GR also rapidly initiates short-acting, non-genomic signals though kinase engagement. However, this activity is less well understood and its role in modulating the transcriptional activity of GR is poorly defined.

The Gc-phosphoproteome was evaluated to characterise the spectrum of non-genomic signals. Following 10-minute exposure, distinct GR ligands differentially phosphorylated common protein targets involved in diverse cellular functions. Three G-protein coupled receptors (GPCR) were identified and preliminary assessment of Gc responsiveness by immunoblot and luciferase reporter assays indicates that Gc has an inhibitory effect upon their activity.

Gc also induced the differential phosphorylation of nuclear targets and cyclin-dependent kinase (CDK)-mediated phosphorylation of RNA Polymerase II was a predicted effector pathway. Selective inhibition of CDK12 and CDK13 reduced Gc-induced expression of target genes. However, repression of cytokine genes was maintained. Global transcriptomics defined groups of GR-regulated genes which are affected by CDK inhibition. Differential expression of transcription factors implies significant involvement in transcriptional processes including regulation of inflammatory pathways and cell differentiation. Collectively this suggests a synergistic GR-mediated mechanism, whereby rapid non-genomic signals feed-forward into the nucleus to modulate subsequent genomic action.

In addition, using fibronectin-coated micropatterns, this study describes a model to explore the influence of cell-matrix interactions and cell geometry upon GR nuclear shuttling and GR-transcription factor cross-talk. Such mechanical signals may underlie heterogenic responses to Gc within cell populations.

Overall, this study provides an integrated assessment of Gc-GR signalling activity. Such insight provides new mechanistic concepts with implications for therapeutic development and understanding how GR contributes to pathogenic disease progression.

Table of Contents

Table of Figures

List of Tables

Abbreviations

11β-HSD	11β-hydroxysteroid dehydrogenase enzyme
ACTH	Adrenocorticotropin hormone
AMPK	5' AMP-activated protein kinase
ANOVA	Analysis of variance
AVP	Arginine vasopressin
BCR	B cell receptor
BSA	Bovine serum albumin
cAMP	Cyclic AMP
CBG	Cortisol binding globulin
CDK	Cyclin-dependent kinase
cDNA	Complementary DNA
ChIP	Chromatin immunoprecipitation
CRH	Corticotropin-releasing hormone
CRM	Cis-regulatory modules
DBD	DNA binding domain
Dex	Dexamethasone
DMSO	Dimethyl sulfoxide
DUSP1	Dual specificity protein phosphatase 1
EGFR	Epidermal growth factor receptor
ER	Oestrogen receptor
ERK	Extracellular signal-regulated kinase
FKBP	FK506-binding protein
FVP	Flavopiridol
GBS	GR binding sequences
Gc	Glucocorticoids
GILZ	Gc-induced leucine zipper
GO	Gene Ontology
GPCR	G-protein coupled receptors
GR	Glucocorticoid receptor
GRdim	GR dimerisation deficient
GRE	Glucocorticoid response element
GRIP1	Glucocorticoid receptor-interacting protein 1
GSK-3	Glycogen synthase kinase 3
HAT	Histone acetyltransferase
HDAC	Histone deacetylase
HPA	Hypothalamic-pituitary-adrenal
HSP	Heat-shock protein
IFN	Interferon
IR-GBS	Inverted-repeat GBS
IRF	Interferon-regulatory factor
JNK	c-Jun N-terminal kinase
LBD	Ligand binding domain
LPS	Lipopolysaccharide
MAPK	Mitogen-activated protein kinase
MED14	Mediator of RNA polymerase II transcription subunit
MKP-1	Mitogen-activated protein kinase phosphatase
MS	Mass spectrometry
N:C ratio	Nuclear: cytoplasmic ratio
NCOA1	Nuclear receptor co-activator 1
NCOR	Nuclear receptor co-repressor
NES	Normalised enrichment score

NF-κB	Nuclear factor kappa-light-chain-enhancer of activated B cells
NGS	Next generation sequencing
NLS	Nuclear localisation sequence
NTD	N-terminal transactivation domain
P-TEFb	positive transcription elongation factor b
PFA	Paraformaldehyde
PKB	Protein kinase B
PLC	Phospholipase C
PMA	Phorbol-12-myristate-13-acetate
PTM	Post-translational modifications
PWM	Position weight matrices
ROS	reactive oxygen species
RT-qPCR	Real-time quantitative reverse-transcriptase Polymerase Chain Reaction
SEC	Super elongation complex
SEM	Standard error of the mean
SILAC	Stable-isotype labelling with amino acids in cell culture
siRNA	Small interfering RNA
SNP	Single nucleotide polymorphism
Src	Proto-oncogene tyrosine-protein kinase
SRC1	Steroid receptor co-activator1
T-ALL	T-cell acute lymphoblastic leukaemia
TFIIF	Transcription Factor II F
TLR	Toll-like receptor
TNBC	Triple negative breast cancer
TNF-α	Tumour necrosis factor-α

Chapter 1: Introduction

Glucocorticoids (Gc) are a class of corticosteroids, a collective term for cholesterol-derived steroid hormones, produced in the adrenal gland and are essential for life. Gc act to regulate the systemic stress response and maintain the homeostasis of a multitude of physiological processes. The term Glucocorticoids can refer to both the endogenous hormone, cortisol in humans and corticosterone in rodents, and synthetic therapeutics which have been designed to mimic naturally occurring cortisol.

Endogenous Gc, are biosynthesised by the adrenal cortex which are released in a diurnal cycle and increased in response to stress. In particular Gc mediate diverse regulatory functions on energy metabolism and immunomodulation (1). The potent capacity of Gc to limit the damaging effects of inflammation during infection and injury, have been harnessed through the development of synthetic steroids. Synthetic Gc have subsequently become one of the most widely prescribed class of anti-inflammatory agents. Large gaps remain in the understanding of the function of Gc, which must be carefully controlled as dysregulation can result in the development of a variety of disorders.

1.1.1 Glucocorticoids: Health and Disease

The diverse action of endogenous Gc is both tissue specific and context dependent. However, in most circumstances Gc initiate the transient activation of systems required to respond to stress and restore homeostasis.

Gc are important during embryonic development for the maturation of organ systems. Gc signals have been shown to make a key contribution to maintaining cardiac function, hepatocyte energy metabolism in addition to lung and brain development(1, 2). Therapeutic Gc are routinely administered to pre-term infants in order to accelerate lung development and surfactant production to prevent respiratory distress (3).

Gc responsive metabolic tissues include the liver, lung, adipose, and central nervous system (**Figure 1.1**). Stimulated elevation of circulating glucose levels by Gc in response to stress, acts to fulfil the increased energy demands of the immune system and maintenance of brain function. Gc stimulate the upregulation of genes encoding enzymes involved in gluconeogenesis in the liver. To complement this action, Gc mobilise amino acids and fatty acids for uptake by the liver to serve as substrates for the synthesis of glucose. This occurs in muscle tissues through a reduction of glucose uptake and protein synthesis, coupled with an increase in protein catabolism while lipolysis in adipose tissue stimulates release of free-fatty acids. Further metabolic effects of Gc include stimulating β-cells of the pancreas to reduce insulin secretion

and the upregulation of factors which oppose insulin signalling in the liver to maintain high circulating glucose levels (4).

Gc have an immunomodulatory role and have been shown to regulate the action of a plethora of cell types at sites of pathogen challenge or trauma. Gc-mediated regulation occurs across all phases of the immune response and acts to prevent the overactivation of immune cells and promotes inflammatory resolution. However, following resolution wound healing processes: re-epithelialisation, collagen deposition and angiogenesis are all suppressed by Gc. Therefore, reduced Gc levels are more favourable under these conditions (5).

The essential homeostatic role of endogenous Gcs upon various tissues and the necessity of tightly coordinated action is highlighted by cases of Addison's disease and Cushing's syndrome; rare conditions defined by Gc deficiency and chronic hypercortisolism respectively. Patients with Addison's disease display weight loss, hypoglycaemia, hypotension, impaired stress resistance and often develop autoimmune disease. These pathologic phenotypes manifest as a result of disturbances in metabolism of carbohydrates, protein and fat in addition to uncontrolled immune activation. Whereas the excessive, chronic secretion of cortisol exhibited by patients with Cushing's syndrome is associated with the development of metabolic syndrome (central obesity), insulin insensitivity (hyperglycaemia), cardiovascular disease (hypercholesterolemia), osteoporosis, neuropsychiatric disorders, impaired wound healing and immune function (2).
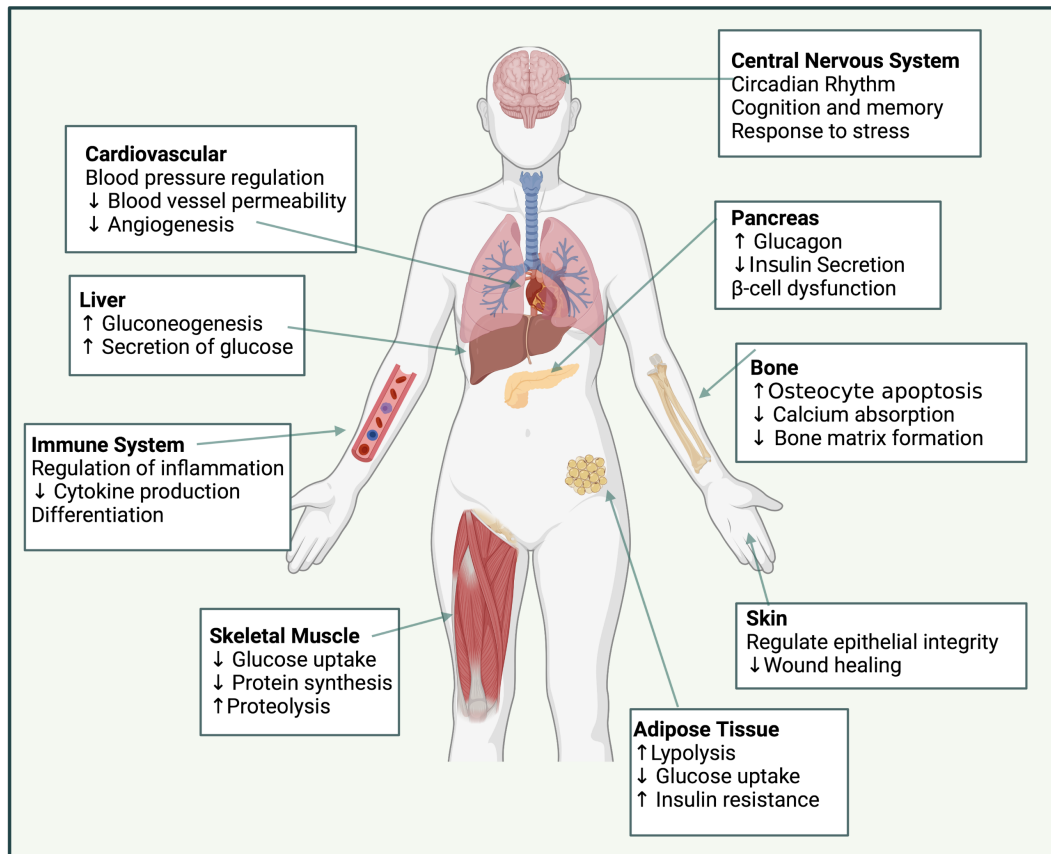
Figure 1.1. Glucocorticoid responsive tissue

Glucocorticoids act systemically and exert their actions upon multiple organ systems to restore homeostatic balance. Major functions of Gc include: synchronisation of circadian rhythms, modulation of immune responses and to suppress damage induced by excessive inflammation and the regulation of glucose and lipid metabolism.

1.1.2 Glucocorticoids: Clinical Usage

Since their initial discovery in the 1940's, Gc remain the first-line treatment for conditions with an inflammatory component. It is estimated that 1-3% of the adult population hold a prescription for Gc (6) furthermore, long term oral prescriptions in the UK have risen by 34% over the last 20 years (7). This widespread usage of synthetic Gc to treat chronic inflammatory diseases is a testament to their effective broad-targeting immunosuppressive properties, whilst their anti-proliferative, anti-angiogenic properties have been harnessed for cancer therapy (2). Such conditions for which Gc are routinely used are outlined in **Figure 1.2.** Despite successful management of disease symptoms, the clinical application of Gc is severely limited by unwanted action of Gc on metabolism. Such effects reflect the phenotypic symptoms of Cushing syndrome including: development of type 2 diabetes, osteoporosis, increased adiposity, muscle atrophy and fatty liver disease (8). Gc can also reduce bone mineral density which increases the risk of osteoporosis and fractures. This occurs as a result of reducing intestinal absorption of Ca^{2+} and negatively regulating the activity of osteoblasts and inhibiting the secretion of factors which facilitate bone mineralisation (9).

Clinical uses of Glucocorticoids

Autoimmune Disease
Rheumatoid arthritis
Multiple Sclerosis
Systemic lupus erythematosus

Allergy

Prevent Transplant Rejection
Solid Organ: Acute rejection
Stem Cell: Graft vs Host Disease

Respiratory disease
Asthma
COPD
COVID-19

Inflammatory bowel disease

Sepsis

Alongside Chemotherapy
Solid tumour
Heamatological malignancy
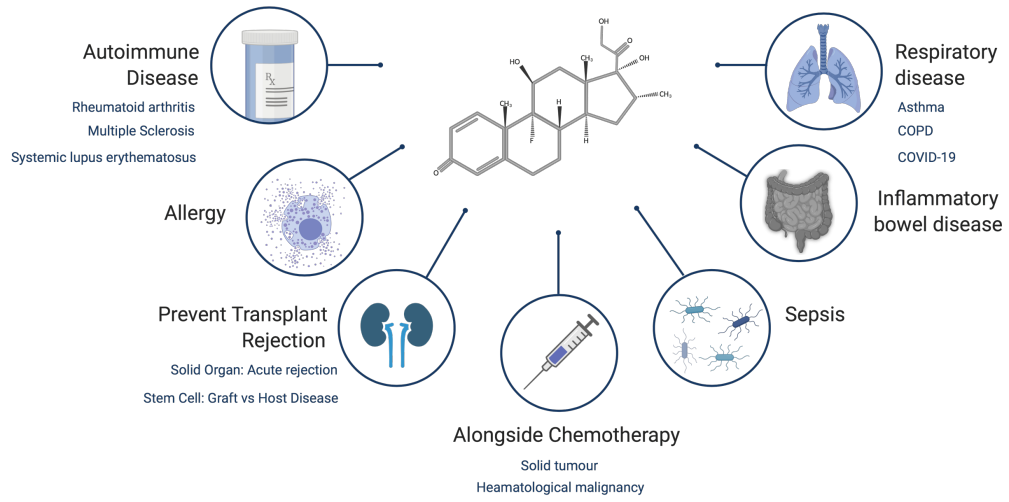
Figure 1.2. Clinical uses of Glucocorticoids

Therapeutic Glucocorticoids such as Dexamethasone have a range of clinical uses. They broadly act to prevent and limit the damaging effects of inflammation.

A range of Gcs which differ in their potency, duration of action and mode of delivery have been developed in order to limit these systemic adverse effects. Local application enables a more targeted delivery of Gc to the desired area and avoids the use of systemic doses. Topical creams containing Hydrocortisone, the synthetic form of endogenous cortisol, are used to treat skin conditions. While inhaled Gc Fluticasone and Budesonide are used to treat asthma (2). Where topical treatment is not possible, to mitigate the risk of fractures, some patients may receive bone-active treatments such as bisphosphonates alongside long-term corticosteroid prescriptions (6). Systemic Gc delivery is necessary for rheumatic disease and as part of cancer therapy as there are currently no alternative options. Maintaining the lowest possible therapeutic dose is the current strategy to limit side effects however, this is confounded by the fact that as inflammatory disease progresses, patients develop localised Gc resistance. Some reports suggest that as many as 30% of patients become Gc resistant (10, 11). This necessitates patients requiring higher doses for the same clinical benefit, which in turn increases both the incidence and severity of side effects (1). Resistance is particularly common in asthma (12, 13) and presents a large challenge in the treatment of lymphoid malignancies (11, 14). Therefore, understanding the molecular mechanisms of Gc function and identifying relevant factors that modify their efficacy is fundamental to the management of inflammatory diseases in the longer term.

1.2 Endogenous Gc: Synthesis and Regulation

Dynamic circadian and ultradian rhythms regulate endogenous Gc synthesis and release, which occurs rapidly upon stimulation (2). The hypothalamic-pituitary-adrenal (HPA) axis integrates systemic neural, endocrine and cytokine signals which ultimately results in cortisol secretion **(Figure 1.3)**. In response to physiological signals and stressors, corticotropin-releasing hormone (CRH) and arginine vasopressin (AVP) are released from the paraventricular nucleus of the hypothalamus. These factors stimulate corticotroph cells of the anterior pituitary to produce and release adrenocorticotropin hormone (ACTH) into the circulation. ACTH feeds forward to the adrenal glands to induce steroidogenesis, the enzymatic synthesis of endogenous cortisol from cholesterol. This occurs within the adrenal cortex leading to cortisol secretion into the blood (1). Negative feedback mechanisms at each stage of the synthesis pathway are tightly controlled which maintains the fine balance of input signals to prevent an excessive release of endogenous hormone.
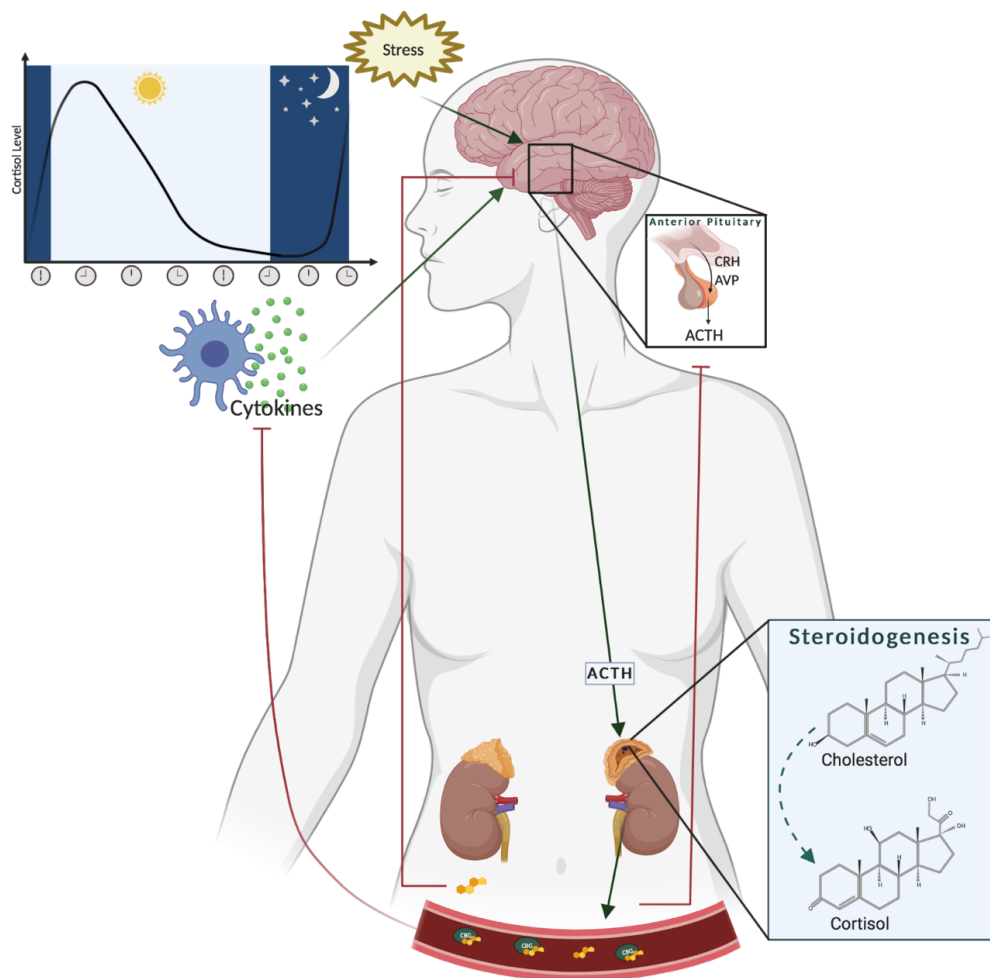
Figure 1.3. Endogenous glucocorticoid synthesis and regulation

The hypothalamic-pituitary-adrenal (HPA) axis regulates the synthesis of cortisol. Daily circadian rhythms regulate cortisol release which is increased in response to stress and inflammatory signals such as cytokines. Corticotropin-releasing hormone (CRH) and arginine vasopressin (AVP) are released from the paraventricular nucleus of the hypothalamus which stimulate corticotroph cells of the anterior pituitary to produce and release adrenocorticotropin hormone (ACTH) into the circulation. ACTH induces steroidogenesis, the enzymatic synthesis of endogenous cortisol from cholesterol, within the adrenal cortex of the adrenal glands. Cortisol is secreted into the circulation and is transported systemically bound to cortisol binding globulin (CBG). Negative feedback signals maintain the balance and prevent excessive hormone release.

The HPA axis is the primary regulator of Gc secretion. Although, Toll-like receptor 2 (TLR2) and TLR4 signals within adrenocortical cells have also been shown to promote steroidogenesis which links steroid production with inflammatory stimuli. Additionally, local production has been reported within the skin (15), thymus and intestine (16) and may reflect local control at critical immunological interfaces.

Although Gc are released systemically, the local availability and activity is regulated in a tissue specific manner. Approximately only 5% of circulating cortisol is biologically active as binding to high-affinity carrier protein, cortisol binding globulin (CBG) or albumin distributes the hormone systemically in an inactive state (5). At sites of inflammation CBGs are subject to degradation and increased temperature reduces their affinity to bind cortisol; serving as an efficient delivery system to inflamed tissues (17). Unbound Gc has a low molecular weight and is highly lipophilic therefore is able to freely diffuse into cells across the plasma membrane. The conversion towards active Gc is regulated at a cellular level by 11β-hydroxysteroid dehydrogenase enzymes (11β-HSD) located within the cytosol. 11β-HSD1 catalyses the conversion of cortisol from the inactive precursor cortisone, while 11β-HSD2 favours the converse reaction to rapidly inactivate cortisol (18). Expression of 11β-HSD1 is high in key Gc metabolic organs such as liver, skeletal muscle and adipose tissue (19) whilst expression in immune cells is inducible by pro-inflammatory cytokines (20). This demonstrates that the concentration of bioactive cortisol is dictated by the local balance in cellular enzyme expression levels allowing for rapid inflammatory resolution.

1.2.1.1 Cortisol and Dexamethasone Chemical structure

Synthetic steroids such as hydrocortisone and Dexamethasone (Dex) were developed based on the structure of endogenous cortisol **(Figure 1.4)**. The structure of corticosteroids is formed of a cyclopentanoperhydrophenanthrene backbone. Dex differs to cortisol by the addition of a fluorine atom, an additional methyl group and double bond between two carbon atoms.
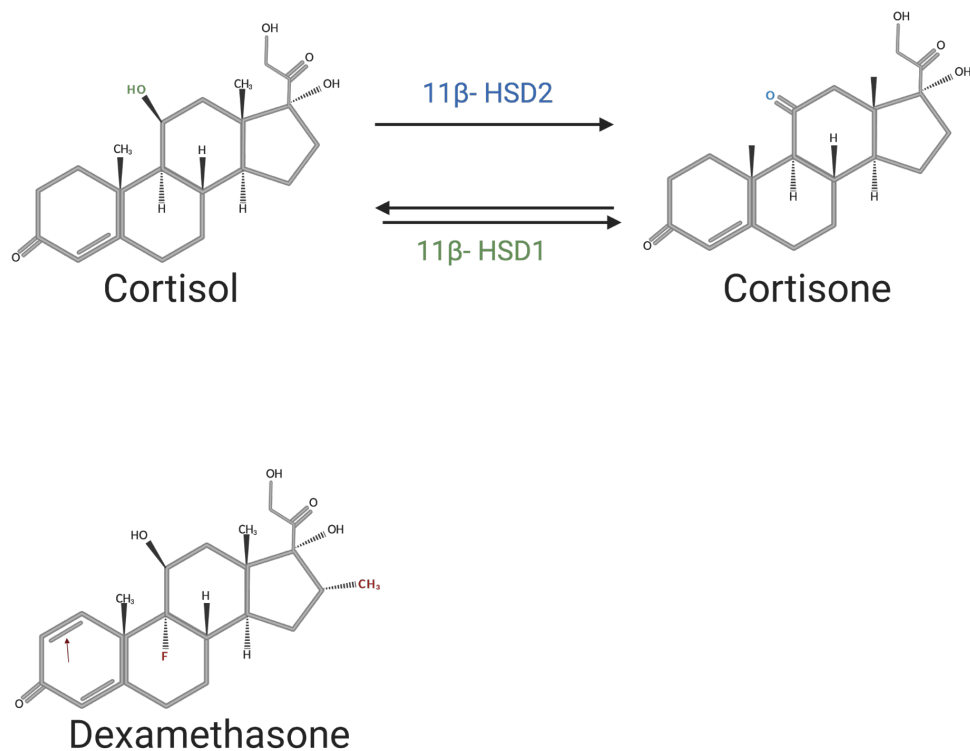
Figure 1.4. Chemical structures of Cortisol and Dexamethasone

The common glucocorticoid chemical structure of is formed of 21 carbon atoms forming a cyclopentanoperhydrophenanthrene backbone, with three cyclohexane rings and one cyclopentane ring. The interconversion of endogenous hormone cortisol and the inactive form cortisone, is regulated by the 11ß-HSD enzymes which control the availability of bioactive cortisol. 11ß-HSD1 catalyses the reduction reaction at carbon 11 position (coloured elements) which converts cortisone into cortisol. The 11ß-HSD2 catalyses the oxidation reaction to convert cortisol into cortisone. Dexamethasone differs to cortisol by an extra double bond between carbon 1 and 2 in the A-ring. Dex is fluorinated at position 9 and contains a methyl group at position 16 (highlighted red).

1.2.1.2 Regulation of Synthetic Steroids

Pharmacologic Gc are not subject to the same regulatory mechanisms as endogenous cortisol as they are unable to bind CBG which results in increased circulating levels of bioactive Gc. Prednisone/Prednisolone are substrates for 11β-HSD enzymes but 11β-HSD2 fails to inactivate Dexamethasone (21). Given the circadian rhythmicity of endogenous hormone, the timing synthetic Gc administration is an important consideration for the optimal efficacy of therapy as well as preventing side effects resulting from disturbance of the circadian cycle.

1.3 The Glucocorticoid Receptor (GR)

Gc exert their functional effects by binding and activating the glucocorticoid receptor (GR), a ligand-activated transcription factor and member of the nuclear receptor superfamily. The GR is ubiquitously expressed. The human NR3C1 gene encodes GR which comprises nine exons and is located on chromosome 5q31-32 (2).

1.3.1 Structure

GR is a modular protein composed of an N-terminal transactivation domain (NTD), central DNA binding domain (DBD) and is separated from the C-terminal ligand binding domain (LDB) by a flexible hinge region, as shown in **Figure 1.5A**. The NTD contains a ligand-independent domain of strong transcriptional activation function (AF1) which is important for the interactions with transcriptional co-regulators and with elements of the transcription machinery (2, 22). The DBD recognises and binds directly to glucocorticoid response elements (GRE) throughout the genome through two zinc finger motifs, and can also mediate protein-protein interactions. Within the DBD is a 5 amino acid sequence termed the D-loop important for GR dimer formation (23). The LBD contains a hydrophobic ligand-binding pocket where Gc bind. The LBD region also contains a further region of transcriptional activation (AF2) which functions to interact with co-regulators in a ligand-dependent manner (1, 2). The receptor also contains two nuclear localisation sequences (NLS1/NLS2) located at the DBD/hinge region and LBD, which are important controls for GR subcellular shuttling (24).

1.3.2 Isoforms

The NR3C1 gene comprises of 9 exons which can be alternatively processed to produce, 8 translational isoforms which differ by their subcellular localisation, ligand affinity and capacity to regulate transcription (25). The major GR species is GRα, which is typically defined as 'full length GR' and constitutes 90% of all GR transcripts in healthy tissues. The second major isoform is GRγ, which comprises 8-10% and is almost identical to GRα, except for retention of 3 bases at the exon 3/4 boundary which introduces a single arginine into the DBD. The resultant disruption between the two alpha helices in the lever arm confers different preference for DNA sequence binding but does not alter DNA binding affinity (26). Further alternative splicing of GR mRNA gives rise to minor receptor isoforms; GRβ, GR-A, GR-P which differ by their C-terminal regions, and are linked to Gc resistance in disease states (27) **(Figure 1.5B)**. GR-β is transcribed from alternative exon 9 (exon9β), which lacks a functional LBD due to loss of helices 11 and 12, therefore the receptor is unable to bind ligand. It is thought that GRβ can dimerise with and antagonise the actions of GRα, and increased expression of GRβ is thought to be linked to steroid resistant asthma (28).
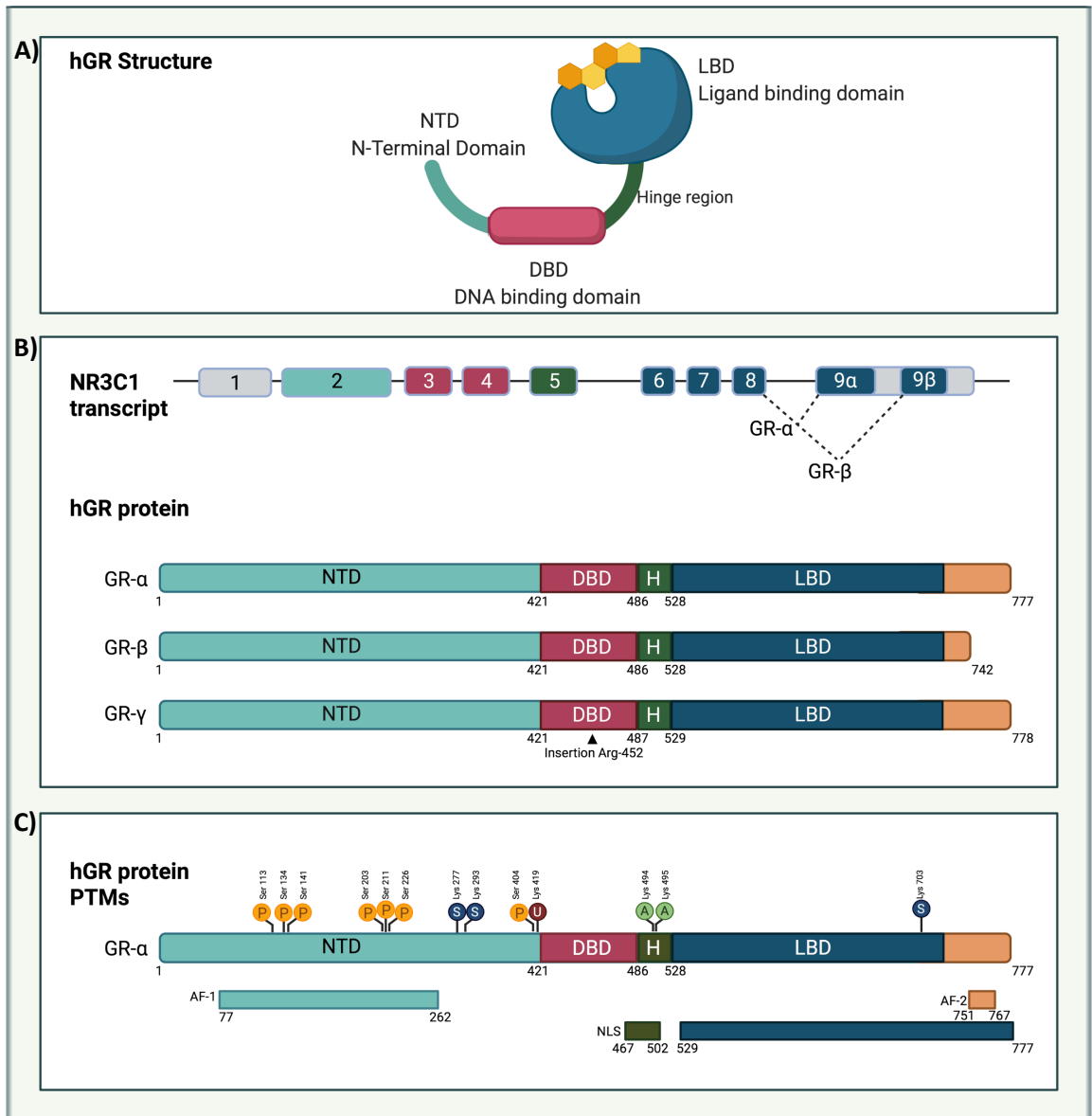
Figure 1.5. Glucocorticoid Receptor structure

(A) GR protein is formed of a N-terminal transactivation domain (NTD) a central DNA binding domain (DBD), hinge region and a C- terminal ligand binding domain The NTD contains area of transcriptional activation 1 (AF-1) which interacts with transcriptional machinery. Once the ligand is bound within the hydrophobic pocket of the LBD the second area of transcriptional function is able to interact with co-regulator proteins. Two nuclear localisation sequences are located within the GR: NLS1 spanning the DBD and hinge region and NLS2 within the LBD. (B) The NR3C1 gene contains 9 exons. Exons 2-9 form the protein coding region of the GR, exon 9 has two alternative transcripts: α and β and alternate splicing generates different GR isoforms. The three major GR variants generated by alternate splicing are outlined. GRα includes exons 2-8 and variant exon 9α, and accounts for approximately 90% of all transcripts. GRγ uses exons 2-8 and variant exon 9α, but retains 3 bp at the exon 3/4 boundary which results in a single amino acid insertion. GRβ includes exons 2-8 and variant exon 9β. (C) Post translational modifications of the GR protein. The NTD is the primary site for post-translational modifications such as phosphorylation (P), sumoylation (S), ubiquitination (U) and acetylation (A) which alter the functional properties of the GR.

1.4 Mechanism of Action

In the absence of ligand, the GR is held within the cytoplasm in a multi-protein complex formed of chaperones: heat-shock protein 90 (hsp90) hsp70, heat-shock organising protein (hop) and associated co-chaperone molecules: hsp40, p23, p14 and immunophilins; cyp40, FK506-binding protein (FKBP)51/FKBP52 (**Figure 1.6**) (29). The assembled oligomer is essential for hormone responsiveness as it orientates the ligand binding domain in a competent state such as to assist high affinity ligand-binding (24). Once GR binds to its ligand, the receptor translocates into the nucleus where it functions as a transcription factor. The nucleocytoplasmic shuttling of GR is a dynamic process through the macromolecule nuclear pore complex, embedded in the nuclear envelope (30). A dynamic equilibrium controls the localisation of unliganded GR which is predominantly maintained in the cytoplasm, while a small population is actively transported to the nucleus and diffuses back into the cytoplasm (31).

Ligand binding induces a conformational change in GR which exposes the two NLS and the receptor becomes hyperphosphorylated through interaction with cellular kinases. Formation of the nuclear transfer complex occurs following the exchange of FKBP51 for FKBP52 facilitating recruitment and direct interaction with dynein motor complexes for transport along the microtubules (32, 33). The receptor dissociates from restraining accessory proteins for rapid, ligand-dependent, active transport into the nucleus. Importin-α, importin-ß1 heterodimers and importin-7 interact with GR through NL1 while importin-7 and importin-8 recognise NL2. Hsp90 is required for efficient translocation and remains bound to the LBD during nuclear import (30). Once in the nucleus, GR interacts with other proteins and DNA to control transcription. The localisation of GR at a given time depends on the balance of import and export dynamics. In the presence of ligand, GR is predominantly localised in the nucleus.

Following ligand withdrawal GR rapidly dissociates from DNA and re-associates with the co-chaperone complex but remains with the nucleus. Redistribution of GR to the cytoplasm is subject to a slow rate of nuclear export due to a nuclear retention signal within the GR hinge region (34). Active export is mediated by calreticulin and binds GR through a motif between the 2 zinc fingers in the DBD (31).
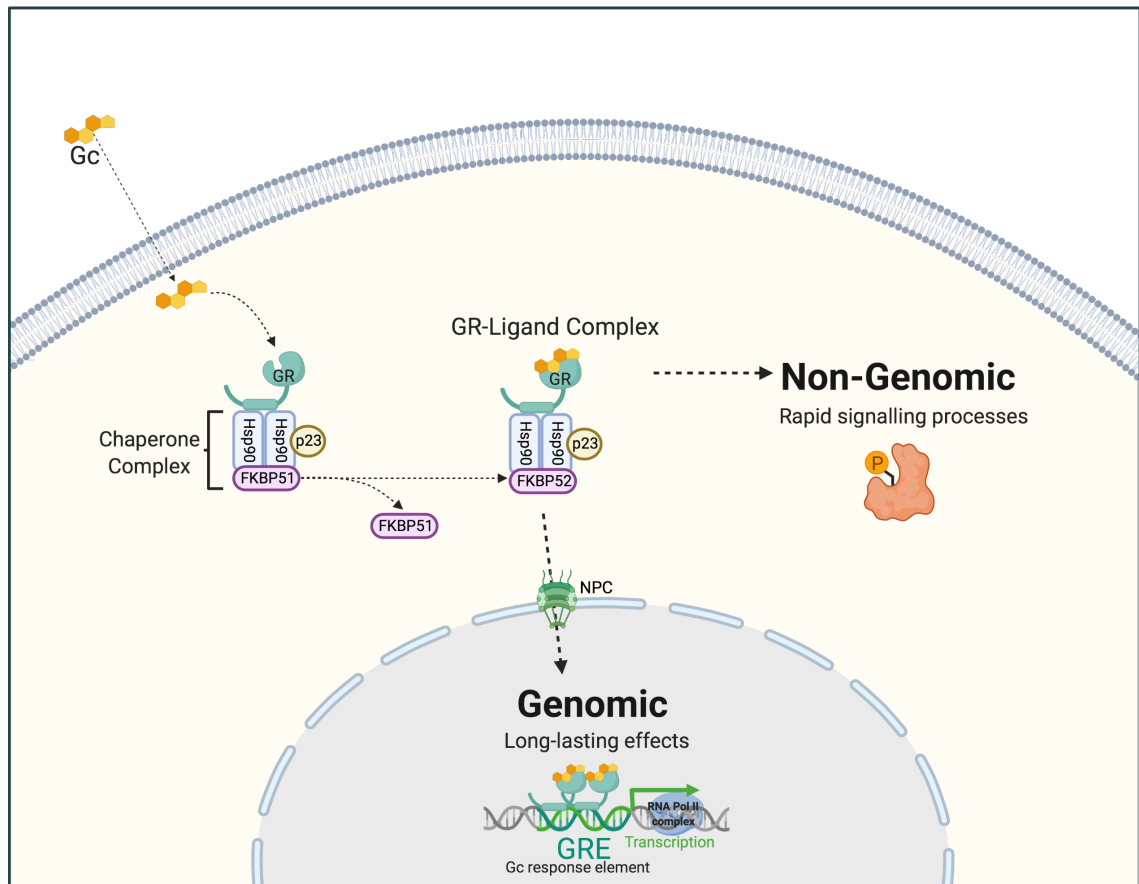
Figure 1.6. GR nuclear translocation

The GR is held in an inhibitory chaperone complex in an active conformation to promote ligand binding. Glucocorticoids diffuse through the plasma membrane into the cytoplasm and GR-ligand binding drives a conformational change which promotes the dissociation of chaperone proteins including the substitution of FKBP51 for FKBP52. Upon ligand binding, GR immediately interacts with kinases to initiate rapid non-genomic signalling involving second messenger cascades. This results in fast-acting signals and cellular changes. The GR-ligand complex subsequently docks and is transported along microtubules into the nucleus through the nuclear pore complex (NPC). In the nucleus GR modulates transcription which is known as the genomic action of GR, which controls the expression of genes to generate long-lasting transcriptional changes. Hsp: heat shock protein. NPC: nuclear pore complex.

1.4.1 Post translational modifications

Post-translational modifications (PTM) on the GR protein alter the functional activity, stability, localisation and diverse signaling capabilities induced by Gc. The receptor is subject to regulation by phosphorylation, ubiquitination, sumolation and acetylation which are outlined in **Figure 1.5C**.

GR phosphorylation occurs as a result of ligand binding and cross-talk with other signaling pathways. The NTD is the primary site of GR phosphorylation in particular within the AF-1 region (35). Phosphorylation patterns influence Gc sensitivity, GR interaction with co-factors and transcriptional capacity, while the functional outcome is dictated by the activating kinase (36).

Various kinases: p38 mitogen-activated protein kinase (MAPK), c-Jun N-terminal kinases (JNKs), glycogen synthase kinase 3 (GSK-3), cyclin-dependent kinases (CDKs), extracellular signal-regulated kinases (ERKs) and protein kinase B (PKB) /Akt have been shown to phosphorylate the GR across multiple serine residues, demonstrating that the array of cellular Gc responses controlled are regulated by a variety of inputs.

GR is basally phosphorylated on [P]Ser203 and CDK1 and CDK5 have been implicated in phosphorylation of this residue (37). [P]Ser203-GR is found located within the cytoplasmic fraction and is responsive to ligand (38) but is unable to bind glucocorticoid-specific gene promoters and is therefore considered to be transcriptionally inactive (39).

The [P]Ser211 phosphorylation mark is highly inducible upon ligand binding and is considered a mark of active GR (38). GR- [P]Ser211 is predominantly localised within the nucleus and has been found in association with the mediator of RNA polymerase II transcription subunit (MED14) a subunit of the mediator complex which forms part of transcription machinery (36). The level of phosphorylation is directly associated with Gc-dependent transcriptional activity and mutation of this residue reduces the expression of the GR target genes Gc-induced leucine zipper (*GILZ*, also known as TSC22 domain family protein 3 (TSC22D3) and interferon-regulatory factor (*IRF)8.* (35, 36, 39) The residue can be phosphorylated by p38 MAPK which subsequently enhances transcription and GR-dependent apoptosis (40). p38 MAPK is activated by 5' AMP-activated protein kinase (AMPK) which regulates Gc action upon carbohydrate metabolism and energy homeostasis in a tissue specific manner. This alters the accumulation of co-factors to GR-bound gene promoters and suppresses genes mediating the catabolic effects of Gc upon glucose metabolism (37, 41). Cyclin-CDK complexes also phosphorylate GR at Ser211 which has a positive effect on transcriptional activity. Furthermore, CDK1 has been shown to alter the localisation of GR to the nucleus which may in-part link the interplay of GR activity with cell cycle phases (37).

JNK has been shown to phosphorylate GR [P]Ser226 and accelerates the nuclear export of GR following ligand withdrawal (42). A mutation preventing phosphorylation at this position showed increased expression of classical GR-target genes *GILZ* and *IRF8* expression.(39) Taken together this suggests the [P]Ser226 modification attenuates the transcriptional activity of GR.

Another post-translational modification shown to alter the repertoire of transcribed genes induced by Gc is [P]Ser404 which is phosphorylated by GSK3β. A conformational change alters the interaction of GR with co-factors and affects the repressive activity of nuclear factor kappa-light-chain-enhancer of activated B cells (NF-κB)-regulated genes. [P]Ser404 phosphorylation may increase the rate of export of GR from the nucleus and at high levels be resistant to Dex-induced cell death. (43)

In response to cellular stress signals p38 MAPK mediates hyperphosphorylation of GR on Ser134. Phosphorylation is independent of ligand and does not alter protein stability or translocation of GR but instead creates a binding site facilitating the binding of 14-3-3 zeta co-factor protein at gene promoter regions. This modification re-directs the Gc-dependent transcriptional response for a subset of genes, showing that cells modify the activation of GR-regulated pathways under stressful conditions. (44) AKT1 has been shown to modify GR nuclear translocation following phosphorylation of the Ser134 residue and subsequent binding by 14-3-3 (14), which, in parallel with other AKT1-mediated mechanisms antagonised Gc-induced apoptosis in T-cell acute lymphoblastic leukaemia (T-ALL) (45). Many of the phosphorylation marks on GR have also been associated with aberrant activation of signalling pathways and may be related to resistance – particularly in lymphoid malignancies.

The GR is targeted for degradation by the proteasome following ubiquitination on Lys-419 which is important for ligand-dependent downregulation of GR to prevent overactivation of Gc-responsive genes (46). SUMOlaytion of GR occurs on Lysine residues -277, -293 and -703 and is increased by ligand binding (46). The SUMO modification was initially associated with receptor turnover but has since been shown to affect GR-mediated transcription chromatin occupancy. This was shown to be important for the regulation of genes associated with proliferation and survival (47) as well as the repression of pro-inflammatory genes (48). Acetylation of GR within hinge region on residues Lys-494 -495 is ligand dependent and fluctuates in a circadian manner (49). Removal of the acetylation mark by histone deacetylase (HDAC2) is required to suppress NF-κB mediated inflammation (28, 50). Overall, the orchestrated balance of PTMs on GR adds further complexity to the regulation of its action and must be tightly controlled to avoid insensitivity or dysregulation.

1.4.2 Polymorphisms

Polymorphisms in the NR3C1 gene have been identified, some of which have been linked to altered GR transcriptional function and partly explain varied degrees of systemic Gc sensitivity within specific subpopulations (2, 27). One example, the ER22/EK23 polymorphism within exon 2, results in an arginine to lysine change within the NTD of the mature protein. This modifies the ability of GR to upregulate target genes and correlates with Gc resistance (51). In contrast the single nucleotide polymorphism (SNP) N363S, also located within exon 2, results in a substitution of asparagine to serine and increases Gc sensitivity (51). A missense variant R714Q, has varied clinical manifestations from mild to severe Gc insensitivity. This is attributable to a conformational change in the ligand binding pocket which reduces the affinity of GR for ligand and transcriptional activity (52). Helix 1 of the LBD is required for GR to interact with key chaperone protein hsp90 while a repeat of 4 leucine residues in helix 8 is important for hsp90

binding maintenance of receptor conformation. Mutations in this region impede the association of GR with hsp90 and due to lack of stability, prevents Gc-induced nuclear translocation and transcriptional activity of GR (53). Other mutations in the CTD alter GR ligand binding capacity conferring a decreased (532-536 LXXLL to LXXAA) or increased (C656G or C656S) ligand binding affinity.

1.5 Transcription

1.5.1 RNA Polymerase II-mediated transcription

RNA polymerase II is a large multiprotein complex which is responsible for the synthesis of all protein coding genes. The transcription of mRNA is a highly dynamic process that is tightly regulated at all stages. The largest subunit of the complex, DNA-directed RNA pol II subunit B1 (Rpb1) (also known as RNAPII subunit A POLR2A) contains a consensus 52-repeated heptapeptide (Y,S,P,T,S,P,S) sequence which forms the CTD. The distinct phosphorylation pattern of the CTD Ser2, Thr4, Ser5, Ser7 residues orchestrates RNA pol II activity, as it provides a scaffold for the binding of transcription-associated factors. This allows for the coupling of transcription with chromatin remodelling and nascent RNA processing (54, 55).

The transcription-associated cyclin-dependent kinases (CDKs) mediate the cycle of reversible phosphorylation of the Rpb1 CTD which corresponds to the transcriptional stage (**Figure 1.7**). General transcription factors and the mediator complex assemble with a hypo-phosphorylated RNA pol II at gene promoters to form the pre-initiation complex. Phosphorylation on Ser7 is present at high levels at early stages and may be important to pave the way for phosphorylation of Ser5 - required to escape the gene promoters for transcription initiation. The transcription factor II F (TFIIF), part of the pre-initiation complex, aids transcription initiation by unwinding double-stranded DNA via the helicase subunit for RNA pol II accessibility as well as phosphorylating the Ser5 residue through the CDK7 subunit during early elongation. This establishes a stable paused complex. Proximal pausing of RNA pol II at an intrinsic pause site between 20-50 nucleotides downstream of the transcription start site (TSS) by negative elongation complexes (DSIF and NELF) can result in dissociation of the complex from DNA. Subsequent recruitment of the super elongation complex (SEC) containing positive transcription elongation factor b (P-TEFb) phosphorylates DSIF, NELF and Ser2 which permits RNA pol II to transition into a stable elongation phase (55). Ser5 phosphorylation of the CTD facilitates the recruitment of RNA capping enzymes, and spliceosome assembly (56) while Ser2 phosphorylation is accompanied by the association of factors to aid the production of mature mRNA transcript including, RNA splicing and polyadenylation proteins and chromatin re-modellers. During the elongation phase, levels of phosphorylated Ser2 increases while Ser5 is

removed. Thr4 is also an abundant modification present in conjunction with Ser2 and facilitates the interaction of the CTD with Rtt103 to mediate 3' end cleavage for robust termination of polyadenylated transcripts (56). Following transcription termination and dissociation of RNA pol II from DNA, phosphatases remove CTD modifications allowing the recycling of hypo-phosphorylated RNA pol II (55).
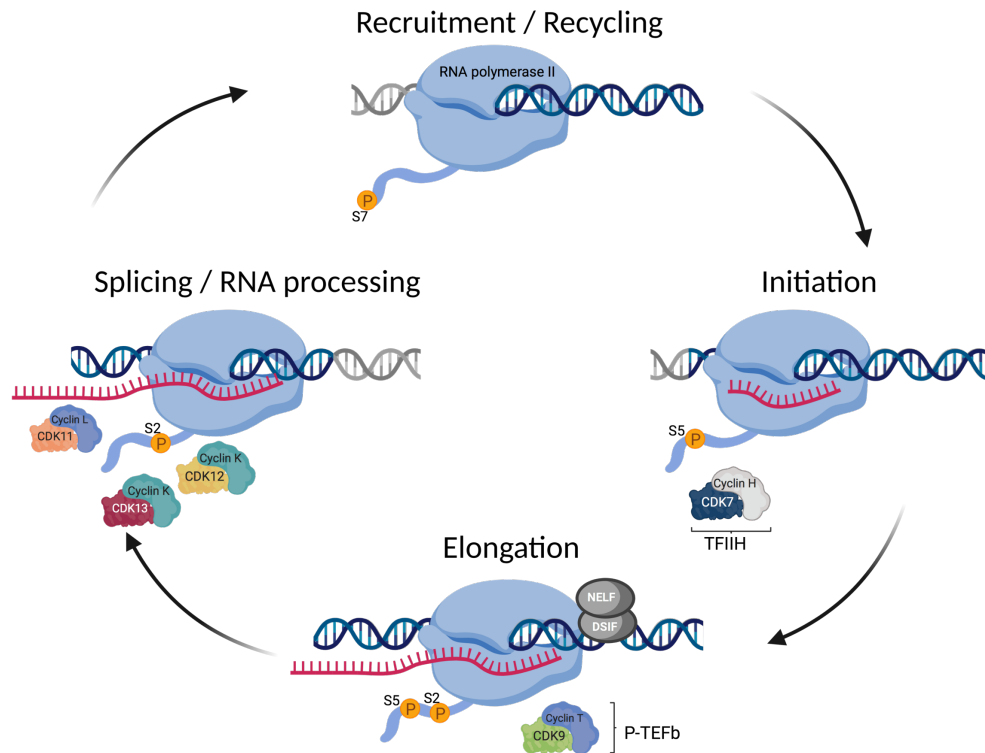
Figure 1.7. The Transcription Cycle

The Rpb1 large subunit of RNA polymerase II has a long C terminal domain (CTD) containing a conserved repeated sequence of 7 amino acids (52 repeats in humans) which are phosphorylated to tightly regulate the progression of transcription. The CTD residues are phosphorylated by the transcription-related cyclin dependent kinases (CDK) and each has a specific phosphorylation pattern that it recognises and regulates. To initiate transcription CDK7 phosphorylates the serine 5 residue which required to escape gene promoters. The complex pauses downstream of the transcription start site held by negative elongation factors: NELF and DSIF. CDK9 as part of the p-TEFb complex phosphorylates the negative elongation factors as well as the serine 2 residue to enable the progression into a stable elongation phase. During elongation serine 2 phosphorylation increases while serine 5 is removed. CDK12 and CDK13 are serine 2 kinases and aid the association of factors to produce a mature mRNA transcript including RNA splicing machinery.

1.5.2 GR-mediated regulation of transcription

GR controls the expression of a multitude of genes and GR has been shown to bind >10,000 sites across the genome. However, as with other transcription factors there is a discord between genomic occupancy and the number of expressed genes (57). The outcome of GR activation, and transcriptional regulation is highly complex and context dependent. GR can bind to DNA directly, or by tethering to other DNA bound transcription factors, and can recruit coactivators or corepressor proteins to mediate changes in gene transcription. These three broad models to describe how GR regulates the activation or suppression of target genes, are outlined in **Figure 1.8**. The expression of Gc-regulated genes is dictated not only by GR-activation status but higher-order chromatin architecture which directs the accessibility of transcription factors to bind to enhancer sites as well as co-factor availability and the presence of other transcription factors.

1.5.2.1 Direct Binding

GRα homodimers directly bind to target DNA sequences via the two zinc finger motifs within the DBD. The consensus glucocorticoid response element (GRE) is an imperfect palindromic sequence comprising of two inverted hexameric half sites separated by three base pairs (**Figure 1.8A&D**) (58). Each subunit of the homodimer occupies one half site which stabilises the interaction with DNA (59). GR directs local chromatin remodelling through the recruitment of co-activators, including histone acetyltransferases (HATs), to facilitate the assembly of the RNA pol II complex to upregulate target genes. However, the direct GR binding sites are more diverse than first appreciated. Conserved variations in GR binding sequences (GBS) within GREs increases the scope for GR-binding across the genome and can affect GR-DNA binding affinity (60, 61). GR-ligand complexes bind to negative GREs (nGRE) also known as inverted-repeat GBS (IR-GBS) and mediate transcriptional repression. Two GR molecules can bind to the non-identical motifs, separated by one base pair, on opposite sides of the DNA. However, biochemical studies suggest that *in vivo* GR may favour binding IR-GBSs as a monomer. (59, 62, 63).

Each specific GBS acts as an allosteric modulator which stabilises the GR structure to direct the appropriate recruitment of transcriptional co-activators or co-repressors through the LBD (58, 63). Similarly, ligands bound within the LBD influence receptor conformations which can direct GR to bind particular DNA regions. Additionally, the exposure of helix 12 following ligand-binding promotes the interaction with co-factors via the AF2 (59).

GR dimers bound at classic GREs, adopt a particular conformation providing an interaction interface with increased affinity for proteins (59). The recruitment of co-activators such as the steroid receptor co-activator (SRC) (p160) proteins: SRC-1 (also known as nuclear receptor co-activator 1 NCOA1), SRC-2 (also known as glucocorticoid receptor-interacting protein 1 (GRIP1)

and SRC-3 (NCOA3), promotes gene expression by directly modifying chromatin accessibility, recruiting secondary co-activators to reorganise chromatin architecture and act as a bridge between GR and the transcription machinery (61). The SRC proteins possess intrinsic HAT activity, the enzymatic transfer of an acetyl group on to histone proteins which relaxes the chromatin to aid DNA accessibility. Through their large protein interaction domains, co-activators form large multi-protein complexes. Binding to BRG1, the central ATPase part of the chromatin remodelling complex SWI/SNF, facilitates the assembly of a transcriptional pre-initiation complex of the basal transcription machinery and activates gene transcription (5, 64).

Conversely, GR bound to nGRE recruits co-repressors such as nuclear receptor co-repressor 1 (NCOR 1) and NCOR2 (also known as silencing mediator for retinoid and thyroid hormone receptors (SMRT)) which recruit HDAC proteins, particularly HDAC3. Together co-repressor complexes alter the post-translational modification signature of histones by removing acetyl groups, which compacts the chromatin and restricts gene accessibility. This has the consequence of repressing gene expression. (65, 66).

The locus specific recruitment of co-regulators by GR permits the regulation of distinct sets of target genes and adds further complexity to Gc-action (67, 68). GRIP1 can act as both a co-activator and co-repressor and has a potent anti-inflammatory role to support the action of GR. Specific phosphorylation of GRIP1 by CDK9 is required for the activation (but not repression) of GR target genes bound by GR at GREs (69).

1.5.2.2 Tethering

Tethering is more transient and occurs through direct protein-protein interactions of ligand-bound GR with DNA-bound transcription factors upon their corresponding response elements (70). Once in these complexes GR is able to alter the affinity of the transcription factor for DNA, recruit co-regulators and may act synergistically (transactivation via coactivators) or in opposition to the transcription factor (transrepression via corepressors). GR can tether to p65 (RELA) of NF-κB or c-Jun subunit of AP-1 complex to inhibit their function **(Figure 1.8B)**. This mechanism is thought to underlie the majority of the immunosuppressive actions of Gc (1, 71). In the case genes encoding major proinflammatory effectors, such as IL-6, GR occupancy at the proximal promoter was shown to be entirely dependent on the presence of an inflammatory stimulus (i.e. activation of p65 and AP1) and only occurred following the binding of p65 and c-Jun, highly suggestive of tethering (72).
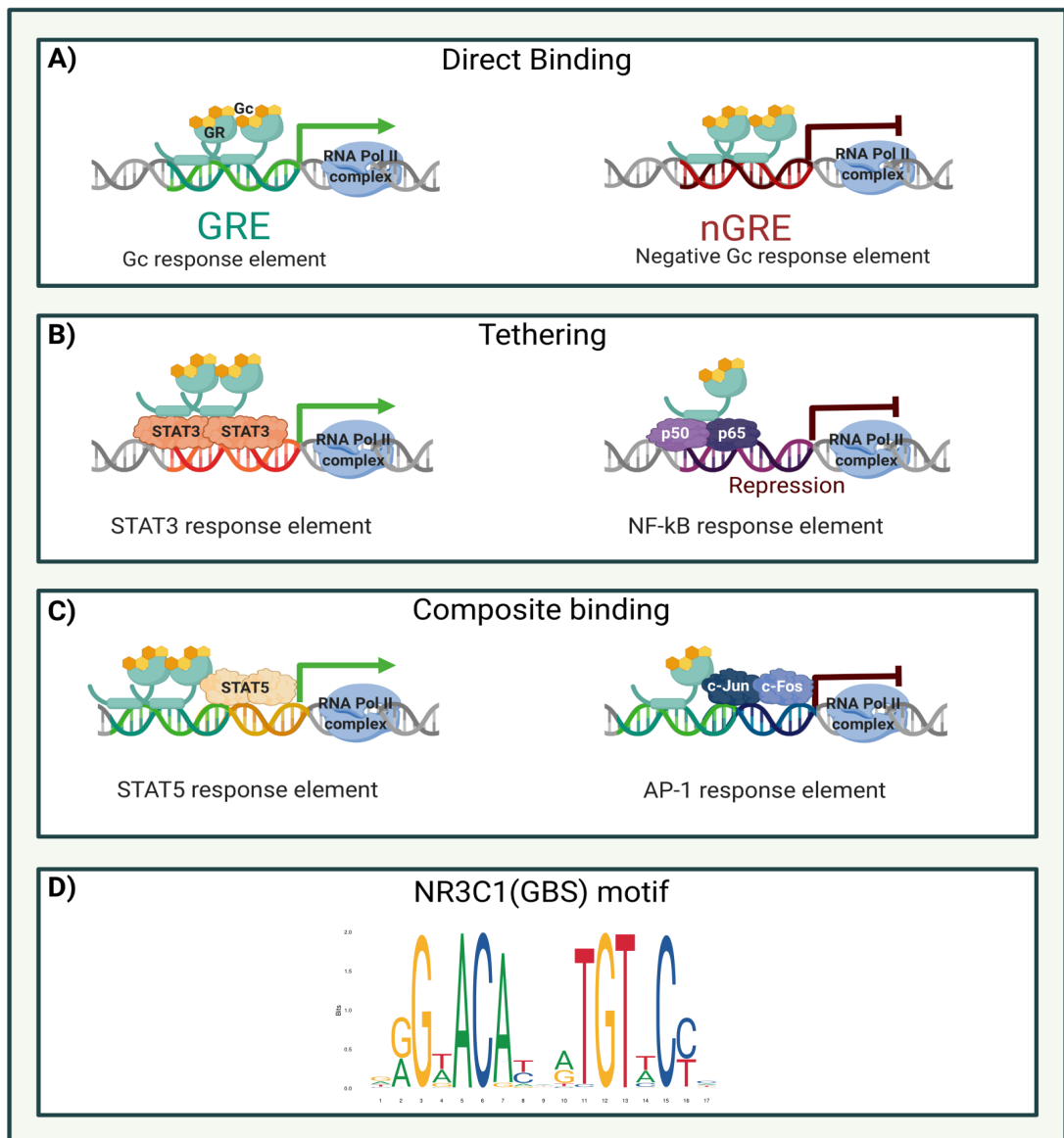
Figure 1.8. Mechanisms of GR genomic activity.

(A) Direct: Ligand-activated GR homodimers bind directly to the imperfect palindromic glucocorticoid response element (GRE) consensus sequence. GR interacts with chromatin remodelling factors and co-activator molecules to recruit the basal transcription machinery (RNA polymerase II) which leads to the direct upregulation of GR response genes. GR can also bind DNA directly at negative (nGRE) sequences. Interactions with co-repressors and histone deacetylases restricts chromatin accessibility to repress the transcription of target genes. (B) Tethering: GR can bind to indirectly to DNA by binding to transcription factors bound at their cognate response elements and modify their transcriptional response. Either to enhance or repress the expression of target genes. (C) Composite: Interactions between GR and transcription factors both bound to DNA directly at adjacent sites. Cooperative or antagonistic actions result in the activation or repression of gene expression respectively. (D) Example of GR binding sequence motif (JASPAR:MA0113.3). GR: Glucocorticoid receptor. GRE: Glucocorticoid response element. GBS: GR binding sequence.

1.5.2.3 Composite interactions

Co-ordinated interactions between GR bound to DNA at canonical half site GREs and other transcription factors bound to their response elements is another mechanism of GR-mediated regulation of gene expression (1, 60). These composite sites contain GR binding motifs alongside motifs for the binding of another transcription factor **(Figure 1.8C)**. Such binding is transient and weak, and therefore requires the cooperative action of the transcription factors to stabilise regulatory complexes and regulate transcription. This adjacent binding has been described for AP-1 (57), NF-κB (73) and signal transducer and activator of transcription (STAT) transcription factors (74). Crosstalk can be reciprocal with resultant antagonism or enhancement of transcriptional activity. Equally the mutual dependence of transcription factors for access to additional binding sites (72, 73) demonstrates interactions are highly complex. In contrast to original assumptions that tethering was the principal mechanism to oppose the pro-inflammatory activity of NF-κB and AP-1, it has been shown that direct binding of GR to DNA is required for both gene repression and activation (72, 75).

1.5.2.4 Complexity of outcome

Genome wide chromatin immunoprecipitation (ChIP)-sequencing studies have revealed that GR occupancy does not reliably correlate with regulatory effects upon proximal genes. Following activation GR occupies regions upstream, within the transcription start site (TSS) or the first exon. However, a significant proportion of GR binding occurs distal to gene promoters and within intragenic regions. Comparison with expression data revealed for repressed genes GR was bound more then 100kb from the TSS whereas for activated genes the median distance was 11kb (76). The distal GR occupancy may regulate expression due to a chromatin folding mechanism. An enhancer-cluster model was proposed by Vockley *et.al* where GR directly bound to DNA also interacts via protein-protein interactions with TFs at tethered sites kilobases away. Synergistic interactions are possible via chromatin loops and clusters of GR-bound to tethered sites may modulate the output of sites directly bound by GR. (57) Further evidence suggests tethering requires GR with the capacity to bind to DNA for anti-inflammatory action. GR containing a mutation within the first zinc finger of the DBD is incapable of binding to classic GRE or half site sequences. The genomic occupancy of this mutant GR at NF-κB and Ap-1 sites and co-immunoprecipitation with p65 support that the tethering capacity is maintained. However, transcriptional repression response to Dex was absent owing to the inability to recruit GRIP1 and assemble co-regulatory complexes (75).

Dynamic interactions between GR and other transcription factors shapes the specific transcriptional outcome. Gc-induced gene expression patterns are highly variable between cell

types (77) due to cell-type specific transcription factor co-expression and activity and areas of active chromatin (78). GR-cistrome comparisons by Uhlenhaut *et al.* revealed that between macrophages, adipocytes, pituitary and mammary cells GR binding has an overlap of less than 1% (72). Therefore, despite the ubiquitous expression of GR, the chromatin landscape and activity of other transcription factor pathways defines the specific actions of Gc (22, 72).

The outcome of GR signalling is also modified by the tissue environment to ensure the Gc response is fine tuned to ensure the most appropriate response in that context. GR may compete for DNA occupancy as GBS have been found within AP-1 response elements and also compete by binding co-factors (59). In the presence of inflammation, GR occupancy across the genome is significantly increased compared to basal levels, suggesting the inflammatory cistrome is more accessible to GR binding. However, regardless of the timing of inflammatory stimulus, GR activation reduces the total chromatin occupancy of NF-κB. This finding opposes the tethering model as GR requires residence of NF-κB on DNA to bind instead increased GR binding may be facilitated in chromatin regions made first accessible by NF-κB (79).

1.5.2.5 GR Oligomerisation

For years it was believed that the metabolic side-effects of Gc treatments were the result of the direct upregulation of metabolic genes from GR homodimers bound to GREs. Therefore, the clinically desirable anti-inflammatory action of Gc were thought to be regulated by GR monomers tethering to pro-inflammatory transcription factors or composite elements. The generation of a GR dimerisation deficient (GR^{dim}) mutant (A458T in humans) compromises the formation of GR homodimers, and initially sought to untangle this specific mechanism of transactivation and transrepression. Equivalent GR $^{dim/dim}$ mice possess an amino acid substitution within the D-loop of the DBD (A465T) which reduces receptor dimerisation and direct DNA binding. This single missense mutation was thought to prevent GRE-dependent transactivation, yet maintain the functionality of monomeric GR and desirable anti-inflammatory effects via tethering (80). In contrast to GR knockout mice, mice harbouring this mutation survive after birth but display impaired cognitive and memory function in response to elevated stress hormone levels (81). GR^{dim} mice are extremely sensitive to inflammatory stimuli, show poor maintenance of intestinal barrier function are highly susceptible to pathologic inflammation such as hypersensitivity and sepsis (82). Overall, GR^{dim} mice have revealed the importance of GR-dimerisation for homeostatic functions and the control inflammation and dissection of metabolic and anti-inflammatory GR effects is more complex.

Chip-seq experiments challenged the understanding that the GR^{dim} mt is incapable of directly binding to DNA and revealed that GR^{dim} binds the genome (in a circadian fashion) but does not

occupy the canonical palindromic GRE motif (83). In fact, GR dimerisation is more complex, and also requires interaction through an interface in the LBD. Therefore, previously described GR^{dim} mts could still dimerise through LBD-LBD interactions. The (L634A) mutation within the LBD reduces the active-GR dimeric population and displays an impaired transactivation mechanism but retains all capacity for transrepression (84). Mutations within GR preventing interdomain interactions are also shown to alter the allosteric effect of DNA upon GR and thus the ability to interact with co-factors (80, 85).

More recent attempts to understand GR quaternary structure and oligomerisation status show that a monomeric GR are non-functional *in vivo*. Given that a dimerisation-defective mutant is incapable of triggering a transcriptional response as chromatin binding is unstable. The transcriptional activity of the GR^{dim} receptor is minimal in comparison to GRwt but is capable of binding sites containing both full and half-GRE motifs. Occupancy at these sites is likely to be as GR dimers though the retained interaction within the LBD and was found to primarily occur at sites of pre-accessible chromatin (86).

GR has also been described as forming a tetramer complex when bound to DNA. Although, it remains unknown whether this quaternary structure is the result of two dimers on adjacent DNA or facilitating looping between distal sites in the genome (85).

1.6 Non-genomic action of Gc

Aside from the long-lasting genomic effects, activated GR induces a number of rapid intracellular kinase signalling events which occur too quickly to depend on transcriptional changes. These immediate cellular responses are part of the GR's non-genomic mechanism of action and were initially considered distinct from the long-lasting genomic effects (**Figure 1.6**). Non-genomic Gc signalling remains poorly characterised by comparison to Gc-mediated genomic action but recent studies have suggested that these rapid extranuclear signals shape genomic activity and long lasting Gc action (87). Therefore, understanding the full extent of Gc signalling and how GR non-genomic action may influence the response to therapeutic Gc is of crucial importance.

The signalling events following GR activation have been shown to modulate calcium mobilisation (88), inhibit ion channel conductivity (89) and promote mitochondrial apoptotic pathways (90); however, such actions appear to be cell type specific. Activated GR can alter the activity of parallel signalling pathways which include MAPKs (91), JNKs (92), ERKs, protein kinase (PK)A, PKB/Akt, PKC and phosphatidylinositol-3-phosphate kinase (PI3K) (89, 93, 94). Many of the non-genomic actions are defined by their rapid onset, insensitivity to inhibition of protein synthesis and in some instances are unperturbed by GR antagonist Ru486 (88). Gcs are thought to exert their non-genomic effects through various mechanisms including: specific interactions with

cytosolic GR and a membrane-bound GR in addition to non-specific interactions with the plasma membrane. Given that the GR does not possess kinase capabilities, how Gc initiates and engages with the diverse range of downstream pathways is not completely understood.

1.6.1 Cytosolic GR

The ligand-induced activation of cytosolic GR (cGR) promotes a conformational change resulting in the liberation of chaperone proteins and freeing them to participate in secondary signalling cascades. Several kinases which mediate MAPK signalling are part of the multi-protein complex which holds GR in the cytoplasm. Proto-oncogene tyrosine-protein kinase (Src) is one such kinase and following rapid release induced by Gc, Src proceeds to phosphorylate annexin 1 which inhibits the epidermal growth factor receptor (EGFR)-stimulated release of arachidonic acid – a precursor molecule to eicosanoids. Gc also reciprocally regulates EGFR signalling by preventing the recruitment of adaptor proteins to the activated receptor. This event is mediated by GR (Ru486 sensitive) but is independent of transcription (actinomycin-D insensitive) and the nuclear translocation of GR (95). Cortisol has been shown to increase reactive oxygen species (ROS)-mediated DNA damage in two breast cancer cell lines. Thought to occur following the dissociation of Src which phosphorylates inducible nitric oxide synthase (iNOS) consequently increasing the production of nitric oxide (NO) to cause oxidative DNA damage (96).

1.6.2 Membrane GR

The existence of a membrane-associated GR has been alluded to in studies demonstrating Gc-induced activation of membrane-proximal second messenger cascades (97, 98). Studies using membrane impermeable steroids conjugated to bovine serum albumin (BSA) have identified rapid changes in phosphorylation status of a number of kinases, including the activation of p38 MAPKs (91) and PKC via phospholipase C (PLC)γ. However, the precise existence and functionality of a membrane GR (mGR) remains unresolved.

Several studies have focussed on trying to identify such a receptor. High-sensitivity immunofluorescent staining techniques are capable of detecting the GR on the cell surface using antibodies recognising epitopes encoded by the NR3C1 gene. This has been demonstrated in cell lines including MCF-7 (99) (ER+ Breast cancer), U2-OS (99) (Osteosarcoma), CCRF-CEM (99) (T lymphoblastoid ALL) and Basophils (100), CD14+ monocytes, B-lymphocytes but not T-lymphocytes from healthy PBMC (101). Exposure to lipopolysaccharide (LPS) increased expression of the receptor on monocytes only; an upregulation which relies on the synthesis and transport of new protein. Monocyte expression of this mGR is positively correlated with disease score in rheumatoid arthritis (101), increased in (SLE) patients and reduced in line with

Gc treatment (102). These observations suggest a regulatory balance exists which increases the membrane localisation with inflammation and Gc control a negative feedback loop.

However, transient RNA interference does not affect the protein expression of mGR but stable knockdown of GR reduces detectable cytoplasmic and membrane GR expression. This supports the hypothesis that the two receptors are expressed by the NR3C1 gene (91). Since over expression of GRα does not increase detectable levels of GR at the plasma membrane, the turn-over, regulation and localisation to the two receptors may be controlled separately (101).

GR is found in association with the integral membrane protein, caveolin-1 (Cav-1) in membrane lipid rafts at the cell surface (99, 103). The molecular mechanism underlying GR membrane localisation and caveolin-1 co-localisation are undefined. Caveolin-1 forms an essential component of caveolae, which are lipid-raft microdomains that form non-clathrin-coated flask-shaped invaginations of the plasma membrane. Caveolin-1 acts as a protein scaffold for the organisation and concentration of signalling complexes. Caveolin-1 facilitates the translocation, assembly and signal transduction of closely related steroid receptor oestrogen receptor (ER) at the plasma membrane (104, 105). This association with Caveolin-1 and ER is promoted by S-palmitoylation - a reversible lipid post-translational modification which increases the hydrophobicity of a protein allowing close association with the membrane. This modification of the LBD of other steroid receptors is necessary for transport to the membrane and downstream signalling through MAPK and PI3K (104). However, despite the identification of a homologous evolutionary conserved sequence in the LBD of GRα, it appears that GR does not undergo S-palmitoylation and is not responsible for the association of GR with caveolin-1, membrane localisation or subsequent MAPK signalling (53, 106).

1.6.2.1 G-protein coupled receptors

G-protein coupled receptors (GPCR) are a large family of protein receptors found at the cell surface. Over 800 members of the GPCR superfamily have been identified within the human genome which all have characteristic 7 transmembrane spanning domain. Collectively GPCRs respond to a large range of extracellular stimuli direct and array of intracellular responses, largely through the coupling to G proteins. This has made GPCRs a major drug target with around 40% of all FDA approved drugs act by binding GPCRs (107).

Downstream cellular responses from GPCRs are often immediate and fast acting, mediated through second messenger cascades but can often converge on transcription factors to activate transcriptional responses. GPCRs become stabilised in an active conformation following the binding of an agonist ligand. This enables the coupling of heterotrimeric G-proteins, composed of G alpha (Gα), G beta (Gβ) and G gamma (Gγ) subunits, which are attached to the plasma

membrane through lipid anchors on Gα and Gγ. Activation results in the exchange of GDP for a molecule of GTP bound to Gα, activates the G protein permitting the dissociation of the heterotrimeric complex whereby proteins diffuse laterally to interact with other proteins situated at the membrane to activate second messenger signalling. The multiple genes encoding G protein subunits accounts for the specificity and diversity of downstream effects (108).

Phosphorylation of activated GPCRs primarily by GPCR kinases, tends to occur on the C-terminal region to promote the high-affinity binding to β-arrestins, scaffolding proteins which desensitises G protein signalling by preventing further G protein coupling and activation. β-arrestins can also participate in downstream signalling activity as well as facilitate the internalisation of activated GPCRs (109).

Gc rapidly induce signalling events which typically originate from GPCRs such as adenylate cyclase and phospholipase C activation. Closely related steroid receptors such as ER and progesterone receptor (PR) and androgen (AR) each have a related family of membrane receptors (GPR30, mPR, GPRC6A respectively) which are encoded by genes distinct from that of the cytosolic receptor (110). Both Gc and BSA-cortisol induce a swift increase in cyclic AMP (cAMP) in primary human airway smooth muscle cells. This is abolished by the knockdown of $G_{\alpha s}$ and unaltered by knockdown or inhibition of GRα. These observations imply that Gc activate the changes in cAMP dynamics though GPCR mechanism (87). Furthermore, acting through a G_i protein coupled receptor, Dex can inhibit the stimulated activity of potassium channels in airway epithelial cells (89).

1.6.3 Non-specific membrane interactions

Gc indirectly affect the biophysical properties and composition of cellular membranes. Endogenous Gc are derived from cholesterol- a constitutive modulator of plasma membrane stability. As both endogenous and synthetic steroids share structural similarities, Gc have been shown to generate changes in the fluidity and permeability of the lipid bilayer (111), this may occur while diffusing into the cell or by intercalating at high levels. High-dose Gc treatment can non-specifically affect energy utilisation of lymphocytes. Disruption to the physiochemical balance of the membrane by Gc impacts the transport of cations (Na^+ and Ca^{2+}) into the cell in addition to increasing proton permeability across the mitochondrial membrane which is important for cellular metabolism and protect against ROS. Cation cycling through ATP-dependent transporter and protein leak across the mitochondrial membrane are two of the main energy consuming processes in activated lymphocytes therefore, an impairment of ATP production and energy re-allocation would obstruct immune functions such as phagocytosis, migration antigen processing and cytokine production (112).

1.7 Glucocorticoid regulation of inflammation

1.7.1 Gc regulation of immune cells

Immune cells are a major target of therapeutic Gc, Dex in particular has well documented effects upon immune cell proliferation, differentiation and viability (61, 77, 113, 114). The transcriptional and pathway responses to Gc are considerably different between non-haematopoietic and haematopoietic cells as well as between specific immune cell types (77).

At the site of infection or trauma, local cells detect signals indicative of pathogen challenge and tissue damage to initiate an immune response. Innate receptors include pattern recognition receptors (PRRs), complement and Fc receptors which rapidly activate the production and secretion of inflammatory mediators such as cytokines, eicosanoids and vasoactive amines. The role of these secreted factors is to alert and activate tissue resident cells and recruit further immune cells to the site.

Gc dampen and attenuate downstream signalling from these innate receptors at multiple levels to suppress the production of secreted factors and prevent immune cell activation. TLR signals converge to activate the transcription factors NF-κB, AP-1 and IRF3; in the nucleus GR can directly antagonise the expression of their repertoire of pro-inflammatory gene targets (72, 75, 115). The parallel activation of genes encoding anti-inflammatory mediators by GR further facilitates the inhibition of TLR signalling. GILZ can directly bind to NF-κB to inhibit nuclear translocation, in addition to NF-κB inhibitor alpha (Iκ-Bα / *NFKBIA*) which sequesters the transcription factor in the cytoplasm (116, 117). Direct DNA binding by NF-κB and AP-1 is also impeded by GILZ to reduce the expression of pro-inflammatory cytokines (118). The dual specificity protein phosphatase 1 (*DUSP1*) gene encodes MAPK phosphatase (MKP-1) which dephosphorylates p38 MAPK to suppress signalling and prevents the downstream activation of pro-inflammatory genes (119).

Gc suppress the expression of adhesion molecules, integrins and chemokines on the vascular endothelium and by tissue resident leukocytes to prevent the migration of further leukocytes such as neutrophils and circulating monocytes. To further prevent migration and maintain tissue integrity, Gc act to reduce the permeability of the endothelial barrier. Through the positive regulation of annexin A1 production and function, and by inhibiting of the production of eicosanoids such as prostaglandins and leukotrienes. These lipid mediators enable cell infiltration by promoting vascular permeability. Increased annexin A1 secretion by macrophages interferes with the release of arachidonic acid by phospholipase A; a key step in eicosanoid biosynthesis (120). In conjunction, annexin A1 functions to reduce immune cell recruitment

through the down-regulation of adhesion molecules which interferes with immune cell migration (121).

Gc shape the inflammatory environment by modulating cytokine networks; suppressing the expression of pro-inflammatory cytokines including; interleukin-1β (IL-1β), IL-1α, IL-2, IL-3, IL4, IL-6, IL-12, IL-17, type 1 interferons (IFNs), tumour necrosis factor-α (TNF-α) and chemokines and promoting anti-inflammatory cytokine release. Modulating the secretion of local mediators and disrupting activating signals required for the adaptive responses can skew immune cell phenotypes to promote inflammatory resolution (5, 27, 122). The transactivation of specific gene programmes by GR promotes anti-inflammatory features such as IL-10 producing cells and increases the anti-oxidative capacity of leukocytes (77, 114, 123). GR upregulates ZFP36 (also known as tristetraprolin, TTP) which binds the mRNA of pro-inflammatory molecules, such as TNF-α, to destabilise and target for degradation and demonstrate how GR also suppresses cytokine expression at a post-transcriptional level (124).

Antigen presentation by macrophages and dendritic cells is a crucial process which links the rapidly activated innate arm with the specific activation of the adaptive immune response. Gc influences the maturation and function of these antigen presenting cells which in turn can shape the activity of T and B lymphocytes. Each of the 3 key signals: MHC presentation of antigen, co-stimulatory molecule expression and appropriate cytokine stimulation are each subject to inhibition by Gc and reduces the capacity to activate T cells or skews differentiation towards T regulatory phenotype.

For T cells which successfully engage their T cell receptor (TCR), Gc impede essential downstream kinase signals at multiple levels. Firstly, by rapidly suppressing kinase activity downstream of the TCR in a non-genomic manner, through the modulating kinase expression and by interfering with transcription factor activity (NF-κB, AP1, NFAT, T-bet). Consequently, Gc reduces the proliferative and secretory response of T cells which are important to control differentiation and survival functions. Gc display lymphocytic properties and T lymphocytes are particularly sensitive to Gc-induced apoptosis the mechanisms of which differ depending on activation and differentiation state (113). Furthermore, the polarization of T helper subtypes towards Th2 and Treg, is favoured over Th1 and Th17 by Gc at high doses which would aid inflammatory resolution (5).

Similarly, Gc downregulate essential genes encoding components of the B cell receptor (BCR) complex and associated kinases. A reduction in the functional cross-talk between the BCR and TLRs has the consequence of diminishing B cell responses and antibody secretion (77). During pathogen challenge, such Gc-mediated dampening of the adaptive response would be

detrimental. However, in the context of autoimmunity, which is driven by unregulated targeting of the adaptive immunity against self-antigens, the broad action of GR to suppress dysregulated activation is a fundamental component of Gc therapy.

During the stages of inflammatory resolution Gc skewing macrophages towards an inflammatory-resolving 'M2' phenotype to aid the clearance of cell debris and to prevent potentiation of immune activation through stimulation of PRRs. Gc also enhance the phagocytic capabilities of macrophages involving the transcriptional upregulation of phagocytic receptors for example mannose receptor (CD206) and scavenger receptors (CD163), which helps the clearance of apoptotic cells (125).

In dose-dependent contexts in macrophages, cortisol has a potentiating effect upon immune stimulation to induce the expression of inflammatory mediators (114) which opposes early views of a purely immunosuppressive mechanism (5). Under physiological contexts the Gc response must be malleable response to act in the most appropriate manner to restore homeostasis. The priming of innate immunity at low doses to first control the insult may be necessary and represents the importance of maintaining a fine regulatory balance. This net effect of Gc is to initially facilitate the immune response, promote resolution and repair and then terminate the inflammatory response to limit tissue damage.

1.7.1.1 NF-κB

The NF-κB signalling pathway regulates pro-inflammatory cytokine expression, cellular stress responses as well as cell proliferation and is a key target of GR-regulated immunosuppression (126). Multiple pathways involved in the acute phase response converge to activate NF-κB which regulates of a plethora of inflammatory genes including: cytokines, chemokines, adhesion molecules, complement components and their corresponding receptors. Five Rel family proteins: p65/RelA, RelB, c-Rel, NF-κB1(p50/p105) and NF-κB2 (p100/p52) co-operate as dimers to integrate signals and fine-tune appropriate cellular responses to inflammatory stimuli (127). The p50/p65 heterodimer is the most abundant of NK-κB dimers which in the absence of inflammatory stimuli are sequestered within the cytosol by inhibitory proteins of the IkB family, which conceal the p65 nuclear localisation signal and limits DNA binding capacity (117). Activation of TLRs, IL-1ß receptor, or TNF receptor (TNFR) (among others) activates signalling kinase pathways which leads to the phosphorylation of IκκB within the IκB kinase (Iκκ) complex (128). IκκB phosphorylates IκB, and then subsequent ubiquitination targets IκB for degradation by the proteasome. p50/p65 is released from the inhibitory complex which permits the nuclear localisation of the p50/p65 dimer (117) where it can bind DNA with high affinity to promote the transcription of pro-inflammatory effectors.

The interaction between GR and p65 is central to the fine-tuned regulation of inflammatory signalling networks. GR modulates p65 activity at multiple levels of the pathway. Firstly, direct interactions between GR and DNA bound p65, inhibits p65 function – the IL-6 promoter provides a classic example of this (129). This establishes that p65/GR cross talk interferes with the production of a pivotal cytokine which acts across both innate and adaptive systems (130, 131).

In addition, GR increases the expression of other proteins known to inhibit p65 function. GR binding to GRE in the *NFKBIA* (Iκ-Bα) gene upregulates the inhibitory protein which in turn sequesters NF-κB to prevent nuclear entry (116, 132). Gc induces the expression of GILZ which physically interacts with p65/p50 and inhibits the nuclear translocation and transcriptional activity of NF-κB (118). The net effect of GR action is to block p65 action on chromatin, and then increase levels of p65 inhibitors to sequester p65 in the cytoplasm to terminate p65 signalling.

1.8 Gc Sensitivity

Monocytes and lymphocytes both show steroid resistance to similar extent in patients with Gc-resistant asthma, whereby Gc are unable to suppress cytokine secretion (34). Signalling inadequacies of GR are thought to underlie reduced responsiveness including: reduced GR expression, decreased affinity of GR for ligand or DNA binding, failure to translocate to the nucleus and increased competition for DNA binding with proinflammatory transcription factors (28). Disease-related factors within the micro-environment are in part responsible for disparity in Gc sensitivity (18). Within the pro-inflammatory milieu both cytokines and oxidative stress have been implicated in limiting Gc responses. IL-2, IL-4, IL-13, which are elevated within the asthmatic airways, reduce GR activity and nuclear translocation (12, 13). Consequently, a failure to respond to therapeutic Gc may result in tissue damage due to unresolved inflammation.

1.8.1 Cell Geometry

Cells integrate biochemical and physical signals to control cell processes. The volume and geometric orientation of a cell is imposed by both cell-matrix and cell-cell interactions such as substrate rigidity, compression and frequency of cell-cell contacts (133). These factors alone can modulate cell fate: proliferation, survival, and differentiation whilst also influencing genomic integrity and the epigenetic state of a cell (133-137). Mechano-transduction describes the way in which cells transform these extracellular spatial cues into intracellular signals to direct cellular responses. The cytoskeleton network is composed of filamentous proteins; microtubules, actin and intermediate filaments which provide mechanical support, internal organisation intracellular transport system, and is also crucial for the perception and translation of dynamic physical signals from the microenvironment to the nucleus. Furthermore, the actin cytoskeleton is physically connected to nucleoskeleton and through the transmission of mechanical forces,

can modulate the morphological properties of the nucleus (136-139). The actin cytoskeleton therefore underpins the ability of a cell to respond and adapt to external signals.

Studies utilising adhesive micropatterns have allowed the comparison of cell shape, size, aspect ratio and volume to assess how geometry can influence the properties and behaviour of single cells. Cells attach to the matrix via focal adhesions however, the frequency and distribution differs between geometries (137-139). Anisotropic/polarised cells attach to underlying substrate through mature focal adhesions at the cell extremity; the total number increases in proportion with degree of elongation (139). This generates local tensile stress and initiates mechanotransducive feedback through activation of Ca2+ signalling and Rho-Rock pathway resulting in stiffening of the actin filament network. In contrast, cells with a circular geometry have an even distribution of focal adhesions around the periphery of the basal membrane, which translates to low cytoskeletal tension and contractility. Short actin filaments are organised into mesh-like structures in isotropic cells unlike the long stress fibres formed along the long axis in cells with elongated geometry (137). The formation of stress fibres correlates to the level of phosphorylated myosin light chain (pMLC), a marker for contractility and cytoskeletal tension, and is greater in anisotropic cells.

The nuclear volume is directly correlated with cell volume - it follows that cells with a greater volume is reflected by larger nuclear volume (138). Nuclear morphology and deformability is influenced by geometry which is governed by actin cytoskeletal contractility while intermediate filaments provide mechanical integrity for nuclear stability (139). Constrained isotropic cells have a more deformable nucleus due to geometry-induced downregulation of nuclear envelope components Lamin A/C. Accordingly, stretched cells exhibit enlarged ellipsoidal nuclei, orientated with the long axis, as the result of flattening by lateral compressive forces exerted by apical stress fibres and have a stiffer nuclear envelope due to increased levels of Lamin A/C (133, 136, 137, 140). These geometry-associated differences in nuclear morphology also influence the organisation of underlying chromatin.

Cell spreading is generally associated with decondensed, more transcriptionally active chromatin; therefore, the spatial density of chromatin is higher in confined cells with smaller nuclear volume in comparison to larger more elongated cells (141, 142). However, this may depend on the extent of elongation and cytoskeletal tension. Versaeval et.al. reported that elongated endothelial cells, displayed an ellipsoidal nucleus but reduced nuclear volume and more compacted chromatin (139). This contrasts other studies where stretched cells with ellipsoidal nuclei have a larger nuclear volume with less compact chromatin, yet suggests nuclear volume is a strong determinant of the extent of chromatin compaction. Compressive force

reversibly increases the amount of transcriptionally inactive heterochromatin, regardless of the initial geometry of the cell (133).

In addition to changes in observable cell features, geometry can induce a shift in the global gene expression profile. As is normally the case, chromatin compaction is accompanied by a reduction in cell proliferation and of transcription initiation measured by ^{P}Ser5 of RNA pol II and large scale down regulation in gene expression (133, 143). However, compaction of chromatin cannot fully explain how transcriptional profiles change in a geometry specific manner particularly when genes are upregulated (141, 144).

Variations in the shuttling dynamics of chromatin modifiers, transcription factors and co-factors are also induced by geometry. Physical signals are known to change localisation of mechanosensitive transcription factors such as yes-associated protein (YAP) and transcriptional coactivator with PDZ-binding motif (TAZ) which detect ECM rigidity through cytoskeletal tension and accordingly alter genomic transcription (145). A growing body of evidence indicates that a cell's mechanical state and actin dynamics can affect the cellular localisation of other transcription factors.

Myocardin-related transcription factor (MRTF-A) is sensitive to changes in the ratio of F/G-actin. MRTF-A binds to G-actin in the cytoplasm and during actin polymerisation is released, permitting its movement into the nucleus. MRTF-A acts as a co-factor and in conjunction with serum-response factor (SRF) regulates the expression of actin-related genes. The transcriptional activity of MRTF-A is differentially regulated based on cell size as larger cell size results in increased MRTF-A nuclear motility and the upregulation of target genes (144). The converse effect on localisation and gene expression is observed in cells under compressive force which induced actin depolymerisation(133).

 Histone deacetylase 3 (HDAC-3)-dependent compaction of chromatin has been shown in response to altered geometry. As shown by studies using chemical disruptors of the cytoskeleton have demonstrated that the nuclear accumulation of HDAC3 is a direct result of a global decrease actomyosin contractility (138, 144). Equally, an increase in histone marks associated with heterochromatin (H3K9me3 and H3K27me3) induced by compressive force was inhibited by HDAC3 knockdown. Inside the nucleus HDAC3 removes acetylation on histone tails which then allows for repressive methylation (133). Higher levels of AcH3K9 (histone H3 acetylated at lysine 9) in cells with a larger cell area correlates to decreased levels of nuclear HDAC3 and more permissive chromatin. Whereas, increased levels of nuclear histone deacetylase 3 (HDAC3) in cells adopting a rounded morphology or facilitates chromatin compaction and a shift in the global gene expression profile (144). Levels of histone acetylation dictates the chromatin landscape, chromatin accessibility and therefore sites of active

transcription are also regulated by cell geometry in this manner (141, 144, 146). This implicates mechanical inputs in the regulation of chromatin accessibility in addition to the transport dynamics and compartmentalisation of transcription factors.

HDAC3 is important for inflammatory gene expression in macrophages (147, 148) Iκ-Bα sequesters HDAC3 in the cytoplasm, which is released upon degradation by either TNF-α signals (149) or inhibition of actinomyosin contractility (144). Higher p65 nuclear localisation and transcriptional activity is also observed under these morphological conditions and is likely due to the degradation of the shared inhibitory molecule.

1.8.1.1 Influence on inflammatory signalling

Steady state NF-κB nuclear shuttling is known to be influenced by morphologic cell features such as nuclear area and number of contacts with neighbouring cells. One study reported that in response to TNF-α stimulation the nuclear: cytoplasmic ratio of NF-κB varied considerably between cell types which could be correlated with their morphological properties (150).

Nuclear translocation of active p65 in response to stimuli occurs more quickly and to a greater maximum level in cells plated on circle micropattern compared to stretched cells. This may be explained by higher resting levels of phosphorylated IKKb. (134). Comparable observations regarding NF-κB localisation have been shown by chemically induced actin depolymerisation or disruption of myosin II ATPase which prevents actin contractibility (150), which further support findings that both simulated and the basal shuttling activity of NF-κB are differentially influenced by the cytoskeleton. Overexpression of Lamin A/C in macrophages enhanced p65 nuclear translocation through a reduction in Iκ-Bα levels, even in absence of activating stimuli (151).

In stretched compared to spherical fibroblasts, TNF-α elicited differential gene expression responses (134). Considering also that LPS and TNF-α, both upstream activators of NF- κB, induce cytoskeletal reorganisation (152), this finding is important as it implies for the same cell type, physical factors can shift the genomic response to cytokine signals and chemical signals can alter the physical state on the cell. In macrophages shape-induced polarisation was observed; where a stretched morphology enhanced skewing towards M2 phenotype and a reduced their response to activating stimuli such as LPS and IFN-γ (153).

This spatial element is likely to be fundamentally relevant in modulating cellular responses of immune cells to inflammatory stimuli *in vivo*. Whilst surveying the tissues and migrating, cells are subject to 3-dimensional, cellular distortion from the compressive pressures of the dense extracellular matrix network and from adjacent cells during trans-endothelial cell migration (154). Therefore, the morphology of an immune cell circulating in the bloodstream differs greatly from that of cells migrating within tissues or interacting with other immune cells (155).

Macrophages display diverse geometries *in vivo* and respond to adhesive cues which can modulate their phenotype (153). Considering p65 activity is potentially increased in larger, stretched cells, this suggests that at sites of inflammation, cells may become pro-inflammatory in the absence of appropriate signals.

Analysing the crosstalk between p65 and GR - two well characterised transcription factors in a key target cell – macrophages provides the perfect model to explore role of cell geometry in modulating immune responses.

1.9 High-throughput methodologies

High-throughput -omics approaches are unparalleled hypothesis generating tools. Such approaches are unbiased and aim to characterise the complete molecular or genetic profile of a cell. The combination of -omics approaches provides large-scale analysis of multiple aspects of cell biology.

1.9.1 Proteomics

Proteomics describes methods which characterise the proteome; which is defined as the overall set of proteins present within a cell or tissue. Such methods can provide in-depth identification of protein structure, function, interactions and post-translational modifications at a given time. Early proteomic approaches such as two-dimensional polyacrylamide gel electrophoresis (2D PAGE), involve first separating proteins in one dimension according to their isoelectric point, followed by their molecular mass in the second dimension. This technique is capable of resolving hundreds of proteins however, this falls short of the thousands of proteins comprising the proteome and such gel-based approaches are laborious, time-consuming and can lack reproducibility (156).

Mass spectrometry (MS) is an important tool for high-throughput protein identification and quantification, which determines the molecular weight of a protein by measuring the mass to charge ratio (m/z) (157). The two main approaches for proteomics differ based on their sample preparation method. The top-down approach analyses whole intact proteins by MS and useful for functional proteomics particularly the analysis of PTMs. This method determines the intact mass of proteoforms and can resolve the modifications present across the whole protein length. However, the number of analysed conditions is limited as it can be difficult to separate complex mixtures.

For bottom up proteomics, proteins are first enzymatically digested then resultant peptides are analysed by MS. This results in more efficient peptide fragmentation. The mass measurement and peptide fragments are used to identify the peptide sequence while the intensity of the mass

aids quantification. Label-free quantification methods allow for the analysis of a greater number of samples however, this method has lower sensitivity compared to labelling methods and each sample is analysed individually which can introduce variability (158).

Label-based quantification involves comparing the ion abundance ratios of metabolically or chemically labelled isotopes. Stable-isotope labelling with amino acids in cell culture (SILAC) is a quantitative proteomic metabolic labelling method. The whole cellular proteome is labelled by incorporating heavy or light amino acids (generally ^{13}C- or ^{15}N-labeled Arg or Lys) into the cell growth medium. Differently labelled samples are treated with the experimental perturbation and are mixed following cell lysis which reduces sampling handling variability. The relative quantification between heavy and light-labelled peptides is detected due to the shift in mass from the isotopic labelling (158). Prior to MS analysis, samples can undergo an enrichment step to select phosphopeptides for phosphoproteomic analysis. A dynamic tool which is provides further depth functional state of the proteome and is useful to identify signal transduction pathways and cellular processes.

1.9.2 Transcriptomics

Transcriptomics defines the characterisation of complete set of RNA transcripts present within the cell or tissue - this can include mRNA, tRNA, non-coding RNA and small RNAs. High-throughput methods identify the complete set of genes which are being actively transcribed with the main goal to compare differentially expressed transcripts between different experimental conditions or cell populations. This functional approach to defining the expression of transcripts can also be extended to analyse splicing patterns and identify the 5' and 3' regions of gene ends.

The microarray technology enables the simultaneous identification of thousands mRNA transcripts. The hybridisation of fluorescently labelled cDNA transcripts to complementary nucleotide oligomers (probes) on a microchip. The transcript abundance for each probe sequence is indicated by fluorescent intensity. The major limitation of microarrays is that probes on the chip contains only known sequences and is therefore constrained to detect a specified set of genes. High-background due to cross-hybridisation can also affect sensitivity and make detection of low abundance transcripts difficult (159).

RNA-sequencing (RNA-seq) was developed with the introduction of next generation sequencing (NGS) and is a highly parallel sequencing technique which provides whole transcriptome analysis. To achieve this, RNA is fragmented then converted to generate a cDNA library with ligated sequencing adaptor molecules (at one or both ends). The library is then sequenced and reads must then be aligned to a reference genome to determine which genomic regions were

being transcribed. In comparison to microarray methods, RNA-seq has a higher specificity and sensitivity particularly for genes with low expression. The sensitivity of an RNA-seq experiment can be increased for example by increasing the sequencing depth or performing prior enrichment for example of mRNA molecules using oligonucleotides binding to poly-A-tails. Sequencing of transcripts can be performed in one direction or both directions (single or paired end) and the most appropriate may depend on the biological question. Single-end is quicker and cheaper and sufficient for differential gene expression studies whereas paired-end sequencing provides more robust alignment to the genome and is useful for more in-depth applications such as isoform identification. RNA-seq has the advantage of also possessing the capability of identifying novel and non-coding transcripts as well as single nucleotide variants.

One of the remaining challenges of RNA-seq is the complex data analysis and standardisation. Differences in transcript lengths can result in gene-length/ fragmentation bias when comparing the expression of genes of different lengths and should be considered in data-analysis pipelines. This arises because the mRNA are fragmented and long transcripts will have more fragments in comparison to an shorter gene that is equally expressed (160). This issue is avoided with 3'RNA sequencing which reverse transcribes mRNAs from the 3' end prior to fragmentation. This method generates only one cDNA copy for each transcript which reduces gene length bias and reflects the true transcript abundance for each gene.

1.10 Hypothesis and Aims

This work aims to assess the genomic and non-genomic cellular response to Gc and the role of factors which modify GR action. The findings of this work will provide insight into the signalling activities of GR to further understanding and inform of how therapeutic Gc function in *vivo.*

The following hypotheses of the study shall be addressed by the following aims and objectives:

Chapter 3. Rapid targets of GR activation

Hypothesis 1: The rapid cellular effects of GR signalling action will differ depending on the activating ligand which will engage alternate kinases and downstream pathways.

Aim 1: To better define the rapid targets of GR activation in order to understand the spectrum of non-genomic signalling by GR.

Objectives:

- Use SILAC phosphoproteomic data to identify proteins which are differentially phosphorylated following GR activation.
- Determine the function of GR regulated phosphoproteins using functional ontology analysis and identify key pathways which are initially engaged following Gc exposure.
- Better understand the involvement of identified GPCRs in the rapid Gc signalling and determine whether the GPCRs are directly activated by Gc.

Chapter 4: Nuclear signals and the role of CDK12 and CDK13 in GR-regulated transcription

Hypothesis 2: CDK12 and CDK13 are involved in the expression of GR-regulated genes.

Aim 2: To understand the effects of Dex on CDK activity, downstream activation of RNA polymerase II and the consequences on Gc-regulated transcription.

Objectives:

- Assess the effect of acute Dex treatment upon the phosphorylation status of RNA polymerase II and measure the effect pharmacologically inhibiting CDK12 and CDK13.
- Define the role of CDK12 and CDK13 upon Gc responsive genes in addition to GR translocation.
- Perform RNA sequencing to identify Gc-regulated genes affected by CDK12 and CDK13 inhibition
- Evaluate the differentially regulated genes and use motif analysis to identify potential transcriptional regulators.

Chapter 5: Cell-matrix interactions and the effect upon transcription factor dynamics

Hypothesis 3. Different cell geometry will affect the nuclear translocation of GR

Aim 3. Develop a model system to investigate the effect of cell geometry upon the nuclear localisation of GR and NF-κB transcription factors

Objectives:

- Characterise Gc sensitivity in monocytic cell lines and establish a method to differentiate into macrophages.

- Utilise matrix-coated micropatterns to model the effects of cell geometry and measure cell features to compare:

    o Polarised vs non-polarised substrates

    o Cell shape, area size, aspect ratio.

- Investigate the effect of cell geometry upon GR & p65 transcription factor subcellular shuttling

Chapter 2: Methods

2.1 Materials

Dexamethasone: (D4902, Sigma) 20mM stock solution was prepared in dimethyl sulfoxide (DMSO; D5879, Honeywell) and diluted to working concentration of 100nM in complete medium.

17β-Oestradiol: (E1024, Sigma) 20mM stock solution was prepared in DMSO and diluted to working concentration of 1nM or 10nM in complete medium.

CDK inhibitors: Flavopiridol (FVP) (26024, Cayman Chemical) and THZ531 (26386, Cayman Chemical) were reconstituted in DMSO purged with N_2 gas, as recommended by the manufacturer. Aliquots were stored at -80°C for no longer than 1 month. For treatments, inhibitors were diluted in cell medium to the desired working concentration (50, 500nM).

Phorbol-12-myristate-13-acetate (PMA): (CAS 16561-29-8, Santa-Cruz Biotechnology) 100 µM stock solution was prepared in DMSO and diluted to a working concentration (5-100ng/ml) in complete medium.

Lipopolysaccharide (LPS): (Ecoli O111:B4, Millipore) used at a final concentration of 10ng/ml.

Cytokines: Recombinant human TNF-α 10ng/ml (PHC3015, ThermoFisher Scientific). Recombinant human IFN-γ 20ng/ml (300-02, Peprotech), Recombinant human IL-4 20ng/ml (200-04, Peprotech). Reconstituted with ddH_2O containing 0.1% bovine serum albumin (BSA). Stored -80°C as instructed by the manufacturer.

Antibodies: Complete list of primary and secondary antibodies used in the study are detailed in **Table 2.1** and **Table 2.2**.

Table 2.1 Primary antibodies used during this study.

Application in immunofluorescence (IF) or western blot (WB). CST: Cell Signalling Technologies.

Target	Species	Clone	Dilution	Technique	Catalogue #	Company
NR3C1 (GR)	Rabbit	Polyclonal	1:200	IF	HPA004248	Atlas Antibodies
NF-κB/p65	Mouse	L8F8	1:500	IF	6956	CST
P65	Rabbit	C22B4	1:100	IF	4764	CST
α-Tubulin	Mouse	DM1A	1:500	IF	3873	CST
Anti-Flag	Mouse	M2	1:2000	IF	F3165	Sigma
GR	Rabbit	Polyclonal	1:1000	WB	L12703-TP1	ProteinTech
^{p}Ser211 GR	Rabbit	Polyclonal	1:1000	WB	SAB4503820	Sigma-Prestige Antibodies
Phospho-Rpb1 CTD (Ser2)	Rabbit IgG	E1Z3G	1:1000	WB	13499	CST
Phospho-Rpb1 CTD (Ser5)	Rabbit IgG	D9N5I	1:1000	WB	13523	CST
Phospho-Rpb1 CTD (Ser2/Ser5)	Rabbit IgG	D1G3K	1:1000	WB	13546	CST
Phospho-Rpb1 CTD (Ser7)	Rabbit IgG	E2V6W	1:1000	WB	13780	CST
Rpb1 NTD	Rabbit IgG	D8L4Y	1:1000	WB	14958	CST
GPR123	Rabbit	Polyclonal	1:1000	WB/IF	PA5-75823	Invitrogen
GPR126	Rabbit	Polyclonal	1:1000	WB/IF	PA5-78542	Invitrogen
GPR126	Rabbit	Polyclonal	1:1000	WB/IF	17774-1-AP	ProteinTech
CD97	Rabbit	Polyclonal	1:1000	WB/IF	13071-1-AP	ProteinTech
Phospho-PKA substrate	Rabbit	100G7E	1:1000	WB	9624	CST
Phospho-PKC substrate	Rabbit	MultiMab mix	1:1000	WB	6967	CST
β-actin	Mouse	AC-15	1:10,000	WB	A5441	Sigma

Table 2.2 Secondary antibodies used during this study.

Application in immunofluorescence (IF) or western blot (WB). GAM: goat anti-mouse. DAR: Donkey anti-rabbit.

Target	Species	Dilution	Technique	Catalogue #	Company
Alexa647 Phalloidin	-	1:200	IF	A22287	ThermoFisher Scientific
Alexa Fluor488 anti Mouse (GAM)	Goat	2 drops/ ml	IF	R37120	ThermoFisher Scientific
Alexa Fluor488 anti-Rabbit (DAR)	Donkey	2 drops/ ml	IF	R37118	ThermoFisher Scientific
Alexa Fluor594 anti-Rabbit (DAR)	Donkey	2 drops/ ml	IF	R37119	ThermoFisher Scientific
Anti-Rabbit IgG -HRP	Donkey	1:5000	WB	NA934V	GE Healthcare
Anti-mouse IgG -HRP	Sheep	1:5000	WB	NA93IV	GE Healthcare

2.2 Cell Culture

2.2.1 Cell Passage

The routine passage of adherent cell cultures, all reagents are outlined in **Table 2.3**. Briefly, cells were washed with DPBS and incubated until detached with appropriate volume of 1x Trypsin-EDTA solution to cover the cells. Appropriate media containing serum was added to neutralise the trypsin and cell suspensions were pelleted by centrifugation (300xg, 5 minutes). Cells were resuspended in complete media and split as appropriate into 75cm^2 or 150cm^2 flasks or counted and seeded at the appropriate density into plates for experiments. Cell lines used and their conditions are detailed in **Table 2.4.**

The human lung epithelial, adenocarcinoma-derived cell line A549 was sub-cultured by trypsinisation when cells reached between 60-90% confluency.

HTLA cells: human embryonic kidney HEK293T cells which stably express tTA-dependent luciferase reporter and β-arrestin2-TEV fusion gene were a gift from the laboratory of Bryan L Roth (109). Cells were maintained as described for A549. For luciferase experiments, cells were transferred into phenol-red free basal media supplemented with: 10% CSS, 1% Sodium pyruvate and selective antibiotics (as **Table 2.4**).

Table 2.3 List of reagents used for cell culture

Reagent	Catalogue #	Supplier
10x Trypsin-EDTA solution	T4174	Sigma
Charcoal stripped serum (CSS)	12676029	Gibco
Accutase solution	A1110501	Gibco
Dimethyl sulfoxide (DMSO)	D5879	Honeywell
Dulbecco's Modified Eagle Medium (DMEM); high glucose (4500mg/ml) with L-glutamine, sodium pyruvate, sodium bicarbonate	D6429	Sigma
DMEM; high glucose with L-glutamine, HEPES. No phenol red.	21063029	ThermoFisher
DMEM/Nutrient Mixture F12 Ham (DMEM/F12)	D8437	Sigma
Dulbecco's phosphate buffered saline (DPBS)	D8662	Sigma
DPBS without Ca^{2+} and Mg^{2+}	D8537	Sigma
GlutaMax	35050-038	ThermoFisher
Heat inactivated FBS (HI-FBS)	10500064	Gibco
Recombinant Human insulin	RP10935	ThermoFisher
Hygromycin B	H007	TOKU-E
Hydrocortisone	H0888	Sigma
Non-essential amino acids (NEAA) 1mM	11140035	ThermoFisher
Penicillin /Streptomycin	P0781	Sigma
Puromycin	P025	TOKU-E
RPMI-1640 medium with L-glutamine and sodium bicarbonate	R8758	Sigma
Sodium pyruvate (100mM)	11360039	ThermoFisher
Trypan blue	T8154	Sigma
Wiliams E medium	A12176-01	Invitrogen

The promyeloblast HL-60, monocytic THP-1 and monocytic U-937 suspension cell lines were cultured in complete medium in 25 cm^2 or 75cm^2 flasks. The suspension cell density was maintained between (0.2×10^5 - 1×10^6 cells/ml) by passage and addition of fresh growth media every 3 days.

For the semi-adherent murine macrophage cell lines, J774A.1 and RAW264.7 subcultures were passaged by gently scraping culture vessels with a cell scraper to dislodge cells. The cell suspension was then centrifuged and split into new culture vessels with fresh medium at a ratio of 1:3 to 1:10.

All cells were maintained at 37°C in a 5% CO_2 humidified atmosphere.

Table 2.4 Overview of cell lines used and their culture conditions.

HI-FCS: Heat inactivated Foetal bovine serum. NEAA: Non-essential amino acids. ATCC: American type culture collection. ECACC: European collection of authenticated cell cultures.

Cell Line	Basal media	Supplements	Species	Description	Catalogue #	Supplier
A549	DMEM	10% HI-FBS	Human	Lung epithelial, adenocarcinoma	CCL-185	ATCC
HEK293T	DMEM	10% HI-FBS	Human	Embryonic Kidney	CRL-1573	ATCC
Caco2	DMEM	10% HI-FBS	Human	Colorectal adenocarcinoma	HTB-37	ATCC
HUH7	DMEM	10% HI-FBS	Human	Hepatocellular carcinoma	01042712	ECACC
HepaRG	Williams E medium	10% HI-FBS, 1% GlutaMax, 5 µg/ml insulin, 50 µM hydrocortisone	Human	Hepatocyte, Hepatocarcinoma	HEPRGC10	ThermoFisher
M059K	DMEM/F12 (1:1)	10% HI-FBS, 1% Sodium pyruvate, 1% NEAA	Human	Glial Cell, Glioblastoma	CRL-2365	ATCC
MCF-7	RPMI-1640	10% HI-FBS	Human	Mammary epithelial cells. Breast adenocarinoma	HTB-22	ATCC
PA-1	DMEM	10% HI-FBS	Human	Ovarian teratocarcinoma	90013101	ECACC
THP-1	RPMI-1640	10% HI-FBS	Human	Monocytic	TIB-202	ATCC
HTLA HEK-293T	DMEM	10% FCS 100U/ml Pen/ Strep, 2µg/ml Puromycin, 100µg/ml Hygromycin B	Human	Embryonic Kidney; stably expressing tTA-dependent luciferase reporter and β-arrestin2-TEV fusion gene	N/A	Gift from the laboratory of Bryan L Roth (109)
HL-60	RPMI-1640	10% HI-FBS	Human	Lymphoblast	CCL-240	ATCC
U-937	RPMI-1640	10% HI-FBS	Human	Pro-monocytic	CRL-1593.2	ATCC
J774A.1	DMEM	10% HI-FBS	Mouse	Monocyte/macrophage	TIB-67	ATCC
RAW264.7	DMEM	10% HI-FBS	Mouse	Macrophage	TIB-71	ATCC

2.2.2 Cryopreservation and recovery of cells

For long term preservation, cells were stored in the vapour phase of liquid nitrogen. Cells were collected and centrifuged (300xg for 5 minutes), the cell pellet was then resuspended in base media with 10% dimethyl sulfoxide (DMSO; D5879, Honeywell). Approximately, $2x10^6$ cells/ml were transferred to 1ml cryotube which were cooled at -80°C in a Mr frosty container (10110051, Thermo Scientific) using 100% isopropanol.

For recovery, cryotubes were warmed in a water bath at 37°C. Cells were diluted with warmed-medium and centrifuged to remove DMSO then added to culture flask (25 cm^2 / 75cm^2 flask depending on recovered cell concentration with complete medium. After 24 hours fresh media was added and subsequently cultured as appropriate.

2.3 Steroid treatment

Cells were transferred into steroid depleted media (base media supplemented with 10% charcoal dextran-stripped serum (CSS) (12676029, Gibco) overnight prior to treatment with Dex. Cells were treated with a final concentration of 100nM Dex for either 1 or 4 hours, dependent on the endpoint measure (1 hour for GR phosphorylation or translocation, and 4 hours to measure transcriptional responses).

2.4 CDK Inhibition

A549 cells seeded at a concentration of $1x10^5$ cells/ml, were pre-treated, for 30 minutes, with 50nM or 500nM of CDK inhibitors, Flavopiridol (FVP) (broad acting) or THZ531 (CDK12, CDK13 specific). For gene expression analysis, cells were then treated with 100nM Dex for 4 hours. In the presence of inflammation, inhibitor pre-treatment was followed by 10ng/ml TNF-α for 60 minutes prior to addition of 100nMDex for 4 hours. Cells were lysed with RLT buffer to extract RNA for assessment of gene expression (described below).

For analysis of phosphoproteins, A549 cells were seeded at $2x10^5$ cells/ml pre-treated as above. Cells treated with 100nM Dex over time course (0,5,10,15,30 or 60 minutes exposure) and lysed with RIPA buffer for immunoblot.

2.5 Cell differentiation

2.5.1 Macrophage differentiation

Three human cell lines were selected due to their capacity to be differentiated into macrophage-like cells (161, 162). HL-60, U-937 and THP-1 cells were seeded at an equal density of $5 x 10^5$ cells/ml in 6 well plates and differentiated using PMA (varying concentrations 5-100 ng/ml) for

48 hours; concentration based on previous literature (163). Differentiated cells were rested for a further 48 hours in PMA free media. During the course of differentiation, cells were visualised and images captured using EVOS Cell Imaging System (ThermoFisher Scientific). The efficiency of differentiation was quantified by cell counting of attached and unattached cells. Supernatants were collected and the wells were washed with PBS and combined with the supernatant. The unattached (supernatant) cells were centrifuged and resuspended in 1ml media and counted by trypan-blue exclusion to determine cell number and viability. Adherent cells were detached by incubating with pre-warmed accutase detachment solution for 20 minutes which was then quenched with growth media containing serum and then removed by gentle scraping. The extent of differentiation was calculated as the percentage of adherent cells out of the total cells counted.

2.5.2 M1 and M2 phenotype

THP-1 cells were seeded at an equal density of 5×10^5 cells/ml in 6 well plates and differentiated using PMA (25 ng/ml) for 48 hours. Differentiated cells were rested for a further 72 hours in PMA free media then cells were treated for 48 hours with cytokines. M1 phenotype: 10ng/ml LPS, 20 ng/ml IFN-γ or M2 phenotype: 20 ng/ml IL-4.

2.6 Manipulation of cell geometry

Activated CYTOOchip Starter A micropattern chips were coated for 2 hours with (20µg/ml) fibronectin (from bovine plasma) F11341, Sigma) diluted in PBS (without Ca^{2+} and Mg^{2+}). Micropattern chips were thoroughly washed with PBS immediately and prior to cell seeding. Micropattern chips containing only crossbow patterns and custom 'HUMEN' micropattern chips purchased from CYTOOchip™ were precoated with fluorescent 650nm fibronectin.

Cells were detached by the appropriate method, centrifuged, thoroughly resuspended to individualise then strained to remove clumped cells and counted and then seeded at the recommended density of 15,000 cells/ml and visualised hourly to determine optimal spreading time. Once sufficient spreading was observed, cells were fixed by adding an equal volume of 8% PFA directly to the culture medium (final concentration 4%) for 15 minutes as instructed by the manufacturer. The chips were then washed by sequential removal and addition of PBS as to dilute the PFA and ensure the chip was not exposed and able to become dry. Subsequent immunostaining was then performed as described below.

2.7 Transfection

2.7.1 Plasmid Purification

Table 2.5. PRESTO-TANGO plasmids used in the study.

All were obtained from Addgene.com in bacteria as an agar stab and were a gift from Bryan Roth (109)

Plasmid #	Plasmid	Antibiotic resistance	Growing temp (℃)	Reference
66311	GPR123	Ampicillin	37	http://n2t.net/addgene:66311;RRID:Addgene_66311
66314	GPR126	Ampicillin	37	http://n2t.net/addgene:66314;RRID:Addgene_66314
66247	CD97	Ampicillin	37	http://n2t.net/addgene:66247; RRID:Addgene_66247
66299	GPER	Ampicillin	37	http://n2t.net/addgene:66299; RRID:Addgene_66299

Plasmids used are detailed in **Table 2.5**. Bacteria were streaked onto LB agar plates containing 100 mg/ml ampicillin (J60977.06, VWR) and cultured overnight at 37℃. Single bacterial colonies were selected and transferred into starter cultures in 5ml 2% LB, containing 100 mg/ml ampicillin and incubated overnight on shaker at 37℃. Cultures used for mini-prep using Qiagen Plasmid mini-kit (12123) as per manufacturers protocol or transferred to larger culture 200ml LB broth for further culture overnight at 37℃. Maxi-prep of plasmid DNA was then performed using Qiagen Plasmid maxi-kit (12362) according to the manufacturer's instructions.

2.7.2 siRNA Knock Down

Small interfering RNA (siRNA) transfections were performed using Lipofectamine^{TM} RNAiMAX transfection reagent (13778150, ThermoFisher Scientific) following the manufacturer's guide. Briefly Lipofectamine was diluted in serum-free RPMI 1640 media. siRNA was diluted separately in RPMI 1640 and then added to lipofectamine reagent at a 1:1 ratio. The siRNA-lipid complex was incubated for 15 minutes at room temperature and added to cells (final siRNA concentration 25pmol per well in 6-well plate) and incubated for 48 hours 37°C/5% CO_2.

2.7.2.1 GPCR siRNA knockdown

Knock down of GPR123/*ADGRA1* (GS84435), GPR126/*ADGRG6* (GS57211) and CD97/*ADGRE5* (GS976) was performed using Flexitube GeneSolution siRNA (Qiagen), which contains 4 individual siRNAs for the gene of interest. Scrambled AllStars non-silencing siRNA (SI03650318, Qiagen) was used as a negative control. siRNA-lipofectamine mixtures were prepared as described above, then added to cells previously plated at density of 1.25 x10^5 cells /well and incubated for 48 hours.

2.7.3 Luciferase Assays

2.7.3.1 TAT3 NRE reporter assay

A549 cells were transfected in 10cm dishes with 2μg plasmid-DNA containing either TAT3-TATAluc or NRE-luc and 0.5μg Renilla-luc. Transfections were performed using Fugene-6 reagent (E2691, Promega) at a ratio of 3.1 volume/weight ratio with DNA as recommended by the manufacturer. Fugene 6 was mixed with serum-free RPMI media for 5 minutes prior to incubation with pDNA (premixed) for 20 minutes at room temperature. Transfection mixture was applied to cultures for minimum 24 hours at 37°C/5% CO_2. Following transfection for 24 hours transfected cells were collected, centrifuged and resuspended in media containing CSS. Cells were then seeded at a denisty of $5x10^4$ cells/well into 24-well plates and allowed to adhere for at least 5 hours before treating overnight with increasing concentrations of Dex (1nM -1μM) in the presence or absence of 10ng/ml TNF-α (NRE-luc) and 500nM THZ531. Cells were washed twice with filtered PBS and lysed with passive lysis buffer (E1910, Promega dual-luciferase Reporter system) diluted x5 in filtered dH_2O in accordance with the manufacturer's instructions. Lysis was allowed to proceed for 30 minutes at room temperature with gentle rocking. Cell-lysates were then transferred to white-bottomed 96-well plates and read on citation-5 plate reader luminometer. To detect firefly luminescence, 25μl LARII was first dispensed and read following a 2-second wait with a 5-second read time. The reaction was quenched and the Renilla reaction was initiated by the addition of 25μl Stop and Glo reagent, which was read using the same parameters as the previous section. Relative luminescence units were per well were obtained by taking the ratio of firefly:renilla luminescence for each well.

2.7.3.2 Tango Assay

HTLA HEK-293 cells were transfected with plasmids containing GPR123-TANGO, GPR126-TANGO, CD97-TANGO, GPER-TANGO or TAT3 at three different concentrations (400ng, 800ng, 1200ng) of pDNA to determine the best efficiency. Fugene-6 reagent was mixed with serum-free RPMI media for 5 minutes prior to incubation with pDNA for 20 minutes at room temperature. Transfection mixes were added to cells for 48 hours. Cells were then trypsinised, counted and transferred into phenol-free media containing CSS. Cells were seeded at a density of $2x10^4$ cells/well into poly-l-lysine coated white-bottomed 96-well plate. Following attachment for 5 hours, cells were treated with varying concentrations (10nM, 100nM, 1 μM) of Dex, (1nm or 10nM) β-oestradiol (GPER only) diluted in phenol-free CSS media, overnight for a minimum of 18 hours. Media was then aspirated and replaced by 50μl Bright-Glo luciferase assay system reagent (E2610, Promega) solution diluted x20 in sterile ddH_2O. Luminescence was then measured using Citation 5 plate reader (BioTek instruments) following 2-second wait and with

5-second read time. Data were normalised to the percentage surviving fraction as quantified by MTT assay (described below).

2.7.4 MTT Assay

Plates for MTT (3-(4,5-Dimethylthiazol-2-yl)-2,5-Diphenyltetrazolium Bromide) assay were seeded with HTLA cells transfected with TANGO-plasmids in parallel the white-96-well plates and treated as previously described. Following 18 hours incubation, a final concentration of 0.5mg/ml MTT reagent (cat. no. 6494, Thermo Fisher) was added to each well for 4 hours. After which the media was removed and the formazan solubilised with the addition of 100µl DMSO to each well. The optical density was measured at a wavelength of 540nm following 5 second shake time, using multiskan MCC 355 microplate reader (Thermo Fisher). The percentage surviving fraction was determined by subtracting the blank values and normalising to the optical density of untreated cells.

2.8 Western Blotting

2.8.1 Protein extraction

Adherent cultures were washed twice with PBS at 4°C, lysed with RIPA buffer (50nM Tris-HCl pH 7.4, 1% NP40 (lgepal), 0.25% Na-deoxycholate, 150 nM NaCl, 1mM EDTA) containing protease inhibitor cocktail set III (Merk) and phosphatase inhibitor cocktail 2&3 (Sigma) and collected by scraping. Treated cell suspensions were collected and centrifuged at 300g for 5 min at 4°C, washed with PBS at 4°C and lysed in RIPA buffer. Whole-cell lysates were cleared by centrifugation at 12,000 x g at 4°C for 20 minutes and the supernatants were retained for protein quantification by bicinochoninic acid (BCA) assay (23227, ThermoFisher Scientific) according to the manufacturer's instructions. Briefly 10µl of each sample were added in triplicate to a 96-well plate, alongside known bovine serum albumin (BSA) standards diluted in RIPA buffer. 200µl prepared working reagent was added to each well and incubated for 30 minutes at 37°C. The colorimetric change was measured by absorbance read at wavelength of 540nM using a multiskan MCC 355 microplate reader. The concentration of protein samples was determined from the standard curve generated from known BSA standards. Proteins lysates were made up to a standard final concentration (0.5-1 µg/ml) in PBS and SDS loading dye (250nM TrisHCl, 10% SDS, 30% glycerol, 5% β-mecaptoethanol. 0.02% bromophenol blue) and were then boiled at 95°C for 5 minutes. Samples were stored at -20°C until required.

2.8.2 Gel electrophoresis

5µg-15µg of protein were subject to electrophoresis on (4-15%) pre-cast Mini-PROTEAN TGX polyacrylamide gels (Bio-rad Laboratories) at 30V followed by wet transfer to 0.45 µm nitrocellulose membrane (GE Healthcare) overnight at 4°C. Membranes were then blocked for 6 hours at room temperature in block buffer (0.15M NaCl, 1% skimmed milk powder, 0.1% Tween-20) and incubated with primary antibodies (diluted in block buffer) overnight at 4°C with agitation. Membranes were then washed (3x10 minutes) in wash buffer (88mM Tris pH7.8, 0.25% skimmed milk powder, 0.1% Tween-20) and incubated with species-specific horseradish peroxidase-conjugated secondary antibodies - diluted in wash buffer, for one hour at room temperature. Following three further washes the enhanced chemiluminescence Super Signal Kit (ThermoFisher Scientific) was used to visualise immunoreactive proteins and developed at various exposure times using X-ray film.

2.8.3 Densitometry analysis

Image J software was used for densitometry quantification. Images were inverted and the background subtracted with a rolling ball radius of 50 pixels. Each lane of the blot was marked using the Gels tool while the 'wand tool' was used to determine the area under the curve for each band as a numerical value of band intensity. The intensity value for each target antibody was divided for the β-actin value obtained for that lane to normalise for differences in gel loading. Phosphorylated protein values were also normalised to the total protein value.

2.9 Real-time Quantitative Reverse-transcriptase Polymerase Chain Reaction (RT-qPCR)

2.9.1 RNA extraction

Cells were cultured as required in CSS and treated before lysis with Buffer RLT containing β-mecaptoethanol, lysates were then homogenised using Qiashredders (79654, Qiagen). Total RNA was extracted using the RNeasy extraction kit (74104, Qiagen) according to the manufacturer's instructions with the inclusion of an on-column DNase treatment (79254, Qiagen) step to remove traces of genomic DNA. RNA concentration and purity were determined using nanodrop spectrophotometer (ThermoFisher).

2.9.2 cDNA synthesis

Complementary DNA (cDNA) was prepared by reverse transcription using high capacity RNA-to-cDNA kit (4387406, Applied Biosystems) following the manufacturer's instructions using the T100^{TM}, Bio-rad Thermocycler. Samples were incubated for 60 minutes at 37°C then heated to

95°C for 5 minutes to stop the reaction, samples were then held at 4°C until required or stored at -20°C.

2.9.3 Taqman qPCR

TaqMan qPCR assays were performed in a MicroAmp^{TM} Optical 96 well plate (Applied Biosystems). cDNA was diluted to 25 ng/µl in RNase free water and 2µl added to each well containing: 1µl TaqMan primer-probe mix (listed **Table 2.6**), 10µl Taqman fast advanced master mix (Applied Biosystems) and 7µl RNase free water. Reactions were carried out in triplicate. Sealed plates were run on QuantStudio 5 Real-Time qPCR System (ThermoFisher Scientific) the programme involved an initial cycle for 50°C 2 minutes, 95°C 10 minutes, followed by 40 cycles of 95°C for 15 seconds then 60°C for 60 seconds. Relative gene expression changes values were calculated using the $2^{-\Delta\Delta Ct}$ method by normalising the CT values of each target gene to the housekeeping gene GAPDH and relative to the untreated control.

Table 2.6 TaqMan primer probes used for qPCR throughout study.

Purchased from Applied Biosystems^{TM} ,ThermoFisher.

Gene	Assay ID	Dye	Amplicon length (bp)	Binding location
GAPDH	Hs02786624_g1	FAM/MGB	157	Probe/primer within exon Within coding region 6/ exon 8 towards 5' end.
ACTB	Hs01060665_g1	FAM/MGB	63	Probe spans exons
FKBP5	Hs01561006_m1	FAM/MGB	75	Probe spans exons
TSC22D2	Hs00608272_m1	FAM/MGB	77	Probe spans exons
PER1	Hs00242988_m1	FAM/MGB	66	Probe spans exons
DUSP1	Hs00610256_g1	FAM/MGB	63	Probe spans exons
NFKBIA	Hs00355671_g1	FAM/MGB	54	Probe spans exons
IL6	Hs00174131_m1	FAM/MGB	95	Probe spans exons
CXCL8	Hs00174103_m1	FAM/MGB	101	Probe spans exons
ADGRA1	Hs00603154_m1	FAM/MGB	69	Probe spans exons
ADGRG6	Hs01089210_m1	FAM/MGB	80	Probe spans exons
ADGRE5	Hs00173542_m1	FAM/MGB	72	Probe spans exons

2.10 Brightfield Microscopy

Brightfield images were captured using EVOS inverted microscope (Invitrogen™) using x4, x10 and x20 objectives.

2.10.1.1 Confluency Analysis

Brightfield images of cultured cells were assessed for confluency. This was performed by capturing minimum of two images per well (three wells per condition). Captured images were then analysed by ImageJ software using the PHANTAST Fiji plugin with the default settings.

2.11 Immunofluorescence Microscopy

Cells were plated in 12 well plates containing 13mm glass coverslips. For suspension cells coverslips were pre-coated for 2 hours with 0.01% solution of poly-L-lysine (P4832, Sigma) then washed with PBS prior to cell seeding. Cells were treated as stated and following three washes with PBS cells were fixed with 4% Paraformaldehyde (PFA) for 1 hour at room temperature (RT). Cells were washed three times and blocked and permeabilised with blocking buffer (1% FBS, 0.1% Triton-X in PBS) for 4 hours, at RT on a rocker. Primary antibodies (as listed in **Table 2.1**) were diluted in block buffer and incubated with cells overnight with gentle rocking, at RT. Cells were washed (3x 10 minutes) then incubated with secondary antibodies (**Table 2.2**)(diluted in block buffer) for 2 hours with rocking at RT and out of direct light. Three further washes (as previous) were followed by Hoechst 33342 staining (1:10,000 in PBS) for 5 minutes. Coverslips were again washed and mounted onto glass slides using Vectashield hard-set mountant (Vectorlabs).

2.11.1 Image acquisition

Fluorescent images were visualised and captured on a Ti Eclipse inverted microscope with Nikon DS-QiMc camera using the x60 oil and x100 oil objectives. Z-stacks were taken with a step size of 0.2μm and by defining the top and bottom stacks of the image.

2.11.2 Image analysis

The publicly available image software Fiji ImageJ and CellProfiler were used to process images and perform image analysis. All images were pre-processed using Fiji Image J and split in individual channels. Cell feature measurements and nuclear:cytoplasmic (N:C) ratios of GR and p65 were then performed using CellProfiler Software (164).

2.11.2.1 Transfection efficiency

Fluorescent images of transfected cells were processed using an image J macro to detect the number of positively transfected cells based on staining in the FITC channel. The transfection efficiency was calculated based on the proportion of transfected cells based on the total number of cells per field of view- determined by staining in the DAPI channel.

2.11.2.2 Transcription factor localisation

Primary objects were defined by nuclear staining and secondary objects associated with each primary object identified using either F-actin or p65 staining (FITC channel). The tertiary objects were then defined by the subtraction of primary object from secondary objects. The mean pixel intensity of the defined object regions for each channel (nucleus and cytoplasm) were then used to obtain a ratio of transcription factor compartmentalisation nuclear: cytoplasmic ratio (N:C) (**Figure 2.1**). Cell and nuclear area measurements were obtained based on the pixel areas covered by the identified objects for the whole cell and nucleus respectively.

2.11.2.3 N:C ratio optimisation

Fiji ImageJ was used to pre-process all images and a macro was developed to aid batch processing. Briefly, the maximum-intensity projections of Z-stacked images were subject to the subtraction of background noise by sliding paraboloid filter with rolling ball radius of 500 pixels for each channel. Greyscale images of each channel were then inputted into CellProfiler (164) for quantitative analysis.

Two different methods of defining secondary objects were used for cells on micropatterns; whole cell and perinuclear region. The comparison is outlined in **Figure 2.2**, which shows a greater level of variability and large calculated ratios for secondary objects defining the whole cell. The FITC channel image (stained for p65) was used to locate the cell boundary (whole cell) or a region expanded a distance of 50 pixels away from the boundary of the nuclear object. The tertiary object is the result of subtracting the primary object from the secondary object (cytoplasm or peri-nuclear cytoplasmic region). The staining pixel intensity for each channel was measured within the region of interest.
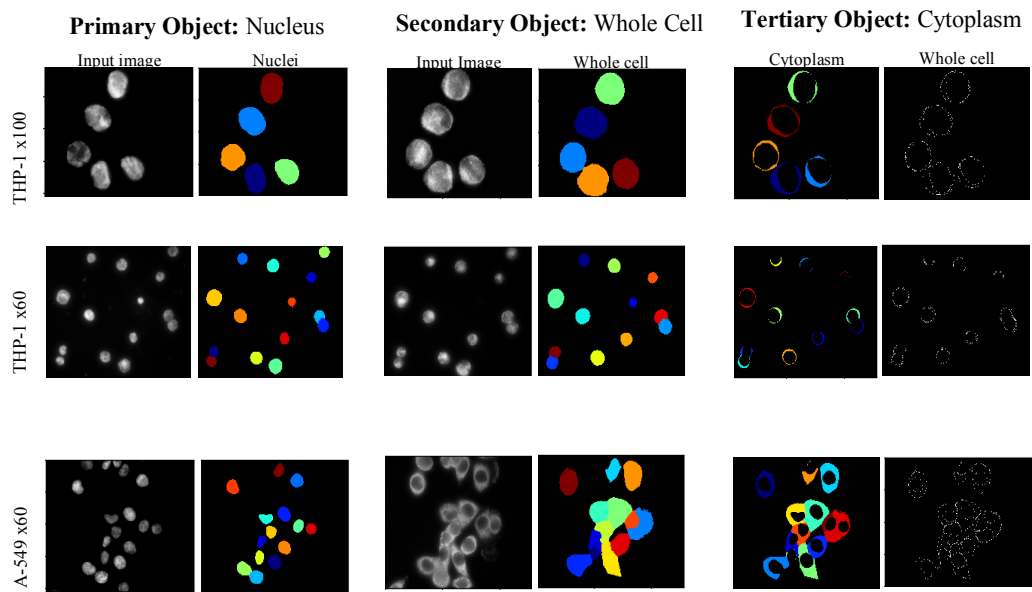
Figure 2.1. CellProfiler pipeline to define cellular regions of interest.

Presented examples of segmentation of cellular regions for THP-1 (images taken at x60 and x100 magnification for comparison) and A549 cells. Grey scale images were pre-processed in Fiji ImageJ to generate maximum-intensity projection and subtract background noise. CellProfiler uses the DAPI channel to identify the nucleus which is taken as the primary object. For each primary object, the FITC channel image (stained for p65) is used to locate the cell boundary (whole cell). This region is taken to define the secondary object. The tertiary object is the result of subtracting the primary object region away from the secondary object.
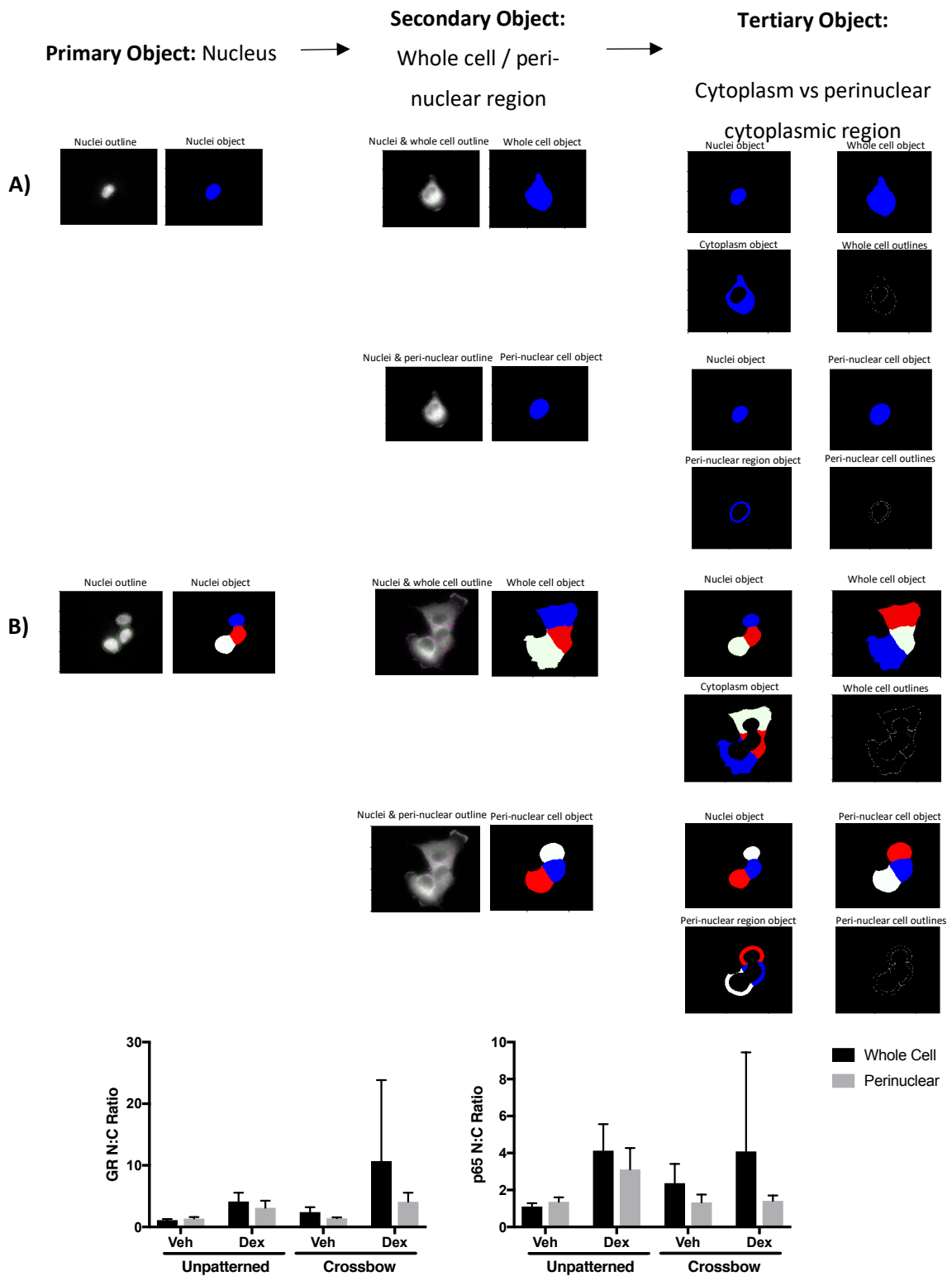
Figure 2.2. Overview of CellProfiler identification of cellular regions.

*A549 cells plated on crossbow micropattern **(A)** and un-patterned substrate **(B)**. CellProfiler takes the DAPI channel to identify the nucleus which is taken as the primary object. For each primary object, the image from the FITC channel (stained for p65) is used to locate the cell boundary (whole cell) or a region expanded a distance of 50 pixels away from the boundary of the nuclear object. These regions are taken to define the secondary object. The tertiary object is the result of subtracting the primary object from the secondary object. The staining intensity of for each channel is measured within the region of interest of the nuclei object and cytoplasmic/ peri-nuclear region objects and then divided to obtain a value for the nuclear: cytoplasmic ratio. Measurements comparing measurements obtained for the whole cell vs peri-nuclear region.*

2.12 ELISA

Quantification of cytokine concentrations was performed using: Human IL-10 Duoset ELISA kit (Dy217B-05, R&D systems) and human TNF-α Duoset (DY210-05, R&D systems) according to the manufacturer's protocol. Samples were assayed neat and plated in triplicate. The optical density was measured at 450nm (with readings measured at 540nm subtracted for correction) using a microplate reader. Cytokine concentrations were determined by reference to the generated standard curve.

2.13 Phosphoproteomics

Identification of phosphoproteins following GR ligand treatment was performed by Dr Stephen Kershaw (University of Manchester School of Medical Sciences) using stable isotope labelling of amino acids in culture (SILAC), followed by liquid chromatography and tandem mass spectrometry (LC-MS/MS), as described (Kershaw, 2018) (165). Triple-SILAC was employed in which three different isotopically labelled forms of arginine and lysine were used, allowing three different treatment conditions to be analysed in a single experiment (166). Briefly, A549 cells were cultured in medium containing naturally occurring L-arginine and L-lysine (containing ^{12}C and ^{14}N- termed light Arg/Lys), or in media containing arginine and lysine substituted with differing amounts of ^{13}C and ^{15}N (termed medium and heavy Arg/Lys). Cells were grown for 10 generations in these media (to allow complete incorporation of these amino acids into protein) and then treated with the GR ligands; Light Arg/Lys cells were treated with vehicle only (DMSO), medium Arg/Lys cells were treated with 100nM Dex (in DMSO) and heavy Arg/Lys cells were treated with either GRT7 (3nM) or (in a separate experiment), 086X (100nM). After ten minutes of ligand treatment, cells were pelleted and proteins extracted. Phosphoproteins were enriched using selection with titanium dioxide (TiO$_2$)-coupled magnetic beads (which bind to phosphopeptides) and digested with trypsin. Samples from the different ligand treatments were pooled and analysed using LC-MS/MS. The LC-MS/MS procedure is quantitative and can resolve the difference in mass between peptides containing light, medium or heavy-labelled Arg/Lys. This allows the side-by-side comparison of the abundance of phosphopeptide species in the different treated samples. The relative quantification of identified phosphopeptides in the different samples was kindly provided by Dr Kershaw.

2.13.1 Data analysis

2.13.1.1 Network Analysis

To perform network analysis, differentially regulated proteins were inputted as a list into Cytoscape (167), to generate protein-protein interaction networks using the StringApp (168). The confidence score of protein-protein interaction either medium (0.4) or high (0.7) is stated in the legend. Line thickness indicate the strength of data support. Network clustering of nodes based on their interactions was performed using Markov clustering (MCL) in the clusterMaker2 Cytoscape app- clusters then used to colour nodes.

2.13.1.2 Enrichment Analysis

Functional enrichment analysis of proteins in the network was performed using StringApp in Cytoscape (167, 168). Using false discovery rate (FDR) to determine significance.

Gene set enrichment analysis was performed using publicly available Enrichr, accessed online: http://amp.pharm.mssm.edu/Enrichr (169). The gene IDs of differentially regulated proteins were imputed as grouped lists. The gene ontology libraries for biological process and molecular function were used, adj-pvalues were used to determine significance.

Kinase enrichment analysis using KEA2: Kinase enrichment analysis 2 website, https://www.maayanlab.net/KEA2/index.html# . Phosphorylated proteins and the modified residue were submitted and enrichment was performed based on literature-based kinase-substrate library with phosphosites.

2.13.2 Kinase Prediction

Prediction of regulatory kinases was performed using the Networkin site accessed at www.networkin.info (170). Protein names were inputted and the modified residues selected to give a predictive output score of the potential phosphorylating kinase.

2.14 Bulk mRNA-sequencing

2.14.1 Sample preparation

A549 cells were cultured for 24 hours in steroid depleted media (CSS) experiment performed with 6 replicates per condition. Cells were pre-treated with 500nM THZ531 for 30 minutes followed by 100nM Dexamethasone for 4 hours. Cells were lysed using RLT lysis buffer with added (B-mercaptoethanol) and total RNA extracted using Qiagen RNeasy kit including sample lysate homgenisation step using Qiashredder columns and on column digestion with DNAase to remove genomic DNA. RNA samples were preliminarily assessed by Nanodrop. For quality control, samples were processed by the Leeds next generation sequencing (NGS) facility, performed using Agilent Bioanalyser (RNA integrity number >9.8) and the RNA concentration determined by Qubit. The best 12 samples for RNA integrity and concertation were chosen and sent for sequencing. The 12 remaining samples were converted to cDNA and the expression of *GAPDH*, *PER1*, *GILZ*, and *BRCA1* was determined by PCR to ensure the inhibitor was working correctly.

2.14.2 Library preparation & Sequencing

Library preparation, sequencing and initial bioinformatic analysis was performed by Novogene. Subsequent methods outlined as stated by Novogene.

Breifly, mRNA was purified form total RNA using poly-T-oligo-attached magnetic beads. After fragmentation, the first strand cDNA was synthesised using random hexamer primers, followed by second strand cDNA synthesis using dUTP. The cDNA was then subject to end repair, A-tailing, adapter ligation, size selection, amplification and purification. The library quality was checked with Qubit and RT-PCR. The library preparations were sequenced on Illumina platform and paired-end reads of 150bp were generated.

2.14.3 Data Analysis

Raw reads of fastq format were firstly processed through in-house perl scripts. All the downstream analysis were based on the clean data with high quality. A List of software used is presented in **Table 2.7**. The sequencing read-mapping showing the distribution of reads mapping to chromosomes shown in **Figure 2.3.** Quantification of transcript abundance is shown in **Figure 2.4.** The read numbers mapped to each gene were counted and then FPKM of each gene was calculated based on the length of the gene and reads count mapped to this gene. FPKM, Reads Per Kilobase of exon model per Million mapped reads, considers the effect of sequencing depth and gene length for the reads count at the same time, and is currently the most commonly used method for estimating gene expression levels (171).

2.14.3.1 Differential expression analysis

Differential expression analysis between biological replicates per condition was performed. Genes with an adjusted P-value <0.05 found by DESeq2 were assigned as differentially expressed.

Table 2.7. RNA-Seq Software list as provided by Novogene

Analysis	Software	Version	Parameter	Remarks	Ref
Mapping	STAR	v2.5	Mismatch =2	Mapping to reference genome GRCh38	(172)
Quantification	HTSeq	V0.6.1	-m union	-	
Differential expression analysis (DEG)	DESeq2	V2_1.6.3	Padj<0.05	For sample with biological replicate	(173)
Enrichment Analysis	Cluster profiler	V2.4.3	Padj<0.05	For GO, DO, KEGG, Reactome enrichment analysis	(174)
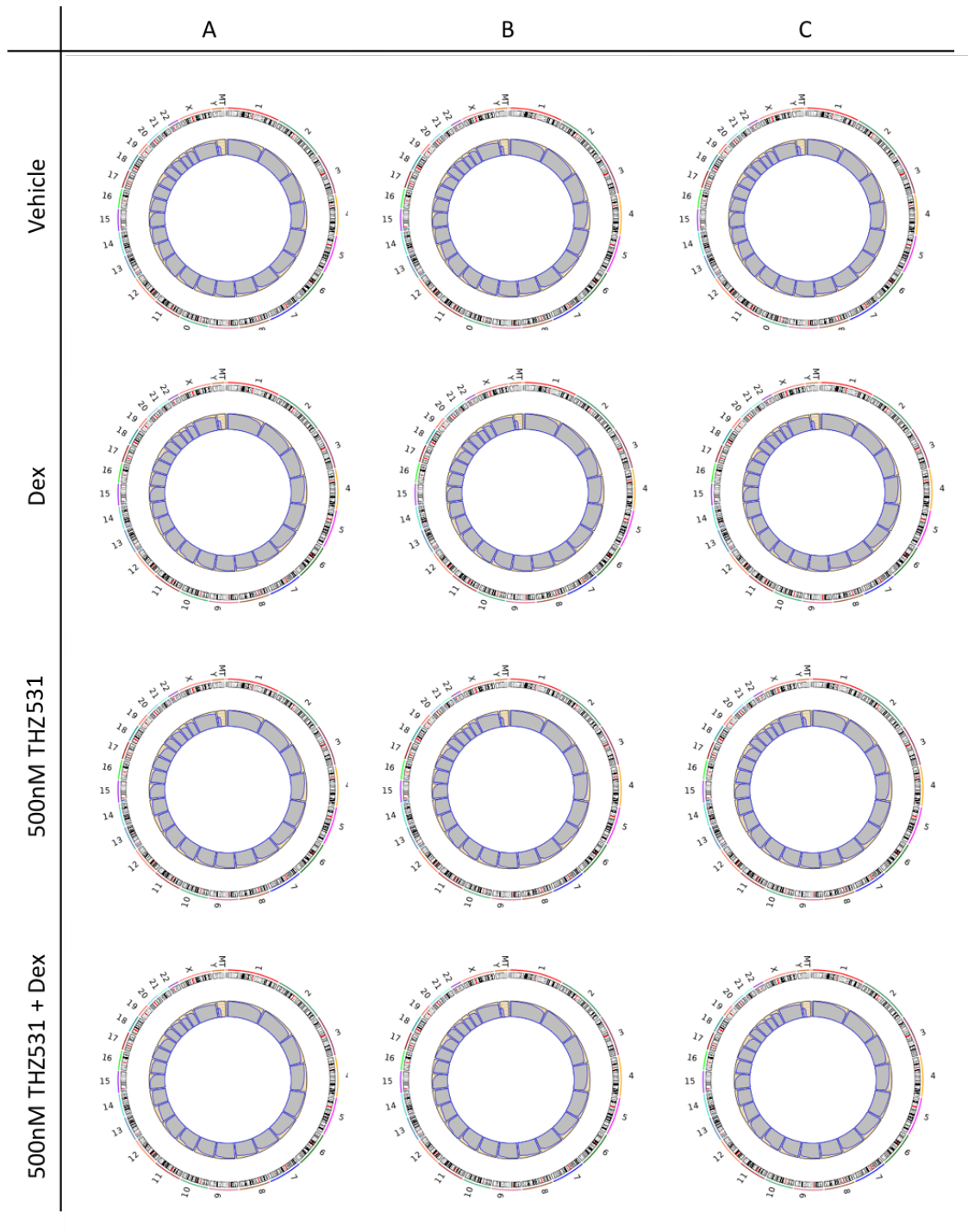
Figure 2.3 Chromosome alignment distribution for each sample

The distribution of mRNA reads mapped to the genome. The outer ring corresponds to the chromosome number, the middle ring is chromosome band type and the inner ring shows the distribution of the reads mapping to each region using 1M base as the sliding window. Each circle represents a sample treated as indicated (down left side). Produced by Novogene.
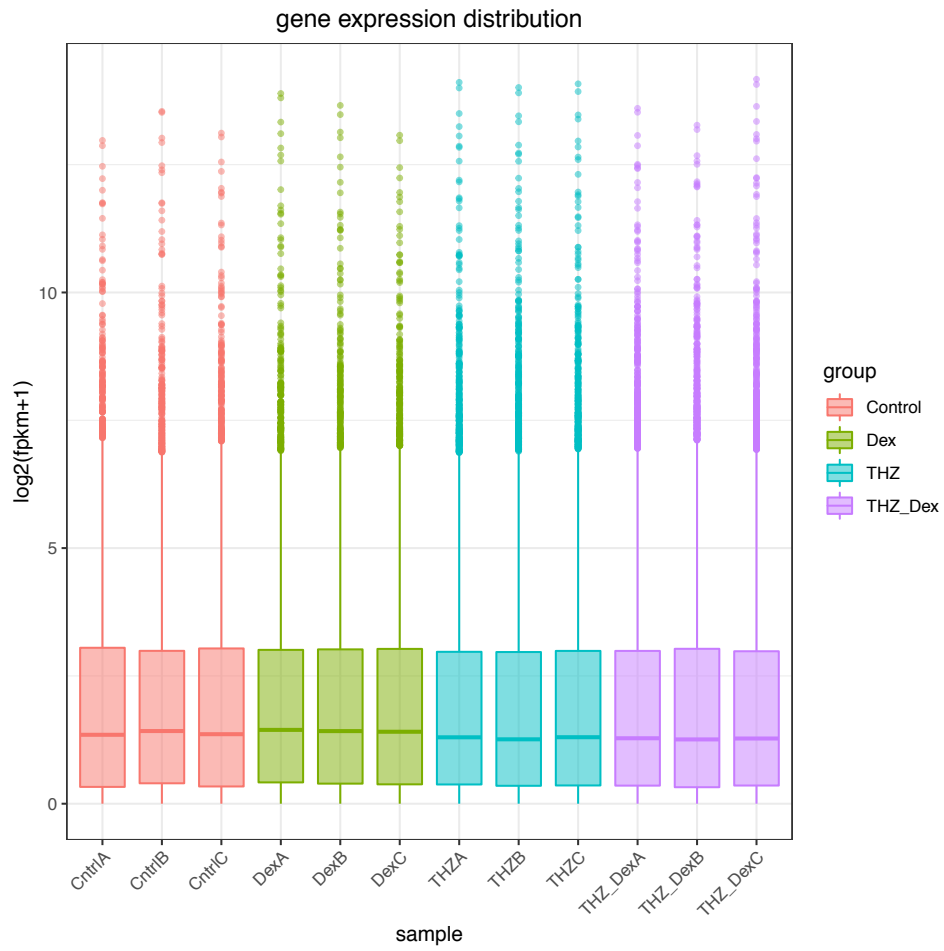
Figure 2.4 Gene density distribution

Comparison of the distribution of the gene expression levels for the different treatment conditions and FPKM for each of the samples. X axis: sample name. Y axis: log2FPKM+1. THZ: 500nM THZ531. THZ + Dex: 500nM THZ531 + 100nM Dexamethasone.

2.14.3.2 GO and KEGG enrichment analysis of differentially expressed genes

Gene Ontology (GO) enrichment analysis of differentially expressed genes was implemented by the clusterProfiler R package. GO terms with corrected Pvalue less than 0.05 were considered significantly enriched by differential expressed genes.

KEGG is a database resource for understanding high-level functions and utilities of the biological system, such as the cell, the organism and the ecosystem, from molecular level information, especially large-scale molecular datasets generated by genome sequencing and other high-through put experimental technologies (http://www.genome.jp/kegg/). The clusterProfiler R package was used to test the statistical enrichment of differential expression genes in KEGG pathways.

2.14.4 Network analysis

To perform network analysis, differentially regulated gene lists were inputted into Cytoscape (167). The StringApp (168) was used to generate a protein-protein interaction network with a medium (0.4) confidence score of protein-protein interaction. Nodes were coloured based on the log2 fold change in expression for treatment groups in comparison to the vehicle. The Reactome functional interactome network, was generated from whole group of Dex-regulated genes affected by THZ531 using the Recatome FI plugin (175).

2.14.5 Motif analysis

2.14.5.1 Analysis of motif enrichment (AME)

The gene promoter region sequences were downloaded from the eukaryotic promoter database (EPD) in FASTA format (176). Lists of ensemble gene IDs for co-regulated genes were submitted with the selection for 'only the most representative promoter for a gene'. Sequences were obtained for the regions of +100kb of the TSS with varying distances: -1kb,2kb, 5kb, 10kb or 20kb downstream. The sequences were then submitted into analysis of motif enrichment (AME) tool using shuffled input sequences mainlining 2-mers, as control sequences (177). Motifs were identified from the vertebrates (*in vivo* and *in silico*) database which searches within the JASPAR CORE vertebrates NON-REDUNDANT (*in vivo* and *in silico*), UniProbe Mouse (protein-binding microarray: PBM) and Jolma2013 Human and Mouse (HT-SELEX) databases. The average odds score was used to score the matches of a single sequence to single motif and the enrichment significance was tested using Fisher's exact test. E-value score (expected number of motifs: adjusted p-value multiplied by number of motifs).

2.14.5.2 I-regulon

Lists of genes were stratified based on the differential expression induced by Dex and/or THZ531 treatment and were inputted into Cytoscape (167). Transcriptional regulators for the gene sets were predicted using the i-Regulon plugin (178).

2.14.5.3 Epigenetic Landscape *In-Silico* deletion Analysis (LISA)

Stratified gene lists (as above) were submitted to LISA.cistrome.org. (179). Gene sets were inputted as to compare genes up-regulated versus down-regulated by Dex. Result files were imported into R for further analysis and visualisation.

2.15 Statistical Analysis

Statistical analysis was conducted using Graph Pad Prism (version 9.10). For the comparison between two variables a Mann-Whitney test was the statistical method used. One-way analysis of variance (ANOVA) was performed to assess group differences (the relevant post-hoc test used stated in results), while two-way ANOVA was used in cases with more than one independent variable. Error bars illustrate ± standard error of the mean (SEM) unless stated otherwise, and number of experiments specified in each figure legend. P values denoted by asterisks, results with a value of $p < 0.05$ were deemed statistically significant.

2.16 Schematic figures

Schematic figures created with BioRender.com.

Chapter 3: Rapid targets of GR activation

3.1 Introduction

Phosphorylation is a reversible post-translational modification added on to proteins to modulate their activity. The chemical addition of a phosphoryl group (PO_3-) by kinases (and the reverse reaction mediated by phosphatases) is important for regulating cellular processes and relaying information through signalling cascades.

Immediate, non-genomic effects of Gc are thought to be exerted by interactions with kinases however, the spectrum of rapid signalling events induced following Gc exposure is yet to be fully determined. Building a clearer understanding of such events may have implications for management of inflammation such as asthma where rapid resolution is required (88, 180). This chapter, explores the non-genomic activity of GR using the unbiased approach of global phosphoproteomics to define the Gc-regulated phosphoproteome.

Three synthetic GR-ligands were evaluated, each with distinct properties. Dexamethasone (Dex) is a highly potent steroid and the 'classic' activating ligand used routinely in GR research and clinical applications (28, 44, 70, 72, 76, 79, 102, 181, 182). 086X, a selective steroid which has the same activation kinetics and potency of Dex but was designed to modulate GR in favour of the trans-repression of genes (183, 184). GRT7, which is a non-steroidal ligand - meaning the compound does not share the core cyclohexane and cyclopentane steroidal structure. This ligand occupies the novel 'meta channel', an extended region within the GR LBD created by the binding of non-steroidal ligands (185). The binding conformation induced by GRT7 results in GR having a greater potency for transcription but displays slower activation kinetics, whereby GR translocation into the nucleus is delayed (165, 186).

GR-ligands were chosen to evaluate the hypothesis that each would generate an individual profile of phosphorylated proteins. Such would reflect their unique transcriptional outputs and be indicative of a distinct set of regulated cellular processes. Therefore, the profile of proteins phosphorylated prior to transcription may be partly responsible for the differences. As ligand binding induces a conformational change in GR protein, the resultant orientation could potentially enable unique protein interactions and association with downstream pathways affecting the subsequent genomic activity (187). If this were the case, new understanding could provide a novel level of modulating the outcome of GR activation.

3.2 Results

Stable isotype labelling by amino acids in cell culture (SILAC) phosphoproteomics was used as a non-biased approach to identify differentially regulated phosphoproteins *in vitro*. Sample preparation and phosphoproteomics was performed by Dr Stephen Kershaw at the University of Manchester proteomics facility. A549 cells, a Gc-responsive lung carcinoma epithelial cell line, were chosen for the phosphoproteomic analysis. These cells are routinely used as a model to study GR biology (181, 188-191). The expression and functionality of the GR protein has been extensively validated in this cell type. Furthermore, the availability of published datasets evaluating Gc activity in these cells can be used for reference (57, 76, 78). Other advantages include their abundance and proliferative capacity allowing for the necessary population doublings within the labelled media (10 generations). As lung-derived cells they are a physiologically relevant model; GR function in the lung is critical during development and represents an important immunological interface.

Briefly, A549 cells, were cultured in medium containing either heavy (Arg10/Lys8), medium (Arg6/Lys4) or light (Arg0/Lys0) stable-isotype-labelled amino acids. This incorporates a known mass difference between the same peptides in the different cultures (157, 192). The metabolically labelled cultures were treated for 10 minutes with three potency-matched, distinct GR ligands. Medium-labelled cells were treated with 100nM Dex and light-labelled cells were treated with DMSO vehicle control. Heavy-labelled cells were treated with either: 100nM 086X or 3nM GRT7. The structures of Dex, 086X and GRT7 are shown in **Figure 3.1A**. These ligands were chosen to compare the acute effects of steroidal vs non-steroidal ligands and ligands with different genomic outputs, at a timepoint when GR is predominantly located within the cytoplasm.

3.2.1 SILAC Phosphoproteomics identifies a common, rapid signature of GR activation

Overall, 388 phosphopeptides were identified as being modified following treatment with GR ligands (**Figure 3.1B**). This corresponds to a total of 155 proteins which were differentially phosphorylated in comparison to the DMSO vehicle control. Despite the different modes of action of the 3 ligands, **Figure 3.1C** highlights that 109 of these protein targets were shared between the three ligands, 24 proteins were shared between Dex and the non-steroidal ligand GRT7 and 16 where shared between Dex and 086X. Yet only two proteins were commonly identified between GRT7 and 086X and not modified by Dex. The signature of modified peptides and specific phosphosites shows a high degree of overlap, indicating that these GR modulators rapidly induce a common phosphorylation signature following GR activation.
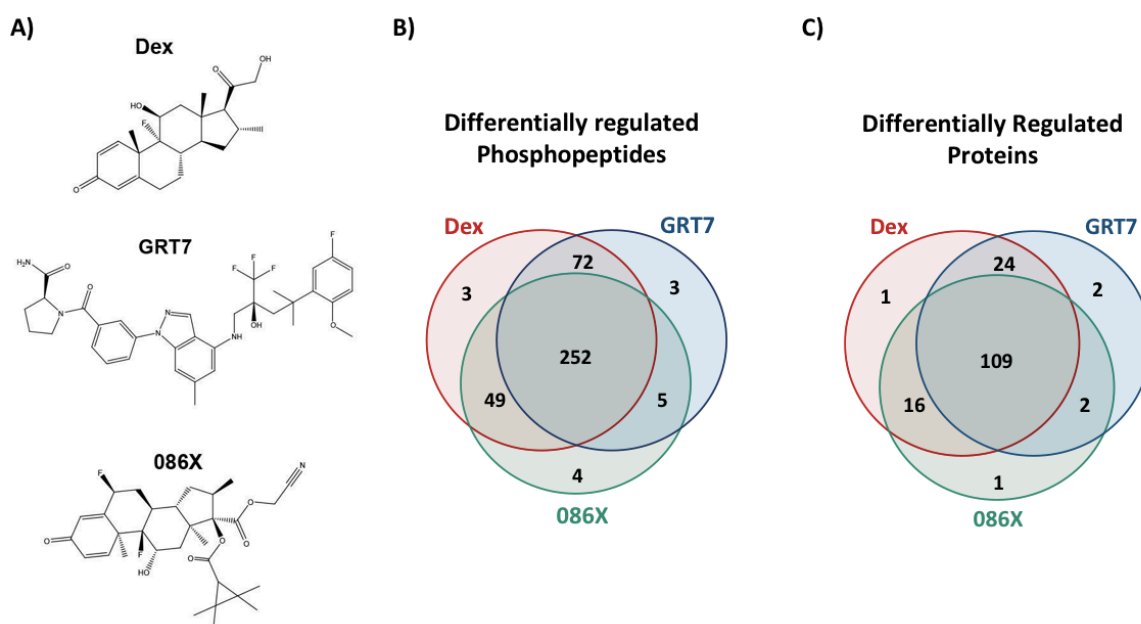
Figure 3.1 Defining the rapid Gc-regulated phosphoproteome

A) Structures of compounds: Dexamethasone, GRT7 and 086X were used define the rapid phosphoproteome. A549 cells in SILAC labelled cultures were stimulated for 10 minutes with one of the GR ligands, lysed and differentially phosphorylated residues were analysed using SILAC phosphoproteomics. B) Venn diagram showing the total number of Gc regulated phosphoresidues. Defined as each of the phosphorylation sites which are differentially modified following 10 minutes ligand treatment - in comparison to the vehicle (DMSO) treated control. C) Venn diagram showing the total number of Gc regulated phosphoproteins. Defined as the proteins which contain the differentially phosphorylated residues following 10 minutes ligand treatment - in comparison to vehicle (DMSO) treated control.

The majority of modified substrates were serine residues (87.01%); threonine represented 13% of residues and only 0.3% of the total phosphopeptides modified by all ligands were tyrosine residues **(Figure 3.2A)**. This corresponds to only one modified tyrosine residue, Tyr15 derived from CDK1, CDK2 or CDK3 (which cannot be distinguished due to sequence similarity in this region). The proportions reflect the enrichment methodology using titanium dioxide, to select for phosphorylated peptides prior to MS analysis, which preferentially selects for serine and threonine residues (192). These proportionalities were maintained for each individual ligand. Analysis of multiplicity indicates that almost half (49.16%) of the peptide fragments had two modifications (double phosphorylation), over a third (38.42%) has a single phosphorylation and 12.41% were triply modified **(Figure 3.2B)**.
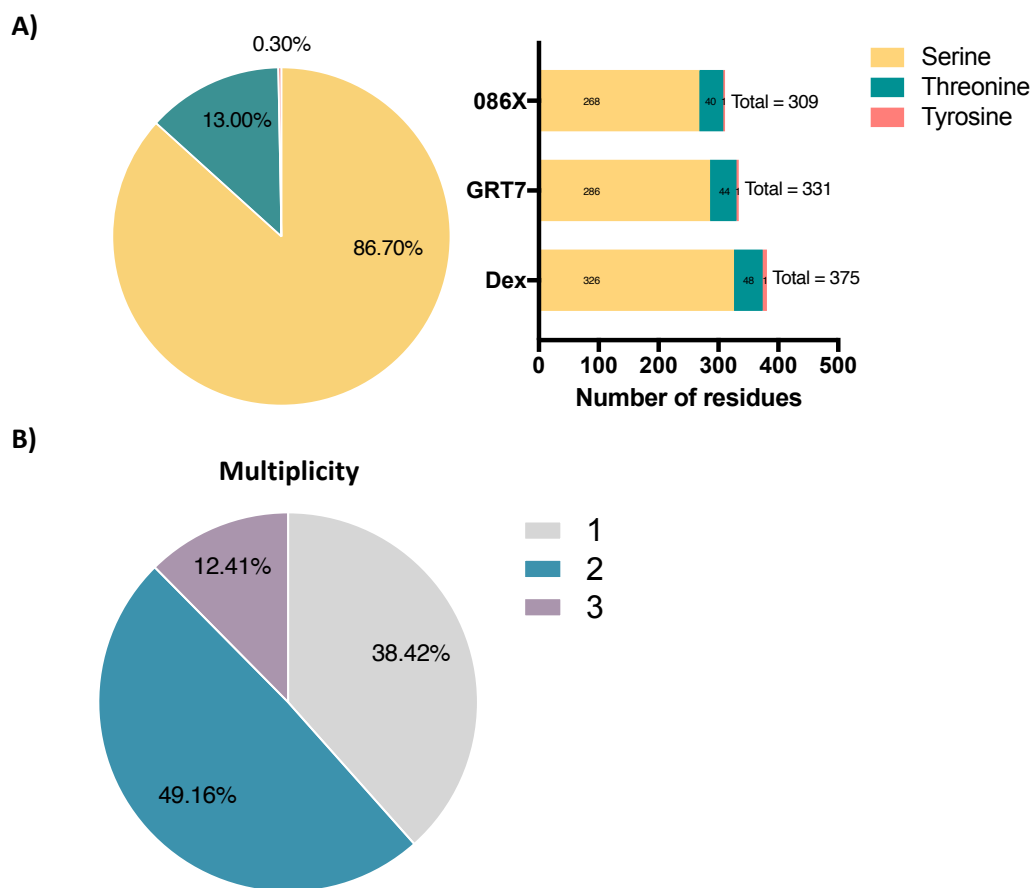
Figure 3.2 Modified amino acids and multiplicity of Gc-regulated phosphoproteome

A) Percentage of modified amino acid residues serine, threonine and tyrosine in pie chart and the accompanying bar chart showing the summarised percentage for the individual ligands. Bar graph outlining the total number of phosphorylated serine, threonine and tyrosine residues measured for each ligand. B) Multiplicity of the modifications at the identified phosphosites. The summarised percentage of multiplicity for all ligands. Indicating whether phosphorylated proteins were found to have single, double or triple phosphorylation marks at a particular site.

SILAC and mass spectrometry allows the quantification of targets before and after treatment and **Figure 3.3A** displays the median log2 fold change for each differentially phosphorylated residue. For each of the ligands there are more residues with a reduction of phosphorylation than addition. The range of the median log2 Fold change induced by Dex treatment is largely between -1 and 1 with only 4 residues surpassing a log2 fold change greater than 1. This is also reflected by GRT7, with a few residues (8 down and 3 up) regulated with a median Log2 fold change <-1 and >1. Overall, the extent of the fold change induced by 086X is greater, with a larger number of residues displaying a greater magnitude of decrease (34 down <-1 and 4 up >1). The directionality of fold change for each specific residue is not always shared between treatments. The heat map **(Figure 3.3B)** compares the median log fold change for each modified residue, and reveals clusters in which the directionality of change is the opposite between ligands. This result demonstrates that despite the shared spectrum of modified proteins, the magnitude of effect exerted by the ligands may differ in regard to cellular outcomes.
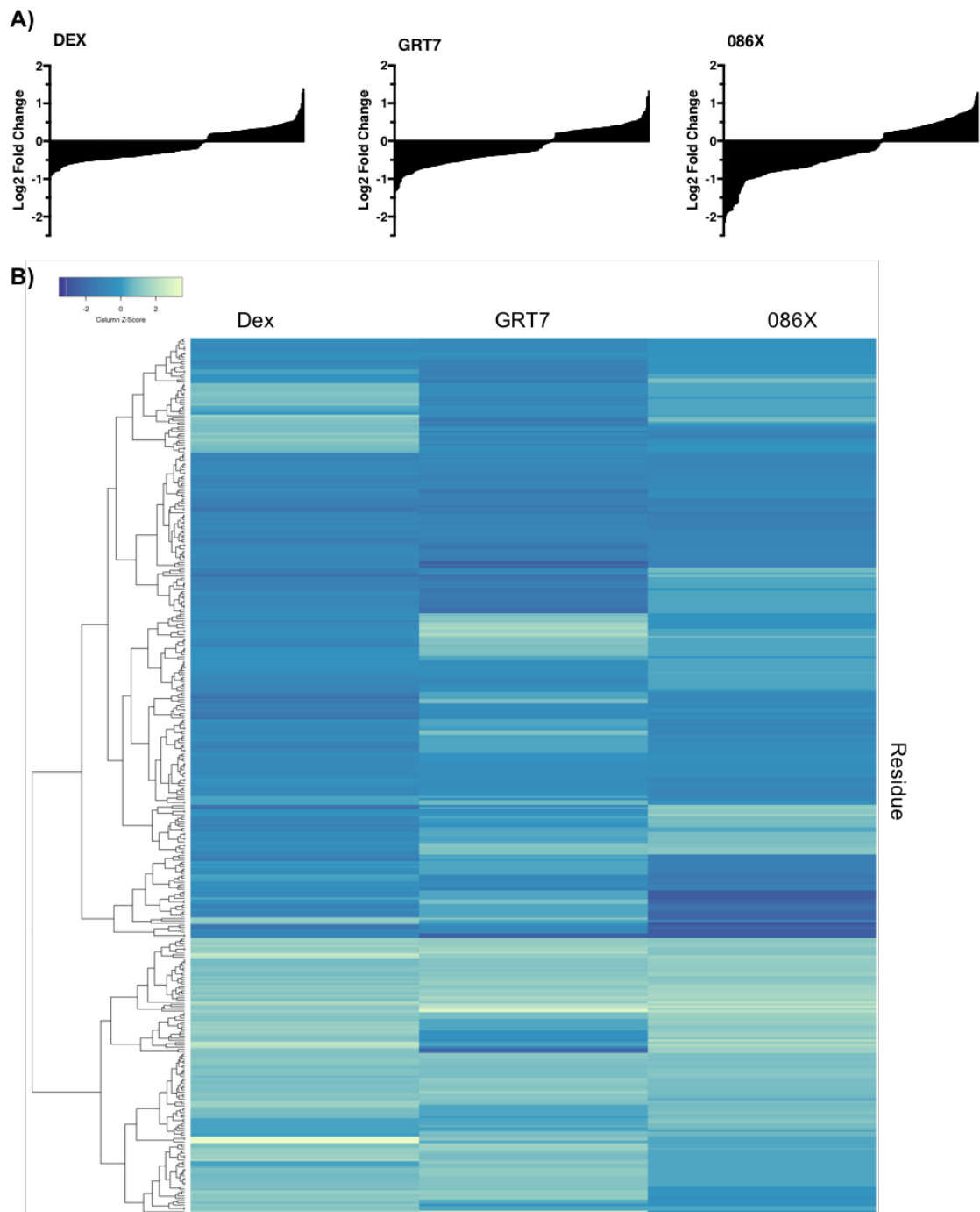
Figure 3.3. Differential regulation of target phosphopeptides induced by GR ligands.

A) *Bar plot showing the median log2 fold change for each of the identified differentially phosphorylated residues induced following 10 minute exposure for each ligand: Dexamethasone, GRT7, 086X.* *B)* *Heat map of the median log2 fold change in phosphorylation, each row represents a modified residue following treatment with each ligand. Made using heatmapper.ca. Cluster methods: complete linkage. Distance measurement methods: Manhattan. Blue corresponds to reduction, yellow corresponds to increase phosphorylation.*

The plots in **Figure A.1** display the identified top 20 up- and down-regulated residues for each ligand, based on the median log2 fold change from a minimum of 3 measurements. Residues from neighbouring sites on the same protein are shown to be regulated in the same direction and to the same extent, for example Dex-induced upregulation of phosphorylation of ADAM9 T761 and S758 (median log2FC 1.29) or ATF7 T51 and T53 (median log2FC -0.82). This likely represents residues which are dually regulated by the same kinase and/or phosphatase.

Figure 3.4 shows all 22 proteins with ≥4 phosphosites which were differentially modified by the Gc ligands. The scaffold protein neuroblast differentiation-associated protein (AHNAK) displays the greatest number of regulated residues for all conditions (Dex:26, GRT7:23, 086X:24) while CHAMP1 had the second greatest number for Dex and 086X (18 sites) yet this was not seen for GRT7 with only 8 sites. This again demonstrates in similarity of the response induced the three ligands.

Number Diff reg Phosphosites — Dex (blue), GRT7 (green), 086X (red)
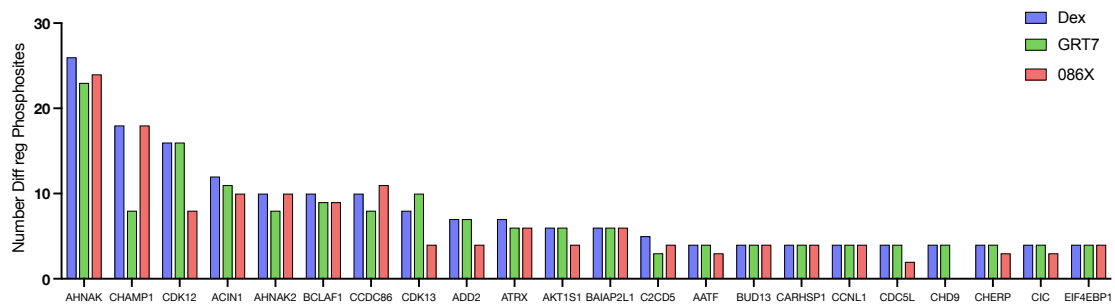
Gene name	Protein name	Protein type	Localisation	Function
AHNAK	Neuroblast differentiation-associated protein AHNAK	Structural scaffold protein	Nucleus/cytoplasm	Predicted role in cell structure and migration, cardiac calcium channel regulation, and tumor metastasis.
CHAMP1	Chromosome alignment-maintaining phosphoprotein 1	Zinc finger protein	Nucleus/cytoskeleton	Required for proper alignment of chromosomes at metaphase and their accurate segregation during mitosis.
CDK12	Cyclin-dependent kinase 12	Kinase	Nucleus	Phosphorylation of RNA POLII, detection of DNA Damage and pre-mRNA splicing
ACIN1	Apoptotic chromatin condensation inducer in the nucleus	Adapter protein	Membrane/nucleus/cytoplasm	Induces chromatin condensation during apoptosis. A component of splicing-dependent multiprotein exon junction complex (EJC).
AHNAK2	Protein AHNAK2	Structural scaffold protein	Membrane/cytoplasm/nucleus	Large nucleoprotein with a role in calcium signaling by associating with calcium channel proteins.
BCLAF1	Bcl-2-associated transcription factor 1	Transcriptional repressor	Nucleus	Death-promoting transcriptional repressor.
CCDC86	Coiled-coil domain-containing protein 86	RNA binding	Nucleus	Cytokine inducible.
CDK13	Cyclin-dependent kinase 13	Kinase	Nucleus	Phosphorylation of RNA POLII, detection of DNA Damage and pre-mRNA splicing.
ADD2	Beta-adducin	Cytoskeletal protein	Membrane/cytoskeleton/nucleus	Membrane-cytoskeleton-associated protein that promotes the assembly of the spectrin-actin network.
ATRX	Transcriptional regulator ATRX	Helicase, SWI/SNF family	Nucleus	Phosporylation controls nuclear matrix and chromatin associations. Involved in transcriptional regulation and chromatin remodeling.
AKT1S1	Proline-rich AKT1 substrate 1	TORC complex	Cytoplasm/nucleus	Subunit of mTORC1 complex and negatively regulates mTOR activity dependent on phosphorylation status.
BAIAP2L1	Brain-specific angiogenesis inhibitor 1-associated protein 2-like protein 1	Adapter protein	Membrane/cytoskeleton/nucleus	Plays a role in the reorganization of the actin cytoskeleton.
C2CD5	C2 domain-containing protein 5	Adaptor protein	Membrane/cytoskeleton	Required for insulin-stimulated glucose transport and glucose transporter translocation.
AATF	Protein AATF	Transcription factor	Nucleus	Antagonises apoptosis and interacts with SP1, RNA POLII. May function as a general inhibitor of the histone deacetylase HDAC1 leading to cell cycle progression.
BUD13	BUD13 homolog	Adapter protein	Nucleus/cytoplasm	Component of spliceosome involved in pre-mRNA splicing.
CARHSP1	Calcium-regulated heat stable protein 1	Adapter protein	Cytoplams	Calcium regulated. Binds mRNA and regulates the stability of target mRNA.
CCNL1	Cyclin-L1	Cyclin	Nucleus	Phosphorylation of RNA POLII, detection of DNA Damage and pre-mRNA splicing
CDC5L	Cell division cycle 5-like protein	DNA binding	Nucleus	Component of the non-snRNA splicosome. Controls G2/M transition. May act as a transcriptional activator.
CHD9	Chromodomain-helicase-DNA-binding protein 9	Helicase	Nucleus	Proposed to be a ATP-dependent chromatin remodeling protein. Has DNA-dependent ATPase activity and binds to A/T-rich DNA.
CHERP	Calcium homeostasis endoplasmic reticulum protein	Adapter	Nucleus/ER	Involved in calcium homeostasis, growth and proliferation. Implicated in mRNA splicing.
CIC	Protein capicua homolog	Transcriptional corepressor	Nucleus	Member of the high mobility group (HMG)-box superfamily of transcriptional repressors.
EIF4EBP1	Eukaryotic translation initiation factor 4E-binding protein 1	Translation repressor	Cytoplasm	Binds ELF-4E and inhibits translation.

Figure 3.4 Proteins with the largest number of differentially regulated phosphosites induced by GR ligands.

The proteins with ≥4 phosphosites regulated by Dex. Of these proteins the number of differentially regulated phosphosites are shown for each of the ligands. Y axis corresponds to the total number of sites detected as differentially phosphorylated for the protein in comparison to the DMSO-vehicle control. Induced by Dexamethasone (blue), GRT7 (green) and 086X (red). The table below details all proteins plotted and summarises the protein name, type, localisation and function.

3.2.1.1 Gc regulated phosphopeptides are located throughout the cell

GR primarily acts within the nucleus to regulate genomic responses, although prior to activation GR resides in the cytoplasm (31) and has been reported to localise to the cell membrane (193-195) and mitochondria (26). In order to gain further insight into the cellular regions subject to rapid-Gc signalling and the processes that the regulated proteins are involved, I investigated their cellular localisation. Information regarding the predicted sub-cellular compartment of the phospho-targets was retrieved from Uniprot and illustrates that rapid Gc-signalling extends throughout the whole cell **(Figure 3.5A)**. The greatest proportion of regulated proteins are located in the nucleus followed by the cytoplasm and the membrane. In addition, proteins associated with the cytoskeleton, mitochondria, Golgi and Endoplasmic Reticulum were identified. A number of the modified proteins are depicted in **Figure 3.5B,** which visually highlights the range of identified targets and their diverse subcellular locations. This shows that ten minutes after ligand addition, a time point when GR is predominantly located in the cytoplasm, GR initiates signals which are broad ranging and reach various cellular compartments.
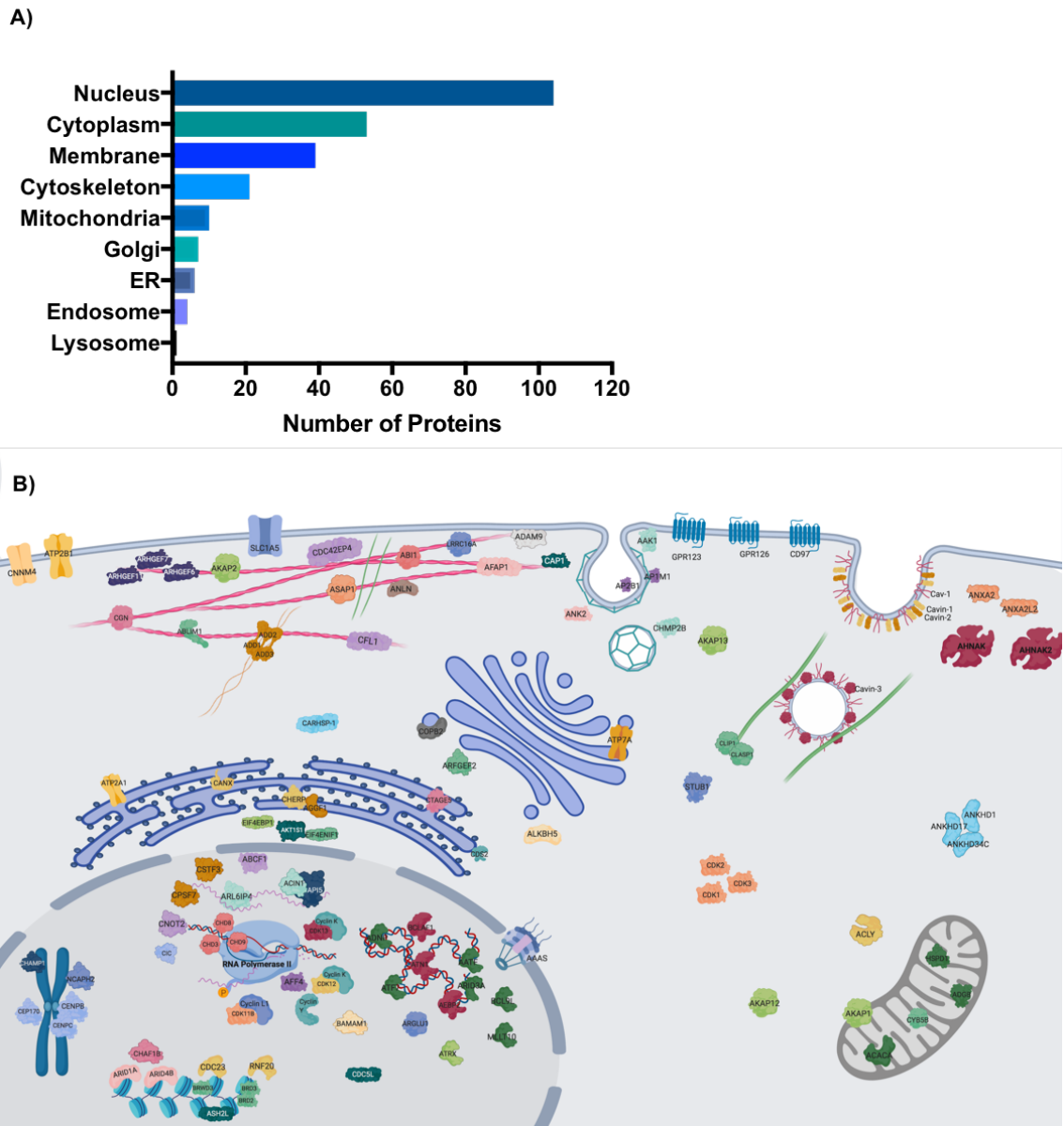
Figure 3.5. Predicted sub-cellular localisation of the identified Gc-regulated phosphoproteins

A) Cellular compartment and corresponding number of differentially regulated phosphoproteins within that compartment, according to the Gene Oontology (GO) enrichment. B) Schematic figure of a number of identified proteins and their predicted cellular localisation. Proteins exist within a diverse range of cellular compartments including at the cell membrane, endosomes, cytoskeleton, Golgi apparatus, endoplasmic reticulum (ER), mitochondria and nucleus.

3.2.2 Phosphopeptide Network Analysis reveals diverse functionalities

In attempt to identify the pathways regulated by these events. I used two approaches, network analysis and gene ontology analysis. Network analysis was performed using the STRINGApp within Cytoscape software, which facilitates the visualisation of the differentially regulated phosphoproteins in context with each other (168). Based on curated protein-protein interaction and association information this analysis helps to infer relationships between commonly regulated proteins. Functional ontology or enrichment analysis, was used to assess the group of co-regulated phosphoproteins to predict common biological functions that they are associated with (169). **Figure 3.6A** shows a functional protein-protein interaction network of all the regulated phosphoproteins which were shared between all three ligands. The network, which contains 158 protein nodes, has 250 edges representing protein-protein interactions. This number of edges is greater than the enrichment number of expected edges (122), defined as the average number of edges expected for a random selection of unrelated protein nodes. Furthermore, the ppi enrichment p value = 1×10^{-16} and overall provides a strong indication that the identified set of proteins are functionally associated. The average degree (number of edges) for each node is 3.16 and so represents a coherent network of proteins rapidly regulated by Gc. Indeed, there was only one protein, Charged Multivesicular Body Protein 2B (CHMP2B), which was unconnected from the network. The node with the greatest degree of connectivity is CDK1 (degree =25) followed by cell division cycle 5-like protein (CDC5L) (degree =22), which is a pre-mRNA splicing factor that regulates mitotic progression(196). This highly interconnected network of proteins identifies common functional processes which are rapidly regulated by the GR ligands following receptor binding.

Gene set enrichment analysis was performed to predict biological functions of the differentially regulated proteins and pathways they may be involved in. **Figure 3.6B** shows that there is diverse range of functions predicted for the regulated proteins. Enriched terms relate to the organisation of cellular organelles, chromatin remodelling, cell-cycle regulation, gene expression and mRNA processing – many of which are functions associated with genomic activity. Although several of these pathways were previously known to be regulated by Gc, this analysis establishes a number of these processes are very rapidly modulated following Gc treatment via a cascade of phosphorylation events.

A) *Functional protein interaction network of all the proteins (oval nodes) differentially phosphorylated by the three GR ligands. Generated using STRING Network within cytoscape. The edges connecting nodes represent protein-protein interactions (line thickness indicates strength of data support). Medium confidence (0.4). Nodes are coloured by mclcluster group.* **B)** *Biological function enrichment analysis from the differentially regulated phosphoproteins generated from the STRING interaction network.*

Figure 3.6 Interaction network and biological function of Gc-regulated phosphoproteins

3.2.2.1 The protein AHNAK had the greatest number of differentially phosphorylated residues

Organelle organisation features as the most enriched biological function and encompasses proteins which act to maintain the assembly and architecture of cellular organelles. This includes two related proteins; AKNAK (neuroblast differentiation-associated protein) and AHNAK2 which are large structural scaffold proteins involved in a multitude of biological processes including calcium signalling and have been associated with metabolism (197). AHANK has also been associated with supressing proliferation in triple negative breast cancer (TNBC) and lung cancer (198, 199); two cancers in which GR-activity correlates with outcome and Gc is administered as part of a standard treatment regime (191, 200).
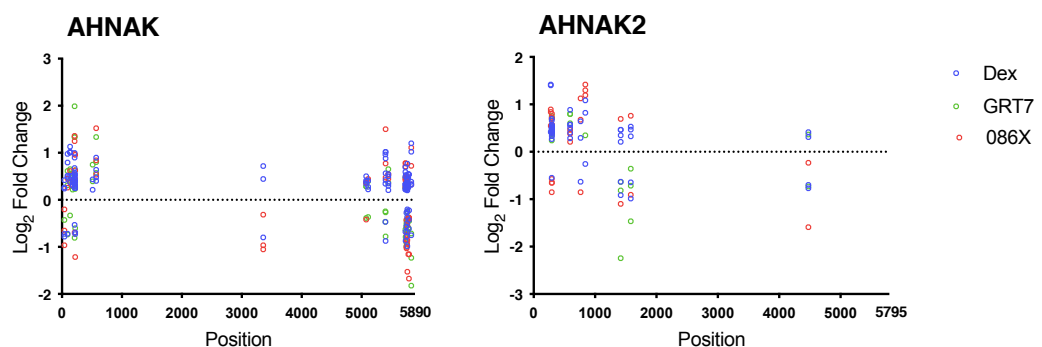
Figure 3.7 Differential phosphorylation of AHNAK and AHNAK2 by GR ligands

Graphs displaying the position of modified residues for AHNAK and AHNAK2, along the protein length (x-axis) and the magnitude of the log2 fold change induced by each ligand (y-axis).

AHANK was identified as the most heavily phosphorylated/ dephosphorylated following GR activation by each of the ligands (**Figure 3.5**) and residues from each of the two proteins featured as top-20 regulated phopho-residues (**Figure A.1**). The position of phosphorylated residue along the protein and extent of the log2 fold change induced by each ligand is shown in **Figure 3.7.** The sites of modification upon AHNAK were primarily within the N-terminal and C-terminal ends which are predicted to be the sites of protein-protein interactions. Whereas, the central domain of 4300 amino acids containing 128-residue repetitive sequence is largely unmodified. Although AHNAK2 shares significant sequence homology, the protein was predominantly modified at the C-terminal end (197). The ligands induced varied extent of change in the level of phosphorylation and this differs between residues.

The potential regulating kinases were investigated using NetworKIN- an online database which predicts which kinase is responsible for the phosphorylation based on consensus substrate motifs (201) (**Table A.2**). This revealed PKCα as the highest scoring for residues Ser5782, Ser5790

and PKCβ for Ser5400 and were the only kinases with a prediction score above 2. Other kinases potentially involved are CAMKIIα and ERK1 ERK2, the same kinases were identified for AHNAK2.

Annexin A2 (ANXA2) is closely associated with the cytoskeleton for vesicle transport and cellular migration (202). In the protein network (**Figure 3.6**) ANXA2 is shown to interact with the AHANK proteins, suggesting these proteins co-operate in a Gc-regulated process.

3.2.2.2 Phosphoproteins are associated with Cytoskeleton Organisation

The proteins in the functional interaction network can be filtered based on shared ontology terms to generate subnetworks of proteins which are predicted to be involved in similar functions. A number of differentially phosphorylated proteins were associated with cytoskeleton organisation, and are shown by the subnetwork (**Figure 3.8A**). Three related adapter proteins: α-adductin (ADD1), β-adductin (ADD2) and γ-adductin (ADD3) were all differentially phosphorylated and are shown as interconnecting nodes. The proteins function as heterodimer/tetramers to assemble the spectrin-actin network and mechanically support the plasma membrane in addition to actin filament capping (203). Two further proteins known to interact to regulate actin dynamics are Cyclase Associated Protein 1 (CAP1) and Cofilin-1 (CFL). These proteins form a complex and participate in actin elongation at the free barbed ends. The identified sites of modification upon CAP1 (Ser308 and Ser310) are modified by GSK3 and regulate binding with cofilin-1 (204).

Cofilin-1 is a small protein involved in the organisation of the actin cytoskeleton by means of regulating the depolymerisation of F-actin filaments and inhibiting G-actin polymerisation (203, 205). Phosphorylation of the cofilin-1 Ser 3 residue, inactivates actin depolymerisation and results in stabilisation of the actin network (205). The SILAC data showed that cofilin-1 was phosphorylated following Gc treatment for 10 minutes (**Figure 3.8B**). Overall, phosphorylation of cofilin-1 Ser3 was enhanced by treatment with all three ligands, suggesting that cofilin-1 is inactivated by Gc**.** However, whilst Dex treatment induced a net increase in phosphorylation in comparison to vehicle, a -0.5 log2 fold change in one of the three replicates was observed. To investigate this finding in more detail, I treated A549 cells with Dex over an acute time course up to 60 minutes and measured the changes in phosphorylation using immunoblotting with a phosphospecific antibody for cofilin-1 Ser 3. The results showed an initial reduction in phosphorylation by Dex at 5 minutes in comparison to untreated cells (**Figure 3.8C**). Following this initial reduction in cofilin-1 Ser3 phosphorylation, the level of ^{P}Ser3-cofilin-1 gradually increased with Dex exposure up to 60 minutes. Based on these findings this suggests that Dex rapidly initiates the removal of phosphate from the Ser3 residue which activates cofilin-1 and destabilises actin. This is followed by the re-phosphorylation of serine 3 and inactivation of

cofilin-1. The increase in cofilin-1 ser3 phosphorylation observed at 10 minutes post-treatment by proteomic analysis likely corresponds to the re-phosphorylation of this substrate following its initial rapid removal.
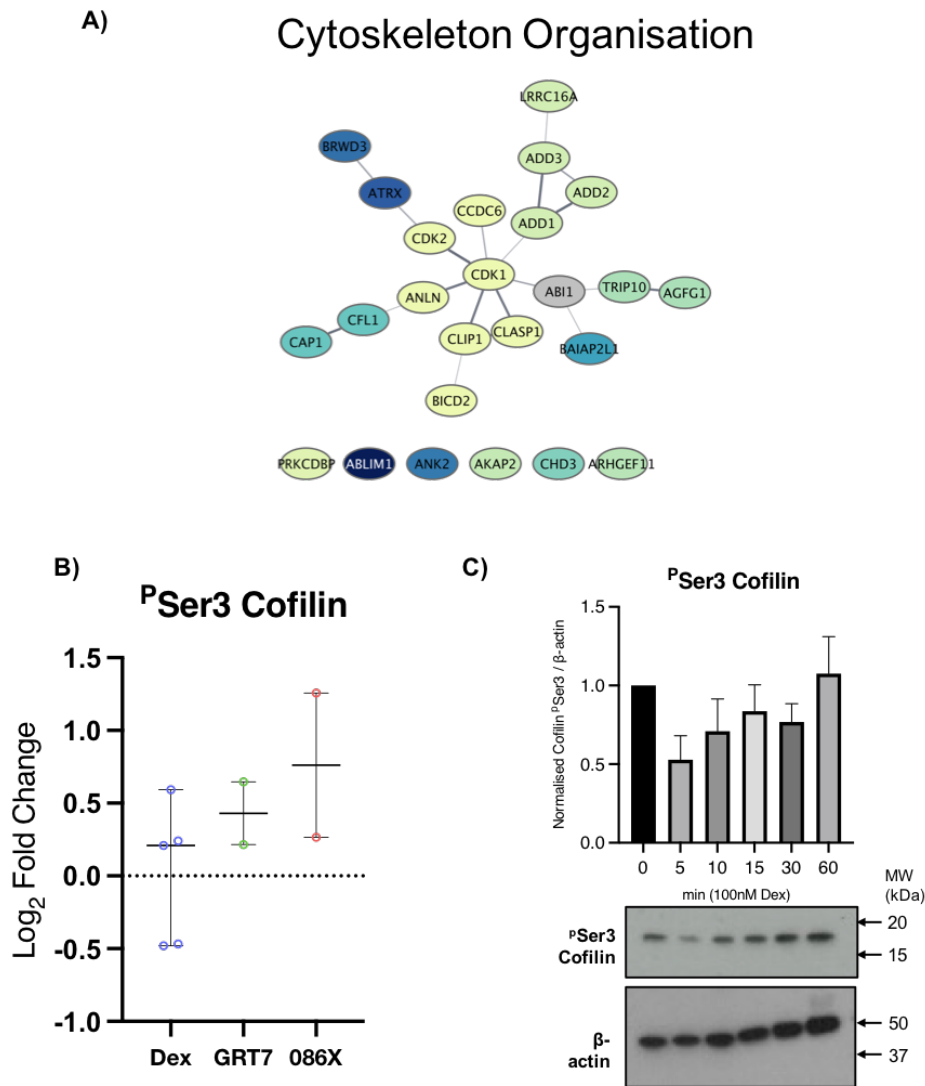
Figure 3.8 Cytoskeletal organisation and phosphorylation of cofilin-1

A) *Protein interaction subnetwork of identified phospho-proteins associated with the enriched biological function: cytoskeleton organisation.* *B)* *Log 2-fold change in cofilin-1 Ser3 phosphorylation relative to vehicle control, quantified by phosphoproteomic analysis. Bars represent median and 95% confidence interval.* *C)* *A549 cells were treated with 100nM Dex over a time course up to 60 minutes. Samples were then lysed and protein expression was analysed by Immunoblot. Specific antibodies against cofilin phosphorylated at Serine 3. Representative blots shown from three independent experiments. Densitometry was used to quantify the relative density of phosphorylation normalised to B-actin. Shown is the mean and SEM of measurements. (n=3)*

3.2.3 Kinase Motif Analysis

Motif enrichment analysis, based on the neighbouring amino acid sequence to the phosphorylation mark, can be used to predict the kinase responsible for the modification and, by extension, the active signalling pathway (summarised in **Figure.3.9A**) Glycogen Synthase Kinase-3 (GSK3), ERK1 (also known as MAPK3), ERK2 (MAPK1) and cyclin-dependent kinase 5 (CDK5) contributed the largest proportion of predicted regulating kinases, followed by: WW domain binding domain, Casein kinase II, GPCR kinase I, PKA Kinase, PKC kinase, MAP kinase-activated protein kinase 2 (MAPKAPK2) and cyclin dependent kinase 1,2,4,6. This indicate activation of a broad range of pathways.

For comparison, kinase prediction was also performed using the web-based KEA2 tool. The lists of phosphorylated proteins and their modified residues by each ligand were inputted. KEA2 performs kinase enrichment probability based on 'kinase similarity and kinase-substrate databases' (206). Analysis again demonstrates the common signature induced by the different treatments (**Figure.3.9B**). Using the KEA2 approach, CDK12 is ranked as the top enriched kinase for Dex and GRT7, closely followed by GSK-3β. However, for 086X CDK12 is the fourth most significantly enriched kinase after GSK-3β, p38α and mTOR. The residues associated with the enrichment were all residues on CDK12 itself, suggesting an autophosphorylation mechanism. These predicted kinases were used to generate a protein interaction network (**Figure.3.9C**) to understand the signalling transduction pathways which are implicated. This is largely clustered into three groups: MAPK, MTOR and CDKs. These kinases largely participate in signalling pathways which are activated by external signalling proteins such as stress, growth factors and cytokines. This suggests that activated GR may modulate the activity of the relayed signals and downstream effectors.
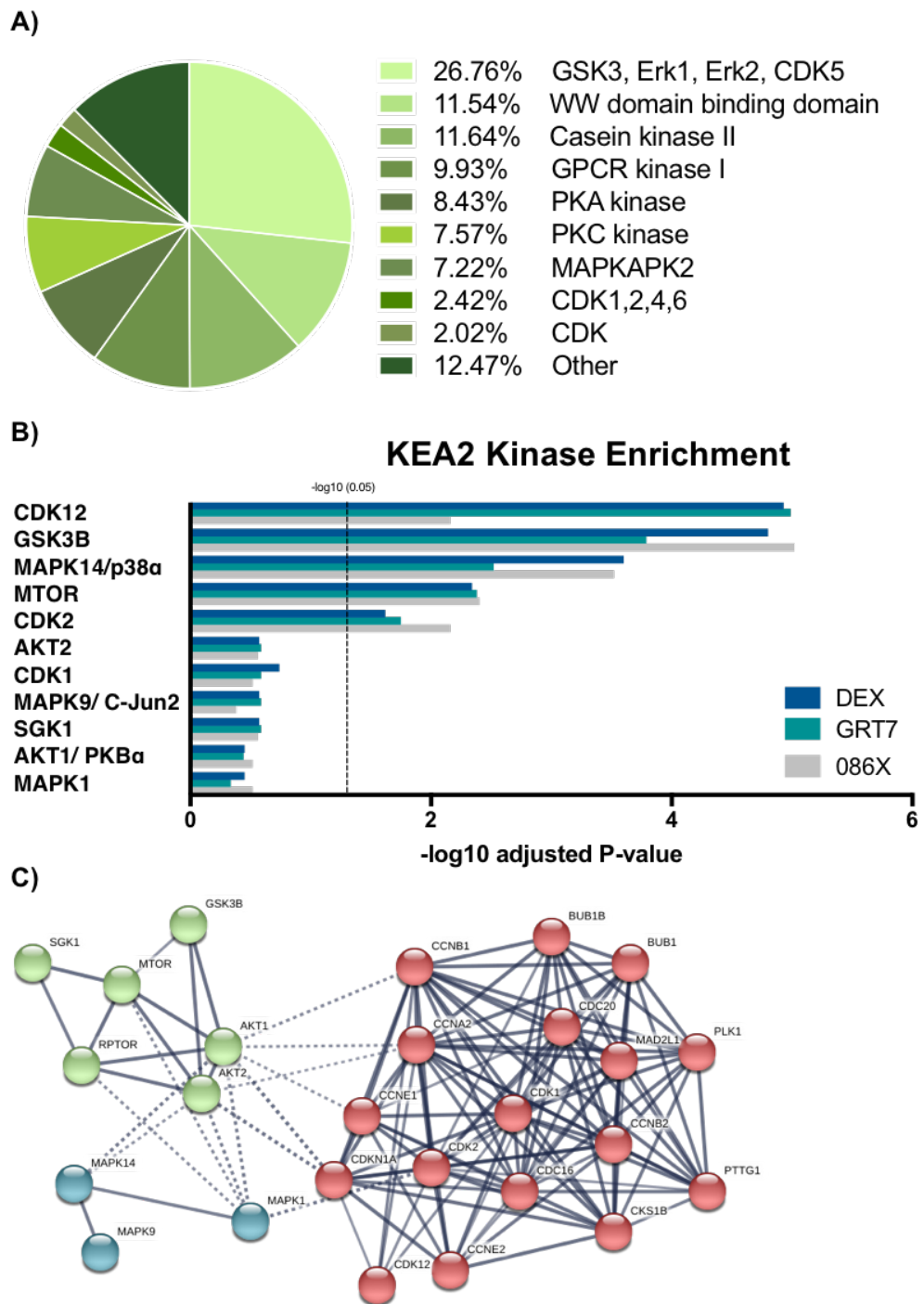
Figure.3.9 Predicted Kinases using motif analysis

A) Substrate motif analysis of differentially phosphorylated proteins. Pie chart of the percentage contribution of each predicted kinase for the total differentially phosphorylated residues induced by all GR ligands. B) Kinase enrichment (by submitting proteins and modified residue location into KEA2 online database). Displayed are the top enriched kinases for each ligand. The dotted line represents the significance cut off set at the equivalent of p<0.05. C) STRING interaction network of the predicted kinases from KEA2 enrichment. Connected by confidence as indicated by line thickness which corresponds to the strength of the data support, filtered using high confidence (0.7). The 11 kinases from kinase enrichment plus 10 interactors in the 1st shell and no more than 5 interactors in the second shell.

3.2.4 Surface Signals

3.2.4.1 Gc differentially phosphorylate G-Protein coupled receptors

Three G-protein coupled receptors (GPCR), GPR123, GPR126 and CD97, were identified as being differentially phosphorylated following treatment with the GR-ligands. This may provide a crucial link between GR activation and implicated kinase signalling pathways (**Figure.3.9A**). Given that GPCR kinase I, and many other kinases which act downstream of GPCRs were identified by the motif analysis, therefore I decided to investigate these receptors further.

The identified receptors are members of the adhesion family. Adhesion GPCRs can be identified structurally by an extended extracellular-region containing versatile functional domains that facilitate cell and matrix contacts. This region typically contains adhesive domains as well as a GPCR autoproteolysis-inducing (GAIN) domain. This GAIN domain contains the highly conserved GPS (G protein-coupled receptor proteolysis site) which is a site of autoproteolytic cleavage where the receptor is cleaved to become a N-terminal fragment and C-terminal fragment which associate by, noncovalent interactions, as a complex at the cell surface (207). Often flanking this region is a hormone receptor (HomrR) domain. Araç *et al* found this region to show a high degree of structural similarity to the hormone binding domain of the corticotrophin releasing factor receptor (CRFR) (207).   Although the complete functional relevance of this domain is uncharacterised, it indicates a potential region that Gc could interact. Therefore, this theoretically indicates the capability of these receptors to have a role in Gc signalling.

GPR123 displayed a positive change in phosphorylation on residue Ser8 by all three ligands, with 086X resulting in the greatest fold change (**Figure 3.10A**). Kinase motif analysis predicted that PKA was a responsible kinase while networKIN method predicted PKCβ (score = 2.49) as an indirect modulator via ezrin (EZR). GPR126 was differentially phosphorylated at position Ser1168 in a negative manner by all GR modulators (**Figure 3.10B**). The predicted regulatory kinases are casein kinase II and MAPKAPK2. A difference in CD97 phosphorylation at position Ser831 was induced by Dex and 086X only (**Figure 3.10C**). A range of kinases were predicted to be responsible based on the substrate motif; these included Casein Kinase II, G protein-coupled receptor kinase 1, PKA and PKC (**Figure 3.10D**).

A) ᴾSer8 GPR123

B) ᴾSer1168 GPR126

C) ᴾSer831 CD97
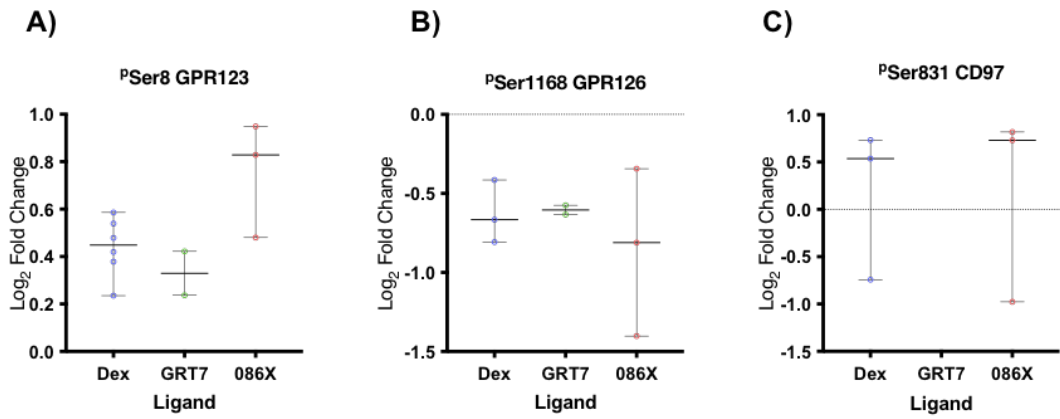
D)

Protein	Gene	Position (Ser)	Predicted Kinase	G protein
GPR123	ADGRA1	8	PKA PKC beta	Unknown
GPR126	ADGRG6	1168	Casein kinase II MAPKAPK2	$G_s G_i$
CD97	ADGRE5	831	Casein kinase II G protein-coupled receptor kinase 1 PKA PKC	$G_{\alpha12/13}$

Figure 3.10 G-protein coupled receptors differentially phosphorylated by GR ligands

The extent of Log2 fold change in phosphorylation induced by each ligand for GPR123 (A), GPR126 (B) and CD97 (C). Each dot represents an individual measurement with the median and 95% confidence interval. Table summarising the modified phospho-residues for each receptor, the predicted kinase from motif analysis (D). (PKCβ identified by Networkin website, the only kinase with a score >1.5 for any of the residues.

3.2.4.2 GPCR Expression

In order to ascertain whether the expression of each of the GPCRs is regulated by GR, A549 cells were treated with 100nM Dex for 4 hours and the expression of genes encoding the identified receptors was determined using qRT-PCR. The results showed that ADGRA1 (which encodes GPR123) was upregulated by Dex treatment and was the only receptor significantly regulated after 4 hours Dex exposure (**Figure 3.11A**).

I hypothesised that these GPCRs might be involved in the transmission of Gc-responsive signals and aimed to investigate the effect of knocking down each receptor. Before performing siRNA-mediated knockdown of these molecules, it was necessary to validate their expression and the suitability of reagents to detect changes in expression following siRNA treatment. The tissue expression pattern of each of the receptors is distinct. GPR123 (ADGRA1) is predominantly expressed in central nervous system (208), while GPR126 (ADGRG6) is expressed in peripheral tissues including the liver and lung (209), which are both major Gc target tissues. CD97 (ADGRE5) is implicated in inflammation and accordingly has high expression on immune cells (210). Therefore, to determine the best model to study the signalling activities of the identified GPCRs, a panel of cell lines with different tissue origins were screened to measure expression. This was initially conducted by lysing cells for protein levels analysis by immunoblotting. However, there are few commercially available antibodies and these proved unreliable and gave inconclusive results (data not shown). The best representative blot for GPR126 after 4 attempts is shown in **Figure 3.11B.** The full-length protein has a predicted molecular weight of 137kDa. However, the protein is cleaved into two fragments for assembly at the membrane, generating a 70kDa *N*-terminal fragment (the extracellular soluble protein) and a 35kDa *C*-terminal fragment. Bands can be seen at 70kDa for most cell lines, although bands of 137kDa are present for MO59K and HepaRG cells, yet the 35KDa fragment is not observed. Longer exposure times resulted in the appearance of multiple non-specific bands (data not shown).
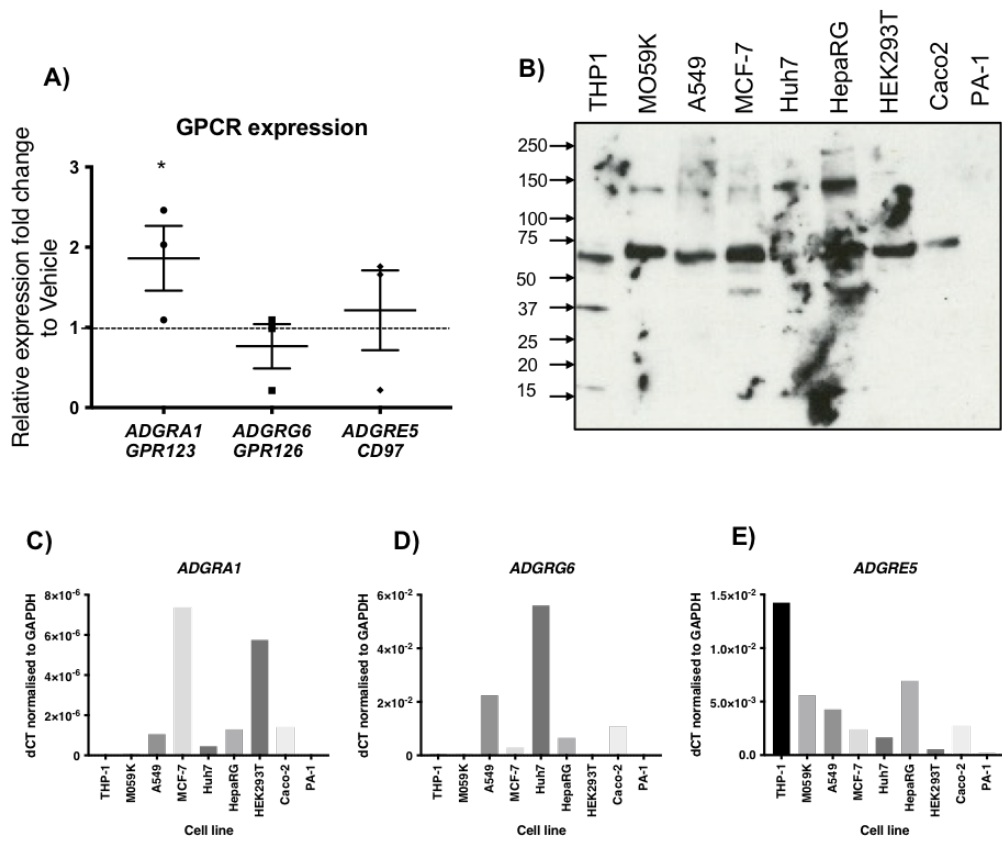
Figure 3.11 Assessment of GPCR expression

A). RT-qPCR analysis of GPCR expression following 4hr exposure to 100nM Dexamethasone. A549 cells were treated with 100nM Dex for 4 hours. Cells were lysed and gene expression was assessed by Taqman qPCR. Fold changes were calculated relative to vehicle treated control and normalised to GAPDH housekeeping gene. Data is presented as the mean fold change and standard error of the mean (SEM) of three independent experiments. Represented as individual points for each experimental repeat (n=3). Statistical analysis performed using Mann Whitney test, comparing expression level of each GPCR gene to the vehicle control only. *P< 0.05. dCT, Δ (delta) CT value. B) Assessment of GPR126 protein expression in various cell lines. Cultured cells were lysed and protein expression was analysed by Immunoblot using 15µg protein lysates using a specific polyclonal antibody against GPR126. GPR126 has a molecular weight of 137KDa but the mature protein on the cell surface is cleaved into two fragments: 35KDa C-terminal fragment and 70KDa N-terminal fragment (the extracellular soluble protein). Cultured cells were lysed and mRNA expression of ADGRA1, GPR123(C); ADGRG6, GPR126 (D) ; ADGRE5, CD97 (E); were analysed by RT-qPCR. Plotted are dCT values for each cell line normalised to GAPDH for that sample mean of triplicate technical replicates.

As an alternative to immunoblotting, the mRNA expression was analysed by RT-qPCR. **Figure 3.11C-E** displays the expression data for each receptor. The breast cancer cell line MCF-7 showed the highest relative expression of ADGRA1 (encoding GPR123). However, for all of the cell lines examined the CT (cycle threshold) was greater than 30 cycles, indicating low level expression of this gene. The hepatocyte carcinoma cell line, Huh7 demonstrated the highest expression for ADGRG6 (GPR126), whereas ADGRE5 (CD97) expression was highest in the THP-1 monocyte-like cell line and reflects their know tissue-level expression. As MRC-5 and Huh7 showed the greatest expression levels for GPR123 and GPR126, respectively, these were taken forward to investigate the effect of knockdown of the GPCRs. A549s were also chosen, to maintain consistency with the phosphoproteomic dataset – as the receptors were detected in the A549 cell line initially.
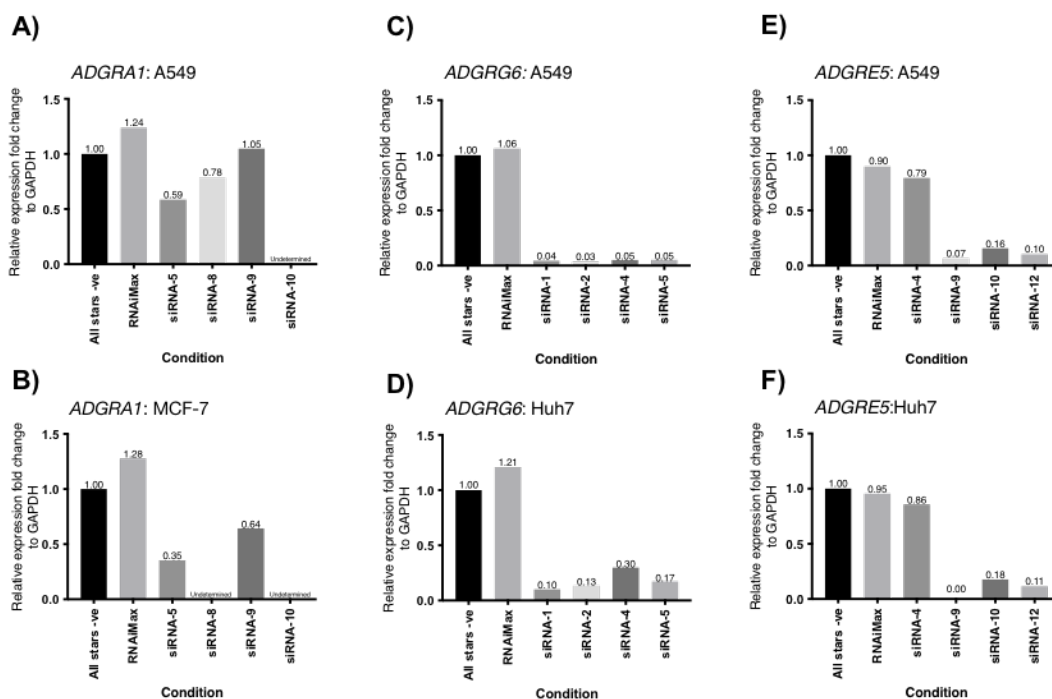
Figure 3.12 Optimisation of GPCR siRNA knockdown

*Various cell lines were treated with siRNA targeting each GPCR for 48 hours. Cells were lysed and GPCR mRNA expression ADGRA1, GPR123**(A,B)**; ADGRG6, GPR126 **(C,D)** ; ADGRE5, CD97 **(E,F)** were assessed by Taqman qPCR. Fold changes were calculated relative to the non-targeting siRNA control (All stars negative control) and normalised to GAPDH housekeeping gene. Values above the bars correspond to extent of knockdown for each siRNA tested. Performed with triplicate biological replicates.*

3.2.4.3 GPCR Activity

siRNAs were evaluated for their efficiency to knock down GPCR targets with the aim of investigating GPCR involvement in Gc signalling. MCF-7 and A549 cells were transfected with siRNA targeting GPR123 **(Figure 3.12A-B)**, while Huh7 and A549 cells were transfected with siRNAs against GPR126 and CD97 **(Figure 3.12C-F)**. The knock down efficiency of siRNAs against GPR123 were more efficient in MCF-7 compared to A549 cells; however, as baseline CT expression was initially very low, any silencing effects of the siRNA would be difficult to validate. Due to the low expression it was decided that the function of GPR123 could not be assessed in knockdown experiments. siRNA-1 and siRNA-2 demonstrated the greatest efficiency (>85%) of GPR126 knockdown in both Huh7 and A549 cells. A knockdown efficiency >89% targeting the CD97 transcript was achieved by two siRNAs, siRNA-9 and siRNA-12 in both A549 and Huh7 cells.

In attempt to elucidate the downstream signalling pathways and involvement of the receptors in Gc signalling, cells were transfected with siRNA for 48 hours and then treated with 100nM Dex over an acute time course. Following lysis, cells were assessed by immunoblot using antibodies which recognise phosphorylated substrates downstream of PKA and PKC activity.

For GPR126, Dex induced an increase in PKA activity up to 60 minutes in A549 and Huh7 cells although, siRNA knockdown had a greater effect in A549 cells **(Figure 3.13).** For both targeting siRNA, the baseline and Dex-induced levels of PKA-substrate phosphorylation is increased over time, suggesting that GPR126 has a suppressive effect upon Dex-induced PKA signalling.

A similar effect was observed for PKC-substrate which was most clearly observed in Huh7 cells. The addition of Dex treatment increased substrate phosphorylation over time which was highest at 60 minutes. The interference of GPR126 expression resulted in greater phosphorylation signals at base line and over time, in response to Dex. This was not as evident in A549 cells and may represent cell-type differences. Similarly, the molecular weight distribution of phosphorylated PKC-substrates was different between the two cell lines, suggesting the potential engagement of different signalling cascades and/or cell type specific expression of particular substrates.
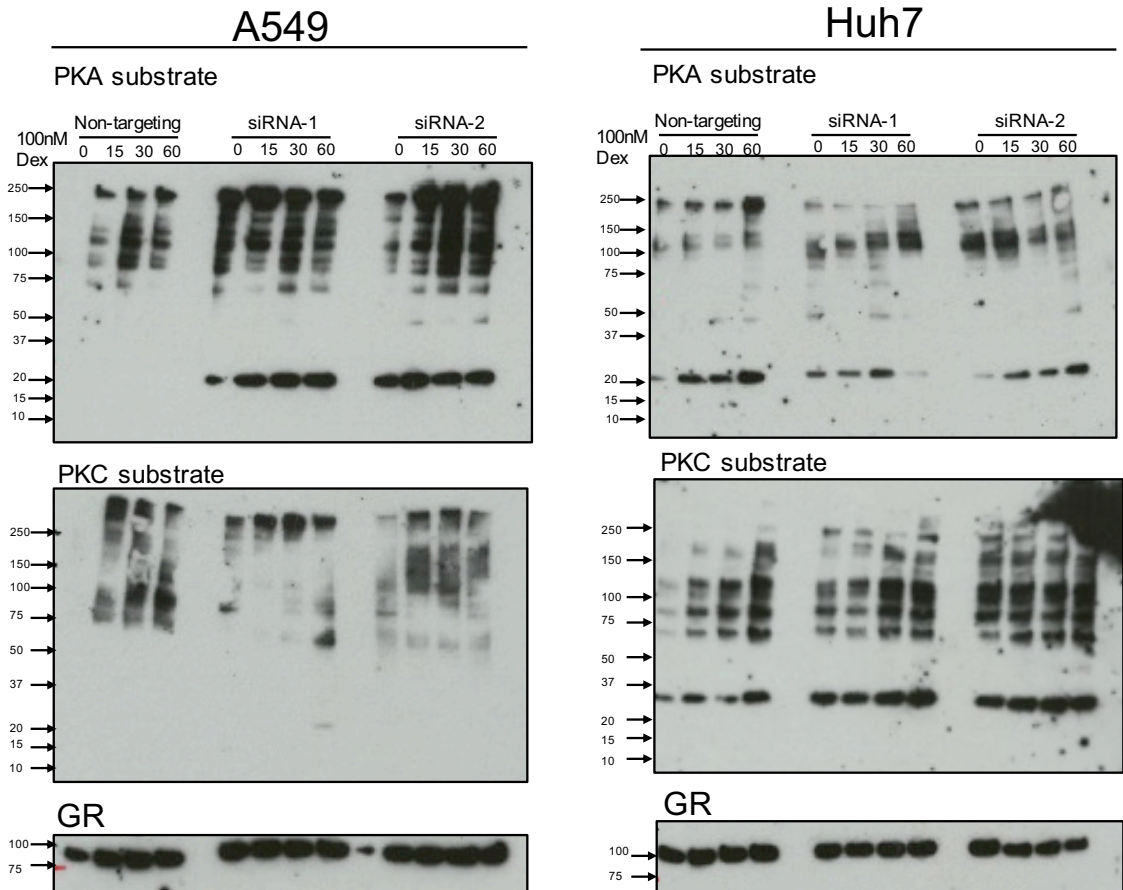
Figure 3.13 GPR126 engagement of PKA- and PKC-mediated signalling activity in response to Dexamethasone

A549 and Huh7 cells were treated with siRNA targeting each GPR126 for 48 hours, the cells were then split between 6-wells of a 6-well plate and allowed to settle. Cells were then treated with 100nM Dex over time course up to 60 minutes and then lysed. Phospho-protein expression was assessed by immunoblot using antibodies specific to the substrate of Protein kinase A (PKA) and Protein Kinase C (PKC).

Knockdown of CD97 in A549 cells and immunoblotting using a PKA substrate motif antibody revealed an increase in baseline phosphorylation (**Figure 3.14**) (i.e. in the absence of Dex treatment). There was no observable increase in phosphorylation upon addition of Dex. Instead, there was a loss of intensity of bands at ~30KDa in cells with CD97 knock down. The converse was seen for Huh7 cells whereby the knockdown of CD97 increased the intensity of the 30KDa band. In the case of PKC, no definitive alterations in phosphorylation could be determined for cells with reduced levels of CD97.

These results investigating activity of PKA and PKC must be interpreted with some caution, as staining patterns and intensities were difficult to replicate between repeats. Furthermore, without a functional antibody for GPCR detection the successful knockdown of the protein cannot be verified.

The localisation of GRP126 and CD97 in response to Dex was investigated using immunofluorescence, to establish whether the localisation of the receptors are responsive to Gc. Cells were treated with 100nM Dex and fixed at varying timepoints following ligand addition (0-60 minutes; **Figure 3.15**). In absence of Dex, GPR126 staining is diffuse throughout the cytoplasm with some regions of increased intensity around the nucleus. However, there are no obvious chances in GPR126 localisation with Dex treatment. A comparable staining pattern was seen for CD97 (**Figure 3.16**) with regions of greater staining intensity around the nucleus in some cells. Nevertheless, the time course of Dex exposure did not reveal anything further about the relationship between the GPCRs and GR activation. These results may, in-part, be attributable to the issue of antibody specificity as encountered previously for immunoblotting.
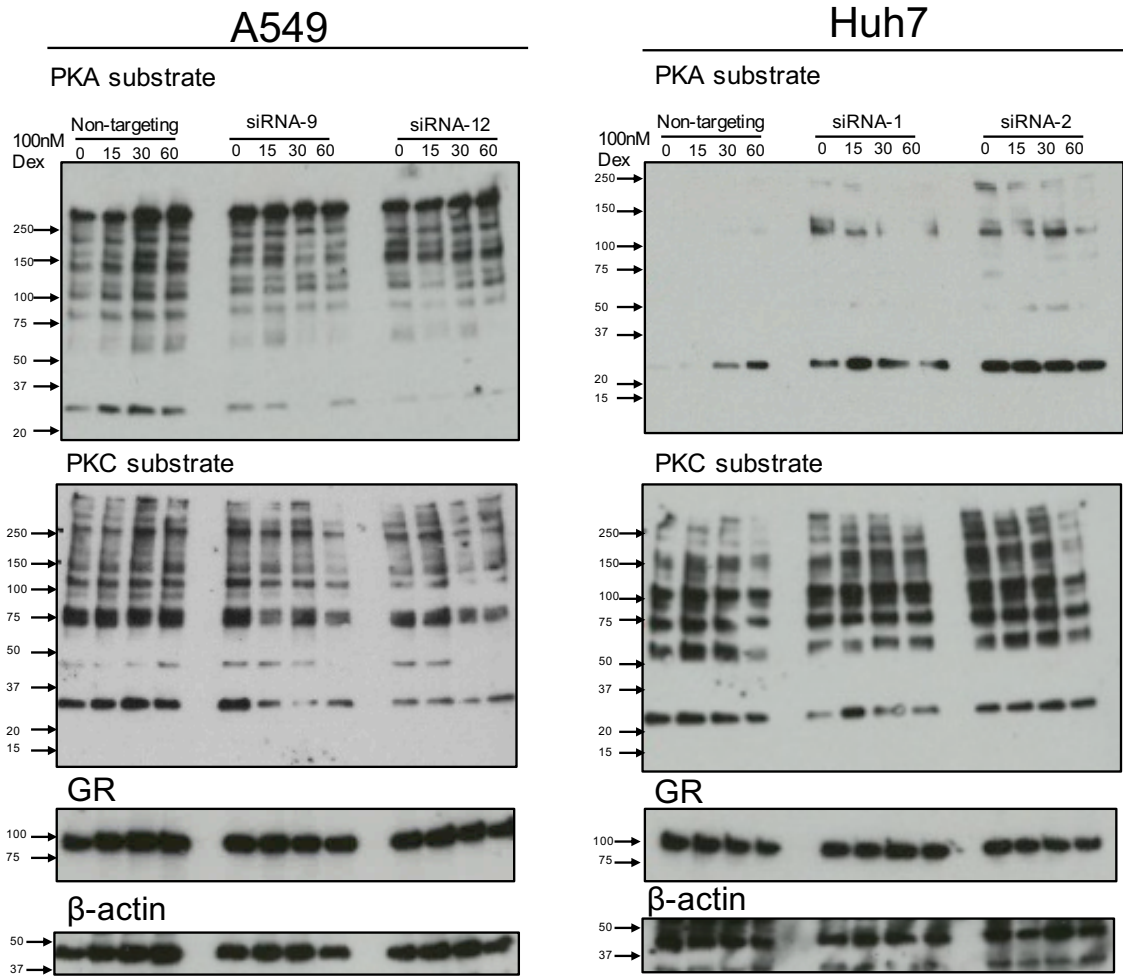
Figure 3.14 CD97 engagement of PKA- and PKC-mediated signalling activity in response to Dexamethasone

A549 and Huh7 cells were treated with siRNA targeting each CD97 for 48 hours, the cells were then split between 6-wells of a 6-well plate and allowed to settle. Cells were then treated with 100nM Dex over time course up to 60 minutes and then lysed. Phospho-protein expression was assessed by immunoblot using antibodies specific to the substrate of Protein kinase A (PKA) and Protein Kinase C (PKC).
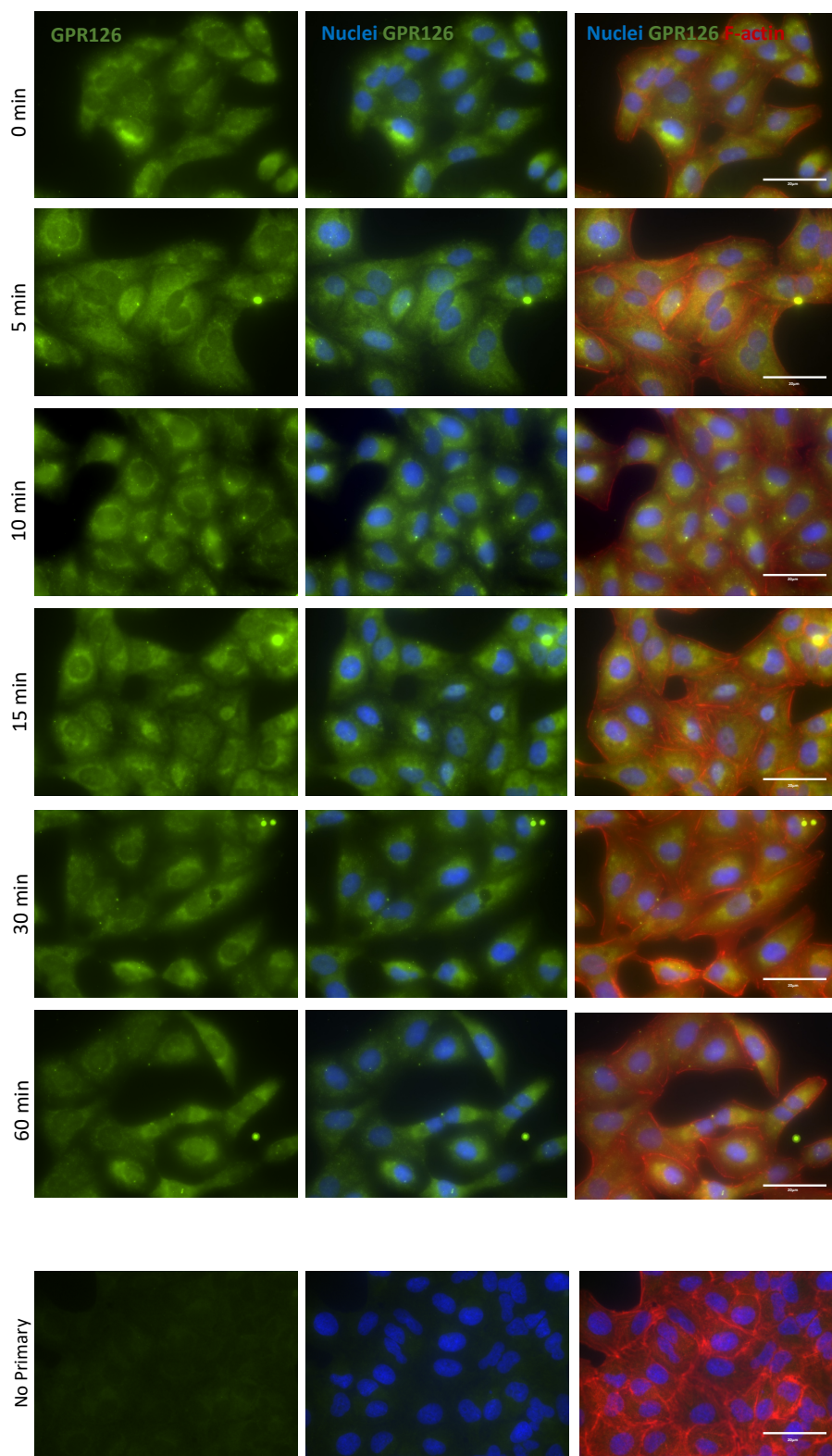
Figure 3.15 GPR126 localisation in response to Dexamethasone.

A549 cells were seeded onto coverslips and treated with 100nM Dex over a time course up to an hour. Cells were fixed, permeabilised and stained for GPR126 (green), F-actin by phalloidin (red) and counterstained with Hoechst 33342 (blue). Representative immunofluorescent images, captured on Widefield microscope x60 magnification. Scale bar: 20µm.
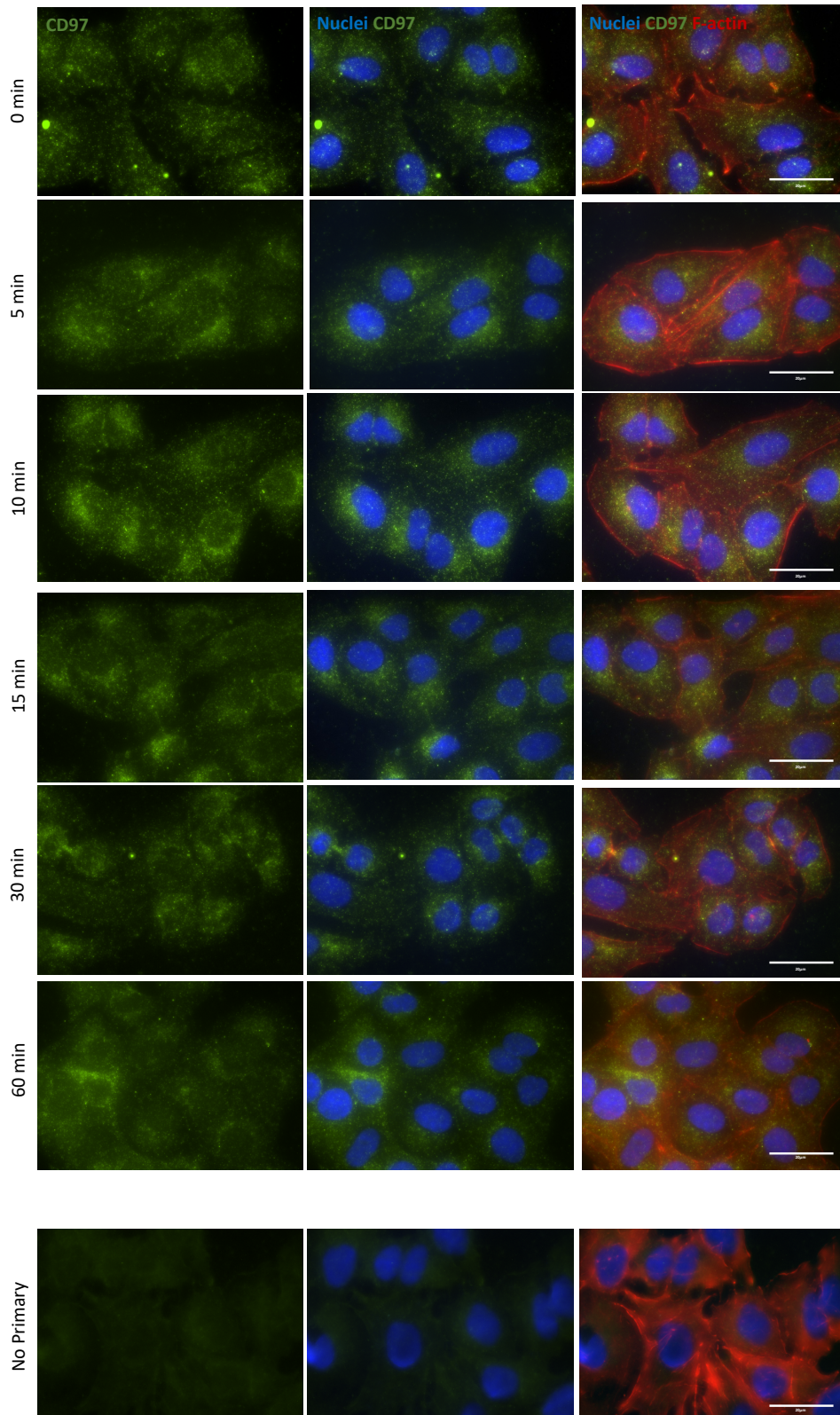
Figure 3.16 CD97 localisation in response to Dexamethasone.

A549 cells were seeded onto coverslips and treated with 100nM Dex over a time course up to an hour. Cells were fixed, permeabilised and stained for GPR126 (green), F-actin by phalloidin (red) and counterstained with Hoechst 33342 (blue). Representative immunofluorescent images, captured on Widefield microscope x60 magnification. Scale bar: 20µm.

3.2.5 PRESTO-TANGO Assay to assess GPCR activity

As an alternate approach to determine whether the identified GPCRs are directly modulated by GR ligands, I used the Tango assay to measure the activity of the GPCRs. This assay was developed by Barnea et al. (211) and subsequently modified by Kroeze et al. (109), generating PRESTO-TANGO (parallel-receptor-ome expression and screening via transcriptional output). In simple terms, this assay system couples GPCR activity to the induction of luciferase expression (**Figure 3.17**). The system uses HEK293 cells stably expressing a fusion protein of B-arrestin linked a protease. These cells (termed HTLA) are then transiently transfected with a construct encoding a fusion protein comprising the relevant GPCR. The main advantage of this assay is that it does not require knowledge of either the G-protein which couples to the receptor of interest or the outcomes of downstream signalling, making it useful for studying orphan receptors such as those identified in this study. Additionally, the measurable response relies only on the recruitment of β-arrestin and so is independent from signalling of other endogenous receptors (212).

I chose to evaluate all three identified receptors; GPR123, GPR126 and CD97 as the assay would not be hindered by low endogenous expression of GPR123. As a positive control I included G protein-coupled oestrogen receptor GPER (GPR30), which is known to be responsive to β-oestradiol (110). The plasmids were transfected at three concentrations into HTLA cells and expression of the construct was assessed by detection of the FLAG-tag epitope included at the *N*-terminus of the GPCR. In order to recapitulate the tango assay procedure, cells were transfected for 48 hours, on day 4 post-transfection, cells were fixed to assess GPCR expression. Images were captured for two magnifications, (x60 shown in **appendix Figure A.2)** and quantified by calculating the ratio of positively transfected (FLAGtag+) cells to the total cells per FOV. Overall the transfection efficiency for all GPCRs remained low at around 10%, however this was in-line with the positive control GRγ. GPR126 showed the lowest efficiency across all concentrations whilst the 800ng and 1200ng concentration showed the highest ratio of transfected cells for GPER. **Figure 3.18** shows a representative image of the distribution and localisation of each of the receptors. GPR123 staining is predominantly at the cell boundary and defined at cell protrusions, with some central speckled regions. GPR126 staining is diffuse throughout the cytoplasm and excluded from the nucleus with regions of more intense staining, an expression pattern similar to that of CD97. GPER shows broad localisation across the whole cell with no particular defined regions of expression.
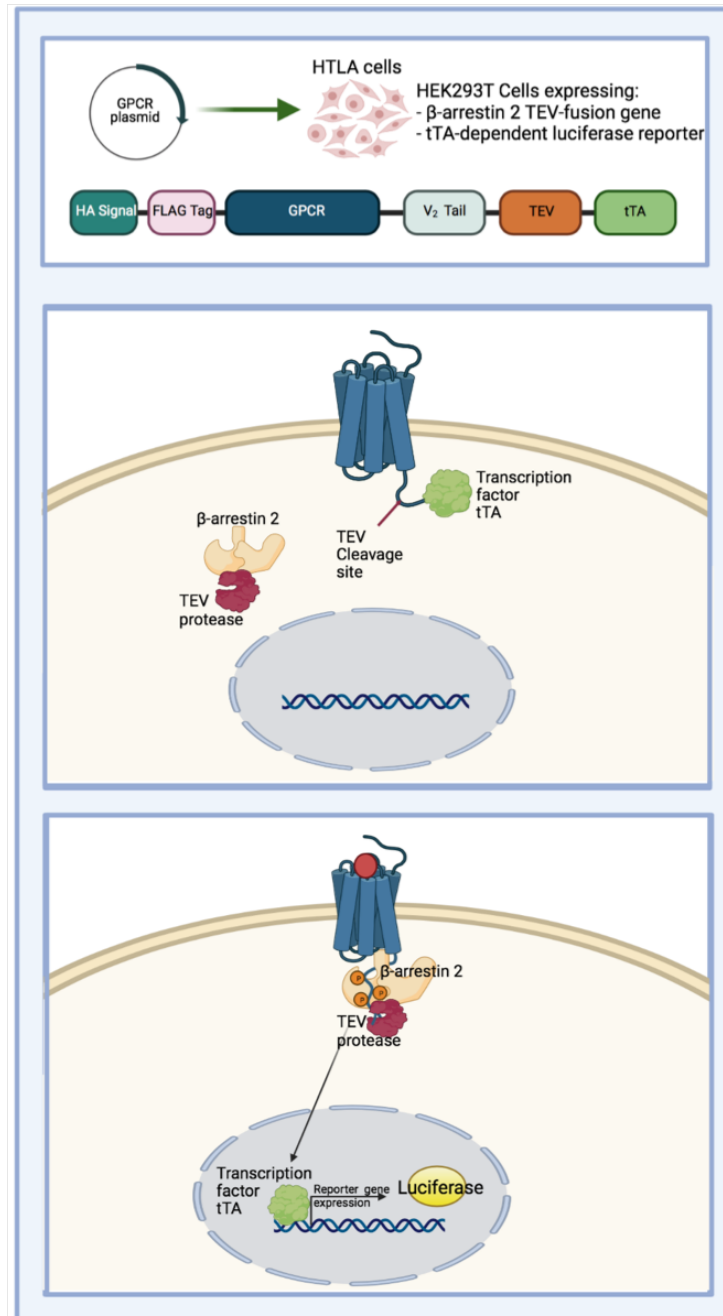
Figure 3.17 Schematic of Tango assay

GPCR PRESTO-Tango HTLA cells stably express the B-arrestin2-TEV fusion gene and tTA-dependent luciferase reporter gene. Plasmid insert structure: contains HA signal for nuclear localisation, FLAG tag, sequence of GPCR of interest, V2tail, TEV cleavage site and tTA transcription factor. HEK293 cells stably express a fusion protein of B-arrestin linked to the TEV protease. Cells are transiently transfected with a construct encoding the GPCR The GPCR and tTA components are separated by a Tobacco Etch Virus (TEV) protease cleavage site.

Resting state the inactive GPCR is expressed at the membrane. The C-terminal tail contains extended V_2 tail containing a TEV protease cleavage site which is joined to a tTA transcription factor. In the cytoplasm cells express B-arrestin 2 coupled to TEV protease. Upon ligand binding and activation of the GPCR, B-arrestin2 is recruited to phosphorylate and inactivate the GPCR. Close proximity of the TEV protease with the cleavage site on the GPCR results in cleavage and release of the tTA transcription factor. This then translocates into the nucleus and drives the expression of luciferase reporter.
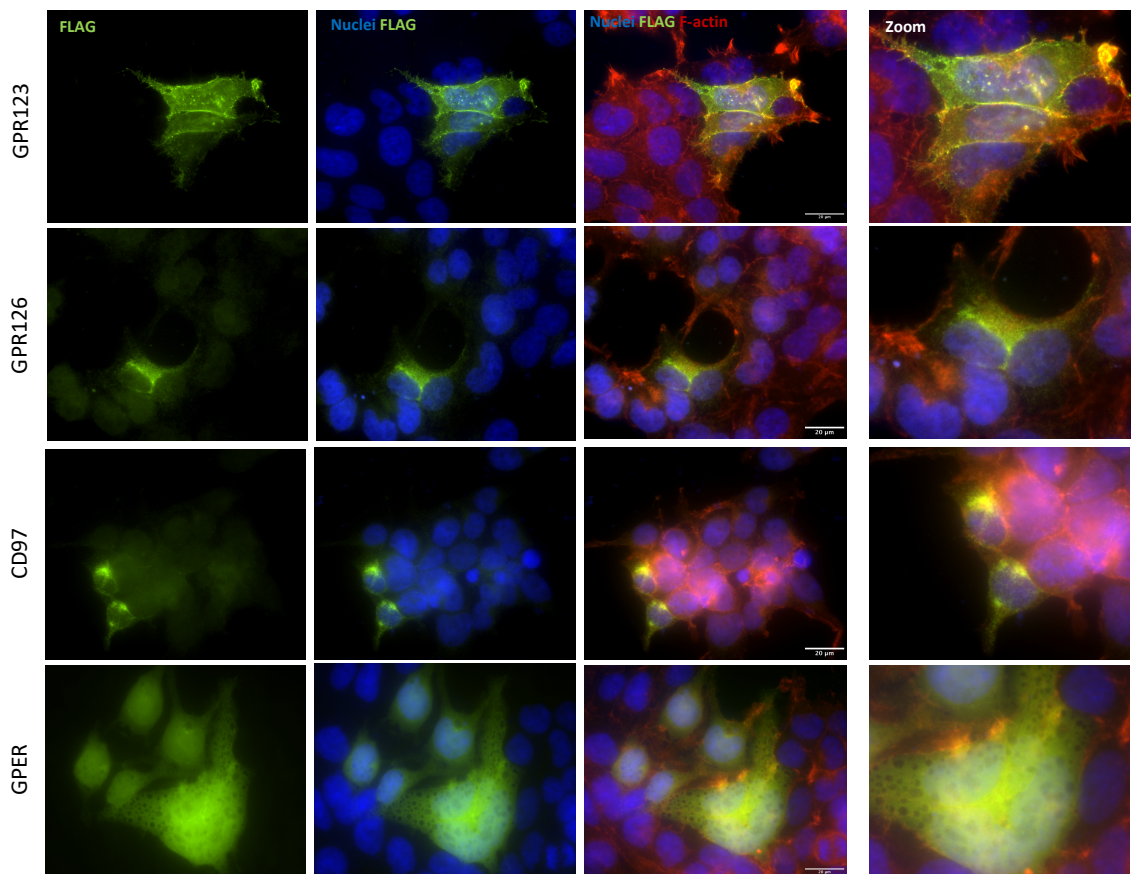
Figure 3.18 TANGO-GPCR expression and cellular localisation

HTLA HEK293 cells were transfected with plasmids containing GPR123, GPR126, CD97 or GPER using fugene 6 reagent. Cells were transfected for 48 hours then media changed to complete media containing steroid depleted serum. Cells were fixed, permeabilised and stained to detect expression of the expressed protein using an anti-FLAG antibody (green), F-actin (red) and counterstained with Hoechst 33342 (blue). Images were obtained on widefield microscope using x60 objective. Representative images are shown for each receptor. Scale bar:20µm

The TANGO assay was performed in HTLA cells, transfected with GPCR of interest and the response to Dex was measured by luminescence. A construct containing the Gc-responsive promoter TAT3 linked to luciferase was included as a positive control to validate Gc-responsiveness and functionality of the assay. During the optimisation of the transfection procedure the cells were detached and counted as an approximate measure of cell survival to ensure the transfection was not resulting in high levels of cell death (data not shown). Overall, a comparison of cell counts did not reveal any large differences between the concentrations of transfected DNA or by overexpression of the receptors. This provides confidence that the cells are viable following the transfection procedure and over expression of the receptors of interest is not altering the growth of the cells.

The viability of the cells was also investigated by MTT assay in parallel with the Dex treatments for the luciferase assay. In each case those transfected with highest plasmid concentration 1200ng, showed lowest surviving fraction, both for vehicle and Dex-treated conditions. There was no difference between increasing concentrations of Dex, suggesting that the Gc are not responsible for reduced survival. Similarly, the pattern of cell survival does not appear to be specific to the receptor of interest as a similar survival pattern is seen for cells transfected with the TAT3 reporter (**Figure 3.19**).

3.2.5.1 GPCR response to Gc

The TAT3 reporter, drives the expression of luciferase as a measure of activated GR binding to DNA directly. The two higher concentrations of transfected pDNA demonstrated a dose-responsive increase in luciferase activity between 10nM and 100nM Dex (**Figure 3.20A**) and demonstrates efficient transfection and measurable responsiveness to Dex. However, the assay efficiency for GPER was low and showed little sensitivity to β-oestradiol, and no consistent trend in response to the treatments between the transfection conditions. As there was no internal control for transfection, luciferase measurements were normalised to the surviving fraction of cells as measured by MTT and the reduced viability seen for GPER may be reflected by the TANGO result (**Figure 3.19**).

A general Dex-induced decrease in luminescence was observed for the GPR123, suggesting that Dex addition reduces the signalling activity of the receptor. For this receptor the highest transfection concentration was the least responsive. A similar effect was observed for GPR126 at the 800ng condition, with a trend towards reduced activity with Dex addition, although the greatest luciferase measurements were recorded for the 1200ng transfected pDNA. The response of CD97 was in close agreement between the 800ng and 1200ng conditions. Although, a slight increase in activity was observed for the 10nM and 100nM Dex conditions compared to vehicle, 1μM Dex was equal to the vehicle baseline levels of activity. Although inconclusive, the assay provides an indication that Dex treatment has a suppressive effect upon the identified GPCRs. For GPR126, this inhibitory activity is consistent with the results obtained when analysing PKA and PKC substrates (**Figure 3.13 and Figure 3.14**). However, further work is required to evaluate the precise activity further.
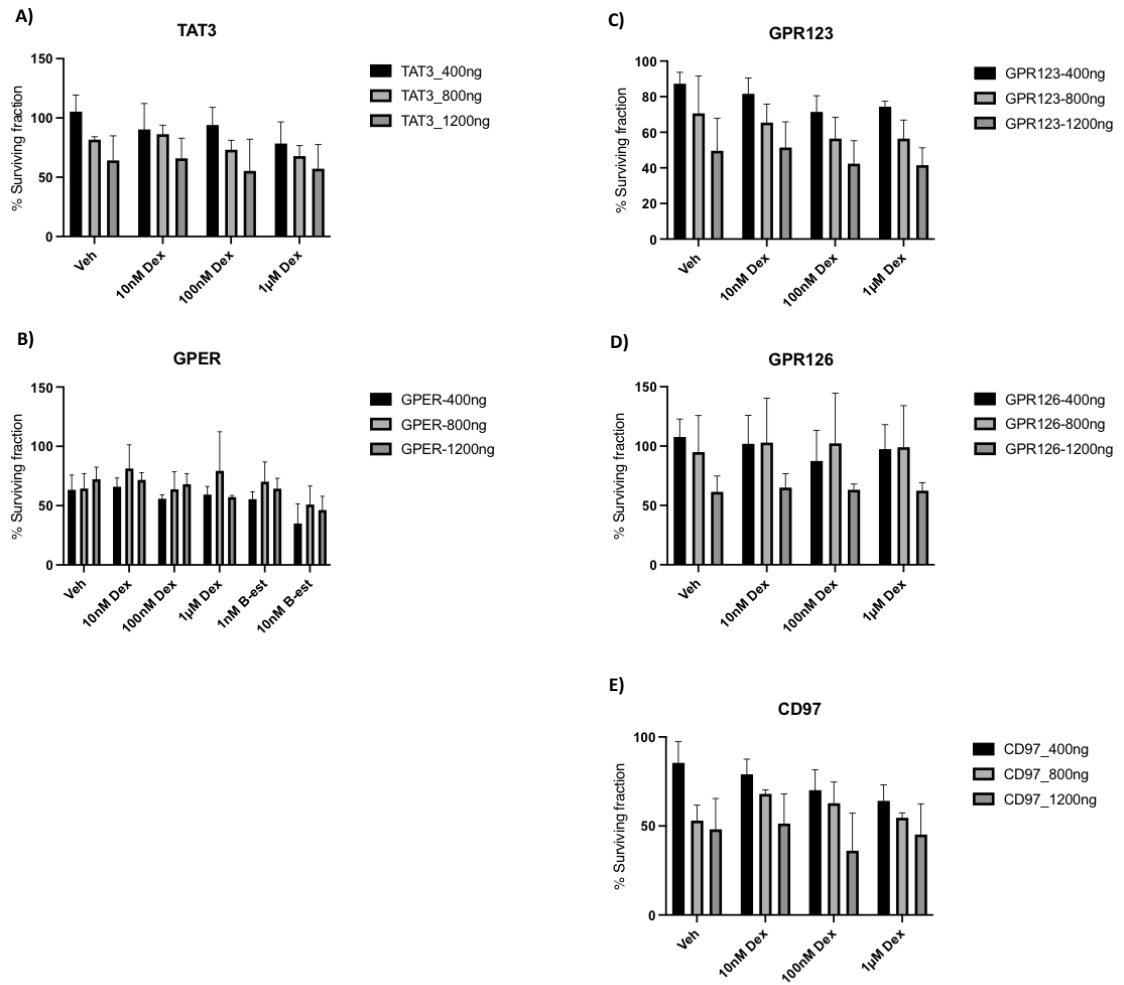
Figure 3.19 TANGO assay assessment of cell viability in response to Dex treatment

HTLA HEK293 cells were transfected with GPR123-TANGO, GPR126-TANGO, CD97-TANGO, GPER-TANGO or TAT3 plasmids using fugene 6 reagent and with 3 different concentrations of pDNA to determine the best efficiency. Cells were transfected for 48 hours then trypsinised, counted and seeded into poly-l-lysine coated 96-well plate in phenol-free media containing charcoal-stripped serum. Cells were allowed to adhere and were then treated with varying concentrations of Dex for 18 hours before adding MTT reagent for 4-hours. (n=3)
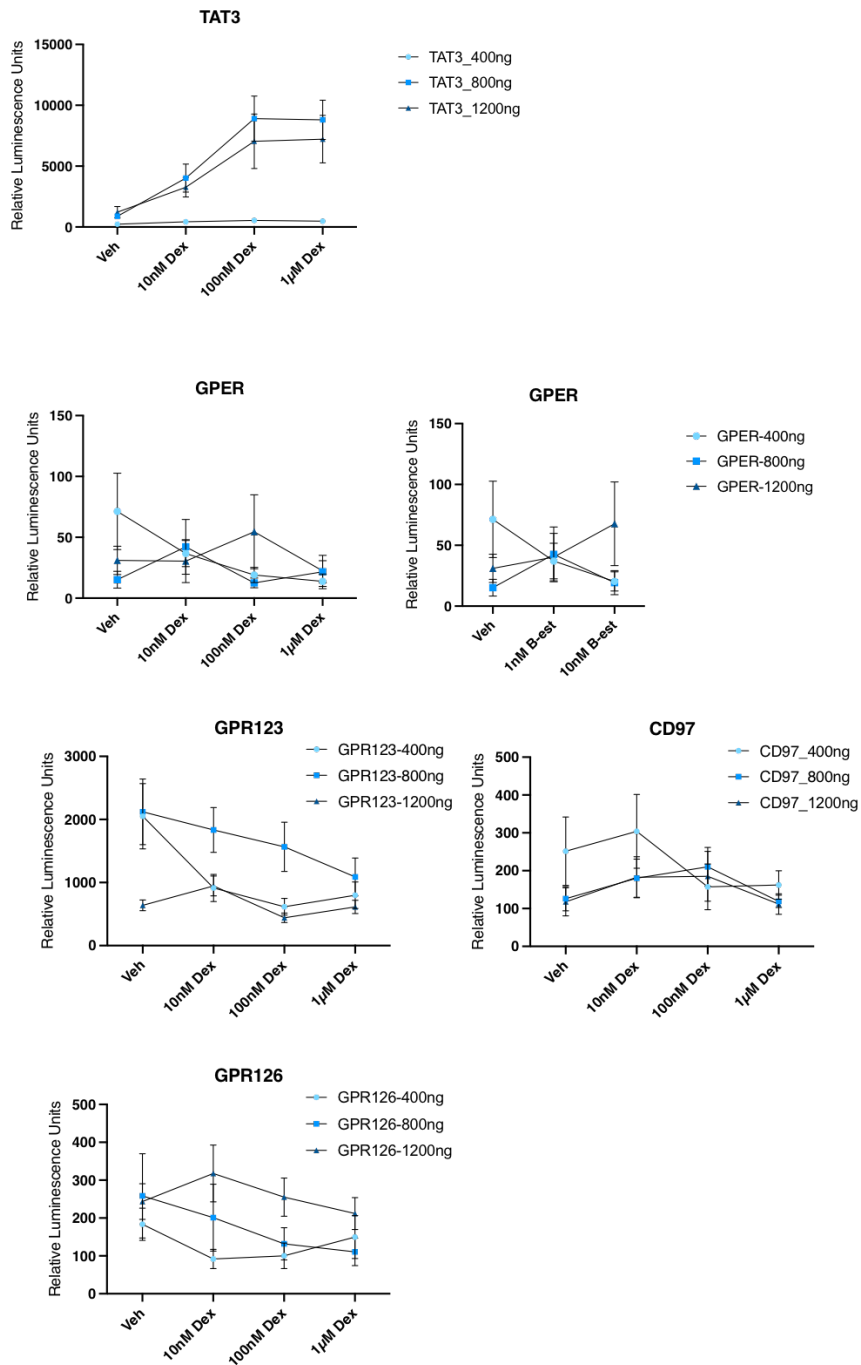
Figure 3.20 GPCR response to Dexametasone by Tango assay

HTLA HEK293 cells were transfected with GPER-TANGO, TAT3, GPR123-TANGO, GPR126-TANGO, CD97-TANGO plasmids using fugene 6 reagent and with 3 different concentrations of pDNA to determine the best efficiency. Cells were transfected for 48 hours then trypsinised, counted and seeded into ploy-l-lysine coated white-96-well plate in phenol-free media containing charcoal-stripped serum. Cells were allowed to adhere and were then treated with varying concentrations of Dex for 18 hours, the media was then removed and bright glo reagent added to each well. Luminescence was read using citation 5 plate reader. Luminescence was normalised to surviving fraction measured using MTT assay. Representative graphs shown from 3 independent experiments performed in triplicate. (n=3)

3.2.6 Nuclear Signals

Many of the identified proteins which were differentially phosphorylated have functional roles related to regulation of transcription and chromatin remodelling (**Figure 3.6B**). A number of chromatin adapter proteins, transcription factors and co-regulatory proteins with potential association with GR-mediated transcription were modified within only 10-minutes of GR-ligand binding. The protein interaction sub-network **(Figure 3.21)** was created by selecting all the proteins associated with the enriched ontology term: 'Chromatin organisation', from the network of proteins differentially regulated by all three GR ligands **(Figure 3.6A)**. This highlights the close association of factors involved in genomic activity to regulate the accessibility of chromatin, such as helicase proteins and members of the SWI/SNF family ARID1A and ATRX in addition to chromatin remodelling factors chromodomain-helicase-DNA binding protein (CHD)3, CHD8 and CHD9. Bromodomain-containing proteins BRD2 & BRD3, are associated BET family kinases which read the chromatin and help to regulate transcription. This prompted further analysis in to the potential functions of these nuclear proteins.
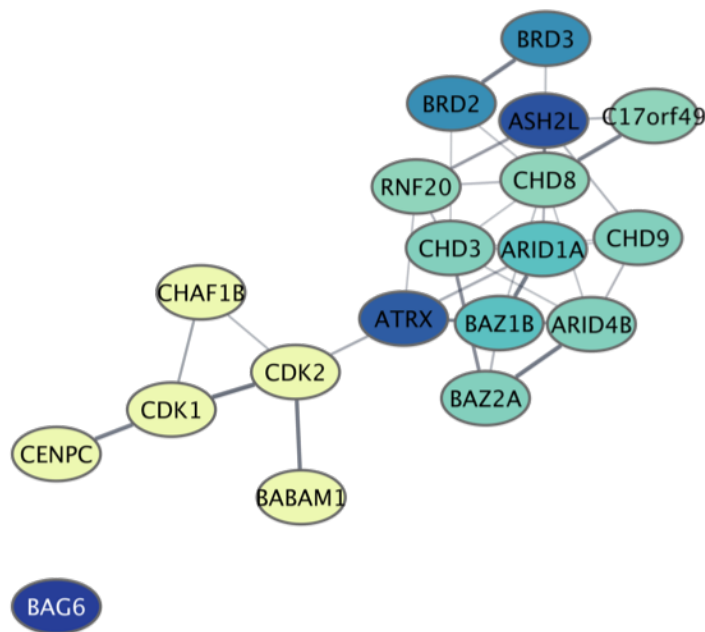
Figure 3.21 Phosphoprotein interaction sub-network of proteins associated with Chromatin Organisation

Protein interaction subnetworks of proteins associated with enriched STRING biological function ontology. The edges connecting nodes represents protein-protein interaction (line thickness indicates strength of data support. Medium confidence (0.4). Nodes are coloured by mclcluster group.

3.2.7 CDKs and partner cyclins were differentially phosphorylated by Gc

Enrichment analysis was performed to assess the molecular function of the proteins which were differentially phosphorylated in response to GR-activation by all three ligands (**Figure 3.22A**). This revealed the top two terms as cyclin-dependent protein kinase activity in addition to RNA polymerase II activity. This was due to a number of cyclin dependent Kinases (CDK)s, CDK11A/B, CDK12 and CDK13, as well as cyclins, Cyclin Y (CCNY), Cyclin-Y-like protein (CCNYL1), Cyclin K and Cyclin L-1, which were differentially phosphorylated in response to treatment with GR ligands. These identified proteins include cyclin-CDK complex-forming partners which are classified as transcription-regulating (213).

Figure 3.22B visualises the position of phosphorylation marks for each of the CDKs and cyclins, against the log2 fold-change induced by each of the ligand treatments and displays both the quantity of phospho-marks as well as the directionality induced by each of the GR-modulators (i.e. whether phosphorylation was increased or decreased).

Two distinct CDK11 genes are expressed as three protein isoforms which form complexes with cyclin L1 and cyclin L2. The CDK11A isoform also known as CDK11^{p110} is ubiquitously expressed whereas, CDK11B (CDK^{p58}) is expressed in G2/M phase of the cell cycle (214) and CDK^{p46} is specifically expressed during apoptosis (215). CDK11B is shown to be dually phosphorylated on residues Ser589 and Thr595 and PhosphoSitePlus database predicts the threonine residue to be regulated by CDK7. Additionally, another serine residue was identified however sequence similarity could not distinguish between the isoforms. Therefore, either CDK11B Ser283 or CDK11A Ser271 was modified which is predicted to be a casein kinase II substrate motif.

Cyclin L1 functions in partnership with CDK11 and mainly showed a reduction in phosphorylation marks by the ligands. With a total of 4 residues which were differentially modified, Cyclin L1 showed the greatest number of modifications out of the identified cyclins. Cyclin Y and cyclin-Y-like protein 1 were differentially phosphorylated by each of the GR ligands but are the only cyclin whose partner CDKs (CDK14 or CDK16), were not identified. Phosphorylation at residue Ser326 occurs independent of CDK14 and such modification permits 14-3-3 protein binding which increases the affinity of the interaction with CDK14 (216). Closely related cyclin-Y-like protein 1 also forms a complex with CDK16. The expression of Cyclin Y is regulated by cell cycle phase and has been shown to localise to the plasma membrane and participate in Wnt/B-catenin signalling cascade.
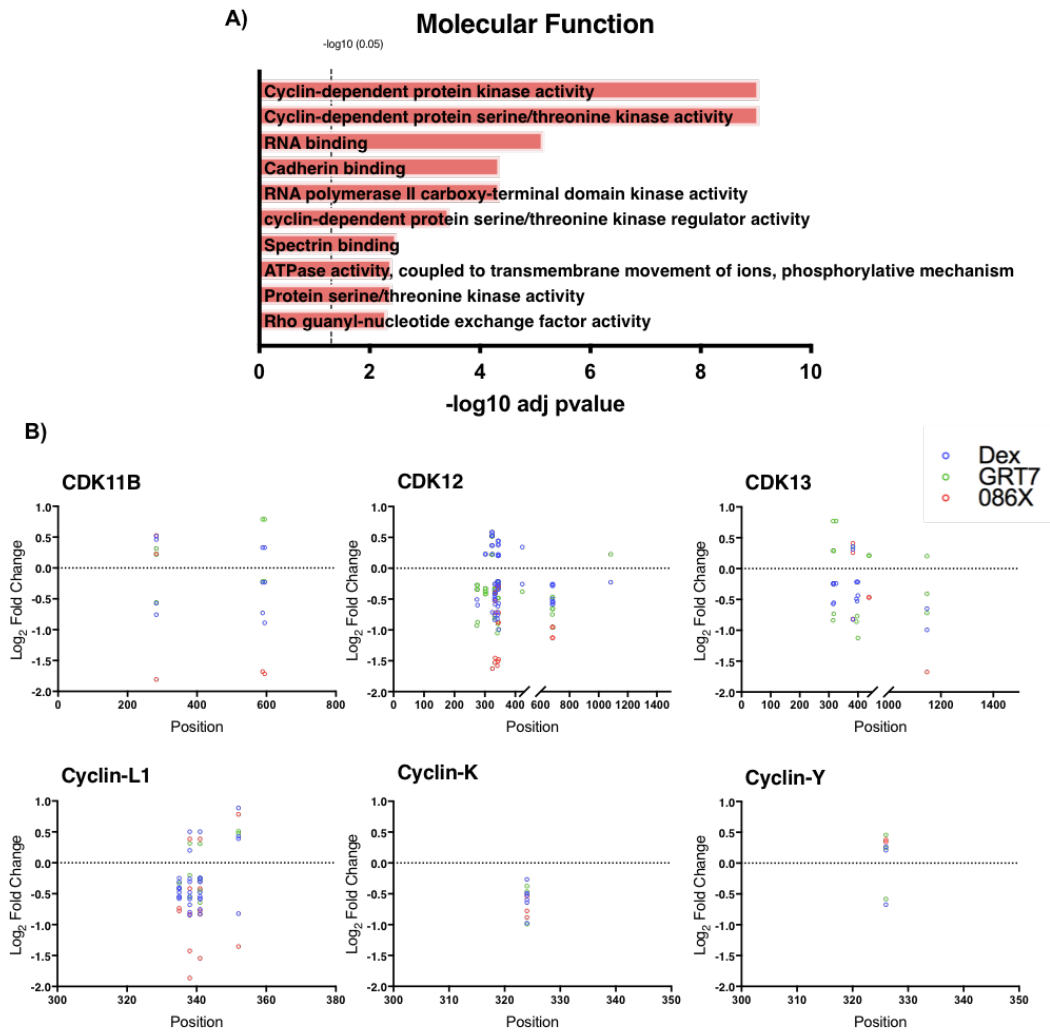
Figure 3.22 Enrichment analysis of Gc regulated phosphoproteins identifies cyclin dependent kinases

A) Functional ontology analysis of all the common proteins differentially phosphorylated by the three GR-agonists. Enriched terms from molecular function database. Dotted line indicating significance equivalent to adj p.value<0.05. B) Plots showing the position of phosphorylation and log2 fold change induced by each ligand for each of the transcriptional CDKs and cyclins identified by the phosphoproteomics.

Cyclin K couples to both CDK12 and CDK13 to form individual complexes. The Cyclin K protein displayed a reduction in phosphorylation upon residue Ser324 by all three ligands. CDK12 and CDK13 were found to show the greatest change in phosphorylation by the number of modified residues. There were a small number of residues within both CDK12 and CDK13 which were modified by Dex and GRT7 but were not significantly modified by 086X, indicating there exists some disparity between the responses induced by each of the ligands.

CDK12 and CDK13 are homologues and both associate with cyclin K to form a complex; the two kinases have very similar kinase domains but have both overlapping and distinct functions (217). Compared to other CDKs, CDK12 and CDK13 are much larger molecules **(Figure 3.23).** In addition to the kinase domain, which is shared with other transcriptional kinases, CDK12 and CDK13 each contain low complexity, arginine-serine (RS) region within the N-terminus (218). This region is thought to facilitate interactions with other proteins of the RS family such as splicing factors. The large majority of residues which were differentially regulated are found within this arginine-serine (RS) region for both CDK12 and CDK13 (marked with arrows **Figure 3.23**). NetworKIN was used to predict the responsible upstream kinases. For CDK12, the highest scoring kinase was CDK4 for Ser334. Other predicted kinases include PKCβ for Ser341 and CAMKIIα for Ser332 and Ser343. The highest scoring predicted kinase for CDK13 was CDK1 for residues Ser325, Ser400 and S1147. CDK2 was also predicted to regulate the same residues in CDK13, although with not as high a predictive score. This provides some indication of cross-talk between cell cycle regulating CDKs and transcriptional CDKs in response to GR activation. The effects of the observed differential phosphorylation of these transcriptional kinases shall be explored further in the following chapter.

CDK12	Ser276	Ser323	Ser332	Ser333	Ser334	Ser341	Ser343	Ser423
CaMKIIα			1.73				1.66	
MCPH1	1.58			1.57	1.58			1.58
BRCA1	1.58			1.57	1.58			1.58
PTIP	1.58			1.57	1.58			1.58
MDC1	1.58			1.57	1.58			1.58
BARD1	1.58			1.57	1.58			1.58
14-3-3 family (αβΘHζεƳ)	1.66		1.66	1.66	1.66		1.66	
MAPK3 (ERK1)		1.57						
PKCβ						1.85		
CDK4					2.01			

CDK13	Ser315	Ser317	Ser325	Ser383	Ser397	Ser400	Ser1147
CaMKIIα	1.90						
MCPH1						1.58	
BRCA1						1.79	
PTIP						1.58	
MDC1						1.58	
BARD1						1.58	
14-3-3 family (αβΘHζεƳ)	1.66				1.66		
MAPK3 (ERK1)		1.63		1.76			
MAPK1 (ERK2)				1.90			
CDK1			2.72			3.14	2.40
CDK2			1.74			1.74	1.74

Figure 3.23 CDK12 and CDK13 structure and differentially regulated residues

Diagram of CDK12 and CDK13 structure (based on figure from Lui et.al 2018). Arrows correspond to all of the differentially phosphorylated residues following 10 min treatment with GR-ligand. Blue arrow for residues appearing in the table below. Orange arrow represents residues with no predicted kinase from NetworKIN. Tables show the differentially phosphorylated residues and predicted phosphorylating kinase generated using NetworKIN using 1.5 as minimum score cut off. Numbers correspond to the score of the kinase for that residue. CDK: cyclin dependent kinase. KD: Kinase domain. PRM: Proline rich motifs. RS: Arginine/Serine rich motifs.

3.3 Discussion

Analysis of the global changes in the phosphoproteome following GR activation is a powerful tool for understanding Gc-induced signalling mechanisms. This approach provided an insightful snapshot into the signalling pathways engaged shortly after ligand exposure, at a timepoint when GR is predominantly located within the cytoplasm. Using three potency matched ligands to compare the acute effect of steroidal vs non-steroidal ligands, as well as compounds which regulate differing genomic transcriptional profiles, and showed there was a common signature of differentially regulated phosphoproteins. This implies that even though the transcriptional response to Dex, GRT7 and 086X is distinct, the initial steps following ligand engagement and GR activation are shared.

The different ligands did however, demonstrate differences in the extent of the log2 fold change and, in some cases, the directionality of change. These differences observed between the ligands are most likely due to ligand-induced changes of GR conformation following binding (186, 219), and would be an interesting insight into selective GR-ligands however, further investigation into this effect was not within the scope of this study.

Phosphorylation is a transient modification which can alter the functional activity of a protein. The presence of a phosphorylation mark requires the integrated balance between both kinase and phosphatase activity. The GR protein itself is subject to phosphorylation by Ser/Thr kinases in both a ligand -dependent and -independent manner (38, 42) (summarised in **Figure 1.5**). However, GR was not identified by the phosphoproteomics as differentially phosphorylated by any GR-ligands. This suggests that ligand induced phosphorylation of the GR protein either: does not occur by 10 minutes; has not reached detectable levels, or the protein has been phosphorylated and dephosphorylated prior to lysis. Most published studies investigating GR phosphorylation use 1 hour of Gc exposure to detect changes in phosphorylation (42, 220, 221) and therefore detection of GR phosphorylation at the 10 minute timepoint is likely to be premature.

3.3.1 Location and functionality of Gc-regulated phosphopeptides

The diversity of the identified Gc-regulated phosphoproteins highlights the range of cellular processes which are affected within 10 minutes of GR-ligand binding. The subcellular localisation of the identified phosphoproteins demonstrates that Gc induce cellular effects reaching multiple compartments of the cell. The majority of proteins were predicted to be located within the nucleus and involved in genomic activities at a time prior to GR-nuclear entry.

3.3.1.1 Membrane and Cytoskeleton

Enrichment analysis implicated the identified proteins involved in processes related to organelle and cytoskeleton organisation. The identification of proteins known to form functional complexes, such as three adductin isoforms (α,β,γ)(203), cofilin and cap1, and the identification of phosphorylation sites with known regulatory activity strongly supports the existence of a coordinated response to Gc which regulates membrane/cytoskeletal dynamics (204). Gc were shown to regulate the stability of the cytoskeleton network and actin filament capping and was detected experimentally as Dex-responsive reduction of cofilin-1 phosphorylation was detected 5 minutes after treatment and returned to initial levels by 60 minutes. Phosphorylation negatively regulates cofilin-1 activity, the unphosphorylated form depolymerises actin resulting in instability (205). This suggests Dex rapidly and transiently destabilises the cytoskeleton. This may be required to redistribute actin for cellular responses such as barrier function, adhesion and migration, all of which are known physiological processes downstream of steroid hormone action (222).

The large structural scaffold protein AHNAK was found to have the greatest number of differentially phosphorylated residues by all GR ligands. Closely related AHANK2 was also differentially modified, although the relevance of these two proteins for Gc signalling is unknown. AHANK has been implicated in TGF-β signalling (199), calcium homeostasis (223) as well as DNA repair (224). Relatively little is known about the function of AHNAK 2, although homology suggests some functions may be shared. Furthermore Networkin-based prediction of regulatory kinases only confidently predicted PKCα to modulate one of the identified residues. Knowledge of the location of the modified residues, largely within N- and C-terminal regions may provide an indication of which processes and functions are regulated as a result of GR activation. The modified domains have been shown to be required for the assembly of molecular complexes, and interactions with actin, voltage-gated Ca^{2+} channels (225) or annexin A2 respectively (197, 226). AHNAK has been shown previously to form a complex with annexin A2 which co-localises with lipid raft components (226); both of which were differentially phosphorylated in this study and were suggested to functionally interact by network analysis. These protein complexes are involved in membrane ruffling, cell-cell contacts and endocytic events which may provide indication as to how AHNAK is associated with epithelial-mesenchymal transition (EMT) and tumour metastasis (197). Future investigation into how Dex affects AHNAK in these processes, particularly in the context of cancer will be important.

3.3.2 Implicated non-genomic pathways

3.3.2.1 Kinase motif analysis

Using motif analysis, I identified potential kinases which are likely involved in relaying rapid-signals following GR activation. For all ligands, the kinases identified from the KEA2 enrichment largely reflect the motif analysis, including the top-identified kinases GSK3, MAPK, MTOR and CDKs. The network analysis highlighted three kinase clusters, CDKs, mTOR and MAPK. These multi-functional kinases and their associated pathways broadly regulate cell-cycle, metabolism and responses to external stimuli respectively, all which are well established to be modulated by Gc (91, 93, 95, 227).

Many of the implicated kinases have previously been associated with Gc signalling, and although not detected, are capable of phosphorylating GR. GSK-3β can affect the activity of GR by direct phosphorylation and is required for transcriptional outputs (43, 221). This has also been shown for CDK5, whereby CDK5 phosphorylated GR upon multiple serine residues and inhibition facilitates expression of anti-inflammatory Gc-target genes (228, 229). The integration of different signalling pathways which converge to modify the phosphorylation profile of GR, has been suggested to direct particular patterns of transcriptional responses (36). Despite GR itself not being shown to be differentially phosphorylated in the phosphoproteomics analysis, the profile of proteins which were identified may provide a clue as to how of these kinases can affect GR-transcriptional outcomes.

3.3.2.2 mTOR and CDK12

The repressor of mRNA translation, eukaryotic translation initiation factor EIF4EBP1 (4E-BP1) was found to be differentially phosphorylated by Gc-ligands on residues Thr37, Ser65 and Thr70. Phosphorylation of these sites has been shown to result in 4E-BP1 inactivation, resulting in its dissociation from the complex which promotes the translation of mTORC1-dependent mRNAs. (227). Phosphoproteomics found acute Dex treatment induced a median reduction in phosphorylation of 4E-BP1, which suggests that translation is suppressed.

Previous studies have shown that the phosphorylation of 4E-BP1 upon residues Thr37 and Thr46 by mTOR, generates a substrate sequence which is recognised by CDK12. This pre-phosphorylation then permits phosphorylation by CDK12 at positions S65 and T70 to release the mRNA 5'cap binding repressor and to promote the translation of mRNAs involved in cell proliferation, DNA repair and mitotic chromosome stability. Furthermore, 4E-BP1 phosphorylated on residues Ser65 and Thr79 is localised to the mitotic spindle, in absence of CDK12 a number of mitotic defects occur including spindle pole detachment (230). As GR also

associates with the mitotic spindle to govern appropriate cell division (231). This demonstrates a potential point of cross-talk between mTOR, CDK12 and GR.

3.3.2.3 Membrane initiated Gc Signals

An important unanswered question in Gc biology is how Gc-signals are relayed from the plasma membrane. Gc-induced signals at the plasma membrane, has alluded to the existence of a membrane-associated GR (97, 98). Closely related steroid receptors each have a related membrane receptor, encoded by genes distinct from that of the cytosolic nuclear receptor (212). This has raised the question of whether Gc-initiated signalling from the cell membrane is through cytosolic-GR activated at the membrane- potentially held within lipid rafts, a spice variant of the NR3C1 gene or mGR encoded by a distinct gene.

Early studies investigating membrane-initiated signalling of Gc, used BSA-conjugated Gc in order to delineate non-genomic effects whereby Gc cannot diffuse through the plasma membrane. Studies using BSA conjugated Dex have been questioned due to the detection of free-non-covalently bound Dex in some commercial preparations. However, this free Dex has since been shown to not be biologically available and cannot cross the plasma membrane (195), which supports the validity of the reported findings.

Increased phosphorylation of p38 MAPK is induced by Dex-BSA in monocytes (91). In hippocampal neurons, stimulation with cortisol-BSA induces activation of PKA upstream of serine kinases including PKC, ERK and non-receptor tyrosine kinase src and phospholipase C (PLC). These responses were G-protein dependent (232, 233) suggesting the involvement of a GPCR in relaying the downstream signals and reveal that a spectrum of signalling activity is directly initiated from the membrane.

Proteomics of cells treated with BSA-cort identified the differential expression of proteins in the cytoplasmic and nuclear fractions. Analysis identified pathways engaged from membrane signals that are known to be regulated at the genomic level by canonical GR signalling. Such pathways included: apoptosis, immunomodulatory and metabolic processes - providing an indication that rapid signals of membrane-origin may orchestrate processes to synergise with genomic effects (99). This corroborates my findings which suggest that non-genomic Gc-signals act to regulate the genomic action of GR.

BSA-Dex has also been shown result in Ser211 GR phosphorylation within 10 minutes and nuclear translocation (97), but did not lead to the upregulation of GILZ expression. However, membrane-initiated stimulation did lead to inhibitory phosphorylation of GSK-β and subsequent the release of β-catenin to translocate to the nucleus and upregulate the target gene c-myc (94). Gc target genes are not affected which is likely to be because GR in this scenario is unliganded

when it traffics into the nucleus, and therefore will not bind to GREs. This suggests that Dex-mediated signalling, arising from the cell membrane can functionally regulate gene expression.

3.3.2.4 Cyclic AMP (cAMP) and Ca^{2+} signals

The second messenger cAMP is rapidly produced following Gc stimulation (87); cAMP synthesis by adenylate cyclase then results in the rapid activation of PKA which can mobilise intracellular Ca^{2+} and activate transcription factor CREB. The G protein stimulatory protein $G_{\alpha s}$ is required for the signalling response and may be important for the regulation of certain Gc responsive genes (87).

Intracellular Ca^{2+} flux occurs within milliseconds and can lead to immediate signalling events. However, the precise effect of Gc upon intracellular calcium signalling, appears be context and cell type dependent and have been shown to both increase and reduce basal intracellular calcium concentrations (88). I found the differential phosphorylation of two calcium ATPases: sarcoplasmic/endoplasmic reticulum calcium ATPase 2 (ATP2A2) and plasma membrane (ATPase1) as well as a number of Ca2+ responsive proteins.

In a study using primary bronchial epithelial cells, Dex has been reported to rapidly decrease $[Ca^{2+}]i$ which prevents ATP-stimulated Cl- secretion. This effect of Dex occurs independently of GR via an adenylyl cyclase, PKA-dependent mechanism, terminating on the sarco-endoplasmic reticulum Ca2+ ATPase-pump (180). Furthermore, Dex has recently been shown to exert an inhibitory effect on $[Ca^{2+}]$ and cAMP-stimulated trans-epithelial Cl^- secretion through three different membrane K^+ ion channels. Modulation of channel activity by phosphorylation by PKA acting downstream of G-protein coupled activation of adenylyl cyclase in conjunction with GPCR-IP3-DAG signalling which activates PKCα to inhibit ion channel conductivity (89). The full significance of Dex regulation of calcium flux and ion channel activity in non-genomic signalling is undetermined but such studies implicate a number of kinase pathways associated with my data.

3.3.2.5 Lipid raft components

Analysis identified the differential phosphorylation of Caveolin-1 (CAV-1) and three Cavin proteins: Cavin-1 (PTRF), cavin-2 (SDPR), cavin-3 (PRKCDBP)) which all components of caveolae lipid rafts. These cholesterol enriched organelles are important for signal transduction by concentrating membrane receptors and signalling proteins together to form a hub of signalling proteins(104, 105). The high cholesterol content of caveolae concentrates ligand for association with steroid receptor. For other steroid receptors (ER, AR, PR), the membrane localisation of the

canonical receptor in association with caveolin, is a significant mechanism for the initiation of extranuclear signals (104-106).

Caveolin-1 has previously been shown to be phosphorylated in response to Dex which is abrogated by disrupting lipid rafts (93). GR and Caveolin-1 have been shown to co-localise (99) and a direct interaction between GR and caveolin-1 has been proven in A549 cells (93, 234). The phosphorylation of PKB is affected by Caveolin-1 KD which abrogates the anti-proliferative effect of Dex by blocking downstream phosphorylation of target kinases GSK-β and mTOR (93). This establishes the importance of the caveolae in the regulation of cell fate. Caveolin-1 knockdown also reduces ligand-induced phosphorylation of GR upon Ser211 in mouse neural progenitor cells (235) and A549 cells (93). This is reflected by changes in the GR-transcriptome. Dex-responsive genes targets associated with proliferation, cell cycle and actin-mediated cell migration and anti-inflammatory processes were all differentially regulated in absence of caveolin-1. (194, 235). Thus, the rapid phosphorylation of caveolin-related proteins following Dex treatment appears to reflect an active role for caveolin-regulated pathways in the transmission and regulation of Dex activity.

3.3.3 G-protein coupled receptors in Gc signalling

Overall, multiple lines of evidence point towards the activation of a G-protein coupled mechanism to initiate Gc downstream signalling. The regulation of many of the predicted regulatory kinases of Gc modulated phosphoproteins, stems from GPCR activity, although the responsible receptor(s) remain unknown.

3.3.3.1 GPER

Similar to GR, ER can localise to the plasma membrane, in association with caveolin-1 (104, 105), but ER also has a distinct membrane receptor. The membrane ER receptor (GPR30 known also as GPER) is structurally unrelated to nuclear ER and mediates non-genomic oestrogen-stimulated processes. Activation of the receptor activates adenylate cyclase to increase cAMP, resultant PKA activation and Ca^{2+} mobilisation occur through direct GPER-mediated activation of Gα subunit (236). Other reported effects include EGFR transactivation, and activation of MAPK and PI3K signalling (212, 236). In cancer GPER can modulate cell growth, migration and ER ligand-responsiveness (236).

3.3.3.2 GPCRs are differentially phosphorylated by Gc

The three GPCRs identified from the phosphoproteomics data set, are adhesion GPCRs - the second largest sub-family of GPCRs. Notably GPR30 has been classified as part of the largest family, the rhodopsin family (110, 211).

3.3.3.3 GPR123

Tissue expression (measured by gene expression from human protein atlas) is largely restricted to the central nervous system, particularly the brain but is also present in the pituitary and adrenal gland – which are Gc-associated tissues (209, 237). Furthermore, the AGDRA1 gene was upregulated by Dex and the only GPCR found to show Gc-responsive expression change, which implicates GPR123 in Gc-activity. I was unable to detect protein level expression of GPR123 in a panel of cell lines, including A549 cells – in which the phosphoproteomics that identified GPR123 as a target, was performed. This was attributed to unsuitable commercially available antibodies, which was also likely to be hampered by low levels of expression; mRNA expression was detectable by RT-qPCR although at low quantities. MCF-7 cells were found to have the highest relative-expression levels, M059K glial cells were the only brain-originating cell line tested but did not appear to express ADGRA1. This may be due to the malignant-transformation of the cells or, most likely, that they were not the most appropriate brain-originating cell-type. Other hormone-responsive tissue, such as brain restricted neuroendocrine cells, may have shown detectable expression.

The *Adgra1* KO mouse phenotype can display preweaning lethality with incomplete penetrance. Other phenotypes of homozygote KO mice include increased lean body mass with increased muscle content and a reduced level of total body fat, in addition to increased bone mineral content and abnormal bone structure (information from International mouse phenotyping consortium (238)). Such effects contrast the metabolic effects of long-term Gc treatment such as visceral obesity, muscle degradation and loss of bone mineral density (4), and implies a potential role of GPR123 in Gc biology.

3.3.3.4 GPR126

GPR126 is encoded by the ADGRG6 gene. The receptor is cleaved within the GAIN domain into the larger N-terminal fragment which forms the extracellular soluble protein part of the receptor and the C-terminal fragment which contains the 7-TM region. The structure of the extracellular N-terminal is formed of: Complement C1r/C1s, Uegf, Bmp1 (CUB), Pentraxin (PTX), Hormone Receptor (HormR), and GAIN domain. Recently, by utilising sequence-based bioinformatics a previously unknown region of the N-terminal receptor structure has been identified in Zebrafish. Between the PTX and HormR is the Sperm protein, Enterokinase and Agrin (SEA) domain which contains an alternative splice site which affects the confirmation of the receptor which consequently varies the basal activity of the receptor (239).

Tissue expression of GRP126 is detectable in most organs but is comparatively low in brain tissue and highly expressed in the lung, liver and bladder (209). I demonstrated that mRNA expression

was highest in Huh7 liver-derived and A539 lung cells, which supports current knowledge of GPR126 expression.

Previous studies identify GPR126 as being involved in regulation of Schwann cell myelination and ear canal formation in Zebrafish (240). The involvement of GPR126 upon peripheral nerve development has since been confirmed as an evolutionary conserved process in mice, and was also shown to affect heart development (241). KO mice generally exhibit embryonic lethality due to cardiac abnormalities and internal hemorrhaging, the few surviving mice are largely characterized by a lack of myelination in the PNS resulting in immobility (241). GPR126 is largely regarded as an orphan receptor although activation has been reported to be activated by type IV collagen – a major constituent of the basement membrane. This may be a developmental autocrine signal as Schwann cells secrete Collagen IV prior to myelination. During this process GPR126 has been shown to activate the $G\alpha_s$ protein to initiate cAMP-mediated activation of PKA signalling to drive differentiation (240). GPR126 is also implicated in angiogenesis; in both developmental and pathogenic contexts through the modulation of VEGFR2 transcription. Acting through cAMP-mediated activation of PKA and subsequent CREB activity, GPR126 stimulates STAT5 and GATA2 expression to positively modulate the formation of blood vessels. GPR126 knockdown aberrantly affected endothelial cell proliferation and migration required for angiogenesis (242).

3.3.3.5 CD97

The final GPCR, CD97 is encoded by the ADGRE5 gene. CD97 is detectable in most organs except parathyroid glands, ovaries, pancreas and skeletal muscle, and expression is largely found on surface of immune cells: lymphocytes, monocytes, macrophages, DC, granulocytes and smooth muscle (except microglia)(209). In line with this association with the immune system, CD97 is unregulated upon immune cell activation. The functional role of CD97 remains unresolved but has been implicated cell adhesion and migration through ECM contacts. There are four known ligands for CD97: CD55, a negative regulator of the complement cascade (243); CD90, a small membrane glycophosphatidylinositol (GPI) anchored protein; integrin α5β1 also known as fibronectin receptor (210) and Chondroitin sulphate (244), a component of the ECM. The specificity for each ligand is thought to be determined by the number and arrangement of EGF-like domains in the extracellular region, itself dependent on isoform expression which is controlled by alternate splicing. Like other adhesion GPRs the CD97 undergoes catalytic cleavage at the GPS motif within the GAIN domain, before reaching the cell surface and contains a hormone binding domain similar to that of GPR126. The N-terminal fragment known as the extracellular α-subunit is formed of 5 EGF domains making CD97 relatively larger than other adhesion GPCRs. The C-terminal fragment or transmembrane β-subunit, facilitates the non-

covalent interaction of the receptor with other subunits to form homo- and heterodimers (210, 244).

I found ADGRG6 mRNA expression to be highest from THP1 monocytic cells supporting that CD97 is highly expressed in immune cells. Expression of CD97 is associated with multiple cancers and is implicated in increased invasion and metastasis. ADGRE5 gene expression is upregulated in breast cancer cells, including MCF7 whereby knock-down has been shown to decrease proliferation and migration (245). CD97 protein expression has been shown to be increased by GM-CSF and reduced by LPS stimulation. Treatment with LPS also alters the mRNA expression of the predominantly expressed isoform (EGF1,2,5). I was unable to measure any significant changes in CD97 expression following Dex stimulation although did not investigate isoform expression.

Over expression of CD97 has been shown to reduce p65 protein expression and LPS-induced secretion of TNF-α, predicted to involve the nuclear translocation of PPARγ to suppress p65. (246) Given the reciprocal nature of p65 and GR, similar effect or involvement of GR may be worthy of future investigation.

3.3.3.6 Substrate identification using immunoblotting

Using substrate specific antibodies, I observed a potential Dex-responsive increase in PKA activity. Knock down of GPR126 greatly increased PKA substrate phosphorylation, particularly in A549 cells which suggests the receptor has an inhibitory effect. GPR126 activity has previously been associated with PKA and cAMP production via Gαs (240) and may induce an opposite effect via coupling to the inhibitory Gαi protein. The different distribution and intensity of the bands observed with CD97 knockdown may imply loss of engagement with particular proteins rather than inhibition of all downstream pathways. The effect of Dex upon PKC appeared to increase with Dex addition and showed greater levels of activity with GRP126 knockdown. Results from immunoblots are inconclusive due to technical disparities between replicates and do not paint a definitive picture of the activity of the GPCRs. However, the RNAi approach provides an indication that the GPCRs do modulate kinase signals following Gc treatment. More rigorous analysis is required and could be achieved, for example, by more specific analysis of direct substrate targets of PKA and PKC.

3.3.3.7 Tango Assay

The tango assay provided a platform to investigate whether the three identified GPCRs are directly activated by GR ligands. This system is advantageous as the assay does not require knowledge of the endogenous downstream signalling pathway or high receptor expression levels. However, even following optimisation of the transfection procedure the results were

inconclusive. The viability of the cells may account for the inconclusive readings which were measured by MTT assay in parallel. Transfection efficiency generally increased with the concentration of transfected pDNA, however for all conditions and treatments the 1200ng resulted in the lowest cell viability. With the exception of GPR123, which had the lowest transfection efficiency at 1200ng but was also reflected by low luciferase readings. Nevertheless, the reciprocal relationship between viability and transfection efficiency may require further optimisation. The TAT3 reporter was included as a transfection control and was successful at inducing luciferase expression in response to Dex. However, there was no dose-dependent increase between 100nM and 1µM which could be due to sub-optimal transfection efficiency. For cells overexpressing the GPCRs, I did not detect an effect of Dex upon cell proliferation at the 18-hour timepoint. Although this may be an interesting factor to investigate further due to the association of GPR126 and CD97 in some cancers (108, 245, 247).

None of the investigated receptors were validated for their activity in the original PRESTO-TANGO publication. The authors reveal that no receptors from the adhesion family were attempted for validation, which is likely due to the large number of orphan members in the adhesion family (109). However, GPER is known to be activated by β-oestradiol and failed to show evidence of stimulation by the assay. A GPER-selective agonist G-1 could be utilised in future to validate activity (248).

GPER is the only GRCR in this study confirmed to interact with β -arrestin 2 (212). Four arrestin proteins exist although, only the non-visual forms β-arrestin-1, -2 are ubiquitously expressed. Some receptors may preferentially interact with a particular arrestin protein (249). The construct used in these cells was for β-arrestin-2 recruitment only. Therefore, a potential explanation for inconclusive results could be that these receptors preferentially interact with β-arrestin-1 which requires further exploration. Particularly, as β-arrestin-1 is reported to affect GR signalling through a direct-interaction (250).

A further way to increase the efficiency of the assay would have been to generate stably expressing cells for each receptor however, this could not have been achieved within the timeframe of the study but would be an important element of future work.

3.3.4 Non-Genomic Signals feed-forward to the Nucleus

Analysis detected that the majority of modified phospho-proteins were located in the nucleus. The differential phosphorylation of chromatin re-modelling factors, suggest the chromatin landscape is modified prior to GR-nuclear entry. SWI/SNF subunits interact to recruit EP300 co-activator protein required to modify chromatin accessibly to permit the transcription of GR-regulated genes (251). Differential phosphorylation was also detected on transcription factor

and co-regulator proteins such as AFF4 - a component of the SEC (super elongation complex) which acts as a central scaffold for the recruitment of other proteins involved in productive transcriptional progression. Furthermore, transcription regulating CDKs and their partner cyclins were identified, supporting the validity of the identified targets. The implications of these CDKs will be evaluated further in the next chapter. Overall, these findings strongly signify that the rapid signals following GR activation and prior to GR's nuclear entry, modify factors potentially in preparation for GR's genomic activity. These two processes are generally considered as independent and distinct processes and considering these processes together will advance understanding of GR's complex mechanism.

3.3.5 Biological Relevance

The movement of GR protein within the cell is often presented in a simplified manner as the exact mechanism is not fully understood. Imaging often provides only a snapshot of the localisation of GR at a given time, which does not capture the dynamic process in its entirety. The conveyor belt hypothesis, presented by *Kolodkin et al (252)* addresses how nuclear receptors, such as GR, can have different localisations at rest, in addition to how cytoplasmic proteins come into contact with hydrophobic ligands that can get trapped in the plasma membrane. The theory suggests that GR is constantly shuttled between the membrane and the nucleus. Unliganded GR is actively transported out of the nucleus – at a faster rate than import therefore, only minor levels of GR are located in the nucleus when low levels of ligand are present. Exported GR is then shuttled back to the membrane in preparation for binding to more of it's lipophilic ligand. Ligand treatment shifts this balance. High concentrations of ligand molecules, in relation to receptor, bind to activate GR. As a result, GR is transported into the nucleus and the nuclear import rate exceeds the export –nuclear GR forms stable interactions with chromatin, which further increases the nuclear retention time.

There are multiple theories regarding how Gc can induce rapid kinase signalling (summarised in Introduction 1.6). However, it is not clear how such a large proportion of nuclear proteins are differentially phosphorylated so rapidly. As GR itself does not possess kinase or phosphatase capacity, signalling must be initiated via other interactions. GR is phosphorylated by a number of kinases including MAPK and CDKs (11, 36, 38, 40) (summarised in Introduction 1.4.1), signifying a direct interaction. These were also putative phosphorylating kinases of the differentially regulated phospho-targets. Signalling cascades, by nature, amplify signals to relay information quickly in order to initiate a change in cellular behaviour. Furthermore, many signalling cascades terminate upon transcription factors resulting in a genomic effect. Given the short time frame that differential phosphorylation was detected following GR ligand addition, it is likely that this initiated a signalling event from the membrane to reach the nucleus (93, 94).

Proposed theories regarding how non-genomic signalling of GR occurs are not mutually exclusive and the regulation of the identified phosphotargets may proceed via multiple mechanisms. Firstly, that the GR-ligand indirectly activates signalling, independent of GR, by integrating within the plasma membrane to alter the fluidity and initiate signalling from lipid rafts (111). Secondly, the release of signalling proteins sequestered in the GR-chaperone complex, permits their activation and interaction with other substrates and downstream signalling pathways. GR is capable of forming large complexes through two protein interaction domains: AF1 and AF2, which could be a potential point of recruitment for kinases and adaptors within the cytoplasm to modulate signalling (1, 60). Finally, GR has been shown to slow microtubule growth in order to shuttle towards the nucleus - which may increase the interaction time and potential with other kinases and substrates on the microtubules (186).

An interesting point for consideration is that GRT7 displayed a similar phophoprofile as the other two ligands yet, GRT7-stimulated translocation of GR to the nucleus is delayed and has been shown to take up to three hours (186). This indicates that ligand-initiated signalling processes do not require nuclear entry of the GR-ligand complex. Similarly, as the GRT7 compound is a non-steroidal ligand it is less likely that the effects are solely due to ligand-induced changes in membrane fluidity.

Each of these theories could be tested in a number of ways. Firstly, using siRNA knockdown of GR, parallel treatment with the ligands to would establish whether changes in membrane fluidity result in the same ligand-induced cellular effect. Microtubule inhibitors could be utilised to disrupt the network and delay GR translocation. This would determine whether the microtubules are important for interactions with effector proteins (187). More in-depth exploration of the GR interactome using nuclear and cytoplasmic fractions, in A549 cells treated with ligands at rapid time points (up to 30 minutes), would help shed light on implicated proteins. The findings could then be confirmed using specific kinase inhibitors or siRNA targeting key upstream proteins shown to interact with GR. Modification of GR protein including a membrane anchored GR or mutant protein lacking NLS1 and NLS2 domains to prevent translocation, would help to delineate the localisation of GR in relation to which pathways are engaged.

One further question to explore would be whether the profile of differentially phosphorylated proteins would also be observed in healthy lung epithelial cells (as opposed to an immortalised cell line) and whether the induced effects are shared across different tissues. GR is ubiquitously expressed yet, the transcriptional outcomes of GR activity are highly tissue specific (72, 78). Given that three GR ligands with distinct transcriptional profiles induced a similar phosphoproteome would support a hypothesis that the rapid cellular response following GR-

ligand binding is a common mechanism. The outcome of which would depend on factors such as tissue-specific protein expression and by extension the importance of the regulated molecular function to that cell type. Similarly, the expression of the identified target phosphoproteins, as well as the effector proteins and kinases in target cells, directly affects which pathways are engaged. Identified biological functions which are ubiquitous such as ''organelle organisation' and 'chromosome organisation', would be predicted to be shared across tissues as they maintain basic cellular homeostasis. Likewise, functions associated with gene expression, 'mRNA processing and splicing' would also be hypothesised to be shared although, the particular expressed genes would be dependent on areas of active chromatin and active transcription factors. More specific process such as 'Cadherin binding' would be predicted to be a particular effect of Gc upon epithelial cells. Identifying the regulating upstream kinases of the regulated proteins would be important for validating such theories in addition to investigating whether similar a Gc-induced phosphoprofile occurs in other cell types.

Biological functions associated with the regulation of the cell cycle are known to be affected by GR activation (93, 103, 253) and a number of predicted regulating kinases of the phosphotargets: GSK3, mTOR, CDKs are mediators of overactivated pathways in cancer. However, as the data set was derived from a cancer cell line then enriched functions associated with cell-cycle regulation could reflect the oncogenic transformation of A549 cells. Nevertheless, the nature of the screening to identify differentially regulated phosphopeptides by GR-ligands, in comparison to the vehicle should mitigate this and only identify processes affected as a result of GR-activation. The effect of activated-GR's rapid engagement with these kinases and pathways requires further exploration to determine functional effect upon cell proliferation but may highlight a point of modulation which could be targeted for clinical benefit.

3.3.5.1 Ligand Specificity

The two compounds, GRT7 and 086X, generated by GlaxoSmithKline were developed to specifically target GR. Given the close evolutionary relationship there is likely to be some affinity of the ligands towards other steroid receptors, particularly mineralocorticoid receptor (MR). During development the compounds were screened to determine activity at other steroid receptors. pIC$_{50}$ values 086X showed activity was >1000-fold greater for GR in comparison to MR (184). Equally GRT7 has been shown to have a minimal effect upon a MR reporter system in A549 cells (187). In order to demonstrate that these ligands are acting through GR-activation, parallel repeat experiments could be performed using a co-treatment with Spironoactone, a specific antagonist of the MR. However, using this approach would only validate that the compounds do not target MR. A more thorough approach to test ligand-receptor specificity would involve repeating the experiments using A549 cells subject to siRNA knockdown to reduce

the expression of GR. Then measurable effects, such as phosphorylation of identified protein targets, could then be directly attributed to ligands acting though GR. An alternate supporting experiment would also involve a tetracycline (TET)-inducible system in cells such as HEK293 deficient in endogenous functional GR. This method, as reported in *Morgan et al* (26)(Fig S4-6), would allow comparison between deficient and cells stably expressing GR in order to confirm GR's role.

3.3.6 Technical challenges

A caveat of the SILAC phosphoproteomic experiment is that it was carried out on only one experimental occasion, which can reduce the robustness of the generated results. In order to mitigate this, a minimum of three biological replicates for each treatment were prepared in parallel and included in the analysis to capture biological variation. In addition, prior to LC-MS/MS quantification samples were pooled at equal ratios to minimise experimentally-induced and sample-handling error. Further biological repeats would be beneficial to corroborating the results with the identification of a comparable phosphotarget profile. Hence, further validation of the findings by western blot to confirm the identified proteins are Dex-regulated phosphotargets is required to improve the confidence and validity of the findings.

Phosphorylation is a highly dynamic process. Therefore, the fluidity of change in phospho-isoforms makes quantification of the directionality of change in comparison to the vehicle challenging. Many identified phospho-marks were not measured with the same directionality of log2FC between replicates. Another limitation of SILAC phosphoproteomics, a bottom-up approach, is that the temporal pattern of phospho- modifications present along the full protein length is lost. As the protein is fragmented prior to MS, it is impossible to tell whether the protein is phosphorylated in two distal locations at the same time (158).

The particular enrichment process, using titanium dioxide to select the phosphopeptides selectively favours serine and threonine phospho-marks and does not enrich for tyrosine residues. Therefore, the activity of tyrosine kinases is not detected, including non-receptor tyrosine kinase c-src kinase which has been shown to mediate some rapid signalling effects of Gc (232).

Data mining attempts to understand the outputs of hypothesis generating methods, such as phospho-proteomics, are limited by the published information within databases. For example, network analysis of protein-protein connections are based on functional evidence and will not show novel-interactions. Similarly, database searches to predict regulating kinases eg Networkin and phosphoSite Plus, can provide an indication of the regulating kinase. However, data is often

from large scale studies and particular queried phosphosites, if present, have no further information due to lack of experimental validation.

In order to validate the findings from the phosphoproteomics, I sought to confirm the rapid Dex-induced change in phosphorylation status of particular residues. However, a major limiting factor was the commercial availability of phospho-specific antibodies, without which, the validation of Gc-induced phosphorylation of specific proteins was difficult. The use of substrate-specific antibodies attempted to mitigate the challenge as they detect the cellular changes in phosphorylation marks regulated by a particular kinase although results were often difficult to interpret. Taken with the lack of functionally validated-antibodies for the GPCRs of interest to conform knockdown, the substrate antibodies were an imprecise method of investigating the downstream signals and functionality of the GPCRs.

Instead, I chose to further investigate the differentially regulated proteins associated with nuclear signalling since Dex is used therapeutically for its long-lasting transcriptional effects upon inflammatory genes. In the next chapter I explore the relationship between two differentially phosphorylated kinases, CDK12 and CDK13 function and their involvement in GR genomic activity.

Chapter 4: Nuclear signals and the role of CDK12 and CDK13 in GR-regulated transcription

4.1 Introduction

Functional ontology analysis in the previous chapter implicated the regulation of RNA polymerase II following the rapid activation of GR. This was due to the modification of a number of transcription-regulating, cyclin-dependent kinases and partner cyclins. Amongst those identified were CDK12 and CDK13, highly homologous kinases which both partner with cyclin K (254) – which was also identified as differentially phosphorylated. Active transcription is tightly regulated by the phosphorylation status of Rpb1, the large subunit of RNA polymerase II. The C-terminal domain (CTD) of Rpb1 contains 52 repeats of a heptad consensus sequence (YSPTSPS); the serine and threonine residues are phosphorylated by these transcription-regulating CDKs. The precise pattern of residue phosphorylation of the CTD consensus sequence, corresponds to active stages of the transcription cycle (outlined in **Figure 1.7**). Therefore, the activity of transcriptional CDKs is co-ordinated to regulate RNA polymerase II processivity and co-transcriptional processing of mRNA transcripts. This chapter aims to explore the involvement of CDK12 and CDK13 in the genomic action of GR using pharmacologic inhibition of CDK12 and CDK13. This entails examining the effect of acute treatment Dex on the phosphorylation status of Rpb1 CTD and subsequent effects upon GR-regulated gene expression.

4.2 Results

4.2.1 Dexamethasone affects the phosphorylation pattern of Rpb1 CTD

In order to investigate the potential effects of acute Gc-induced regulation of RNA polymerase II activity, A549 cells were treated with Dex over a time course of 60 minutes. Cells were then lysed and the phosphorylation pattern of the Rpb1 CTD, was assessed by immunoblot (**Figure 4.1**). Phosphorylation on the second serine residue of the CTD consensus sequence (referred to as Serine 2), showed a gradual increase up to 15 minutes which declined by 60 minutes. Serine 5 (the fifth serine residue within the consensus) phosphorylation showed a similar pattern although, quantification of three independent experiments suggests the level of Ser5 phosphorylation remains unchanged by Dex. Conversely, the level of serine 7 phosphorylation was greatest at 0 minutes and declined over the time course. These rapid changes in phosphorylation on Rpb1 are consistent with the pattern during early stages of transcription initiation, and suggests Gc signalling feeds-forward to the nucleus to prime the transcription machinery in preparation for genomic responses.
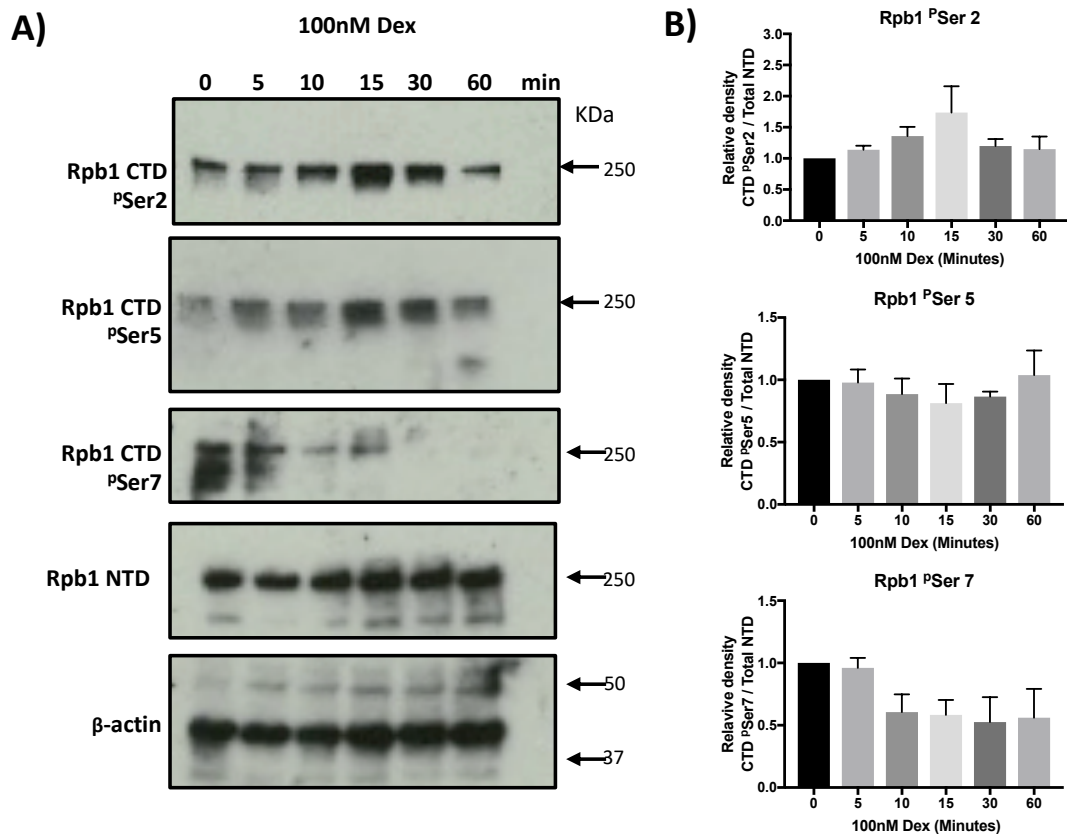
Figure 4.1 RNA Polymerase II CTD phosphorylation in response to Dexamethasone.

*A549 cells were treated with 100nM Dex over a time course up to 60 minutes. Samples were then lysed and protein expression was analysed by Immunoblot using 10µg protein lysates. Specific antibodies against CTD phosphorylated serine residues 2, 5 and 7 of the Rpb1 large subunit of RNA polymerase II and total NTD. **A)** Representative blots shown from three independent experiments. **B)** Densitometry was used to quantify the relative density of CTD phosphorylation in comparison to the NTD and normalised to β-actin. Shown is the mean ± SEM of measurements quantified from three independent experiments (n=3). CTD: C-terminal domain. NTD: N-terminal domain*

4.2.1.1 Assessment of Rpb1 phosphorylation using CDK Inhibitors

To further examine the potential role of CDK12 and CDK13 upon the regulation of GR-target genes I used two compounds to inhibit the activity transcriptional CDKs: flavopiridol (FVP) and THZ531. FVP is a potent CDK inhibitor which acts by binding uncompetitively to the ATP binding site of CDK enzymes to inhibit kinase activity (255). Although FVP preferentially inhibits CDK9, the activity of other cell cycle-regulating and transcriptional CDKs including CDK7, CDK12 and CDK13 are also inhibited. The inhibitor THZ531, was specifically designed to covalently bind to a cysteine residue unique to CDK12 and CDK13 (Cys1039 and Cys1017 respectively). THZ531 therefore, selectively and irreversibly inhibits CDK12 and CDK13 and is x100-fold less effective towards CDK7 and CDK9 (256). CDK12 has been mainly associated with phosphorylating the serine 2 residue on the CTD of Rpb1 (218, 256) which is sensitive to inhibition by FVP. In effort to assess the effect of CDK inhibition upon Rpb1 phosphorylation, A549 cells were pre-treated

with 50nM or 500nM CDK inhibitors for 30 minutes then treated with 100nM Dex for a time course of 60 minutes. The phosphorylation status of Ser2 of the Rpb1 CTD heptad repeat was assessed by immunoblot, as this is the residue in which CDK12 and CDK13 preferentially regulate (254, 257). **Figure 4.2** shows that in absence of inhibition, Dex increases the level of Ser2 phosphorylation up to 15 minutes after which, the level of phosphorylation is reduced. This is consistent with the pattern demonstrated previously. Pre-treatment with 50nM FVP does not reduce global ^{P}Ser2 levels however, the decrease in Ser2 after 15 minutes of Dex exposure as previously shown, is not observed. At higher concentrations of FVP, the phosphorylation levels are significantly reduced, although not completely abolished. This is likely due to the inhibition of both Ser2 kinases, CDK9 and CDK12. Specific inhibition by THZ531 does not significantly reduce levels of phosphorylation at either concentration in comparison to Dex alone. At 500nM pre-treatment shows no effect on the baseline but appears to reduce the Dex-induced increase in phosphorylation. Therefore, CDK12 and CDK13 may be specifically responsible for the Dex-mediated changes in Ser 2 phosphorylation, beyond the activity of CDK9.

I next sought to determine the effect upon phosphorylation of CTD residues at a later time point when activated-GR is transcriptionally active. By pre-treating cells with CDK inhibitors for 30 minutes, cells were then treated with 100nM Dex for 4 hours to investigate the levels of Ser2 phosphorylation. As shown in **Figure 4.3** Dex alone significantly reduces the quantified level of ^{P}Ser2 at this time point. 50nM FVP pre-treatment reduced the vehicle and Dex treated levels of Ser2 below 50% of the normalised level of that in absence of CDK inhibition. At 500nM the effect was maintained but not decreased any further. THZ531 also reduced the relative density of detected Ser2 phosphorylation to below half that of the condition without CDK inhibition, for both high and low concentrations. In addition, Dex treatment demonstrated a significant reduction in the quantified levels of Ser2 phosphorylation in comparison to the vehicle, again supporting that Dex affects Ser2 phosphorylation dynamics upon RNA polymerase II.

A recent study by Tellier et.al (258), suggested that CDK12 may also be a Ser5 kinase therefore I also investigated the Ser5 phosphorylation status as previously described. Pre-treatment with the CDK inhibitors resulted in a small reduction in phosphorylation across all conditions in comparison to the DMSO-vehicle. Although, for both inhibitors, THZ531 in particular, the reduction was not to as great an extent as the reduction in ^{P}Ser2. Likewise, no significant Dex-mediated effects were measured for ^{P}Ser5 in comparison to the vehicle. From this it would appear that Dex increases Ser2 phosphorylation at early timepoints which later leads to a reduction but that the effects on Ser5 phosphorylation are less pronounced.
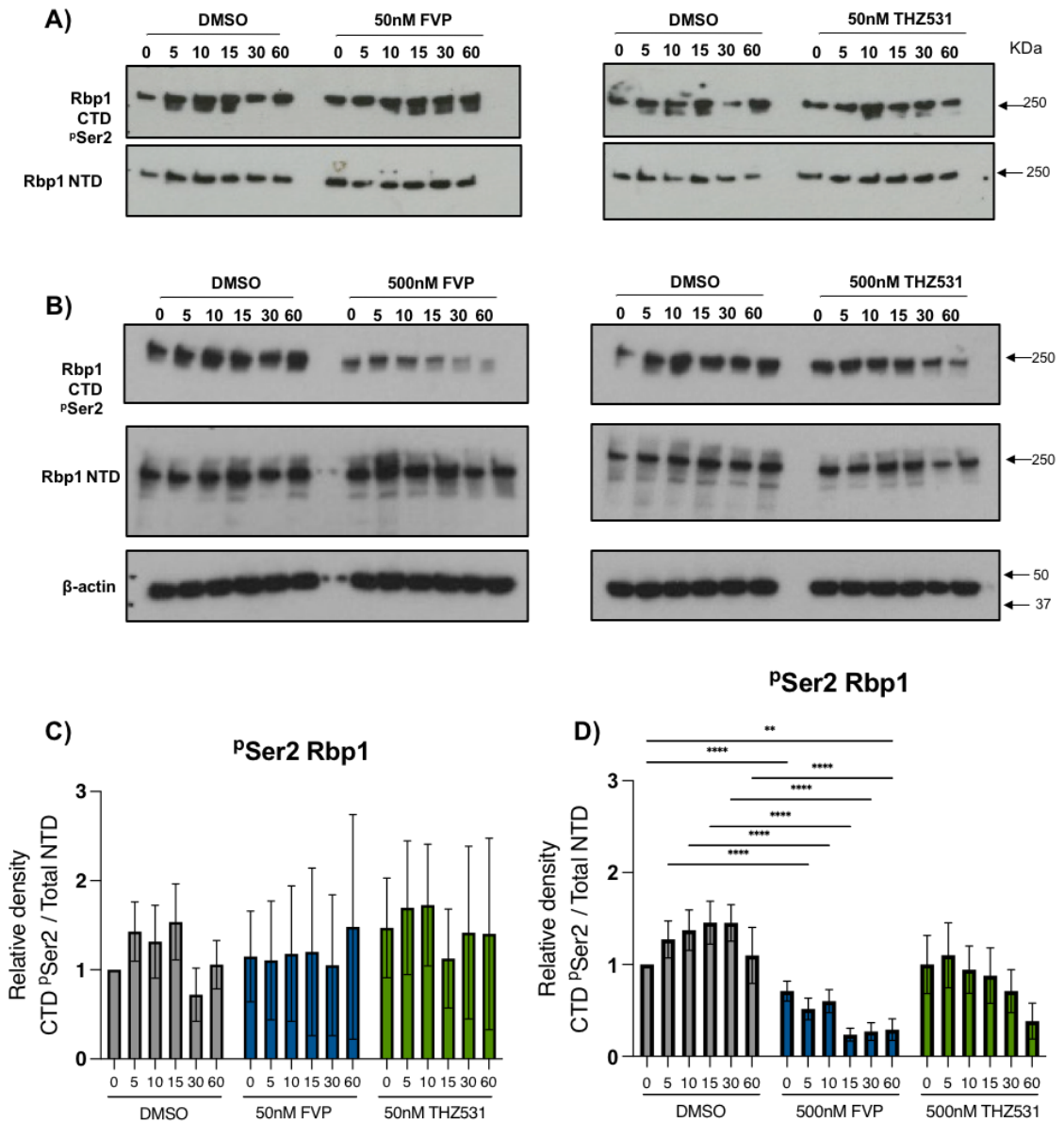
Figure 4.2 Effect of CDK inhibition on Rpb1 CTD Serine 2 phosphorylation with acute Dexamethasone treatment

A549 cells were pre-treated with FVP or THZ531 (either 50nM (A) or 500nM (B)) before being treated with 100nM Dex over a time course up to 60 minutes. Samples were then lysed and protein expression was analysed by Immunoblot using 10μg protein lysates. Specific antibodies against CTD phosphorylated serine 2 residue of the Rpb1 large subunit of RNA polymerase II and total NTD. Representative blots are shown from three independent experiments. Densitometry was used to quantify the relative density of CTD phosphorylation in comparison to the NTD and normalised to β-actin (50nM Inhibitor (C), 500nM inhibitor (D)). Shown is the mean ± SEM of measurements quantified from three independent experiments (n=3). Statistical analysis was performed using two-way ANOVA with Tukey's post-hoc multiple comparisons test comparing the mean of treatment with the mean of every other. **P ≤ 0.01, **** P ≤0.0001. CTD: C-terminal domain. NTD: N-terminal domain.
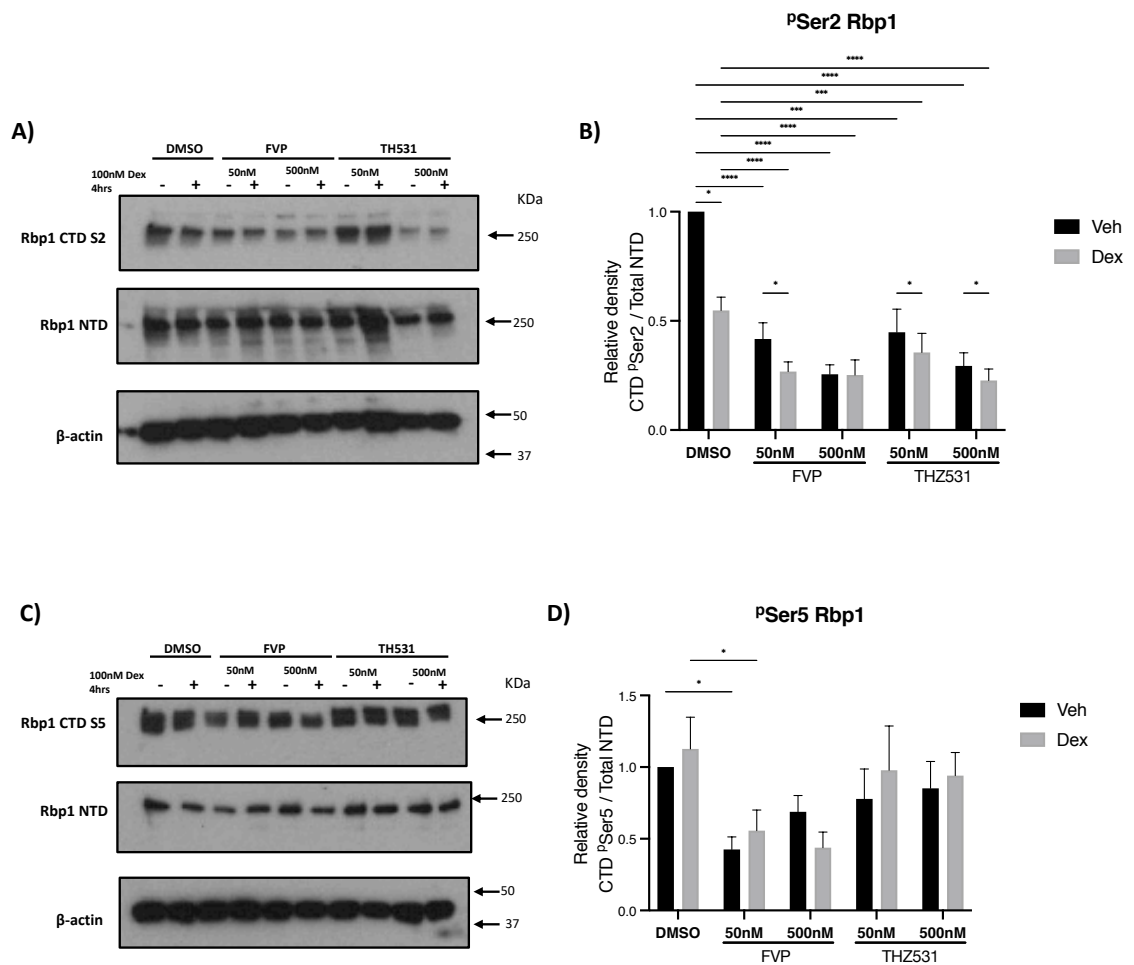
Figure 4.3 Effect of CDK inhibition on Rpb1 CTD phosphorylation with Dexamethasone treatment

A549 cells were pre-treated with FVP or THZ531 (either 50nM or 500nM) before being treated with 100nM Dex for 4 hours. Samples were then lysed and protein expression was analysed by Immunoblot using 10µg protein lysates. Specific antibodies against CTD phosphorylated serine residues 2 (A) and 5 (C) of the Rpb1 large subunit of RNA polymerase II and total NTD. Representative blot is shown from three independent experiments. Densitometry was used to quantify the relative density of CTD phosphorylation in comparison to the NTD and normalised to β-actin (B&D). Shown is the mean ±SEM of measurements of three independent experiments (n=3). Statistical analysis was performed using two-way ANOVA with Tukey's post-hoc multiple comparisons test comparing the mean of treatment with the mean of every other. *P≤0.05,***P ≤ 0.001, **** P ≤0.0001. CTD: C-terminal domain. NTD: N-terminal domain.

4.2.2 CDK12 and CDK13 inhibition reduces Dex-induced target gene expression

In attempt to test whether the observed changes in RNA polymerase II phosphorylation might regulate GR-dependent transcription, I looked at the expression of genes known to be directly activated by GR. A549 cells pre-treated with either FVP or THZ531 for 30 minutes were then exposed to 100nM Dex for a further 4 hours, the mRNA expression of classic Gc-response genes was then analysed by quantitative (q) RT-PCR. In line with the broad suppressive action of FVP upon transcriptional processes, 500nM FVP abolished the relative expression of each of the classic GR response genes for both the vehicle and Dex treated cells (**Figure 4.4**). A 10-fold lower concentration of FVP, maintained Dex-mediated induction of the canonical GR target genes. While the expression of *GILZ* and *DUSP1* display a more pronounced reduction by FVP, *NFKIBA* (IκBα) and *PER1* display little measurable difference comparison to no CDK-inhibition. The dose dependent difference is somewhat reflected by the CDK12 and CDK13 specific inhibitor THZ531. There were minimal differences in the Dex-induced expression of direct GR target genes at 50nM THZ531, compared to no inhibition. At 500nM THZ531 the magnitude of Dex-induced upregulation of genes *GILZ*, *PER1* and *DUSP1* is suppressed in comparison to DMSO. The expression of *NFKBIA* is not reduced to a comparable extent implying selectivity for a sub-set of Gc target genes. Furthermore, in the presence of CDK12 and CDK13 inhibition, the expression level is not significantly different from the vehicle. Importantly, no significant changes in the vehicle baseline expression of genes treated with THZ531, which suggests the observable differences are not due to reduction of global transcription.
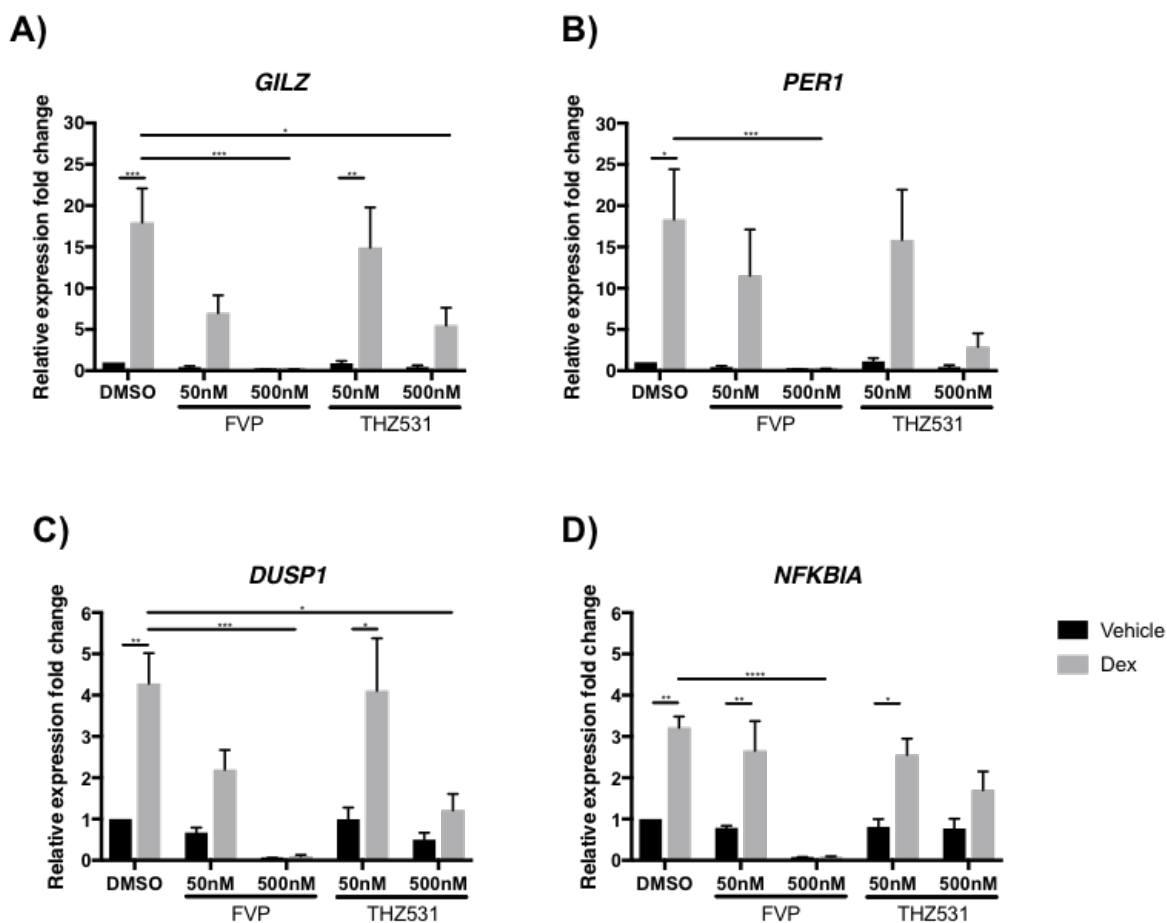
Figure 4.4 Expression of Gc-response genes following inhibition of CDK12 and CDK13

A549 cells were pre-treated with FVP or THZ531 (50nM or 500nM) for 30 minutes followed by 100nM Dex treatment for 4 hours. Cells were lysed, RNA extracted and gene expression was quantified by taqman RT-qPCR. The fold change in expression of Gc-regulated genes GILZ (A), PER1 (B), DUSP1 (C), NFKBIA (D) were calculated relative to vehicle treated control and normalised to GAPDH housekeeping gene. Data is presented as the mean fold change ± SEM of three independent experiments (n=3). Statistical analysis was performed using two-way ANOVA with Tukey's post-hoc multiple comparisons test comparing the mean of treatment with the mean of every other. *P<0.05, **P<0.01, ***P<0.001.

4.2.2.1 Dex-induced gene repression is maintained with CDK12 and CDK13 inhibition

As a potent modulator of inflammatory responses, a vital role of GR function is downregulating the expression of pro-inflammatory cytokines. GR tethers to active pro-inflammatory transcription factors bound to the promoter regions of *IL-6* and *CXCL8* (IL8) to suppress their transcription (116, 129). To determine the effect of CDK inhibition upon genes that GR downregulates, A549 cells were pre-treated with inhibitors as before which was followed by stimulation with inflammatory molecule 10ng/ml TNF-α for 1 hour (to stimulate target gene expression), before Dex addition. A potent Dex-mediated suppressive effect upon TNF-induced *IL-6* and *IL-8* expression was observed in absence of CDK inhibition, whist FVP and THZ531 both reduced the extent of TNF-α -induced induction of both *IL-6* and *IL-8* (**Figure 4.5**). Additionally, the repressive effect of Dex upon cytokine expression was maintained in the presence of the inhibitors. This indicates that CDK12 and CDK13 activity may be important for the TNF-α - induced expression of cytokines but are less important for GR-tethering (and resultant repression) as the Dex-mediated response is comparable to that observed without inhibition.

Upon initial characterisation of the compound THZ531, Zhang and colleagues reported a select number of genes which were significantly downregulated by inhibition of CDK12 and CDK13 alone (256). The observed dose-dependent downregulation identified the most sensitive genes related to the DNA-damage response, including *BRCA1*. I investigated the expression of *BRCA1* in A549 cells treated with Dex following pre-inhibition of CDKs to validate their activity. This found expression to be most greatly reduced by 500nM THZ531 in line with previous association of CDK12 in regulation *BRCA1* expression (259). FVP treatment also significantly reduced *BRCA1* expression in comparison to no CDK inhibition, which is most likely due to suppression of CDK12 activity. For all conditions there were no significant effect of Dex upon the expression of *BRCA1* **(Figure 4.6A)**.

To ensure that the attained differences in gene expression were not a result of a global repression of transcriptional activity, the baseline transcriptional activity of two housekeeping genes *GAPDH* and *ACTB1* was compared for each of the conditions tested. Importantly, the CT values for each gene do not vary with significantly inhibition of CDK through the use of FVP or THZ531 (**Figure 4.6 B&C**).
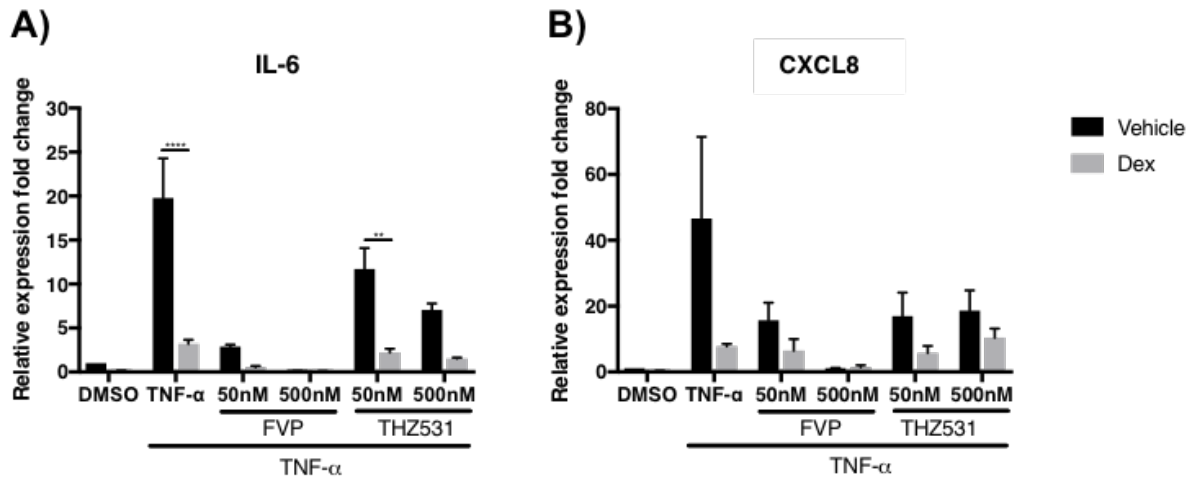
Figure 4.5 Expression of Gc-repressed genes following inhibition of CDK12 and CDK13

Gene expression analysis of GR-repressed inflammatory genes. A549 cells were pre-treated with FVP or THZ531 (50nM or 500nM) for 30 minutes, 10ng/ml TNF-a for one hour then 100nM Dex for a further 4 hours. Cells were lysed, RNA extracted and gene expression was quantified by taqman RT-qPCR. Fold changes of IL-6 *(A)* and CXCL8 *(B)* were calculated relative to vehicle treated control and normalised to GAPDH housekeeping gene. Data is presented as the mean fold change ± SEM of three independent experiments (n=3). Statistical analysis was performed using two-way ANOVA with Tukey's post-hoc multiple comparisons test comparing the mean of treatment with the mean of every other.**P<0.01,****P<0.0001.
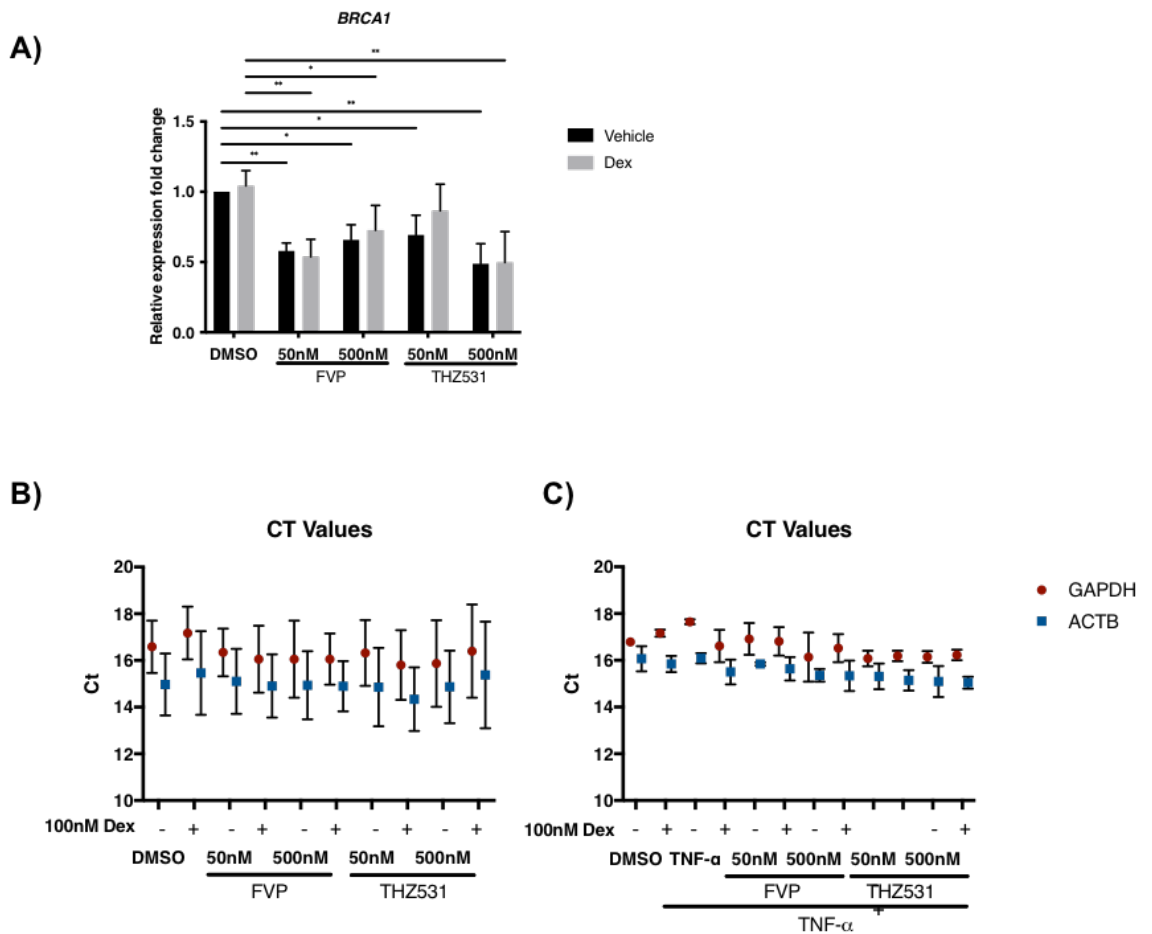
Figure 4.6 Assessment of CDK inhibition upon gene expression

*A) A549 cells were pre-treated with FVP or THZ531 (50nM or 500nM) for 30 minutes followed by 100nm Dex treatment for 4 hours. Cells were lysed, RNA extracted and BRCA1 gene expression was quantified by taqman RT-qPCR. Fold changes were calculated relative to vehicle treated control following normalisation to GAPDH housekeeping gene. Data is presented as the mean fold change and standard error of the mean ±SEM of three independent experiments. (n=3). (B & C) CT values of ACTB and GAPDH housekeeping genes from taqman RT-qPCR, displayed as a measure of baseline transcription for all treatments. Coloured points represent the mean CT value with error bars displaying the standard deviation of measurements from three independent experiments. Statistical analysis was performed using two-way ANOVA with Tukey's post-hoc multiple comparisons test comparing the mean of treatment with the mean of every other. This revealed no significance between housekeeping gene CT values. *P<0.05,**P<0.01.*

4.2.2.2 THZ531 reduces reporter activity by direct TF binding

To further investigate the effect of CDK12/CDK13 inhibition upon the recruitment and activation of transcription at classical GR and NF-κB response elements, A549 cells were co-transfected with firefly and renilla luciferase reporter plasmids. Then cells were treated with TNF-α and/or Dex in the presence of 500nM THZ531. The TAT3-TATA plasmid contains trimerized GRE and is therefore, a site of direct GR binding(260), whilst the NRE reporter contains canonical binding sites for p65 /p50 complexes containing a NF-κB response element, which GR can then tether to (62, 129).

The nature of the assay requires overnight treatment of the cells, to ensure a detectable signal of firefly luciferase is produced. However, is was noted that across three individual replicates that cells treated overnight with inhibitors had reduced cell numbers. This was quantified by assessing the confluency of cells in the wells prior to lysis (**Figure 4.7A**), and confirms a reduction in all conditions treated with THZ531. This effect is mitigated by the inclusion of the renilla reporter which is transfected alongside the firefly constructs to act as an internal transfection control. The signal of firefly luciferase is normalised to the renilla signal which will be proportional to the total number of transfected cells present.

In the absence of THZ531, the cells transfected with the TAT3 construct show an increase in reporter expression with increasing doses of Dex. In the presence of THZ531 the level of expression is reduced suggesting that transcriptional activation is impeded by CDK12/CDK13 inhibition, but not abolished **(Figure 4.7B).** In the context of inflammation, TNF-α increases the expression of the reporter although a Dex-dependent reduction in expression is not observed. CDK12/CDK13 inhibition reduces the TNF-α -induced increase in activity however the addition of Dex appears to have no further effect. This reflects the effect upon gene expression, which strengthens the suggestion that CDK12/CDK13 are involved in the upregulation of genes by the direct binding of transcription factors to promoter regions. The repressive mechanism of GR tethering to transcription factors are less affected by inhibition of CDK12/ CDK13.
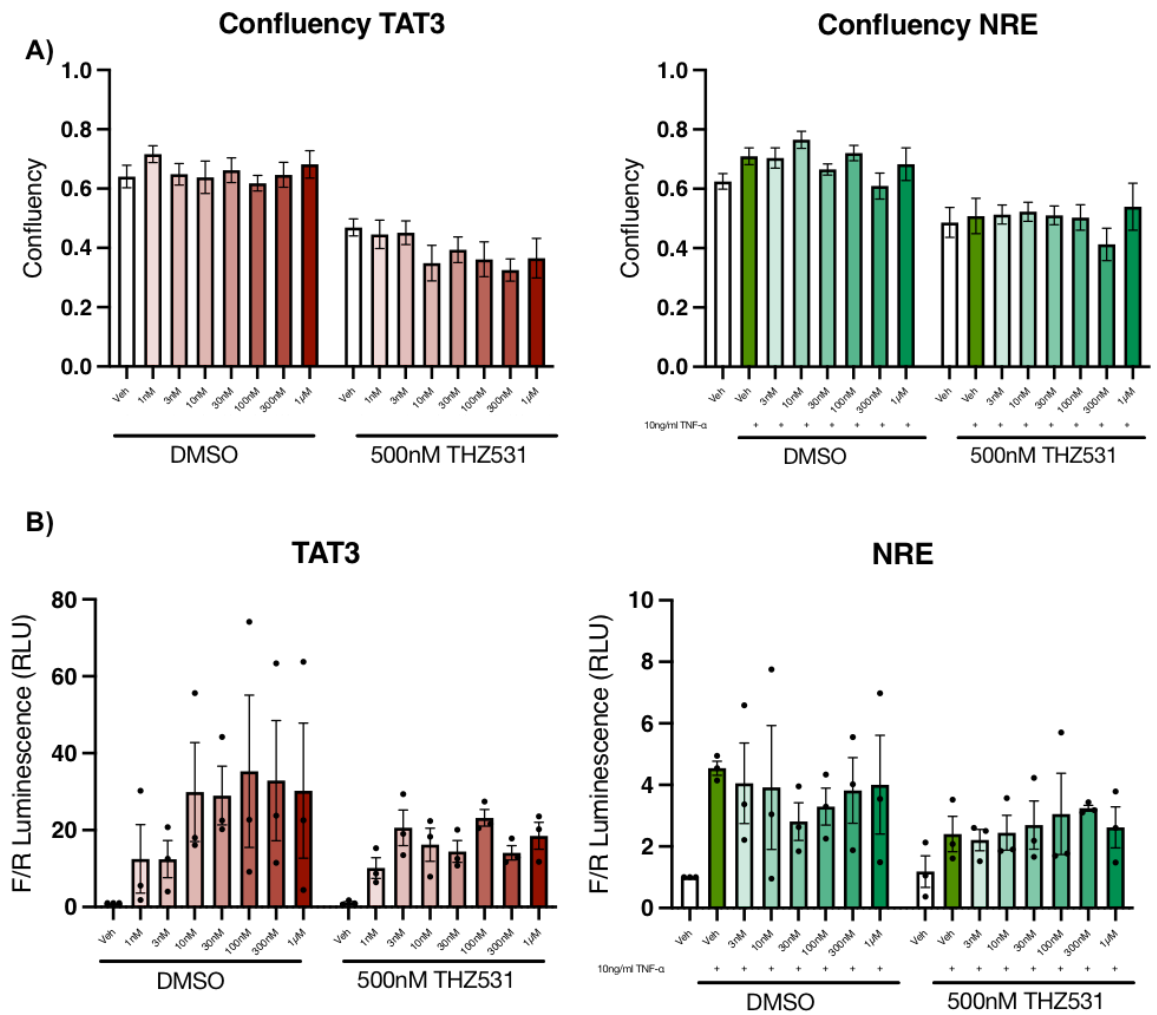
Figure 4.7 The effect of THZ531 at GR and p65-regulated promoters.

A549 cells were transfected with TAT3 or NRE reporter plasmids alongside renilla constitutive reporter vector. At 24 hours post transfection cells were seeded into 24 well plates in CSS media. Cells were then treated overnight with varying concentrations of Dex (1nM-1μM) in the presence of 10ng/ml TNF-α and 500nM THZ531, where indicated. Following treatment and prior to lysis, cells were imaged to assess cell confluency which was quantified using image-J PHANTAST plugin (A). Data is presented as the level of confluency (0-1) for each condition. Cells were then lysed and lysates were assessed to quantify the level of firefly and renilla luminescence (B). Data is presented as the relative luminescent units of firefly:renilla (F/R) for each condition, for the mean ±SEM of each condition, individual dots represent mean values from each experimental repeat. (n=3) RLU, Relative luminescence units.

4.2.2.3 THZ531 does not affect GR and p65 nuclear translocation

I also assessed whether the translocation dynamics of the GR and p65 transcription factors were affected by THZ531, which could underlie differences in genomic responses. A549 cells pre-treated with 500nM THZ531 were then treated with 10ng/ml TNF-α and 100nM Dex. The timing of TNF-α stimulus was added both as a 1-hour pre-treatment and in conjunction with Dex, to ensure the timing of inflammatory stimulus does not affect the extent of translocation. Immunofluorescence staining reveals that Dex and TNF-α treatment induces the nuclear translocation of GR and p65 respectively (shown in **Figure 4.8A** and quantified in **Figure 4.8B)**. THZ531 does not disturb the translocation dynamics of GR or p65 following ligand stimulation and nuclear:cytoplasmic ratios are comparable between conditions based on the status of CDK inhibition. Therefore, any transcriptional differences are not due to reduced entry of the transcription factors into the nucleus.
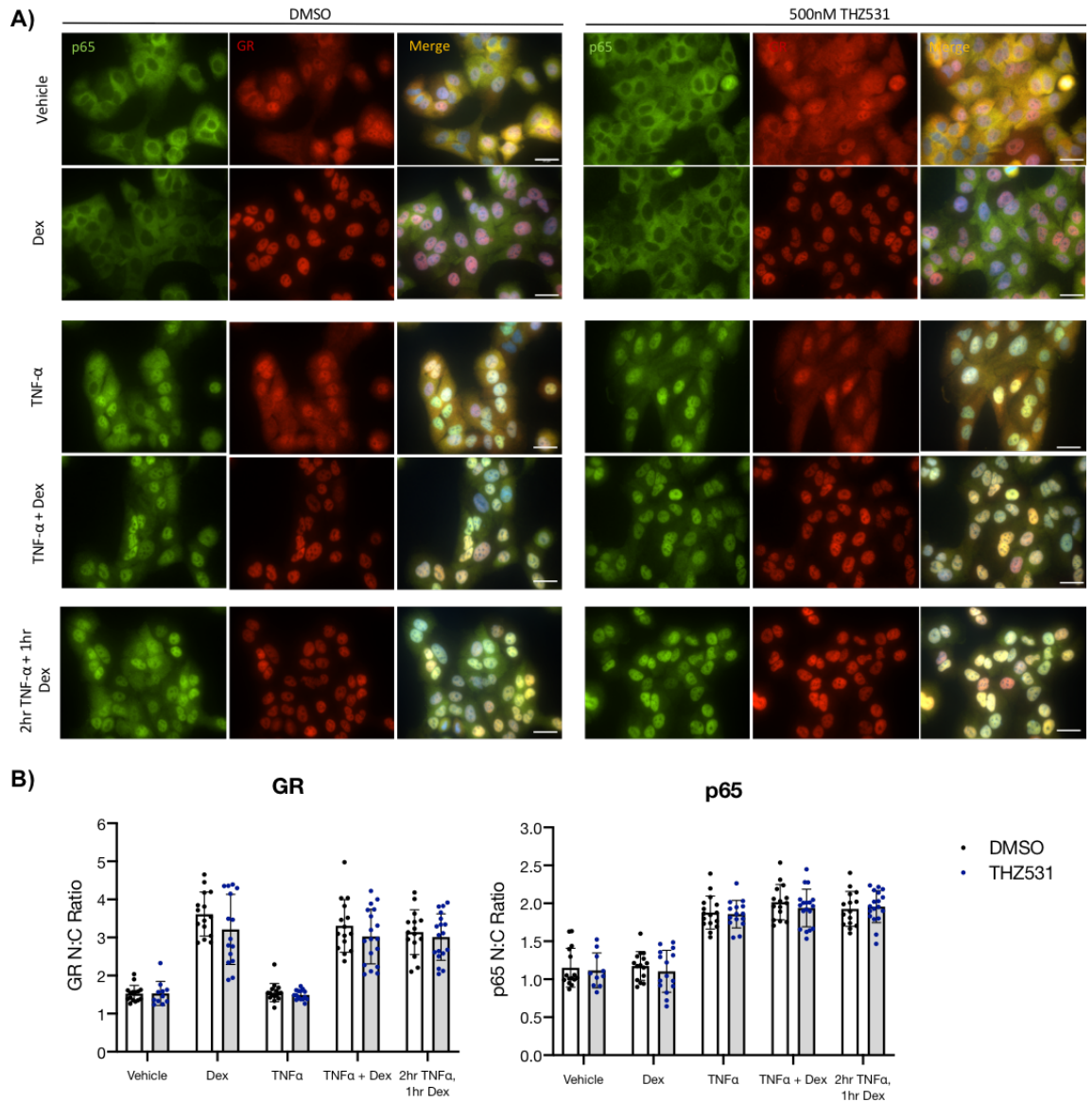
Figure 4.8 Effect of THZ531 upon GR and p65 translocation

*A549 cells were seeded onto coverslips and pre-treated with 500nM THZ531 for 30 minutes. Cells were then treated with 100nM Dex, 10ng/ml TNF-a individually or in combination for 1 hour, or treated with TNF-a for 2 hours with Dex added for the final hour. Cells were fixed, permeabilised and stained for p65 (green), GR (red) and counterstained with Hoechst 33342 (blue). **(A)** Representative immunofluorescent images of three independent experiments captured on Widefield microscope x60 magnification. Scale bar: 20µm Quantification of nuclear:cytoplasmic (N:C) ratio of p65 and GR using Cell profiler software **(B)**. Data is presented as the mean N:C ratio per field of view and standard deviation for three independent experiments. Statistical analysis was performed using two-way ANOVA with Bonferroni's multiple comparisons test and revealed no significance between DMSO and THZ531 treated samples for all conditions (n=3).*

4.2.3 Transcriptome profiling

Results described above suggest that inhibition of CDK12 and CDK13 affects Gc-regulated transcription. I therefore performed RNA-sequencing to gain a more global understanding of the role of CDK12 and CDK13 in GR-mediated transcriptional processes. A549 cells were pre-treated for 30 minutes with 500nM THZ531 followed by a 4-hour treatment with 100nM Dex. These time points were chosen to provide a window to identify the immediate GR-mediated transcriptional effects or defects following the inhibition of CDK12 and CDK13 activity, and to minimise resultant transcriptional effects downstream of GR activity (via GR-Dex mediated changes in the expression of other transcription factors).

The Pearson correlation matrix in **Figure 4.9A** shows an $R^2 > 0.98$ between samples and indicates close gene expression pattern between replicates, which is important to verify reliability of the downstream analysis. The Dex condition correlates most closely with the control group ($R^2 = 0.956$-0.963) and furthest from THZ531 alone ($R^2 = 0.879$-0.886), whilst the two groups treated with THZ531 have the closest similarity ($R^2 = 0.969$-0.972). Principal component analysis reflects the close clustering of the technical replicates and reveals distinct separation of each of the treatments **(Figure 4.9B &C)**.
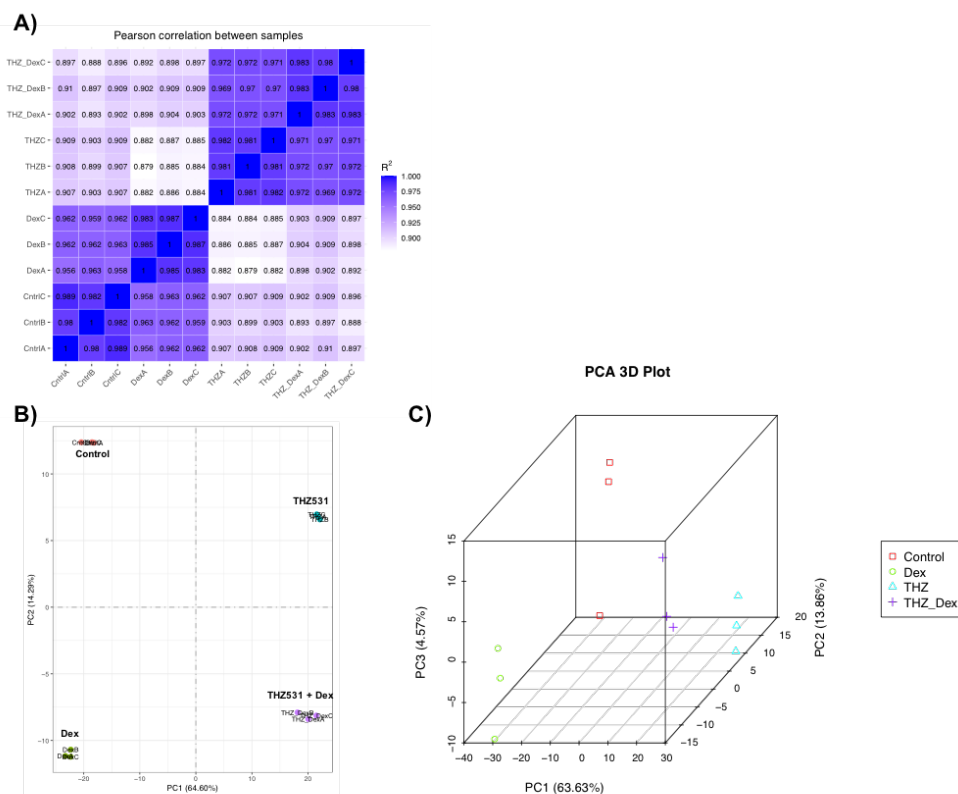
Figure 4.9 Correlation and Principle component analysis.

A) *Pearson correlation coefficient matrix to compare the correlation of gene expression between samples. Colouring based on R^2 value.* *B)* *Principle component analysis (PCA) for each sample in 2 dimensions (2D) and (C) 3D. Produced by Novogene*
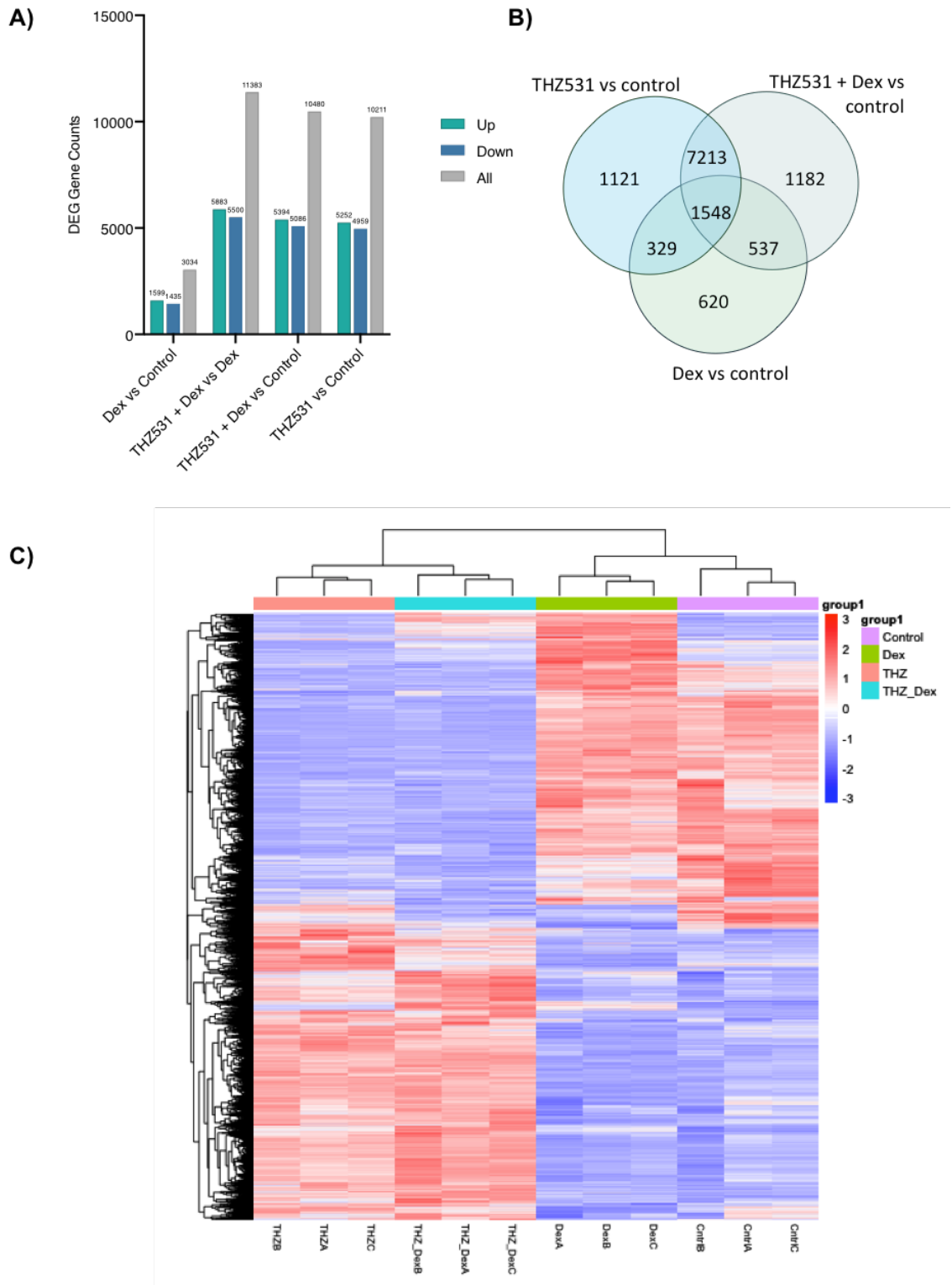
Figure 4.10 Differentially expressed genes and hierarchical clustering for each experimental group.

A) Differentially expressed gene counts, including direction of differential expression (up/down) and total for each group as specified on y-axis. B) Overlapping venn of differentially expressed genes (DEG). Comparison of DEG for each treatment condition in comparison to the vehicle control. Values correspond to all genes with a stringency DESeq2 padj≤0.05 only, no fold change stringency applied. C) FPKM hierarchical cluster analysis for all genes regulated by each condition using the log2(FPKM+1) value of differentially expressed genes, shared for all samples in the four treatment groups. Red represents genes with high expression and blue represents genes with low expression. Stringency: p<0.01. Log2FC ±1. DEG: Differentially expressed gene. THZ:THZ531. FPKM: Fragments per kilobase of exon per million.
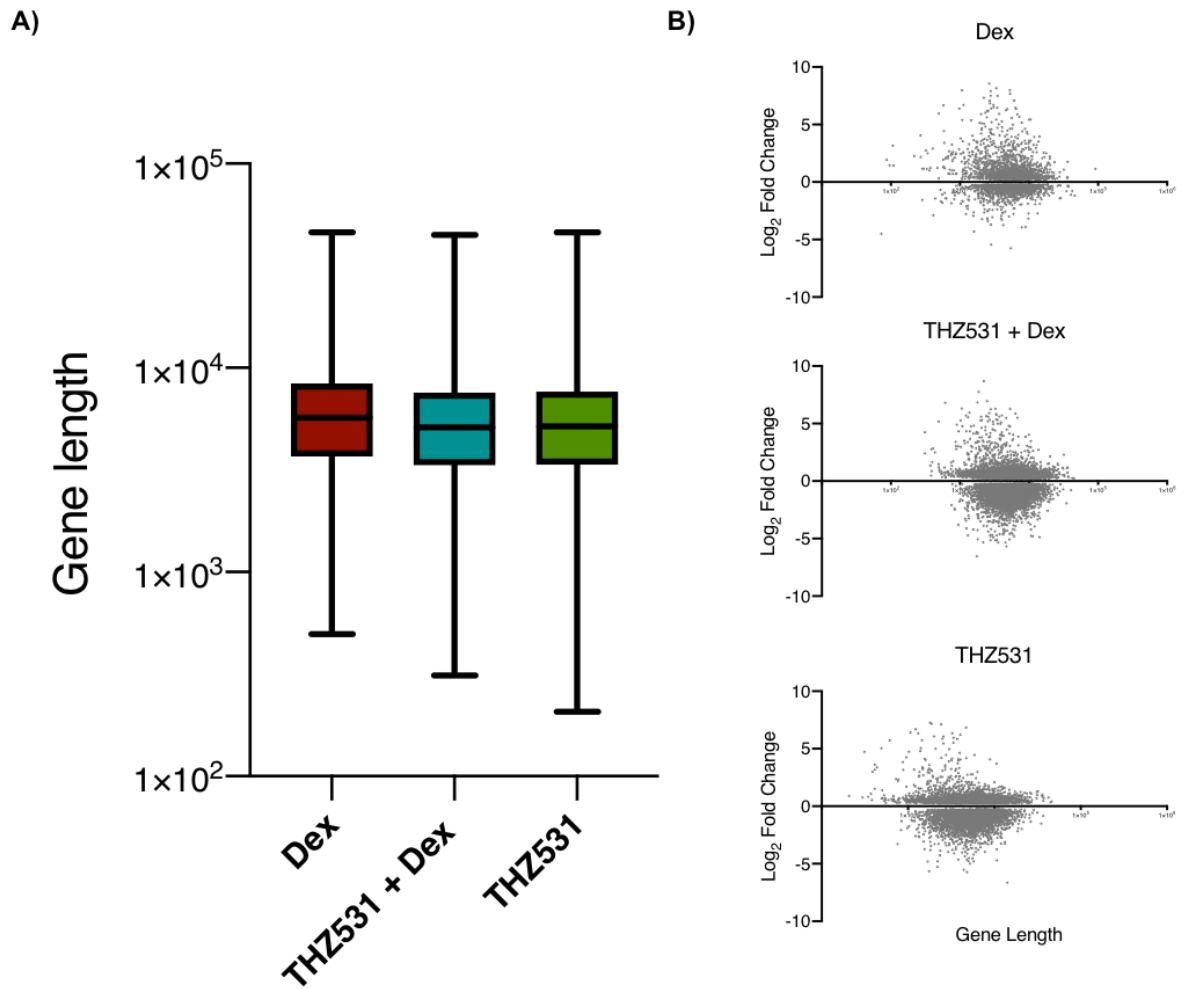
Figure 4.11 Gene length correlation of differentially regulated genes

A) Box plot comparing the length of genes which were found to be differentially regulated in comparison to the vehicle control for each treatment condition: Dex, THZ531 + Dex and THZ531. B) Scatter plots representing individual gene lengths against the log2fold change induced by each condition vs the vehicle control.

4.2.3.1 Differential gene expression analysis

To fully understand the changes induced by each experimental condition, differential expression analysis was performed in comparison to the vehicle control. I also included a comparison of the differential expression between THZ531+ Dex treated samples and Dex alone with aim to define the set of genes which are affected by inhibiting CDK12 and CDK13 away from the expression level induced by Dex. In **Figure 4.10A,** the counts of significantly (DESeq2 padj≤0.05) differentially expressed genes (DEG) are shown for each comparison, as well as the proportion of genes regulated either up or down (prior to any log2fold change threshold) are shown. A total of 3034 genes are regulated by Dex, although a far greater number of genes are regulated in the presence of THZ531 (THZ531 vs control= 10211, THZ531+Dex vs control = 10480). This reflects the fact that Dex targets a single transcription factor (GR) whereas THZ531 modulates CDK12 and CDK13 which themselves modulate several cellular processes, including multiple transcription factors. The largest number of differentially expressed genes (11383) is seen for THZ531 + Dex vs Dex. There were no large disparities between the proportion of up and down regulated genes for any condition; importantly, this suggests that inhibition of CDK12/ CDK13 does not result in a global loss of transcriptional activity at this time point.

The Venn diagram-based comparison of the significantly DEGs for each treatment group in **Figure 4.10B**, confirms that a large number of genes (10,211) are perturbed by THZ531; alone and in the presence Dex. Of these 1548 + 329 are also regulated by Dex alone which accounts for over half of the 3034 genes regulated by Dex. The condition treated with THZ531 in the presence of Dex shows the greatest overlap with THZ531-alone, likely due to the large number of genes affected by THZ531.

The hierarchical cluster analysis on the DEGs for each group indicates two predominant clusters of expression **(Figure 4.10C)**. The first shows down regulation of genes treated with THZ531 (THZ531 alone and THZ531+ Dex) which are upregulated by Dex and the control condition. Whilst the next cluster shows an upregulation of THZ531-treated samples and the same genes are down regulated by Dex and the control group. There are two clusters of genes which are regulated in the same direction by Dex and THZ531+Dex and the opposite direction by THZ531 alone and the control yet these contribute to a small overall proportion of DEGs.

Inhibition of CDK12 and CDK13 by THZ531 has previously been reported to affect the expression of long genes due to preference for intronic alternate poly-adenylation sites(261). Plotting the distribution of the length of all the protein coding genes whose expression was significantly regulated by each of the conditions shows that the median and interquartile range of gene length is similar between the three treatment groups **(Figure 4.11A)**. There is no significant difference in gene length between the two conditions treated with THZ531 however, both the

median and mean gene length of differentially regulated genes is greater in the Dex treated condition. The range is greater for the two groups treated with THZ531 in comparison to Dex alone and extends to include genes with a shorter length compared to Dex treatment alone. When comparing the gene length against the induced log2fold change **(Figure 4.11B)**, the treatment with THZ531 does not reveal an enrichment or bias towards a greater perturbation of the expression of longer genes.

4.2.3.2 Enriched Ontologies

The volcano plot of Dex-regulated genes **(Figure 4.12A)** identifies some of the most significant up-regulated (DEG) as well established Gc targets such as *DUSP1* and *FKBP5* in addition to cell adhesion protein cadherin 16 (*CDH16*). The most significantly down regulated genes following Dex treatment were cytochrome p450 family 24 subfamily member (*CCP24A1*), growth differentiation factor 15 (*GDF15*) and solute carrier (*SLC7A11*). Application of a log2fold change threshold of 1 **(Figure 4.12B),** displays the distribution Dex-regulated genes which shows a predominance towards gene upregulation.

Dex-regulated genes have previously been classified into two broad categories: stress response and development which encompasses accepted functions of Gc-signalling (76). KEGG enriched pathway analysis of the genes regulated by Dex identifies: Osteoclast differentiation, ErbB signalling and TNF signalling pathway as the top three terms **(Figure 4.12C)**. ErbB family of tyrosine kinase receptors relay downstream signals in response to extracellular growth factors. The response encompasses a vast spectrum of cellular responses involving kinase signalling required for cell proliferation, differentiation, migration and survival (262). Similarly, cross-talk between GR and TNF-α signalling is a fundamental aspect the anti-inflammatory action of GR. Therapeutic does of Gc promote osteoclast maturation and survival, whilst favouring osteoblast apoptosis. The skewed balance between bone ossification and resorption underlies the pathogenesis of Gc-induced osteoporosis (263) - a detrimental characteristic of Gc therapy. Such terms reflect the involvement of GR regulated genes in both developmental cell differentiation and the homeostatic response to stress.

Other enriched pathways denote the well-known involvement of Gc in the regulation of inflammation pathways including NF-κB signalling pathway and cytokine-cytokine receptor interaction (5, 9, 72). Further assessment of the ontology of the Dex-regulated genes reveals biological processes related to circulatory system, response to steroid hormone in addition to cell migration and adherence (**Figure 4.13**).

The enriched molecular function of the regulated genes is associated with transcriptional activity such as RNA polymerase II proximal promoter-sequence specific binding and transcription

corepressor activity, consistent with the action of liganded-GR as a transcriptional regulator. Cell adhesion molecule binding, actin binding and GTPase binding are enriched terms which indicate processes associated with cellular response to external signals and is reflected by enriched terms associated with cellular component relating to the actin cytoskeleton, cell-cell junctions, focal adhesion and membrane rafts. Together these enriched processes and functions, highlight how genes-regulated by Dex underlie many know aspects of Gc biology associated with development, wound healing and immune regulation(5, 46).

Assessment of the most significantly upregulated genes following treatment with THZ531 alone **(Figure 4.14)** reveals a number of early response genes including AP-1 proteins Jun and JunB, immediate early response (*IER)3*, *IER2*, *IER5* and EP300 interacting inhibitor of differentiation (*EID3*). Genes with reduced expression included mitochondrial antiviral signalling protein (*MAVS*), tensin 4 (*TNS4*) and protein phosphatase 1 regulator subunit 10 (*PPP1R10*). **Figure 4.14B** shows the distribution of the differential-expression change of THZ531-regulated genes and shows the large majority of genes are downregulated as a result of CDK12/CDK13 inhibition. KEGG pathway analysis identifies terms including proteasome, ribosome and oxidative phosphorylation as well as disease-related terms such as Parkinson disease and prion disease which may indicate a role in protein folding and turnover (**Figure 4.14C**). The top identified biological processes associated with THZ531-regulated genes relate to mRNA catabolic processes and protein targeting to the ER which again suggest CDK12 / CDK13 are important for the correct processing of mRNA for translation by ribosomes and subsequent protein folding and sorting (264). The enriched molecular functions of the regulated genes include cell adhesion molecule and cadherin binding, ubiquitin-protein ligase binding as well as transcription co-repressor activity (**Figure 4.15**). Ribosome-related terms are a predominant cellular component reflecting involvement in protein translation while the terms cell-substrate junction and focal adhesion indicate cellular sensing of the external ECM.

THZ531 treatment in the presence of Dex, reveals the top upregulated genes to include classic Gc response genes *TSC22D3* (GILZ), *PER1* and serum glucocorticoid kinase 1 (*SGK1*). Other upregulated genes include the AP-1 constituent FOS and cyclin dependent kinase inhibitor 1C (*CDKN1C*) which can both regulate cell proliferation (**Figure 4.16A**). The top downregulated genes *MAVS* and *PPP1R10* are the same as that seen with THZ531 alone, other factors include proto-oncogene c-Src and oxidative stress induced growth inhibitor 1 (*OSGN1*). As with THZ531 alone, this condition favours the down-regulation of target gene although a large number are significantly upregulated Log2fold change (FC)>1 indicating that global transcription is not inhibited (**Figure 4.16B**). The enriched KEGG pathways also largely reflect the terms enriched by THZ531 with the addition to carbon metabolism and glycolysis / gluconeogenesis (**Figure 4.16C**).

The similarities are likely due to the large number of genes where are significantly affected by inhibiting CDK12/CDK13. Likewise, the enriched biological processes as associated with mRNA catabolic processes and localisation and protein targeting. The top molecular function of the regulated genes is chromatin binding which indicates a role in genome accessibility and stability, whilst the top cellular components are again associated with cell-substrate junction, focal adhesion and ribosomes (**Figure 4.17**). Given the large number of genes which are affected by inhibition of transcriptional kinases CDK12/CDK13, I found little separation between the THZ531 and THZ531 + Dex conditions. In order to understand the relationship between CDK12/CDK13 and GR, the analysis required a more specific approach to identify the particular gene subsets of interest.
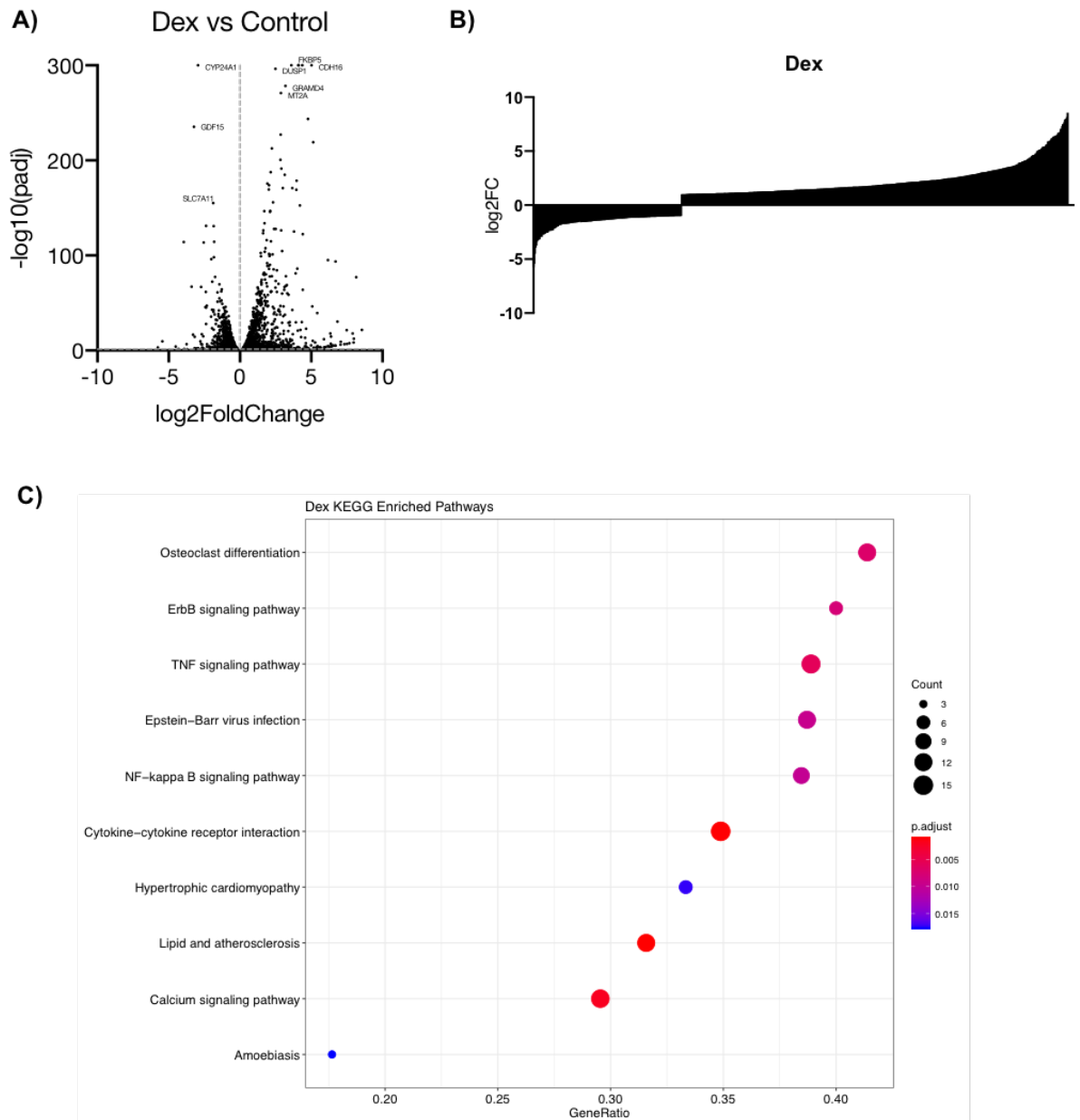
Figure 4.12 Dexamethasone-regulated genes

(A) Volcano plot of all genes differentially regulated by Dex in comparison to the vehicle. No stringency cut off. (B) Distribution plots of differentially expressed genes against their log2FC in comparison to the vehicle. Padj <0.01. Log2FC ±1. (C) KEGG enriched pathways from genes differentially regulated by Dex. Gene ratio calculated based on the number of genes in the gene set against the total number of genes associated with the term. Dot colour corresponds to the padj value, for the significance or term enrichment. Dot size corresponds to the number of genes implicated in the term. Created using clusterprofiler

Figure 4.13 Enriched functional ontologies of all Dexamethasone-regulated genes.

*Gene ontology analysis of genes differentially regulated by Dex in comparison to the vehicle control. For Biological processes **(A)**, molecular function **(B)** and cellular component **(C)**. Gene ratio calculated based on the number of genes in the gene set against the total number of genes associated with the term. Dot colour corresponds to the padj value, for the significance or term enrichment. Dot size corresponds to the number of genes implicated in the term.*
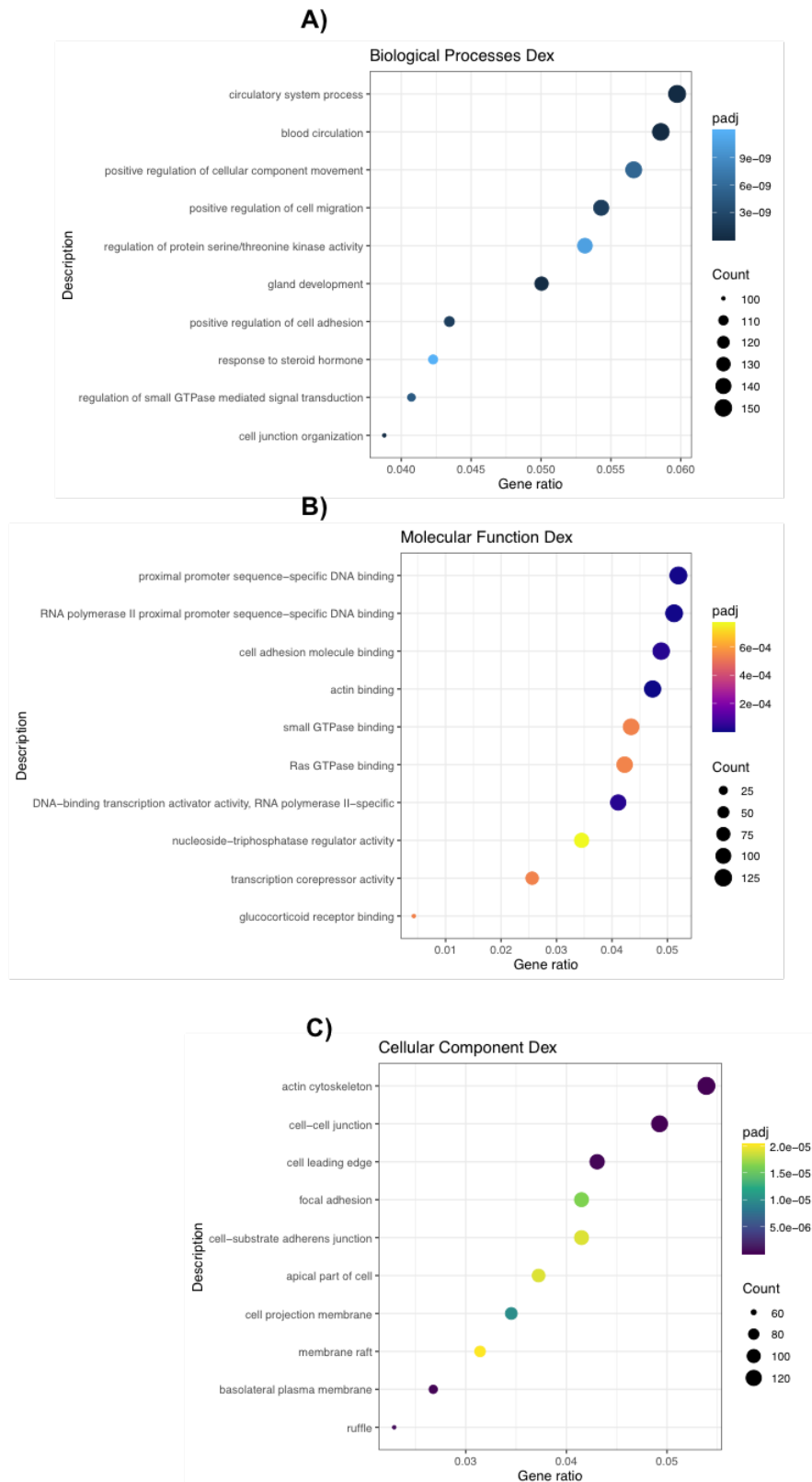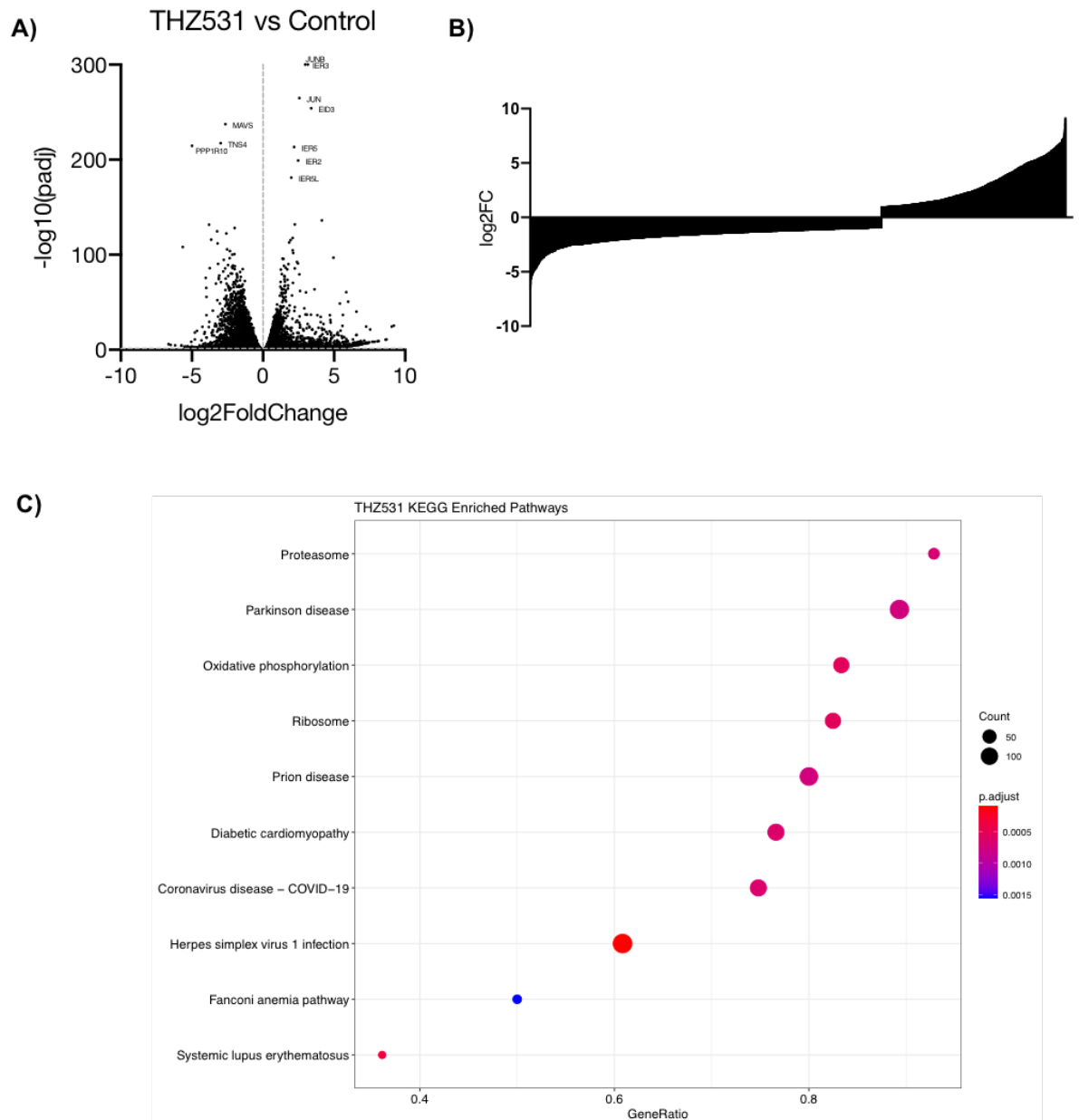
Figure 4.14 THZ531-regulated genes

(A) Volcano plot of all genes differentially regulated by THZ531 in comparison to the vehicle. No stringency cut off. (B) Distribution plots of differentially expressed genes against their log2FC in comparison to the vehicle. Padj <0.01. Log2FC ±1. (C) KEGG enriched pathways from genes differentially regulated by THZ531. Gene ratio calculated based on the number of genes in the gene set against the total number of genes associated with the term. Dot colour corresponds to the pAdj value, for the significance or term enrichment. Dot size corresponds to the number of genes implicated in the term. Created using clusterprofiler.
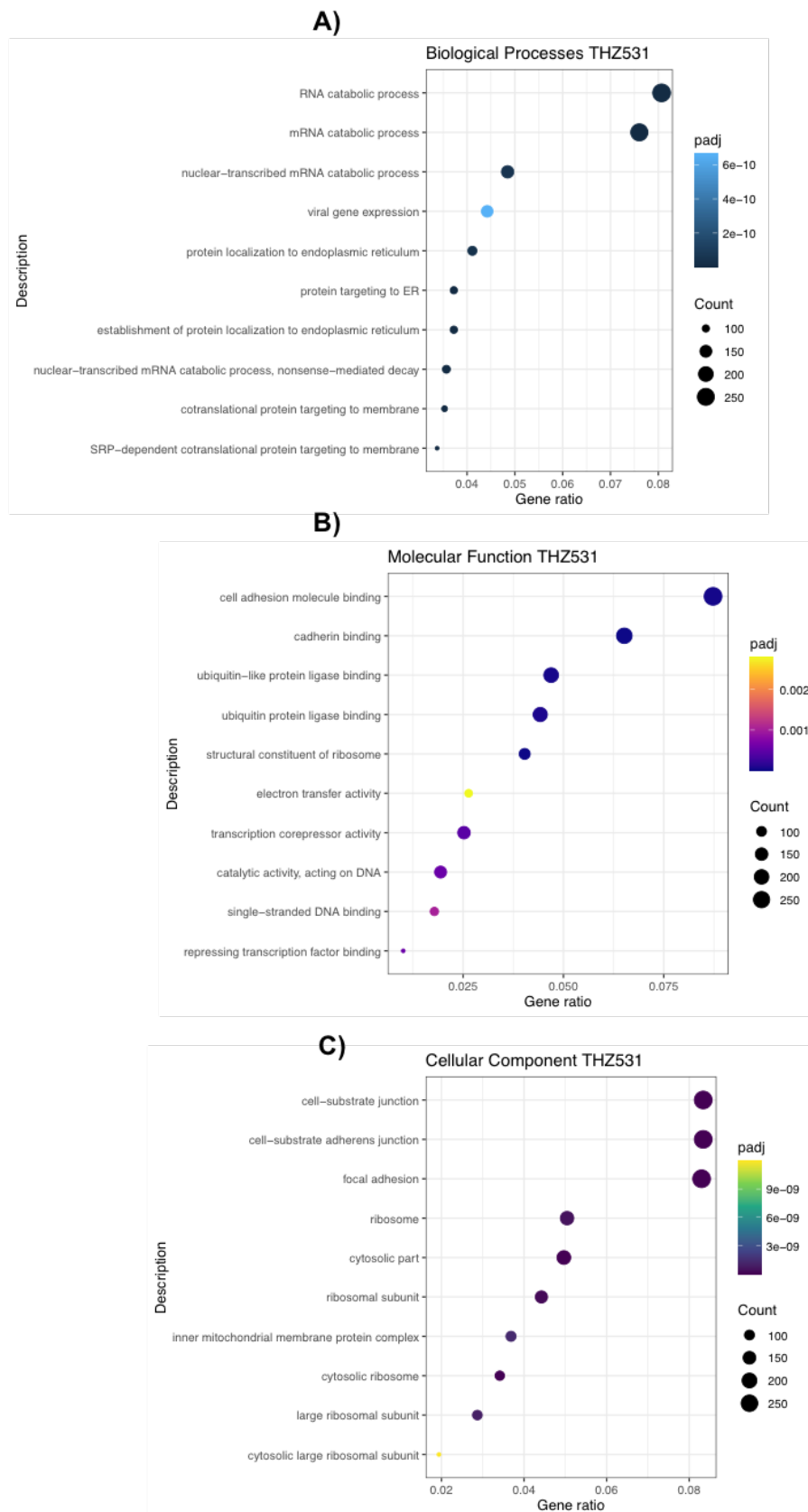
Figure 4.15 Enriched functional ontologies of all THZ531-regulated genes.

Gene ontology analysis of genes differentially regulated by THZ531 in comparison to the vehicle control. For Biological processes (A), molecular function (B) and cellular component (C). Gene ratio calculated based on the number of genes in the gene set against the total number of genes associated with the term. Dot colour corresponds to the pAdj value, for the significance or term enrichment. Dot size corresponds to the number of genes implicated in the term.
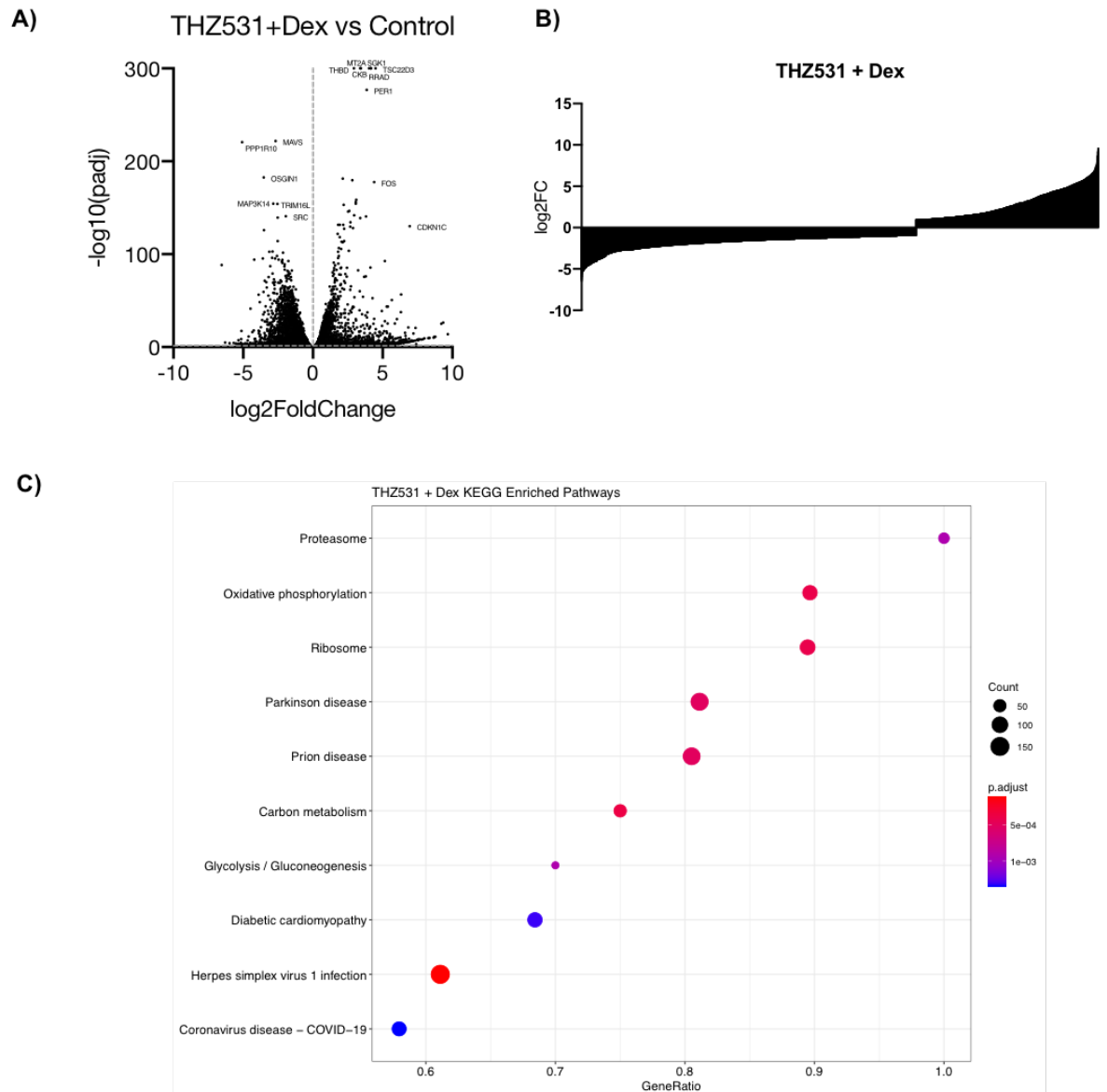
Figure 4.16 THZ531 and Dexamethasone -regulated genes

(A) Volcano plot of all genes differentially regulated by THZ531 + Dex in comparison to the vehicle. No stringency cut off. (B) Distribution plots of differentially expressed genes against their log2FC in comparison to the vehicle. PAdj <0.01. Log2FC ±1. (C) KEGG enriched pathways from genes differentially regulated by THZ531 + Dex. Gene ratio calculated based on the number of genes in the gene set against the total number of genes associated with the term. Dot colour corresponds to the pAdj value, for the significance of term enrichment. Dot size corresponds to the number of genes implicated in the term. Created using clusterprofiler
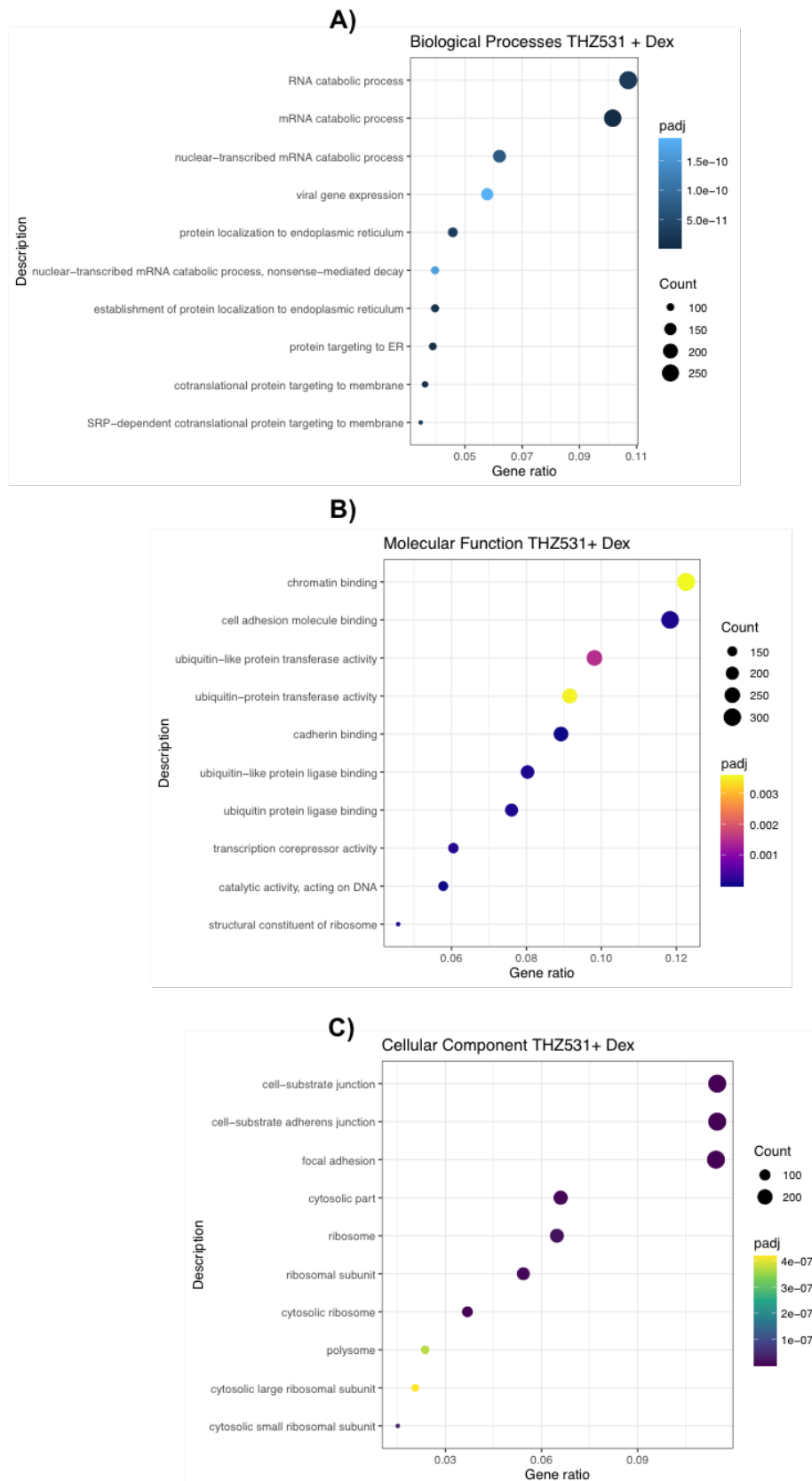
Figure 4.17 Enriched functional ontologies of all THZ531 and Dexamethasone-regulated genes.

Gene ontology analysis of genes differentially regulated by THZ531 in comparison to the vehicle control. For Biological processes (A), molecular function (B) and cellular component (C). Gene ratio calculated based on the number of genes in the gene set against the total number of genes associated with the term. Dot colour corresponds to the pAdj value, for the significance of term enrichment. Dot size corresponds to the number of genes implicated in the term.

4.2.3.3 Dex-regulated genes which are affected by THZ531

The primary goal of the RNA-seq analysis was to understand the relationship between GR and CDK12/CDK13, most importantly the role of the CDKs upon the regulation of GR-target genes. To achieve this, I aimed to identify genes constituting two key groups for further analysis: Group 1 - Dex regulated genes which are affected by inhibition of CDK12 and CDK13 and Group 2 - Dex regulated genes which are independent of CDK12 an CDK13. Using DEG gene lists (Dex vs Control and THZ531+Dex vs Dex) to define these gene sets - group one consisted of shared genes which were regulated by Dex whose expression was significantly altered with THZ531 pre-treatment, away from the level of expression induced by Dex alone. Group two represents genes from the aforementioned gene lists which were significantly regulated by Dex and excluded from the set of genes that a significantly regulated by THZ531+ Dex.

For enrichment analysis, I compared different thresholds and determined that a log2 fold change threshold of ± 0.5 with an adjusted p value threshold of p<0.01 was acceptable. As to include a high P value stringency but lower fold change cut off to include a larger number of genes sufficient to obtain significantly implicated gene ontologies with aim to understand regulated processes.

The overlapping groups of genes including the directionality of differential expression using this stringency, are shown in the Venn and proportionality in the pie charts (**Figure 4.18A&B**). 60.6% (594 genes) of Dex-up-regulated genes and 46.6% (292 genes) of Dex-down-regulated genes are affected by THZ531, which indicates that THZ531 has a greater effect upon the expression of genes up-regulated by Dex. There also remains a proportion of genes which are not significantly altered by inhibiting CDK12/CDK13 (387 up and 335 down) which reflects the notion that CDK12/CDK13 affect the expression of a subset of GR-regulated genes.

4.2.3.4 Ontology of Dex-regulated genes affected by THZ531

Gene ontology analysis of all the intersecting genes (total 886 genes) (**Figure 4.18C&D**) reveals an enrichment of biological processes associated with regulation of transcription from RNA polymerase II promoter, regulation of cell proliferation and apoptotic processes. The enriched molecular functions of this gene set mostly relate to regulatory region DNA binding and transcription factor activity implicating a significant impact on transcriptional processes and regulation of gene expression. This contrasts the processes associated with the 722 genes which are regulated by Dex only. Enriched terms for these genes are associated with protein phosphorylation and kinase activity, which may represent a connection to genes encoding proteins involved in the non-genomic signalling activity of GR. For example: *CAV1* which was differentially phosphorylated by Dex after 10 minutes, and components of MAP kinase signal

transduction pathway and cAMP second messenger cascade– both implicated as pathways regulated by rapid non-genomic GR action (87, 93).

Another identified function for Dex-regulated genes affected by THZ531 includes GTPase activator activity. A number of G-protein signalling (RGS) proteins as well as β-arrestin 1, and proteins involved in Rac1, RHOA and CDC42 signalling were responsible for the term. This suggests that cell motility and cytoskeleton dynamics are regulated by GR and CDK12/CDK13, yet is not necessarily a unique process as genes regulated by Dex alone were also linked to cell motility and wound healing.
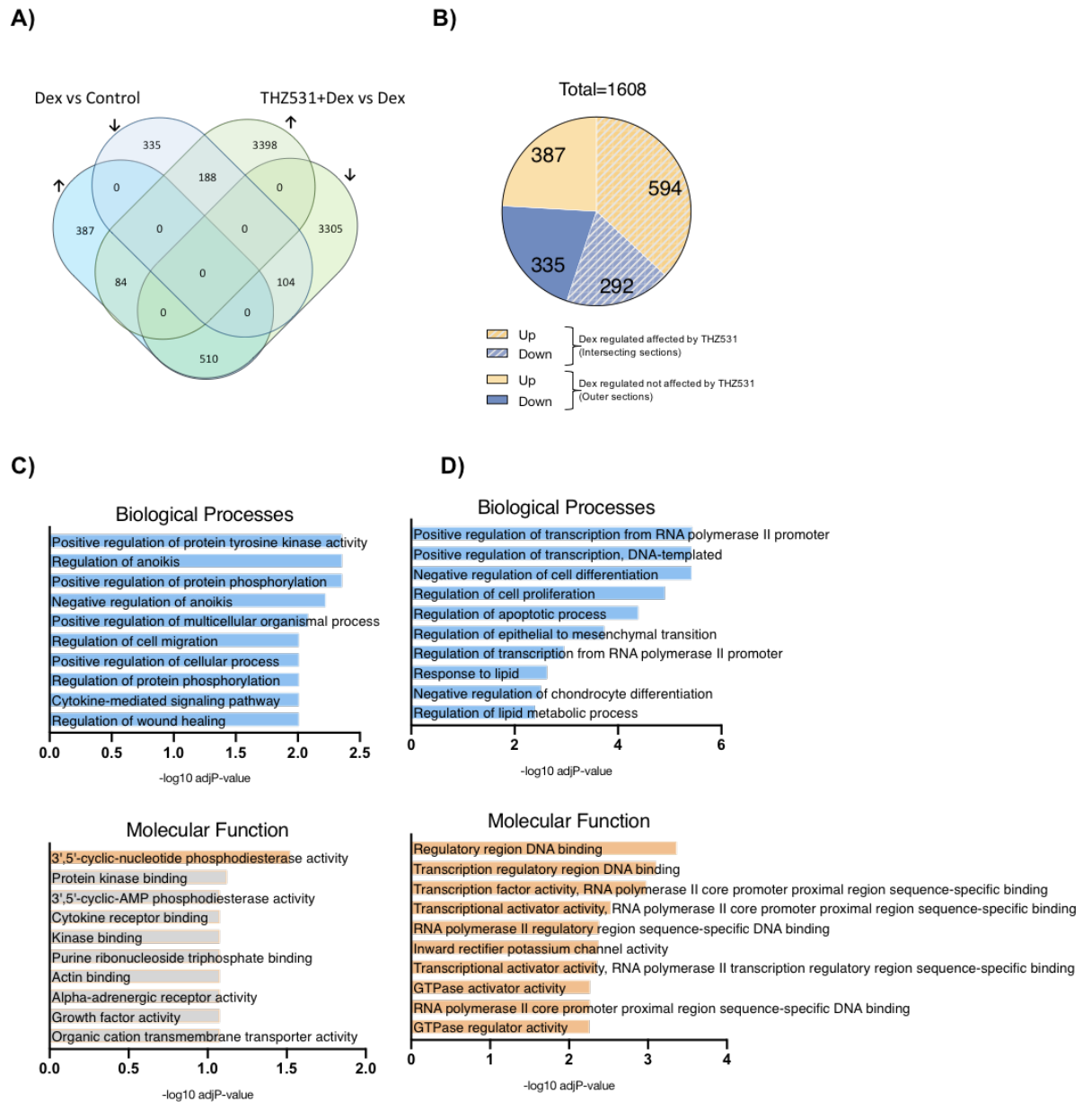
Figure 4.18 Defining the set of genes differentially expressed by Dexamethasone and affected by THZ531

A) Venn diagram comparing genes which are differentially expressed by Dex vs vehicle and THZ531+Dex vs Dex alone. Groups stratified by directionality of log2fold change up or down. Numbers correspond to number of genes. B) Pie chart corresponding to of the total number of Dex-regulated genes: up=yellow, down=blue, the proportion of genes significantly affected by THZ531 indicated by the shaded regions. Stringency cut off adj p<0.01 and log2FC ±0.5. Gene ontology of biological processes and molecular function performed using Erichr software for genes exclusively regulated by Dex alone (722 genes). C) and regulated by Dex and affected by THZ531 (886 genes) D). Coloured bars indicate significantly enriched terms.

One enriched ontology relating to inward rectifier potassium ion channel activity revealed the expression of a number of potassium and sodium ion channels to be affected by Gc and THZ531. The term included the gene encoding the serine/threonine kinase, serum glucocorticoid kinase (SGK1) which is known to regulate ion channel and membrane transporter activity (265). Expression was upregulated by Dex but increased further by THZ531 pre-treatment (data not shown). In most cases Dex increased gene expression whereas the effect is reduced by pre-treatment with the inhibitor. With the exception of *KCNK3*, where Dex reduced expression and is reduced further by CDK12/CDK13 inhibition. Closer inspection of the FPKM values of the genes encoding the ion channels, revealed low expression counts. These observations may implicate an important Gc-regulated mechanism but given such low levels of expression were not investigated further.

The functional interaction network generated using information from the Reactome database (266), highlights modules of highly interacting nodes from the gene set (**Figure 4.19)**. This was generated regardless of the directionality of change induced by Dex and helps to generate an indication of the key genes and regulated processes. Here the K^+ channels form an independent sub-network of factors which are all inter-connected supporting their associated function. Central nodes include EGFR, SRC (c-Src) and ARRB1 (β arrestin-1) implicating membrane-associated signalling. While other central nodes highlight transcription factors, FOXA1, JUN including nuclear receptors RXRA and AHR and nuclear transcriptional co-activator HELZ2 (helicase with zinc-finger 2) and strongly implicate perturbed genes in affecting transcriptional responses.

The network in **Figure 4.20A** shows the directionality of regulation by the groups in addition to implicated genes associated with the positive regulation of transcription. The genes associated with the sub-ontology regulation of transcription of RNA polymerase II promoter (**Figure 4.20B**) identifies a large number of transcription factors which are differentially regulated by the treatment groups. Plotting the log2fold change for each gene and condition, highlights three sub-groups of expression: genes regulated by Dex whose expression is reduced by CDK12/CDK13 inhibition; genes regulated by Dex whose expression is potentiated by THZ531 and genes regulated by Dex whose expression is regulated in the opposite direction following inhibition with CDK12/CDK13. This demonstrates how THZ531 has differential effects upon the expression of Dex-regulated genes.
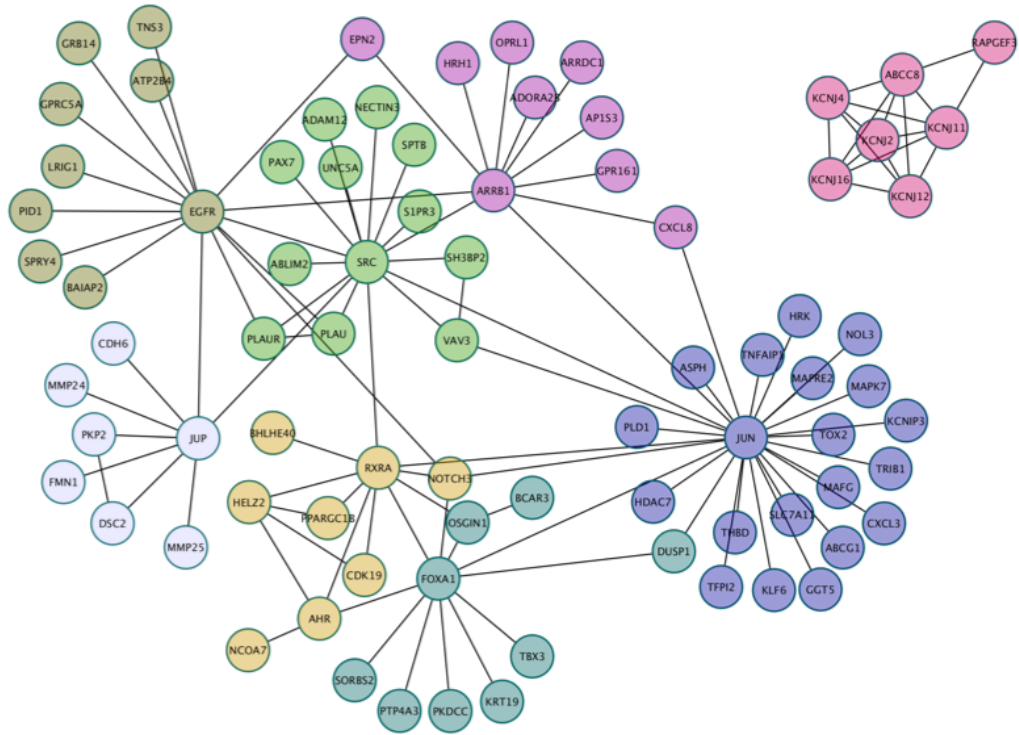
Figure 4.19 Functional interaction network of genes regulated by Dexamethasone and affected by THZ531

Reactome functional interaction network generated from all genes identified as being regulated by Dex and affected by THZ531. Modules of highly interacting groups of genes coloured by cluster group.

A)
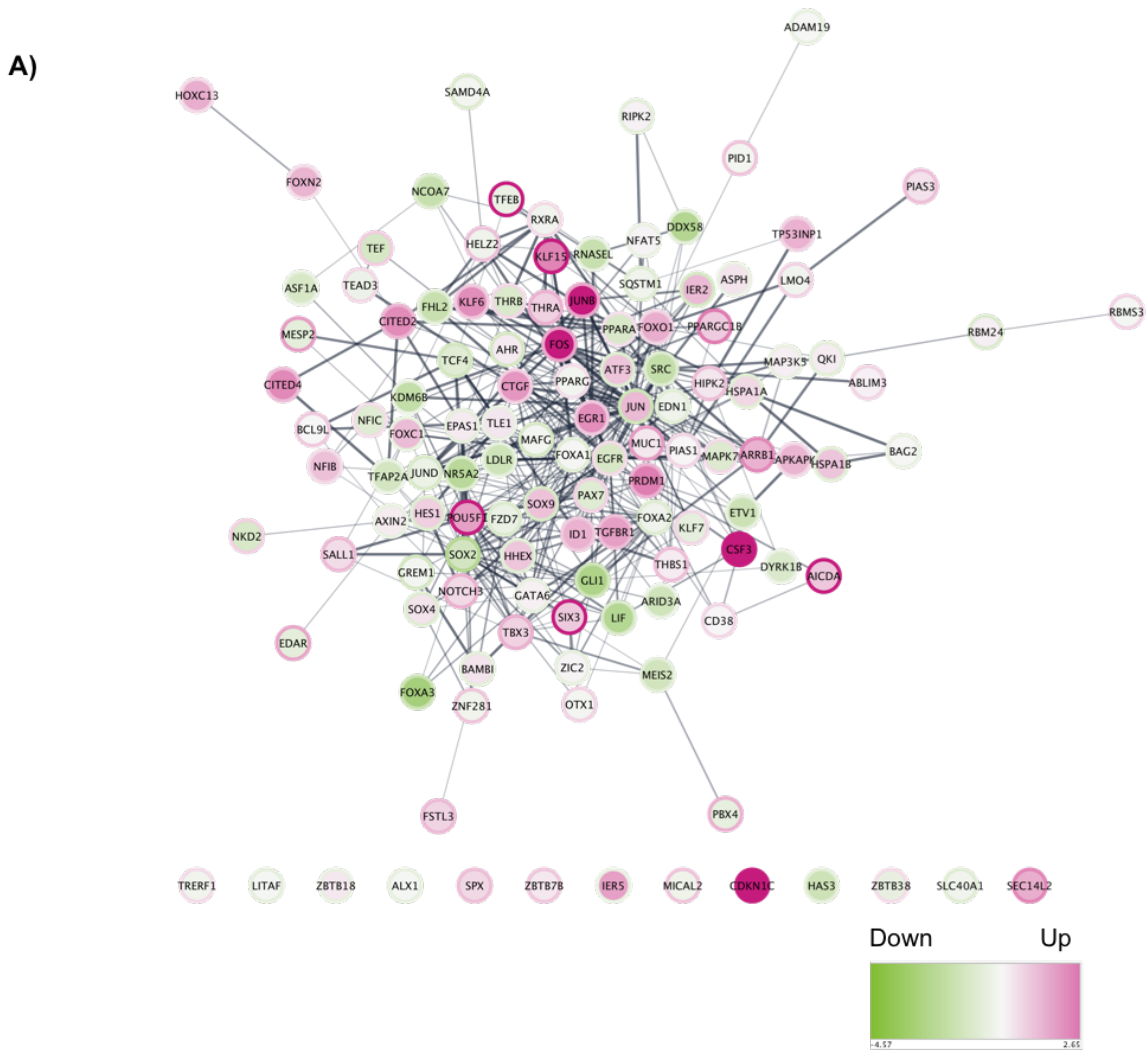
B)

Regulation of Transcription from RNA Polymerase II promoter
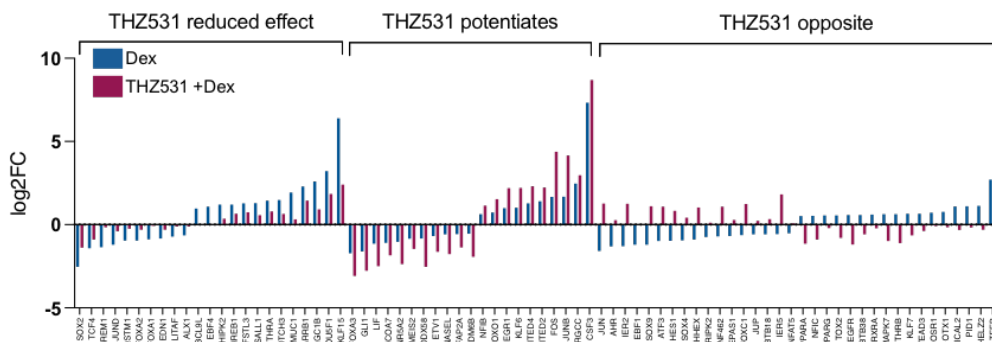
Figure 4.20 Dexamethasone-regulated genes affected by THZ531 and associated with regulation of transcription.

(A) String interaction network of all genes regulated by Dex and affected by THZ531 associated with the ontology positive regulation of transcription. Node centre coloured based on log2FC induced by THZ531+Dex vs vehicle and node outline coloured by log2FC by Dex vs vehicle. (B) Plotted log2FC for genes associated with the term regulation of transcription from RNA polymerase II promoter. Organised into groups based on effect of THZ531 and ordered by Dex-induced change.

The AP-1 transcription factors were featured as genes underlying multiple significantly enriched ontologies for example: positive regulation of transcription and regulation of cell proliferation differentiation – reflecting the cross-talk between GR and AP-1 factors (48, 72, 267). Plotting the expression changes in AP1 components (**Figure 4.21**) reveals how the expression pattern is modified by THZ531 and Dex treatments. For example, expression of *JUN* is downregulated by Dex alone but upregulated by THZ531+Dex and further still by THZ531-alone. Whereas, *FOS* expression is upregulated by Dex which is upregulated further and to a similar level by THZ531+Dex and THZ531 alone. This would lead to an altered composition of AP-1 factor expression which may influence dimer pairings and transcriptional outcomes.
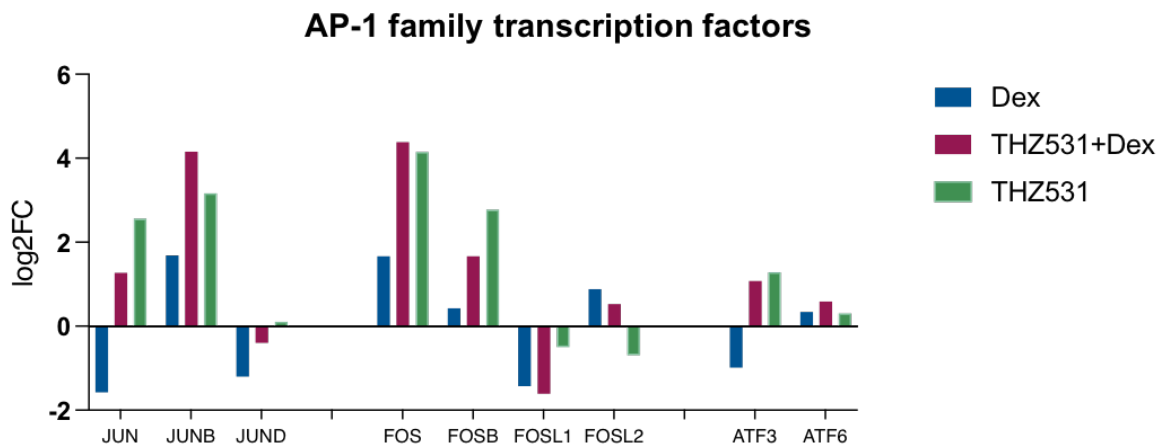
Figure 4.21 Differential expression of AP-1 transcription factors.

Plotted log2 fold change in expression for AP-1 transcription factor genes for 100nM Dex, 500nM THZ531 and 500nM THZ531+ 100nM Dex treated conditions in comparison to the vehicle control.

4.2.3.5 Comparison to genes not regulated by THZ531

Once the set of genes which are regulated by Dex and affected by the inhibition of CDK12/CDK13 had been established, I sought to assess whether the observed regulation was impacted by THZ531 alone. I found that the large majority of the potentiated and opposite gene groups (166 out of total 173 (166+7+94) and 233 out of total 327 respectively) (**Figure 4.22A**) were also genes which are significantly differentially regulated by THZ531 treatment alone. Whereas the greatest proportion of the reduced gene group (20 out of total 293) were not differentially expressed by THZ531 in comparison to the baseline. For the genes which are shared (highlighted in green circles), plotting the log2FC of shows the correlation between the direction of differential expression for each treatment THZ531 alone and THZ531 + Dex, in comparison to the vehicle. The potentiated and opposite genes show positive correlation in the direction of regulation by the two conditions. Conversely the expression of reduced genes is negatively correlated (**Figure 4.22B**). This analysis does suggest that THZ531 has a large impact on the expression of genes and directionality of change, regardless of Dex.
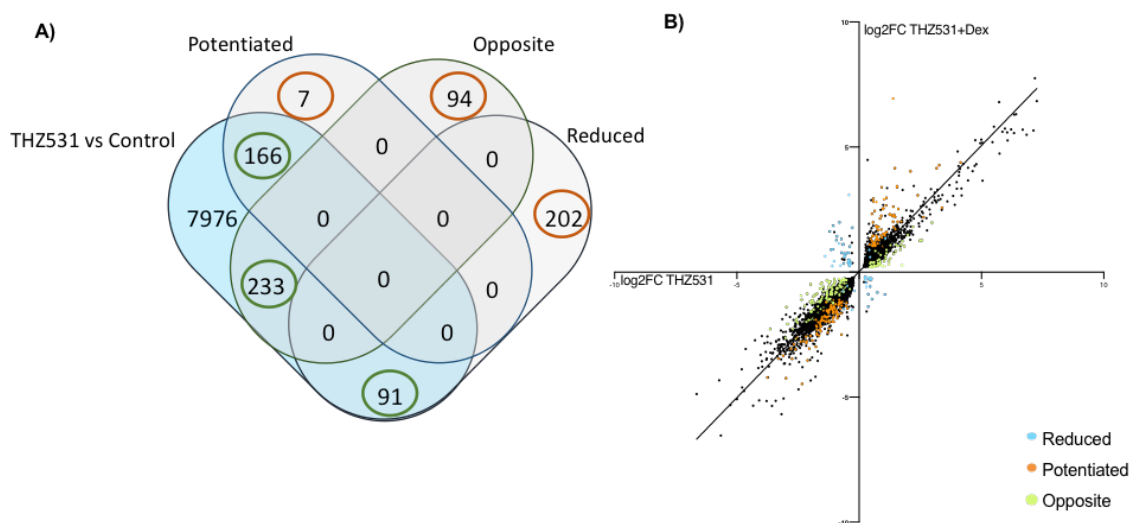
Figure 4.22 Comparison of genes regulated by THZ531 + Dexamethasone with the effect of THZ531 alone

A) Venn diagram comparing genes which are differentially expressed by THZ531 vs vehicle and Dex-regulated genes affected by THZ531 split into three groups: potentiated, opposite, reduced. Orange circle genes not significantly regulated by THZ531 alone. Green circle overlapping genes also significantly regulated by THZ5531. B) Scatter plot of log2FC of overlapping genes (green circle from Venn), differential expression change induced by THZ531 alone on x-axis and THZ531+ Dex on y-axis. Coloured points correspond to genes regulated by Dex and affected THZ531 split into three groups: potentiated, opposite, reduced.

4.2.4 Promoter analysis

4.2.4.1 AME

I used promoter analysis in attempt to understand the regulatory mechanisms underlying the differential gene expression patterns. This aims to identify candidate transcriptional regulators from a given set of co-modulated genes and assumes that the promoters of the differentially expressed gene sets are bound by the same transcription factors. First, I used motif enrichment analysis which scans promoter region genomic sequences of a set of genes to detect the presence of known transcription factor binding motifs. Previous ChIP-sequencing studies have found GR to bind genomic regions many kilobases (kbs) away from the transcription start site (TSS) of regulated genes (76). With this in mind, I obtained the promoter sequences for +100 bases downstream of the TSS in each case and either -1kb, 2kb, 5kb, 10kb or 20kb upstream to determine the best region for analysis.

To first validate the methodology, the sequences for genes which are significantly ($p < 0.01$ and log2FC ±1) up and down regulated by 100nM Dex were inputted into the AME server (177). The AME algorithm takes the inputted sequences of co-regulated genes and calculates the relative enrichment of known transcription factor motifs within the dataset. The identified enriched motifs were then compared to assess the differences between the size of the upstream sequence interval.

For the upregulated set of genes (407 total genes), the majority of enriched motifs were mutually identified between the different size regions (287 common motifs) (**Figure 4.23).** The greatest number of unique motifs were found for the -1kb region (185 unique motifs) followed by the -20kb region (36 unique motifs) which shared a proportion of with the -10kb region and 5kb region. The shared motifs found to be most significantly enriched in the gene sequences (**Table 4.1**) include motifs for forkhead box proteins: FOXC1, FOXC2, FOXL1; Zinc finger protein ZNF263, Interferon regulatory factor 1 (IRF1) and serum response factor (SRF). The enriched motifs which were identified for the set of genes downregulated by Dex (157 total genes) were again largely shared between the different size genomic regions (163 motifs). However, in comparison to the upregulated gene set, there was more variation in the extent of overlap between the sequence regions. The top most significantly enriched motifs which were found within all sequence regions included ZNF263, SP2 and SRF. Furthermore, 8 of these top motifs were the same motifs as identified for the upregulated gene set. Given the lack of distinction between the gene groups which are regulated in alternate directions by Dex, combined with the absence of GREs or any NR3C1 binding sites identified in the sequence regions, this lead to exploring a different motif-detection approach.
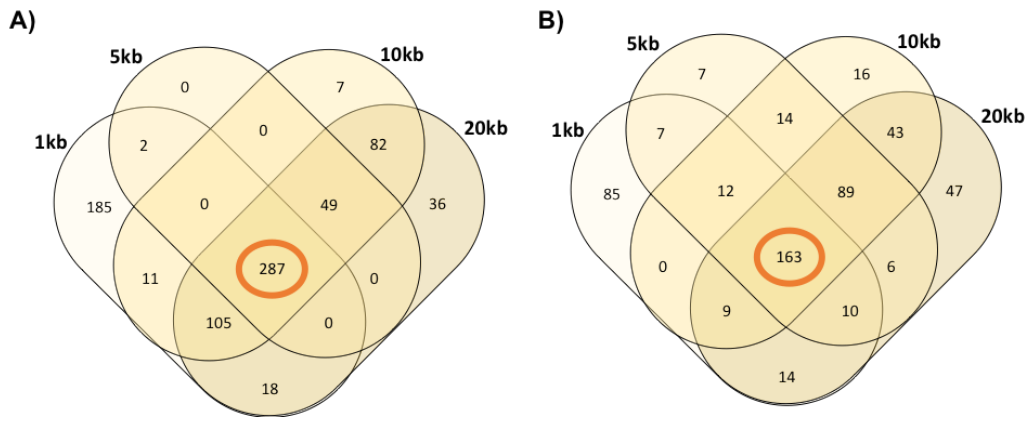
Figure 4.23 AME motif analysis of genes significantly regulated by Dexamethasone

*The promoter sequences were obtained for the 407 genes which were significantly (p<0.01, log2fold change ±1) upregulated by Dex **(A)** and for the 157 genes which were significantly downregulated by Dex **(B)**. Sequences corresponding to +100 bases downstream of the TSS in and either -1kb,2kb, 5kb, 10kb or 20kb upstream to determine the best region for analysis. Venn diagram displaying the number of identified motifs for each sequence region.*

Table 4.1 Top common motifs upstream of genes significantly upregulated by Dexamethasone.

The top scoring and shared motifs, which were identified within the promoter regions of the upregulated and downregulated genes, based on significance score (e-value). The unique identifier of the particular motif (columns 1 & 2) and name of the binding factor (column 3)

Up		
Motif_ID	Alternative ID	Binding factor name
FOXC1_DBD_1		Forkhead box protein C1
MA0528.1	ZNF263	Zinc finger protein 263
UP00029_1	Tbp_primary	TATA box binding protein
UP00037_1	Zfp105_primary	Zinc finger protein 105
Foxj3_DBD_4		Forkhead box protein j3
UP00097_2	Mtf1_secondary	Metal regulatory transcription factor 1
MA0050.2	IRF1	Interferon regulatory factor 1
UP00077_2	Srf_secondary	Serum response factor
FOXC2_DBD_2		Forkhead box protein C2
UP00090_2	Elf3_secondary	ETS-related transcription factor 3
FOXL1_full_2		Forkhead box protein L1

Down		
Motif_ID	Alternative ID	Binding factor name
MA0528.1	ZNF263	Zinc finger protein 263
MA0516.1	SP2	SP2 transcription factor
UP00077_2	Srf_secondary	Serum response factor
UP00037_1	Zfp105_primary	Zinc finger protein 105
MA1125.1	ZNF384	Zinc finger protein 384
FOXC1_DBD_1		Forkhead box protein C1
UP00028_2	Tcfap2e_secondary	Transcription factor AP-1ε
UP00029_1	Tbp_primary	TATA box binding protein
MA0050.2	IRF1	Interferon regulatory factor 1
UP00090_2	Elf3_secondary	ETS-related transcription factor 3
UP00097_2	Mtf1_secondary	Metal regulatory transcription factor 1

4.2.4.2 i-Regulon

The i-Regulon plugin for cytoscape (178) builds a transcription regulatory network using cis-regulatory sequence analysis of co-regulated genes with aim to identify master regulatory factors. Groups of differentially expressed genes are analysed against databases of motifs and ChIP-seq tracks. I-regulon uses a 'ranking-and-recovery enrichment calculation' for motif identification which briefly involves ranking all human genes for each motif within a library of position weight matrices (PWM). This is performed by taking the regions around the TSS of each gene which are then scanned for cis-regulatory modules (CRMs)– regulatory features of the genome outside coding regions, with dense sites for the binding of multiple TF (includes enhancers and promoter regions). The genes are ranked according to the likelihood it is a target of a particular motif. Gene rankings are then compared to the set of inputted query genes and based on area under the cumulative recovery curve to obtain a normalised enrichment score (NES). Motifs with a NES score ≥3 (corresponds to FDR between 3% and 9%) indicates that a large proportion of the query genes are ranked highly for that particular motif. The programme then uses a 'motif2TF' procedure to link enriched motifs from PWMs to a candidate binding factor based on annotations of motif-Tfs binding, orthology and motif similarity (178). The i-regulon programme has the added advantage that it reveals the underlying genes from the co-regulated list which are enriched for the motif or transcription factor. Therefore, the identified motifs and corresponding transcription factors can be placed in context of their gene targets.

4.2.4.3 Dex regulated genes

First, all the genes which were significantly regulated by Dex, regardless of THZ531 effect were analysed (as with the AME analysis). The tables of predicted transcription factors **(Table 4.2)** demonstrate that NR3C1 (GR) and FOXA1 are the only significant factors associated with upregulated genes. A number of transcriptional regulators were identified for the downregulated gene set, including histone acetyl transferase EP300, GATA3 and FOSL2. Other identified transcription factors JUND and RXRA, as well as FOXA1 were also genes differentially regulated by Dex and affected by THZ531, indicating a potential regulatory loop.

Table 4.2 Predicted transcriptional regulators of Dexamethasone-regulated genes

*Candidate transcriptional regulators, based on the identification of motifs enriched in the upstream regions of co-regulated genes. Performed using iregulon 'ranking-and-recovery enrichment calculation'. Groups of differentially expressed genes: 407 genes which were significantly (p<0.01, log2fold change ±1) upregulated by Dex, 886 genes regulated by Dex and significantly (p<0.01, log2fold change ±0.5) affected by THZ531 or not affected by THZ531 (722 genes). Each split into up- and down-regulated genes depending on directionality induced by Dex. Orange shading indicates factors in which the corresponding genes were identified as differentially regulated by Dex and affected by THZ531. * Indicates transcription factors unique to that category. NES: normalised enrichment score.*

| | Up | | Down | |
	Transcription Factor	NES	Transcription Factor	NES
Dex	NR3C1	9.08	EP300	5.47
	FOXA1	6.05	GATA3	4.46
			TEAD4	4.11
			JUND	3.99
			FOSL2	3.82
			TCF12	3.58
			MEF2A*	3.08
			RXRA*	3.00
Dex affected by THZ531	NR3C1	9.53	EP300	4.79
	FOXA1	4.90	GATA3	3.78
			TEAD4	3.6
			FOXA2	3.49
			FOSL2	3.45
			ERM* (ETV5)	3.41
			JUND	3.22
			TCF12	3.06
Dex not affected by THZ531	NR3C1	7.44	EP300	5.41
	FOXA1	7.38	GATA3	4.64
			FOSL2	4.19
			TCF12	4.04
			JUND	3.58
			TEAD4	3.51
			FOXA2	3.33
			FOSL1*	3.07

4.2.4.4 THZ531 affected vs not-affected

The analysis was then performed using the two groups of Dex-regulated genes: Group 1 - Dex regulated genes which are affected by THZ531 (genes in the intersecting region of the Venn) and Group 2 - Dex regulated genes which are independent of THZ531 as previously described. For both groups of genes, NR3C1 and FOXA1 were again associated with genes up-regulated by Dex, indicating that THZ531 does not alter the primary regulatory factors associated with upregulated genes. Although the NES score for NR3C1 was higher for Dex-regulated genes affected by THZ531 in comparison to those not affected whereas the converse was observed for FOXA1.

Overall, the associated regulators and NES scores, corresponding to genes down-regulated by Dex were largely shared between the two groups and all genes regulated by Dex. However, some factors were unique to the groups; as indicated in the table for example: affected by THZ531 ERM (ETV5) and not affected by THZ531 (FOSL1).

To further investigate these regulatory factors, I performed the analysis for the intersecting genes split in to subgroups and based on the directionality of the change induced by THZ531 (ie reduced, potentiated or opposite) **(Table 4.3).**

The reduced group was only associated with GR and FOXA1 for upregulated genes. The two factors were also identified for the opposite and potentiated groups. The latter groups had other implicated transcriptional regulators and a number of regulators were unique to that category eg ZBTB7A for opposite and FOXP2, POLR2A, TBP and CEBPD for potentiated groups. The NES was the greatest for NR3C1 for genes reduced by THZ531 and the score of FOXA1 was lower than that of all Dex upregulated genes. The identification of more factors in the opposite and potentiated groups likely account for the lower NES score for NR3C1, suggesting the contribution of other transcriptional regulators is important. Some of these factors were also associated with down-regulated genes for a different group (eg EP300, TCF12, NFIC, FOXA2, RDBP) which may indicate a shift in the regulatory balance caused by THZ531 treatment for those particular gene groups. By stratifying the gene lists based on the directionality of change induced by THZ531, a greater number of associated transcription factors were identified for down-regulated genes. A number of these factors such as ZNF263, JUN and CEBPB, among others, were unique to the category they were identified to be associated with. These factors may provide insight into the differential regulation of each gene groups and the effect of CDK12 and CDK13.

Table 4.3. Predicted transcriptional regulators of Dexamethasone-regulated genes affected by THZ531

Candidate transcriptional regulators, based on the identification of motifs enriched in the upstream regions of co-regulated genes. Performed using iregulon 'ranking-and-recovery enrichment calculation'. Groups of differentially expressed genes as indicated for up- and down-regulated genes: opposite by THZ531 (327 genes), potentiated by THZ531 (173 genes), reduced by THZ531 (293 genes). Orange shading indicates factors whose genes were identified as differentially regulated by Dex and affected by THZ531. * Indicates transcription factors unique to that category. NES: normalised enrichment score.

	Up		**Down**	
	Transcription Factor	NES	Transcription Factor	NES
Reduced	NR3C1	10.85	EP300	5.06
	FOXA1	4.93	GATA3	4.02
			FOXA2	3.95
			ZNF263*	3.58
			TCF12	3.36
			JUN*	3.29
			SMC3*	3.29
			TEAD4	3.16
			FOSL2	3.07
Opposite	NR3C1	6.43	PML*	4.38
	FOXA1	3.77	RDBP	3.97
	NFIC	3.50	EP300	3.69
	ZBTB7A*	3.38	JUND	3.49
	TCF12	3.15	TEAD4	3.28
	EP300	3.11	CEBPB*	3.27
			GATA3	3.19
			TAF1*	3.11
			REST*	3.04
Potentiated	NR3C1	4.36	NFIC	4.59
	FOXP2*	4.07	ERM (ETV5) *	4.17
	FOXA2	3.81	FOXA1	3.84
	RDBP	3.72	NFIC	3.74
	POLR2A*	3.30	TEAD4	3.62
	TBP*	3.18	JUND	3.40
	CEBPD*	3.18	EP300	3.30
	FOXA1	3.14	FOSL2	3.18
	EP300	3.13	FOSL1*	3.13

4.2.4.5 LISA

The LISA (epigenetic landscape *In Silico* deletion analysis) takes lists of differentially expressed genes with the aim of predicting the transcriptional regulators responsible for co-regulation. This approach integrates chromatin accessibility data (DNAase-seq and ATAC-seq) with known transcriptional regulator binding information from ChIP-seq databases. The analysis can be performed on the same gene list to produce two outputs: firstly, by using ChIP sequencing data of transcriptional regulators (transcription factors and chromatin regulators) to infer the peak-based regulatory potential upon a gene. Peaks are taken to represent binding in a binary manner 100kb up- and down-stream of the TSS. The second uses a similar approach but is a motif-based method which identifies the number of motif-hits within the promoter of target genes. An assumption of these models is that regulatory effect upon the target gene bound by a particular factor is reduced with increasing genomic distance from the TSS. Also, that the presence of multiple binding sites has an additive effect on target gene regulation. The LISA uses this peak-regulatory potential model accounting for binding distance and number of sites, combined with a model of chromatin landscape- accessibility to identify regulators of the query gene set in comparison to a set of unrelated background genes (179).

4.2.4.6 ChIP-Seq approach

I first assessed the same set of genes most significantly regulated by Dex. By inputting two gene sets corresponding to up and down regulated genes, the output provides an adjPvalue for the contribution of a factor towards the regulation of the genes perturbed in a particular direction, which can be plotted (as in **Figure 4.24A** and zoomed **Figure 4.24B**). Each point represents a factor investigated in a publicly available ChIP seq experiment.

NR3C1 is identified as the most significant factor associated with up-regulated genes, evident by the distribution of points along the x axis. The DNA repair protein and part of the cohesisn complex (268) RAD21 was another factor closely associated with upregulated genes. CEBPB and pioneer factor FOXA1 were significantly associated with both up- and down-regulated genes; evident by the distribution of points between the two axes. Some of the top significant factors associated with the down regulated genes set were AP-1 family members FOSL2 as well as FOS and JUN, although, showed a similar distribution to CEBPB. Factors GATA3 and RELA were also clustered towards the down regulated gene set.

To further understand how the inhibition of CDK12 and CDK13 may affect Dex-regulated genes, I performed the same LISA model analysis by inputting the two groups of genes, described previously: based on the effect of CDK12 and CDK13 inhibition. The corresponding adjPval scores were plotted and **Figure 4.25** shows the predicted contribution of the transcriptional regulators for genes either up vs downregulated by Dex. Again, NR3C1 is the most significant factor associated with upregulated genes for both groups. In addition, the RAD21 is associated with up-regulated genes and is more prominent for genes regulated by Dex and affected by THZ531 compared to those not affected. However, the distribution of FOXA1 shows a shift (compare

Figure 4.25B vs **Figure 4.25D**) from closely associated with upregulated genes towards downregulated genes that are affected by THZ531. This is also apparent for CEBPB and FOSL2. Comparison of all the significant transcription regulatory factors identified for each group reveals a large overlap, with 369 factors predicted to regulate the two gene sets. Although, a number of regulators were uniquely identified for each group, there are more factors associated with the genes regulated by Dex and affected by inhibition of CDK12 and CDK13 compared to genes not affected by THZ531 (174 and 58 respectively).

In attempt to understand effect of CDK12 and CDK13 inhibition, the analysis was then performed for the three gene groups regulated by Dex and further stratified by the direction of expression change by THZ531. For all three groups; opposite, potentiated and reduced by THZ531, NR3C1 was again identified as being the most significantly associated with genes upregulated by Dex (**Figure 4.26**). Although, the level of significance was lower for the genes potentiated by THZ531 NR3C1 was still the most predominant factor for upregulated genes (**Figure 4.26 B&E**). Similarly, for all groups, RAD21 maintained a close association with upregulated genes. The genes regulated in the opposite direction by THZ531+Dex compared to Dex alone show FOSL2 and CEBPB contributing towards the expression of genes in both directions (**Figure 4.26 A&D**). FOXA1 and GATA3 are the predominant factors associated with downregulated genes and reflects the distribution observed for the whole group of genes affected by THZ531 (**Figure 4.25 C&D**). The potentiated group shows a similar distribution for CEBPB and FOSL1 to the opposite genes. Whereas, FOXA1 and GATA3 show a shift in distribution to be equally centred between up and down regulated genes. RELA shows the closest correlation with down-regulated genes. The distribution of factors for the reduced gene set is most comparable to the opposite group except FOXA1 and GATA3 are not as closely associated with down regulated genes.

A large proportion (338) of transcriptional regulators are shared within all three groups. However, identification of common factors does not necessarily indicate the same effect as the contribution towards up and down regulated genes set is not considered.

Figure 4.24 LISA Model ChIP-seq: Analysis of genes significantly regulated by Dexamethasone

Scatter plots of -log10 p-values for transcriptional regulators corresponding to gene sets both up- and downregulated by Dex. Analysed using LISA cistrome ChIP-seq based method, each dot represents a single transcriptional regulator. The spread of all the identified factors (A). Zoom of the above graph showing factors between the values of –log10(pval) 20 up / down (B). DEG: Differentially expressed gene.
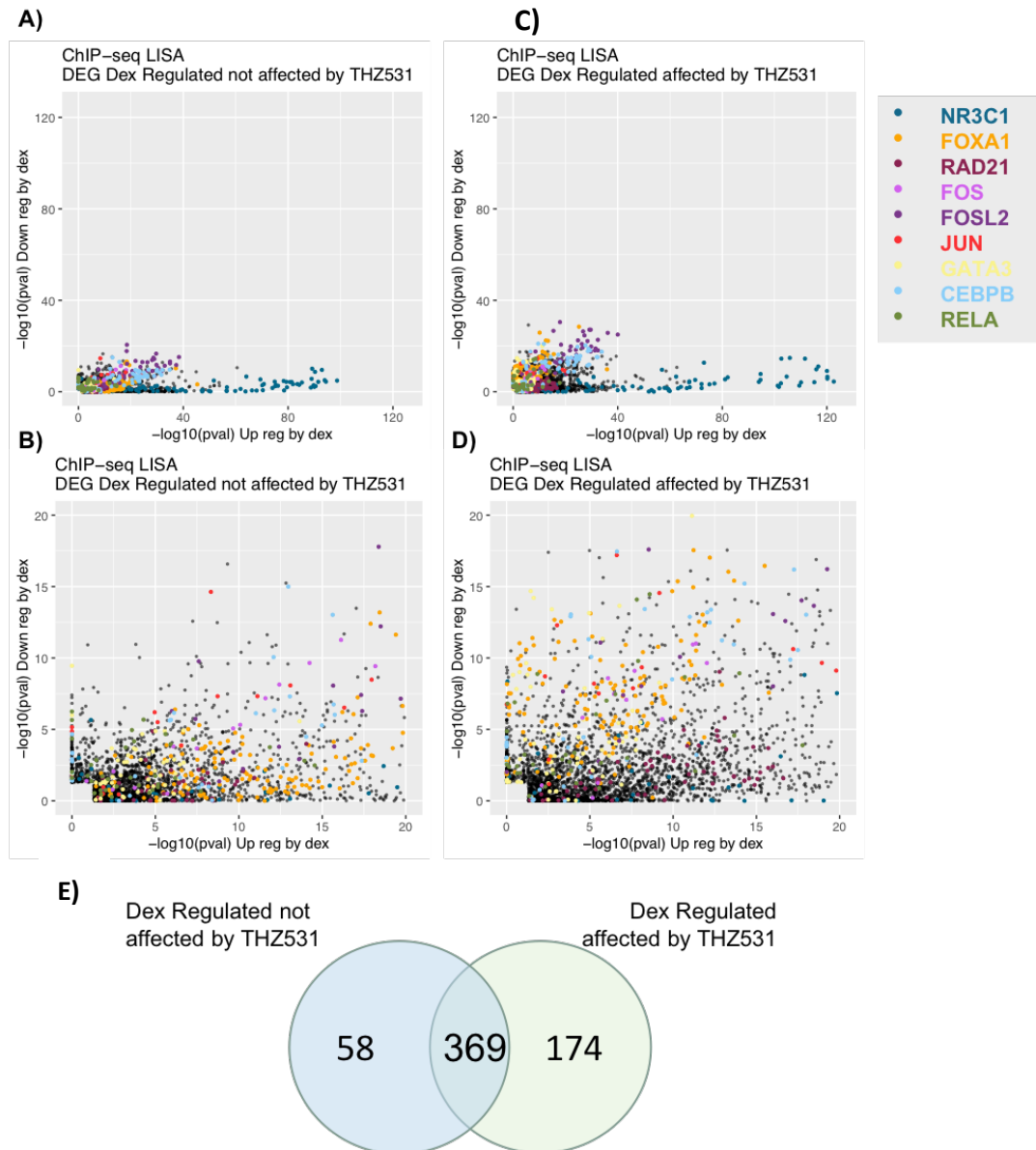
Figure 4.25 LISA Model ChIP-seq: Analysis of genes significantly regulated by Dexamethasone and affected or not affected by THZ531

*Scatter plots of -log10 p-values for transcriptional regulators corresponding to gene sets both up- and downregulated by Dex. Analysed using LISA cistrome ChIP-seq based method, each dot represents a single transcriptional regulator. The entire set of identified factors for the gene sets: **A)** regulated by Dex and not affected by THZ531, **C)** regulated by Dex and affected by THZ531. Zoom of the above graphs **B)** not-affected by THZ531 and **D)** affected by THZ531 showing factors between the values of –log10(pval) 20 up / down. DEG: Differentially expressed gene. **E)** Venn diagram comparing the shared predicted regulatory factors between genes regulated by Dex*

Figure 4.26 LISA Model ChIP-seq: Analysis of genes significantly regulated by Dexamethasone and stratified based on the effect of THZ531

*Scatter plots of -log10 p-values for transcriptional regulators corresponding to gene sets both up- and downregulated by Dex. Analysed using LISA cistrome ChIP-seq based method, each dot represents a single transcriptional regulator. The entire set of identified factors for the gene sets: **A)** opposite by THZ531, **B)** potentiated by THZ531, **C)** reduced by THZ531. Right column, zoom of the adjacent graphs **D)** opposite(**E)** potentiated **F)** reduced, showing factors between the values of –log10(pval) 20 up / down. DEG: Differentially expressed gene.*

4.2.4.7 Motif-based approach

The motif-based approach of the LISA analysis identifies enriched transcription factor binding-motifs located in the promoter regions of the gene set of interest. As with the ChIP-method, it can assess gene sets corresponding to up and down regulated genes with an adjPvalue for the contribution of a factor towards the direction of regulation. As before, the gene sets were analysed, all significant motifs are plotted (each point representing a single motif), with transcription factors of interest shown in colour. In addition to the top, most significant motifs for the up and down regulated genes are labelled (**Figure 4.27**). For all Dex-regulated genes, the motif for ZNF219 was most significantly associated with upregulated genes, closely followed by NR3C1 and other nuclear receptors PPARG and AR. Myeloid zinc finger factor MZF1 was also a top factor closely associated with the upregulated genes. Motifs for AP-1 family proteins, FOS, FOSL1 and JUN, JUNB, JUND were identified as being associated with downregulated genes. Whereas, RELA is more significantly associated with up-regulated genes.

Motif enrichment performed for genes regulated by Dex and not affected by the inhibitor, reveals significantly enriched motifs are situated between the axes - indicating a similar correlation with both up and down regulated genes (**Figure 4.28A**). Of these factors NR3C1 is the dominant factor for upregulated genes. The AP-1 factors are the top identified motifs for downregulated genes despite showing equal significance with upregulated genes. This contrasts the Dex-regulated genes affected by THZ531 (**Figure 4.28B**), there is a clear definition between factors associated with either up or down regulated genes. NR3C1 does not feature as the most significant motif for upregulated genes which was found to be MZF1. FOXP1, FOXA2 and FOXA1 contribute to the top motifs associated with down regulated genes and were not identified for genes not-affected by THZ531. Almost all identified motifs for genes not affected by THZ531 were shared with those that were affected (219/233). However, 432 motifs were unique to the affected category potentially indicating the modulation of a much greater number of factors.

The motif- based detection method was again applied to the gene groups based on directionality of change induced by THZ531 (**Figure 4.29**). The opposite by THZ531 group displays a similar distribution of factors to that of the Dex-regulated-THZ531 affected group, including a significant association with the MZF1 motif for upregulated genes. Whereas, the motifs identified for the potentiated by THZ531 group, are largely clustered in between up and downregulated genes with inflammatory factors such as NF-κB2, RELA and STAT4 occupying the region. NR3C1 and AR motifs are most significant for upregulated genes and AP-1 factors are most prominent for the downregulated gene set. The contribution of the FOX transcription factors is less significant than for the genes regulated in the opposite direction by THZ531. In contrast to the CHIP-based analysis opposite regulated genes have more associated motifs yet many of the identified transcription regulatory factors are again shared between the groups (265 shared motifs).

The use of promoter, motif analysis helps to identify potential transcriptional regulators involved in the expression of specific gene sets. Rather than identifying an individual

transcriptional regulator perturbed by THZ531 as initially hypothesised, the integration of the findings from different methods demonstrates both the complexity of transcriptional regulation and how the balance of multiple factors contributes to gene expression. However, this analysis must be further validated to fully understand the contribution of CDK12 and CDK13 to the regulation of Dex-modulated transcription.

4.2.4.8 Bioinformatic Analysis Summary

In summary, the integrated bioinformatic analysis was utilised to understand the relationship between GR genomic regulation and the activity of transcriptional kinases CDK12, CDK13 and their partner cyclin K. Inhibition of CDK12 and CDK13 activity by THZ531 does not affect all Dex-regulated genes, rather a substantial subset ~55% genes; with a greater number of upregulated genes perturbed (594 out of 886, 67% of genes regulated by Dex and affected by THZ531). Ontology analysis suggests that CDK12 and/or CDK13 are involved in GR-regulated expression of proteins involved cell proliferation and apoptosis in addition factors regulating transcriptional processes. Ultimately, this suggests that CDK12 and/or CDK13 are essential for GR genomic outputs and functional outcomes associated with cell survival and differentiation.

Stratification of Dex-regulated gene subsets based on the directionality of the expression change incurred by THZ531, reveals three groups: reduced potentiated and opposite. Promoter analysis supports the involvement of AP-1 factors – both as regulatory proteins mediating the expression of genes regulated by Dex, CDK12 and CDK13 and as genes whose expression is affected by the loss of CDK12 and CDK13 activity. Analysis using both cistrome binding patterns and motifs was employed in attempt to identify a key transcriptional regulator for each gene group. Candidate transcription factors such as FOXA1/FOXA2, members of the AP-1 family and CEBPB among others, were identified as potentially involved in the expression pattern of the DEG groups. However, this analysis revealed that the measured effects were not clearly attributable to the expression or activity of unique factors. Rather, inhibition of CDK12 and CDK13 indicates a potential transcriptional shift in GR-crosstalk with multiple transcriptional regulators.
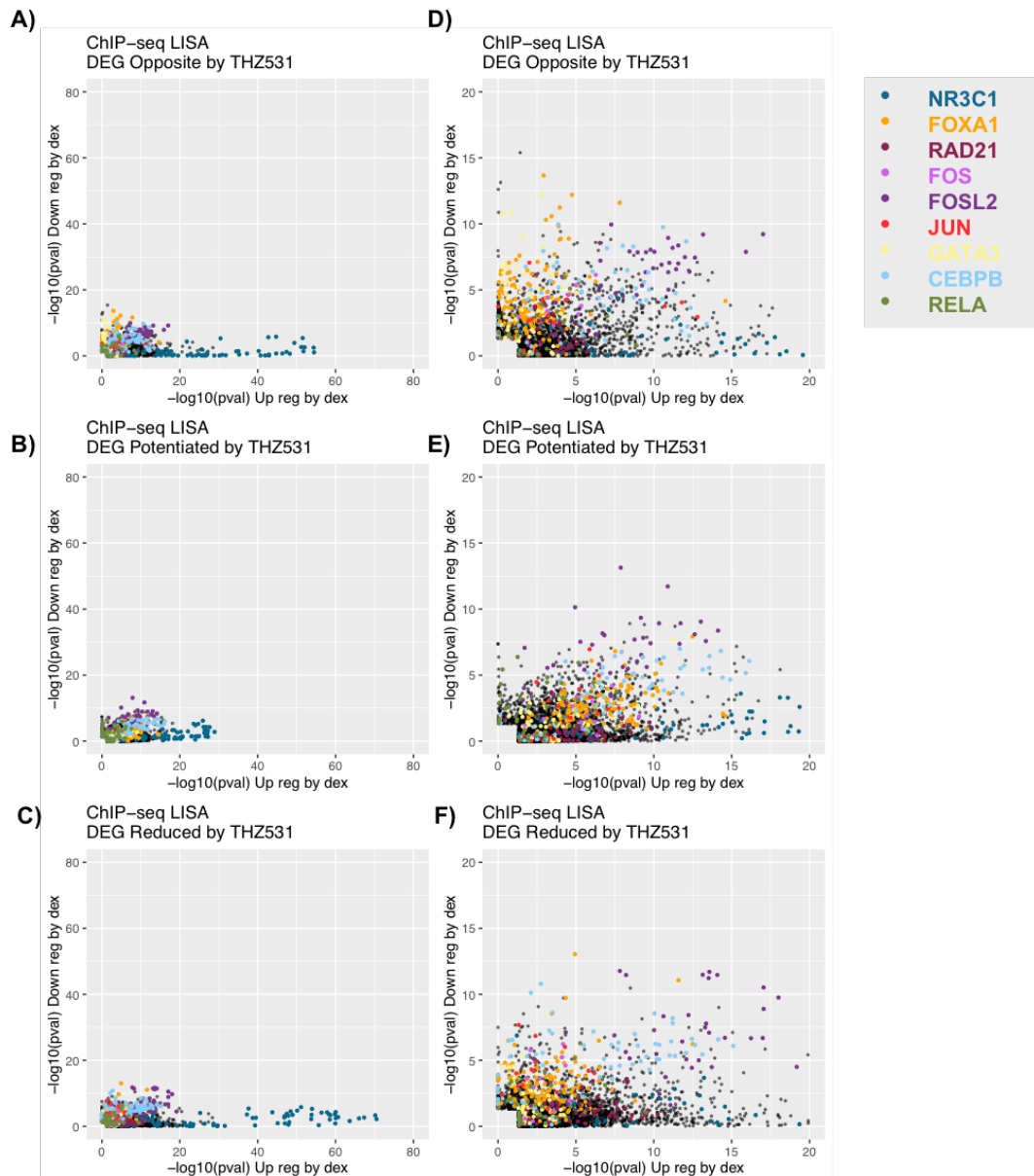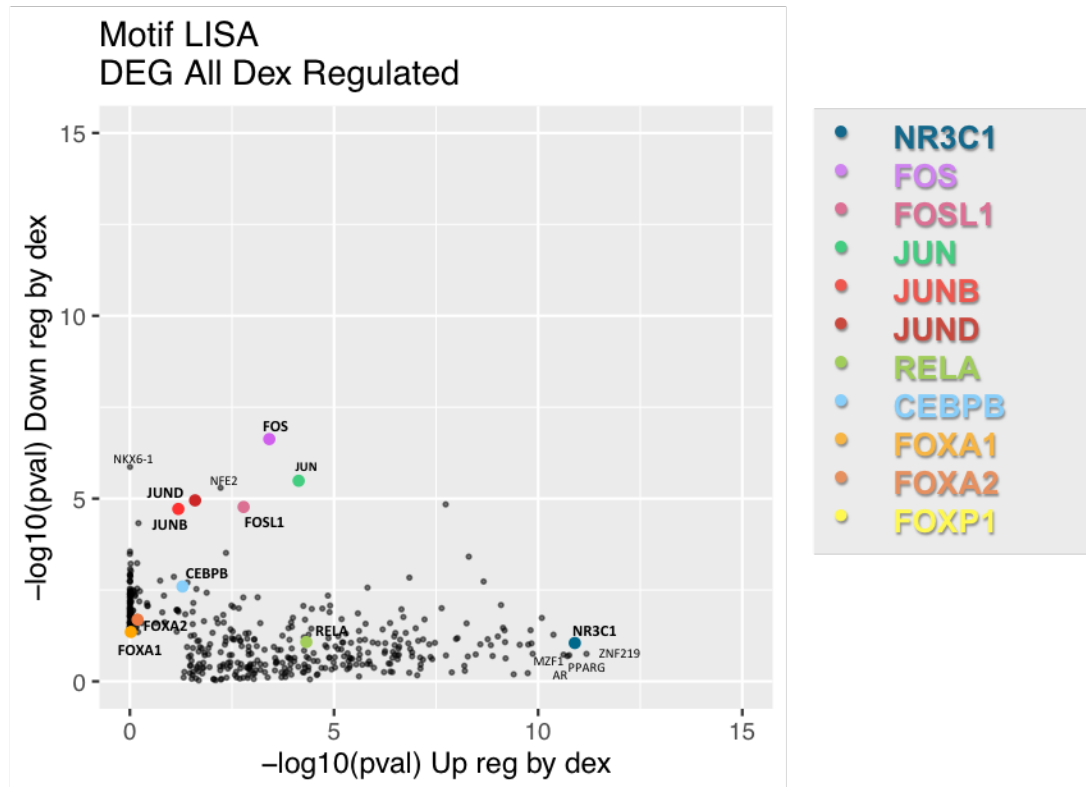
Figure 4.27 LISA Model Motif: Analysis of genes significantly regulated by Dexamethasone

Scatter plots of -log10 p-values for motifs of transcriptional regulators corresponding to both gene sets both up- and downregulated by Dex. Analysed using LISA cistrome motif-based method, each dot represents a single transcriptional regulator binding motif. Coloured dots represent defined transcription factors in order to compare between data sets. Labelled factors without coloured dot, represent the motifs identified as having the top significance ranking for the up / down- regulated genes. DEG: Differentially expressed gene.
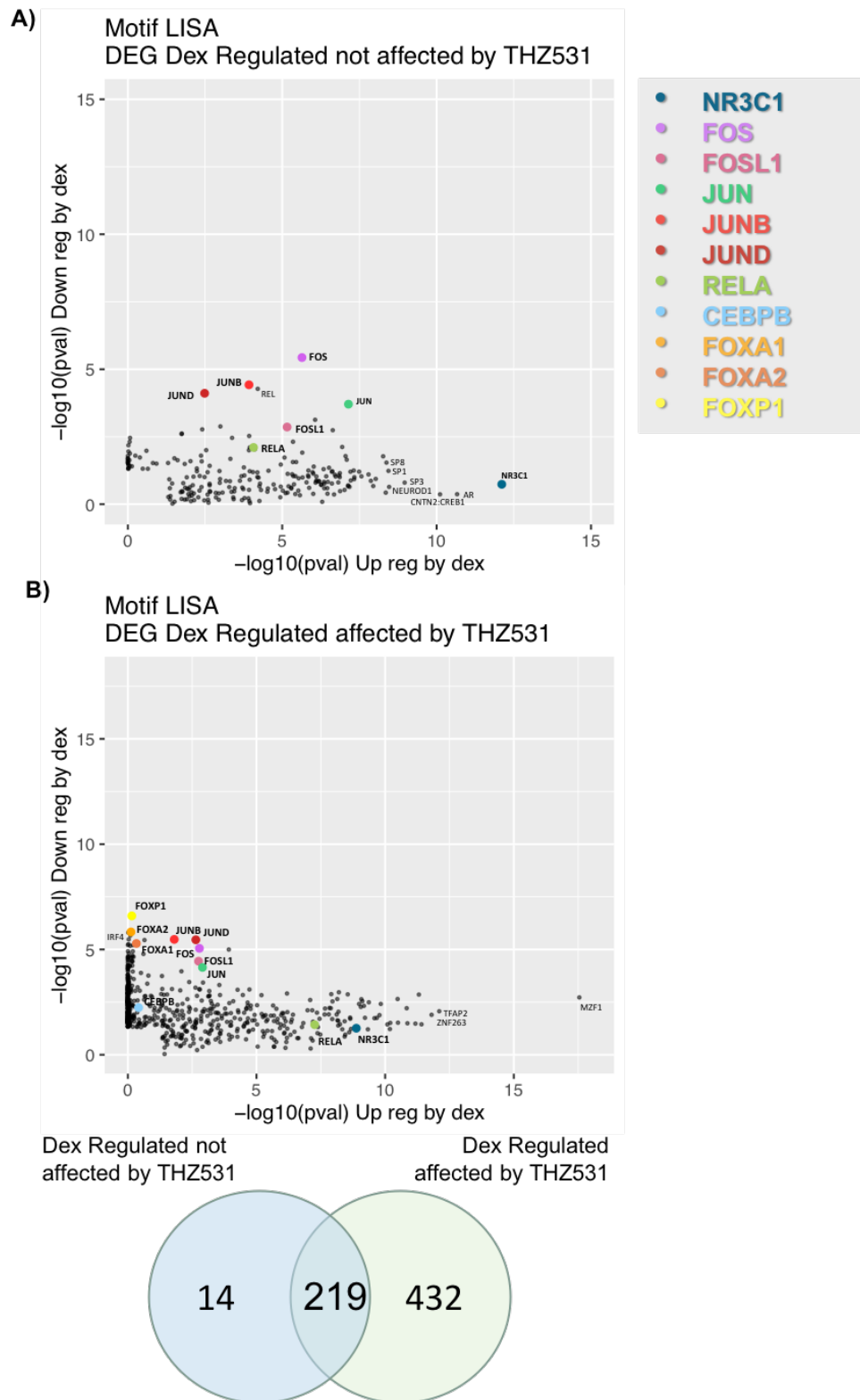
Figure 4.28 LISA Model Motif analysis of genes significantly regulated by Dexamethasone and affected or not affected by THZ531

*Scatter plots of -log10 p-values for motifs of transcriptional regulators corresponding to both gene sets both up- and downregulated by Dex. The entire set of identified factors for the gene sets: **A)** regulated by Dex and not affected by THZ531, **B)** regulated by Dex and affected by THZ531. Analysed using LISA cistrome motif-based method, each dot represents a single transcriptional regulator binding motif. Coloured dots represent defined transcription factors in order to compare between data sets. Labelled factors without coloured dot, represent the motifs identified as having the top significance ranking for the up / down- regulated genes. **C)** Venn diagram summarising the number of identified motifs for each gene set. DEG: Differentially expressed gene.*
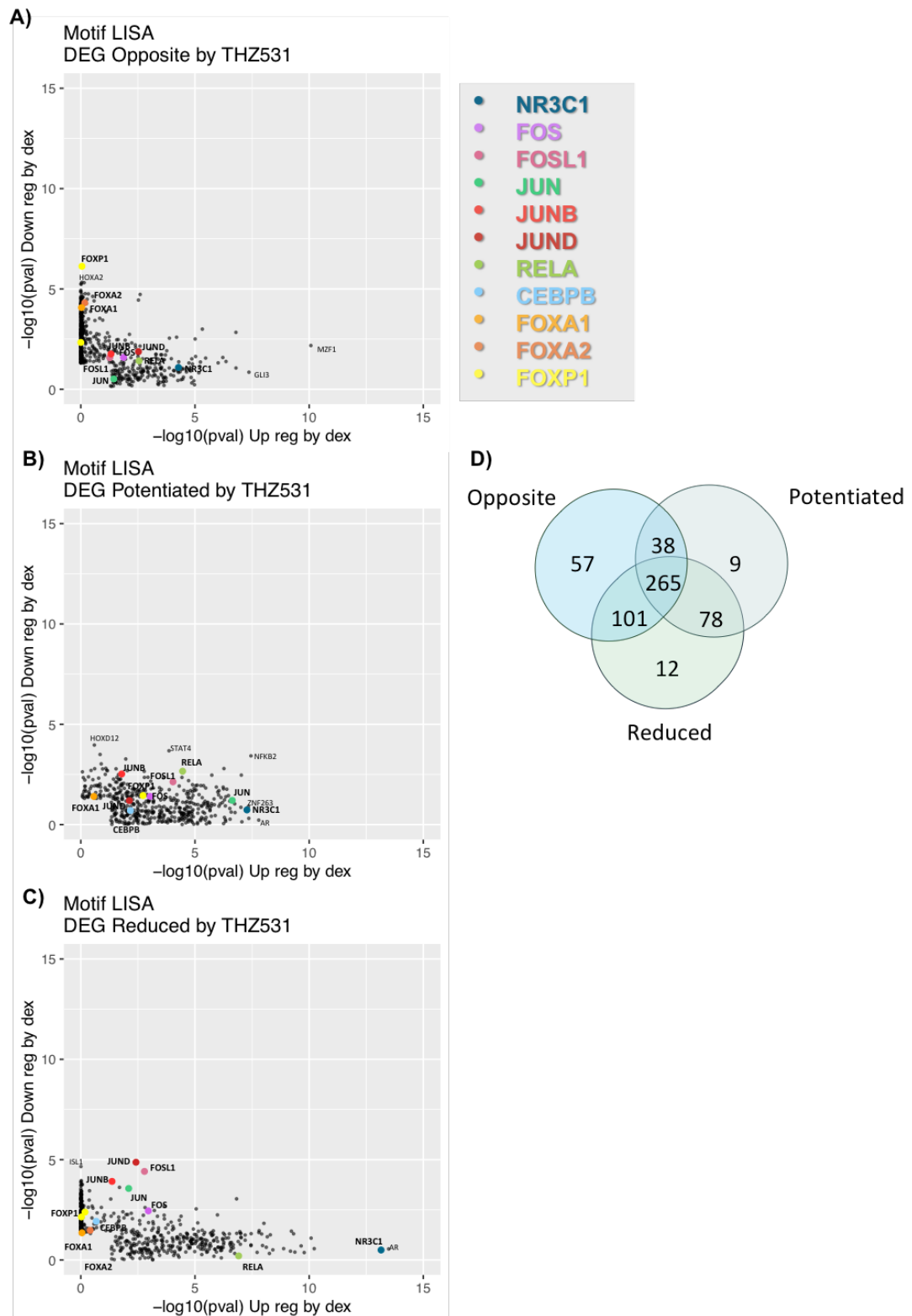
Figure 4.29 LISA Model Motif Analysis of genes groups significantly regulated by Dexamethasone and affected by THZ531

*Scatter plots of -log10 p-values for motifs of transcriptional regulators corresponding to both gene sets both up- and downregulated by Dex. The entire set of identified factors for the gene sets: regulated by Dex and **A)** regulated in the opposite direction by THZ531, **B)** potentiated by THZ531, **C)** reduced by THZ531. Analysed using LISA cistrome motif-based method, each dot represents a single transcriptional regulator binding motif. Coloured dots represent defined transcription factors in order to compare between data sets. Labelled factors without coloured dot, represent the motifs identified as having the top significance ranking for the up / down- regulated genes. **D)** Venn diagram summarising the number of identified motifs for each gene set. DEG: Differentially expressed gene.*

4.3 Discussion

4.3.1 The Rpb1 phosphorylation status

The phosphorylation of the CTD serine residues of RNA polymerase II is crucial for cell survival by mediating productive transcription (269). The changes in phosphorylation of the Rpb1 CTD observed following Dex treatment, revealed a decline in Ser7 phosphorylation over-time, concomitant with a gradual increase in ^{P}Ser2 which peaked at 15 minutes and declined by 60 minutes following Dex-exposure. This may suggest there is a global increase in elongating RNA polymerase II by 15 minutes following GR-activation. Ser2 phosphorylation is considered a mark of active transcription as levels increase along gene bodies peaking at the 3' end (254, 270). This reflects the dynamics of Rpb1 whereby the number of actively elongating complexes was shown to peak at approximately 25 minutes following Dex addition (271). These changes in phosphorylation patterns were measured at time points understood to be prior to GR nuclear entry. Theories regarding how nuclear proteins are phosphorylated in context to GR localisation are discussed in the previous chapter (3.3.5 Biological relevance). In this context one hypothesis would be that Dex initiates a cytoplasmic signalling cascade terminating on kinases capable of modifying RNA polymerase II. The result of such action primes the transcription machinery for more efficient, large-scale genomic activity upon GR translocation and subsequent chromatin binding.

Many studies have attempted to define the precise substrate specificity of the transcriptional CDKs, which has revealed contextual complexity with multiple kinases able to phosphorylate Rpb1 CTD. Using pharmacological inhibition of CDKs I show that Ser2 phosphorylation is reduced but not abolished. The broad targeting inhibitor, FVP is capable of inhibiting multiple CDKs including the primary Ser2 kinases CDK9 and CDK12 (254, 272), this transpired to the greatest measured reduction in Ser2 phosphorylation - both from the baseline and the Dex-induced increase. This effect was sustained at later time points and also reduced phosphorylation of Ser5, although not to as great an extent.

For THZ531 treated samples, CDK9 remains active which has been implicated as the predominant Ser2 kinase for regulating the pause-release step to proceed into productive elongation (272). The retained activity of CDK9 would explain the residual level of Ser2 phosphorylation in the presence of CDK12 and CDK13 inhibition. Although, after 4.5 hours phosphorylation was reduced to half that of the baseline potentially indicating a delayed effect upon global Ser2 phosphorylation. Furthermore, at this later timepoint Ser2 phosphorylation was reduced between vehicle and Dex-treated samples an effect not observed for Ser 5 phosphorylation, which was upheld to an extent in the presence of THZ531. These temporal

differences in Dex-induced dynamics of Ser2 phosphorylation levels indicate an involvement of CDK12 and /or CDK13 although, the true mechanism remains to be determined. Alternatively, it may not be that Dex alters the activity of the kinases but the rather a phosphatase (269) or CDK inhibitor such as CDKN1C (273) which alters the dynamics of Rpb1 CTD regulation.

CDK12 has been implicated as a Ser5 kinase (258). However, I investigated the effect of the CDK inhibitors upon the level of Ser5 phosphorylation, and show THZ531 has no significant effect on the phosphorylation levels of Ser5 in comparison to basal levels. The precise role of CDK12 is still debated and may potentially only phosphorylate Rpb1 at a select number of genes. Knockdown of CDK12/13 or cyclin K has been shown to not result in a measurable reduction in Ser2 phosphorylation (254); an effect also seen using analogue sensitive-inhibition of CDK12 (a competitive ATP analogue which, when added, specifically abolishes the kinase activity of the protein) (258). Likewise, inhibition of the kinases using THZ531 has not been shown to conclusively impede total Ser2 phosphorylation (256) and corresponds with my findings.

As part of TFIIH complex, CDK7 facilitates transcription initiation with the addition of phospho-modifications upon positions Ser5 and Ser7 of the Rpb1 CTD. The Ser5 modification, disrupts the interactions between RNA Polymerase II and the mediator complex, allowing the transcription machinery to escape gene promoters (274). Phosphorylation of the Ser5 residue is recognised by 5' capping enzymes to prevent degradation and demonstrates the involvement of Ser5 modification during early stages of mRNA transcription. CDK9 is the catalytic subunit of P-TEFb which phosphorylates the Ser2 residue, but displays preference towards a substrate pre-phosphorylated at Ser7 (272). CDK12 and CDK13 are important for RNA processivity and also phosphorylate Rpb1 CTD at Ser2, thought to occur sequentially following CDK9-mediated activity. Similarly, CDK12 requires substrate pre-phosphorylation of Ser7 for substrate recognition and optimal activity (257). This Ser7 modification is present early during the process and can be bound by the integrator multiprotein complex and associate with RPAP2 – a phosphatase which removes Ser5 phosphorylation (270). Despite CDK9, CDK12 and CDK13 regulating the phosphorylation of the same residue, the kinases have distinct but overlapping roles and synergistically maintain enriched levels of Ser2 along gene bodies (256). CDK9 has been shown to indirectly recruit CDK12 via polymerase-associated factor 1 complex (PAF1C) (258, 275). Overall, this preferential specificity demonstrates the precise temporal co-ordination of the transcriptional stages.

4.3.1.1 Antibody limitations of CTD phosphorylation

The detection of specific phospho-epitopes on the CTD of Rpb1 subunit can differ based on the monoclonal antibody clone used. Furthermore, it has been proven for the 3E10 mAb (to detect

p-Ser 2) and 3E8 (p-Ser 5), that the detectable signal-strength on a particular residue is affected by the presence of modifications on nearby residues. This is due to adjacent modifications obscuring the accessibility for antibody binding. Although in this study different antibodies to the ones described above: E1Z3G (Ser2) and D9N5I (Ser5) mAbs (Cell Signalling Technology) were used, it is still important to take into consideration. Therefore, interpretation of CTD phosphorylation status measured by immunoblot should be done with caution. The use of antibodies is capable of accurately indicating a change in CTD phosphorylation but due to the potential confounding effect of adjacent modified residues, not the quantified directionality (264). To overcome this limitation a more accurate approach would be to determine the CTD phosphorylation dynamics such as using mass spectrometry.

4.3.1.2 Other CTD Serine 2 Kinases

One study determined that the proteins which constitute the interactome of each phosphorylated residue of the CTD of Rpb1, reveal little cross-over between stages of the phosphorylation cycle. This indicates that each phosphorylation-mark has a unique and distinct part to play during the orchestration of transcription (56). Furthermore, the involvement of other non-CDK transcriptional regulatory kinases suggests there exists a context-dependent mechanism to regulate the expression of particular gene sets in response to stimuli.

CDK11^{p100} phosphorylates the Ser2 residue of RNA polymerase II to enable elongation and 3' processing of replication dependent histone (RDH) genes (214). While, CDK7 has been implicated in splicing processes and inhibition leads to splicing defects distinct from those associated with CDK12 and CDK13 (276). This would indicate that splicing processes are controlled independently and is not a downstream consequence of preventing CDK12 and CDK13 activation.

GSK-3 is also involved in alternate splicing in response to DNA damage. Furthermore, GSK-3 itself has been implicated as a CTD kinase in response to UV-induced DNA damage. Both Ser2 and Ser5 residues are phosphorylated by GSK-3 but is most efficient when the CTD substrate is pre-phosphorylated by CDK9 (277). BRD4, is a kinase with HAT capabilities, and also travels with the SEC to couple chromatin organisation with productive transcriptional progression. BRD4 recruits PTEFb and has been shown to phosphorylate Ser2 (278) whilst also regulating alternative splicing patterns through interacting with the splicing machinery. (279) These two kinases both share similarities with CDK12 as they couple the phosphorylation of Ser 2 with the regulation of splicing.

It may also be noteworthy that CDK11 was identified as being differentially phosphorylated by Gc (previous chapter) and GSK-3 was one of the most significantly implicated kinases for the set

of Gc-regulated phosphoproteins. Furthermore, epigenetic readers of histone acetylation BRD2 and BRD3, are also BET family members along with BRD4 and were also differentially phosphorylated by Gc. Therefore, the Dex-mediated effects upon Rpb1 phosphorylation could plausibly involve activity of these kinases.

4.3.2 CDK12 & CDK13: Implications for GR-regulated transcription

I found THZ531 has a suppressive effect upon Dex-induced upregulation of a luciferase reporter which was utilised to assess the activity of GR acting via direct-binding to DNA. These transcriptional effects had comparable outcomes to gene expression measured by PCR whereby THZ531 blocked the Dex-induced upregulation of classic Gc target genes *GILZ, PER1, DUSP1* but not *NFIKBA*.

In contrast, Dex suppressed the TNF-α -mediated induction of *IL6* and *IL8* expression but inhibition of CDK12 and CDK13 did affect expression further. THZ531 reduced the extent of cytokine up-regulation by TNF-α, and reduced TNF-α-stimulated reporter gene expression. This suggests that CDK12 and CDK13 are also important for the direct induction of *IL6* and *IL8* by NF-κB. Therefore, it appears that CDK12 and/or CDK13 are involved in GR-dependent transcription acting through transactivation but are less important for GR-tethering. If THZ531 was preventing GR from tethering to pro-inflammatory transcription factors then Dex would be incapable of reducing the TNF-α induced upregulation. This points towards CDK12 and CDK13 regulating specific subsets of Gc-regulated genes through a direct DNA-binding mechanism. These findings are similar to a previously reported role of CDK9, required for the expression of genes up-regulated by GR (69).

4.3.2.1 GR regulation and other CDKs

CDK9 regulates the expression of GR target genes through the phosphorylation of GR co-factor GRIP1. This phosphorylation occurs at GR bound at GREs and is required for GRIP1 co-activator function, to induce the expression of anti-inflammatory genes but not co-repressive functions at tethered sites. Additional complexity and transcriptional specificity is provided by the phosphorylation-status of GRIP1 as multiple phospho-isoforms in complex with GR were observed across GR binding sites (69). This demonstrates cross-talk between GR and CDK9 and reflects my findings that inhibition of CDK12 and CDK13 has a greater effect on genes that are up-regulated by Dex.

The accessibility of the CDK9/cyclinT1 P-TEFb complex to the *IL8* gene promoter, bound by NF-κB following TNF-α stimulation, is suggested to be physically blocked by GR. The tethering interaction of GR upon p65 does not impede RNA polymerase II recruitment but prevents the

CDK9-mediated ser2 phosphorylation of RNA polymerase II. TNF-α-regulated expression of IκBα is not unaffected and P-TEFb was not recruited to the promoter, although it is now known that *NFKBIA* is gene also transactivated by Dex (280). This reported role of CDK9 again suggests there is a gene specific mechanism of regulation between GR-mediated direct activation and transrepression. However, ChIP PCR or sequencing would be useful to determine whether CDK12 binds at these promoters, particularly for the gene encoding IκBα (*NFKBIA*) which I show to be unaffected by CDK inhibition. Moreover, if CDK9 is required for CDK12 recruitment (258, 275), studies such as those described above which inhibit or KD CDK9 may have indirect effect on downstream transcriptional processes mediated by CDK12.

CDK8 has an inhibitory-regulatory role upon STAT3 transcriptional responses following IL-6 stimulation. Phosphorylation of STAT3 by CDK8 and CDK9 is initiated downstream of IL-6 signalling in CD4 T cells. Yet CDK8 reduces the dwell time of STAT3 upon chromatin and consequently reduces target gene expression (281). This dynamic modulation of CDK8 expression levels may serve as a mechanism to fine-tune cytokine sensitivity and differentiation programmes and demonstrates how transcriptional CDKs modulate transcription factor activity. Knowledge of such processes may provide potential insight into how GR and CDK12/CDK13 are associated and raise the possibility that CDK12 and CDK13 act to modify the scale of GR response.

4.3.2.2 Genomic effects of THZ531

Multiple studies have assessed the transcriptional effects of inhibiting CDK12 and/or CDK13 both with specific inhibitors: THZ531 or SR-4835 and analogue sensitive models. These studies have determined that CDK12 and CDK13 are responsible for the efficient transcription of particular gene subsets - namely those involved in the DNA damage response (DDR) (217, 254, 256). Down-regulation of the expression of *BRCA1* by THZ531, is well reported and has gained significant attention due its function to maintain genome stability and implications for cancer treatment (256). I measured the expression to *BRCA1* gene to demonstrate the activity of the two inhibitors. THZ531 reduced expression to half that of the vehicle at 500nM and reflects what has been shown previously (256). FVP also reduced expression which would likely be due to the parallel inhibition of CDK12 with CDK9 however, could not be proven definitively. I detected no effect of Dex on expression of *BRCA1*, yet functional cross-talk between BRCA1 to regulate GR protein activation has been reported with implications for breast cancers therefore, the relevance may extend beyond gene level expression (282).

I confirm that inhibition of CDK12 and CDK13 does not suppress global transcription as I observed no significant changes between the expression of two housekeeping genes measured

by qPCR or the baseline expression of Gc-regulated genes treated with vehicle by qPCR and reporter assay. These findings corroborate those of Bohmann et al. who showed that knockdown of CDK12 decreases the reporter activity of Nrf2 in *Drosophila* cells whilst a renilla control gene was unaffected - indicating that global transcription was not disturbed (283).

4.3.2.3 Cell viability

THZ531 was first described as exhibiting anti-proliferative and apoptotic effects (256). I identified regulation of cell proliferation and regulation of apoptotic processes within the top five enriched biological functions for the group of genes regulated by Dex and affected by THZ531 by RNA sequencing. THZ531 is known to affect transcription (256). The measure of confluency was included to provide an additional measure of cell number to complement the Renilla luciferase control, independently of transcription. I observed that THZ531 pre-treatment appeared to reduce the confluency of cells used to measure luciferase reporter activity, however I did not investigate effects on cell viability any further. This reduction was more evident in cells transfected with the TAT3-luc reporter in comparison to the NRE-luc reporter plasmid. TAT3-luc is a simple GR reporter developed in the 1990s (284), whereas NRE-luc is a newer, commercially available reporter designed with lower toxicity. It is likely that the Tat3-luc had greater toxicity to the cells, which would account for the measured reduction in confluency.

Studies have suggested that for cell viability and proliferation, the actions of CDK12 and CDK13 are functionally redundant. Rather the loss of their shared partner cyclin, cyclin K is more detrimental to cell survival than loss of either CDK alone (217). Bartkowiak et.al failed to generate a CDK12 knockout using CRISPR and suggested that the kinase is essential for cell survival. The group instead generated an analogue sensitive protein containing a single mutation which enables the inhibition of the kinase by the addition on an inhibitory adenine analogue. In contrast to the findings described above, when CDK12 was inhibited they reported suppression of cell proliferation despite CDK13 and cyclin K retaining their functionality (218). Although, this does not answer what the combined effect of GR and THZ531 would have upon survival. Given the defined effect of GR upon inhibiting cell proliferation and the cell cycle (253), this suggests CDK12 and CDK13 inhibition in the presence of Dex would synergise and result in a loss in cell viability, particularly over long treatment time periods.

4.3.3 RNA Sequencing data

Previous studies have shown that treatment with FVP stalls RNA polymerase II at the proximal promoter whereas THZ531 reduces the amount of elongating polymerase II found on gene bodies (256). This is likely to be because the P-TEFb complex, is required to phosphorylate the negative elongation factors to allow progression to the elongation stage. As THZ531 does not

inhibit CDK9 activity, P-TEFb retains the capacity to phosphorylate the factors which would otherwise prevent the pause-release stage to enable RNA polymerase II advancement. The activity of CDK12 and CDK13 are then required for the progression of the transcription machinery through elongation and facilitates interactions with RNA processing factors (254). In order to fully understand the full contribution of CDK12 and CDK13 towards Dex-regulated gene expression I required a global transcriptomic approach.

4.3.3.1 CDK12 and long genes

CDK12 and CDK13 have structural similarity which reflects their close evolutionary relationship (217) but the precise individual functions of the two kinases remains an outstanding question. Given the association with DNA-damage response genes (256) and alternation in cancers (261), CDK12 has become a recent focus for research. The specific transcriptional regulation of certain genes by CDK12 has previously been proposed to be an inducible mechanism to upregulate genes involved in stress responses (283). Other theories implicate CDK12 in the expression and co-transcriptional processing of long genes; particularly those associated with DNA-repair, genome stability (230) and cell cycle regulation (285). As GR regulates the expression of genes involved in these processes (231), it may not be unreasonable to hypothesise some co-operative action between GR and CDK12 in the regulation of cell cycle and genome stability.

CDK12 progresses with the elongating RNA polymerase II along the body of the gene (256) and CDK12 deficiency can thus result in transcription elongation or termination defects. The loss of both CDK12 and CDK13 results in RNA processing defects, as CDK12 and CDK13 are involved in regulating the concurrent processing of mRNA transcripts during progression of elongation complex. CDK12 has been found in association with exon junction complex and SR splicing factors which are recruited to elongation complex (218, 254). Therefore, post-transcriptional mRNA processing is a key function of the two kinases. Since long genes have more intragenic polyadenylation sites, inhibition of CDK12 in mouse embryonic stem cells resulted in an increased usage of these sites. Therefore, the expression of the full-length mRNA transcripts was reduced for long genes - such as those involved in DNA repair. Other features sensitive to CDK12 KD are low GS content and lower ratio of U1 snRNA binding to polyadenylation sites (261, 286).

By comparing correlation of differential expression against the gene length of identified targets I sought to consider this previously reported effect. This simple method of assessment did not show any preference towards longer genes being more significantly perturbed by THZ531 treatment. However, this method gave no indication into which transcript isoforms were produced or their length, which would indicate what the effect of Dex would have upon mRNA

processing following CDK12 and CDK13 inhibition. More in-depth bioinformatic analysis would be required to confirm the result.

Many of the proteins identified as part of the both GR and CDK12 interactome, are involved in mRNA splicing and translation (26, 257).In addition, splicing factor CDC5L was identified as differentially phosphorylated following Gc treatment and a central protein within the interaction network. Similar to CDK12, CDC5L has been shown to be important for regulating expression of DNA damage response genes and mitotic progression (196). Therefore, investigation into alternative splicing of changes induced by THZ531 may have provided further insight into the point of regulation between CDK12 and GR. However, to perform such analysis accurately a read depth of 30-60 million reads per sample is required (287) in contrast to the 20 million reads obtained for this study and would be an important component of further investigation.

Following siRNA knockdown of CDK12 or CDK13, Geyer et al. (288) reported a dissimilarity between the two profiles of differentially expressed genes, with little overlap. However, in another study, the transcriptome of cells with CDK13 knockdown were found to largely overlap with that of CDK12 knockdown (73% of transcripts shared). Although KD of CDK12 affected the expression of 2.5 times more transcripts than CDK13 and 1.3 times more than CDK9 (254). In this study, I was unable to delineate the distinct contribution of CDK12 and CDK13, as THZ531 inhibits both kinases. Future studies using knockdown of each protein individually (e.g. using RNA interference) and treatment with Dex would be useful to determine these specific gene signatures.

The effect of THZ531 on the inhibition of Dex-responsive genes in the RNA-seq data is not directly comparable to that first observed with PCR. The detected fold-change differences in the RNA seq were not as large as those measured by qRT-PCR. This is likely due to the relatively low depth of sequencing and therefore cannot detect changes to such a resolution. However, transcriptomics could not properly investigate the tethering mechanism as performed for the PCR as there was no activating inflammatory stimulus for the AP-1 or NF-κB transcription factors. Nevertheless, this would be an important question for future research to definitively define any effects of CDK12 and CDK13 both upon GR tethering and inflammatory pathways.

4.3.3.2 Dex regulated genes affected by THZ531

I defined a set of ~800 protein coding genes regulated by Gc whose expression is significantly altered with prior inhibition of CDK12 and CDK13 by THZ531. By normalising the expression of genes treated with THZ531 and Dex against the Dex-only samples, I identified genes whose expression was significantly perturbed (log2FC= 0.5) away from the effect of Dex alone. I then

used this group of differentially expressed genes to attempt to understand the mechanism linking GR activation to CDK12 and CDK13 activity.

One significantly enriched ontology of Dex-regulated affected by THZ531 highlighted the close association between the regulation of SGK1, potassium and sodium channels. Dex has been previously shown to rapidly inhibit the action of three airway K+ channels to reduce epithelial secretions (89), although the channels differ from those identified in this study. This finding implicates Gc and CDK12 and/or CDK13 in the modulation of genes involved in ion channel activity and regulation of electrolyte homeostasis. The expression of SGK1 was potentiated to greater levels by Dex in the presence of THZ531. Expression of this ubiquitous kinase is known to be upregulated by hormones including Gc and in response to stress (265). The further potentiation by THZ531 may represent a stress-responsive gene regulated by CDK12 and would be interesting target for further investigation.

4.3.3.3 Transcription factors and super enhancers

A predominant molecular function of the Dex-regulated THZ531-affected gene set is transcription regulatory-region DNA binding, and signifies many differentially expressed genes are associated with transcriptional processes. Further analysis confirmed the expression of a broad-range of transcription factors and regulators are altered by CDK12 and CDK13 inhibition. This supports the results from the initial microarray analysis of THZ531 in Jurkat cells (256), which showed that at lower concentrations (50nM) DNA damage response genes were extremely sensitive to downregulation by the inhibitor. At higher doses (200 & 500nM) there was a significant loss of the expression of genes encoding transcription factors, particularly those associated with super-enhancers such as RUNX1 and GATA3 (256). Super-enhancers are defined as hyper-active genomic regions with an enriched occupancy of master transcriptional regulators and co-activators. These sites are generally associated with cell-type identify and modulate chromatin structure accordingly (190) and previous ChIP-seq has found CDK12 to be enriched at these regions (256). Gene ontology identified cell differentiation as a top process for Dex-regulated genes affected by THZ531 and taken together this may implicate CDK12 and/or CDK13 in establishing cell identify and differentiation processes.

4.3.3.4 AP-1 factors

Basal genomic occupancy of AP-1 factors directs chromatin accessibility to facilitate Dex-responsive GR binding to specific regulatory sites (72, 267). GR can functionally affect AP-1 transcriptional outputs both by tethering and cooperative binding (181).

Genes encoding components of AP-1 transcription factor dimer-complexes (members of JUN, FOS and ATF gene families), were identified as differentially regulated by Dex and affected by

THZ531. In addition, these were enriched as regulatory factors by the promoter analysis, suggesting a regulatory role in the expression of the investigated gene sets. Dex exposure reduces expression of *JUN*, *JUND*, *FOSL1* while increases *JUNB* and *FOSL2* expression (190) which I also established by RNA sequencing in this study. However, THZ531 in the presence of Dex, altered the level of gene expression by potentiating (*JUNB, FOS, FOSB, FOSL1, ATF6*), reducing (*JUND, FOSL2*) or mediating the opposite directionality (JUN, ATF3) in the level of AP-1 factor expression. RNA-sequencing performed by Fan et.al, following dual inhibition of analogue sensitive CDK12 and CDK13, found upregulation of immediate early response genes. *IER2, IER3, IER5* and *JUN* and *JUNB* were included as the top identified factors (217) which corroborates the top up-regulated genes regulated by THZ531 in this study. CDK12 has previously been shown to be required for EGF-mediated induction of c-FOS (289), however I found that THZ531 up-regulated the expression of *FOS* and *FOSB* genes, both alone and in the presence of Dex. The disparity may be a result of the differing method of inhibition, cell line used and/or time point. Nevertheless, these conflicting findings implicate CDK12 and/or CDK13 in the regulation of the expression of AP-1 factors.

AP-1 transcription factors function as dimers, the composition and combination of which were once thought to direct specific genomic responses. The co-localisation of JUNB-FOSL2 has been shown to increase after Dex stimulation, but is most likely a result of their increased expression. The genomic binding patterns of AP-1 subunits have been characterised at sites termed 'AP-1 hotspots'. These sites are promoter distal regions, distinct from super-enhancers and highly enriched for AP-1 motifs. These AP-1 hotspots are found close to GR binding sites and were shown to have a pronounced effect upon Dex-dependent gene expression. Furthermore, the AP-1 factors were recruited indiscriminately at these sites with little evidence of dimer-specific preferences (190). Therefore, whether the THZ531 would induce changes in AP-1 factor dimer-composition and the subsequent effect upon GR genomic action remains unknown. Given the close genomic interplay between the factors this may have implications for the regulation of inflammatory responses.

In resting macrophages, the transcriptional start sites (TSSs) of inflammatory genes are pre-loaded with proximal-paused-RNA polymerase II. This release is regulated by NELF, DSIF and P-TEFb in response to activating stimuli (290). The induction of early inducible factors is regulated by NELF, and the loss of which results in an enhancement of anti-inflammatory gene expression, in response to LPS. NELF also negatively regulates the AP-1 transcription factors and deletion enhances the expression of genes regulated by c-Jun and c-Fos. The phosphorylation and release of paused-polymerase II and NELF could not conclusively be attributed to CDK9 activity (291)

therefore, another CTD kinase such as CDK12 and / or CDK13 may also be involved in the post-initiation control of inflammatory genes.

One factor affected by the loss of NELF is CBP/EP300-interacting trans-activator (CITED2), a transcriptional co-regulator implicated in dampening proinflammatory gene expression (291, 292). CITED2 was identified as a factor upregulated by Dex and potentiated further with prior THZ531 exposure. As it appears NELF has a role in suppressing anti-inflammatory over activation, the co-regulator may represent a target of interest for further investigation.

4.3.4 Promoter analysis

I used the groups of identified Dex-regulated genes to perform motif or promoter analysis. In doing so three different methodologies were evaluated; using AME, i-Regulon and LISA software. The approach is not conclusive but provides an indication of transcription regulatory factors which are significantly associated with a set of perturbed genes. These candidate factors will then serve as initial targets for further experimental validation.

4.3.4.1 Method evaluation

GR principally binds at promoter-distal sites (189), which lead to comparing different size genomic regions upstream of the TSS of regulated genes. The AME method scans the promoter region sequences and identifies motifs based on sequence similarity from a library of motifs PWMs. However, initial attempts of promoter-based motif analysis using the AME server yielded largely similar results between the different size upstream regions. Also, given the absence of NR3C1 motifs for Dex-upregulated genes and lack of distinction between the results for genes up and downregulated by Dex, the method was not used further. Instead I utilised programmes with algorithms that also consider experimental data to provide a more biologically relevant approach. The integration of ChIP-sequencing data by both iRegulon and LISA therefore, assesses perturbed gene sets both as a co-regulated group and in context with other experimental data.

The results using the iRegulon plugin were limited in-terms of the number of identified regulatory factors and presented a high degree of overlap between the predicted-regulatory transcription factors. With almost all groups of genes upregulated by Dex predicted to only be regulated by NR3C1 and FOXA1, the lack of distinction does not help to understand the potential underlying mechanisms. Although, in some cases specific differences were found between the particular motifs identified for the same factor – indicating that the same transcription factor is enriched yet binding at different motif between gene groups. This highlights the importance of considering both the bound transcription factor and specific motif to which the factor may be

bound. Furthermore, the motif strength and combination of motifs for different factors (e.g. CEBPB and GR) can influence enhancer activation in response to Dex (189). This adds further complexity to the identification of factors imparting regulatory control.

The LISA ChIP based analysis found NR3C1 to be most closely associated with upregulated genes. This follows the canonical model of GR directly binding to GREs (23)(**Figure 1.8**). However, the distribution of FOXA1 between up- and down-regulated genes was shifted towards down-regulated genes when comparing genes affected vs those not-affected by THZ531. Similarly, the FOXA1 motif was strongly associated with Dex downregulated genes in the motif-based LISA. Furthermore, the FOXA1-motif was not identified for the set of genes not affected by THZ531. This signifies that FOXA1 has a more dominant role in co-operating with GR to downregulate specific gene subsets in a mechanism involving CDK12 and/or CDK13.

Overall this shows the greater level of complexity provided by the LISA in comparison to iRegulon analysis. This reflects what was shown in the publication validating the LISA method to identify known regulatory factors. The ChIP-based LISA method performed better at identifying correct regulatory-transcription factors within the top 10 for different gene sets in comparison to the motif approach. However, both methods outperformed the iCisTarget methods (developed form iRegulon)(179).

In order to incorporate the full scope of potential regulatory factors in the promoter and motif analysis, all the factors from datasets were included – regardless of experimental cell type. Filtering was performed to remove mouse datasets in addition to applying a significance threshold equivalent to an adjusted p value <0.05. The results could have been filtered further to only include Lung specific cell types – given that sequencing was performed using A549 cells. However, filtering to only include datasets from A549 would greatly reduce the number of included data sets and reduce the potential to identify regulating transcription factors. For an initial analysis I wanted to investigate any transcriptional regulators which could provide a link between GR and CDK12/CDK13 in a hypothesised conserved mechanism. As GR and CDKs are ubiquitously expressed proteins datasets from different experimental cell sources were included to support the rationale that the relationship between GR and CDK extends beyond A549 cells. Of the most significant identified transcription regulators such as RELA, JUN and FOS, expression and GR-crosstalk with these factors occurs across various tissues (72, 92, 116). Whereas the lineage specific transcription factors including members of the GATA and FOX family, are more likely to represent their role as pioneer factors and cooperative binding with GR during development (293, 294). Although, the activity of tissue specific factors such as GATA3 are less important in A549 cells, preliminary knowledge of a putative transcriptional-mechanism could

be applied to more relevant contexts, such as breast cancer where GATA3 (295) and CDK12 (264) are implicated.

4.3.4.2 Identified factors

Both iRegulon and LISA algorithms detected factors which are known to participate in concert with GR at regulatory regions (eg., CEBPB, FOX, TEAD, GATA, AP1)(181, 188-190). This provides confidence that the results are biologically relevant. However, the ChIP-based LISA analysis indicated that the differences in gene expression between groups, stratified depending on the effect of THZ531, might not be due to the presence or activity of unique factors. Rather, inhibition of CDK12 and CDK13 could result in the shift in activity of the shared factors or differential cooperation between factors.

GR binding across the genome depends on established regions of accessible chromatin. Therefore, GR binding requires factors associated with active enhancers such as bound pioneer factors, EP300 and H3K27ac (189). This is thought to be fundamental mechanism underlying GR-context dependent responses. Genomic binding of the histone acetyltransferase EP300 is dynamic and responsive to Dex in addition, GR colocalises with EP300 at enhancers which is an important factor in accessibility. Gc- stimulation results in a shift in the binding of transcription factors at enhancers, including JUN, JUNB, FOSL2, CEBPB (189). EP300 was enriched by iRegulon analysis irrespective of whether the expression of target genes was affected by THZ531 suggesting that GR-EP300 interaction is important for the expression of GR-responsive genes but is a mechanism independent of CDK12 and CDK13.

RAD21 was strongly associated with Dex-upregulated genes, for the CHIP-seq analysis. This protein is a member of the cohesin complex, and has many functions including in the repair of double-strand DNA breaks, correct chromosome segregation, DNA replication and transcription regulation (268). Although present for both groups of Dex-regulated genes, RAD21 was more significantly associated for genes affected by THZ531. RAD21 has been shown to cooperate with tissue specific transcription factors and CCCTC-binding factor (CTCF) which directs RAD21 to DNA binding sites. Furthermore, CTCF cooperates with the cohesin complex to maintain high-order chromatin structure and enable long-range interactions. This process can facilitate both transcriptional activation and repression, but CTCF is generally associated with inactive chromatin regions (296).

CTCF was identified by ChIP-based LISA analysis (data not shown). In agreement with RAD21, CTCF was most significantly associated with upregulated genes, particularly Dex-regulated genes affected by THZ531. Further to this, both factors had a greater association with the reduced gene set followed by the potentiated set. Based on these results, CTCF and RAD21 appear to be

an associated mechanism for these sets of upregulated genes. However, a recent study has shown Gc responsive chromatin interactions are correlated with enriched RAD21 but depleted CTCF occupancy (188). Although, the aforementioned study was comparing Dex-responsive occupancy. As CTCF has previously been shown to be irresponsive to stimuli, including Dex, (189) identification of CTCF by the analysis is likely a result of CTCF's role in maintaining basal chromatin interactions.

At sites of high DNase accessibility, GR co-binds with pioneer factors including FOXA1. FOXA1 and AP-1 motifs have been shown to be enriched sites of GR-binding which regulate repressed genes. AP-1, FOXA1, GR and CEBPB motifs are significantly enriched for activated genes (188) which largely reflects the distribution of factors observed from the LISA-ChIP analysis. FOXA1 and FOXA2 are essential for cell specification and differentiation during development (297). GR also contributes to the later-stage maturation of the lung epithelium - from which A549 cells are derived. The close association may reflect their role, in addition to other developmental transcription factors ETS and GATA6, in development.

The binding of FOXA1 has been is closely associated with steroid receptors which has been described as a reciprocal relationship for chromatin interactions and accessibility (294). The promoter analysis approaches implicate FOXA1 in the expression of genes differentially expressed both up and down in response to Dex. iRegulon identified NR3C1 and FOXA1 as exclusively responsible for genes with Dex-responsive increase in expression. The interplay between GR and FOXA1 has been previously demonstrated and a redistribution of GR binding has been shown in absence of FOXA1 (298). Co-binding of FOX proteins can facilitate direct GR binding at nearby GREs as well as, tethered-binding (298). Taking the LISA ChIP-seq analysis, THZ531 appeared to shift the association of FOXA1 from upregulated genes towards downregulated gene groups. Of the genes whose expression was potentiated in presence of THZ531, FOXA1 were correlated with genes upregulated by Dex. As the expression of these genes increased further with CDK12 and CDK13 inhibition, one explanation could involve direct binding of GR and FOXA1 at proximal sites to directly upregulate genes. In absence of CDK12 and CDK13 an inhibitory co-factor may be inactive or removed, permitting increased expression. Although, a confounding finding would be the lack of FOXA1 motif associated with Dex upregulated genes. The LISA motif approach implicated motifs for FOXP1, FOXA1 and FOXA2 all associated with genes downregulated by Dex and affected by THZ531. Moreover, these factors were absent for genes not affected by THZ531. The most significant association was for genes regulated in the opposite direction by THZ531. The predominance towards Dex-mediated downregulation signifies a mechanism involving GR tethering to FOX factors bound directly to their specific sequence or a looping mechanism as a means for regulating distal promoters (188,

191). However, this cannot explain how loss of CDK12 and CDK13 activity can modulate expression in opposing directions. Transcription factors can bind regions in different orientations resulting in allosteric modification which could underlie such differences (59, 80, 298). More-in-depth analysis of the precise binding pattern and proximity of identified motifs to GRE is required. In addition, investigation of specific genes of interest may help to further decipher the mechanism.

Finally, one identified transcription factor motif, myeloid zinc finger protein MZF1 was significantly associated with upregulated genes affected by THZ531, surpassing NR3C1. MZF1 regulates transcription during haematopoietic development and has been implicated as a proto-oncogene in both solid tumours and hematopoietic malignancies (299). MZF1 is associated with invasion and epithelial to mesenchymal transition (300), an enriched ontology for Dex-regulated genes affected by THZ531.

RNA-sequencing provides broad coverage of the entire genome and the sequencing depth can be a limitation, particularly for genes with low expression. Although RNA-seq is an unbiased approach, analysis relies on computational alignment of sequences to the reference genome which is not a standardised process. Furthermore, bias towards a greater expression for longer genes must also be considered because mRNA transcripts are fragmented prior to sequencing long transcripts produce more fragments in comparison to a shorter transcripts with equivalent expression. A more precise, albeit lower throughput, approach to confirm the differential regulation would be qPCR with primers specifically targeted to the sequence of the gene of interest. This is more sensitive to detect treatment induced changes especially for genes with low expression. Therefore, independent verification to confirm the differential expression of key genes of interest by means of qPCR is necessary to validate transcriptional the effects of Dex and THZ531.

Overall, further investigation into the relevance of these identified transcription factors in relation to CDK12 and CDK13 in the regulation of GR-mediated transcription may have importance for the understanding transcriptional regulation during development and cancer progression. Future unbiased approaches such as ChIP-seq would shed light on the genomic binding patterns of CDK12, CDK13 and GR in response to Dex and could also be investigated in the presence of inflammation.

Chapter 5: Cell-matrix interactions and the effect upon transcription factor dynamics

5.1 Introduction

Macrophages are central governors of local tissue homeostasis and highly receptive to microenvironmental cues, making them a fundamental target of Gc action in inflammatory disease (301). As part of the first-line of host defence, macrophages initiate innate inflammation following the recognition of pathogen associated molecular patterns (PAMPs) by innate pattern-recognition receptors (PRRS), including toll-like receptors (TLRs). The presentation of antigen by macrophage along with their secretory repertoire of chemokines and cytokines, connects both the innate and adaptive arms of inflammation. The phagocytic capacity of macrophage primarily aids in the removal of inflammatory tissue debris for resolution and contributes to wound healing (127, 301). However, under pathologic conditions, macrophages can contribute to the perpetuation of chronic inflammation. Macrophages are capable of these divergent functions through distinct transcriptional programmes influenced by the local tissue environment in which local factors determine the phenotypic activation state. Tissue architecture is significantly altered in disease states such as fibrosis, chronic inflammation and the tumour microenvironment.

To date, studies have not considered the potential contribution of such mechanical signals in the context of GR action. Stretched cell geometry reduces the rate of translocation and level of p65 nuclear occupancy (134) while a stretched-induced skewing towards an 'M2' phenotype has been described in macrophages (153). One hypothesis would be that a stretched cellular morphology positively affects the rate and level of GR nuclear translocation, which, in conjunction to reduced levels of nuclear p65, promotes a more anti-inflammatory cell state. Considering the converse whereby GR translocation is hindered by alternate, confined geometries, could result in a compromised capacity of GR to respond to ligands and subsequently enter the nucleus to dampen pro-inflammatory p65-mediated transcription. Such morphology-associated reciprocal effects would modulate a cell's responsiveness to inflammatory signals. Therefore, I aimed to investigate how macrophage responsiveness to Gc could be altered by cellular geometry.

5.2 Results

5.2.1.1 GR is expressed and phosphorylated in response to Dexamethasone

Each of the three-human leukaemia-derived cell lines, used in the study were selected based on their capacity to be differentiated towards a macrophage-like phenotype. Firstly, it was important to characterise and assess the responsiveness of each of the cell lines to Gc and determine which would be the most suitable to model GR signalling.

In order to confirm the expression of the GR and its ligand-dependent activation induced by Dex; HL-60, U-937 and THP-1 cells were cultured in steroid depleted media overnight and treated with 100nM Dex. The presence of total GR and phosphorylated GR (^{P}S211-GR) protein was assessed by immunoblot using specific antibodies (**Figure 5.1**). All the cell lines express GR and no significant differences in total protein expression were observed by treatment. Ligand-dependent phosphorylation of GR at position serine 211 (Ser211) is associated with nuclear translocation of GR and therefore serves as a marker of GR activation. ^{P}Ser211 GR was detected and increased in response to Dex treatment (**Figure 5.1**), with measurable increases detected in HL-60 and THP-1 cells (the latter showing a statistically significant effect) and indicates steroid responsiveness. Treatment induced phosphorylation was not robustly observed in U-937 cells suggesting a potential defect in GR activation in these cells.
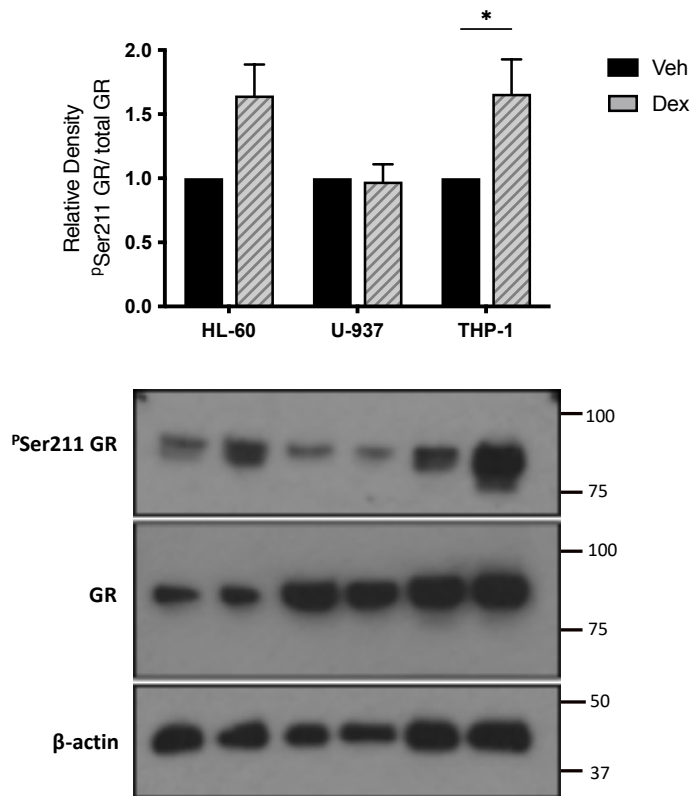
Figure 5.1 Evaluation of cell line responsiveness to Dexamethasone

*HL-60, U-937 and THP-1 cells were treated with 100nM Dex for 1 hour. Protein expression was analysed by immunoblot using 5µg protein lysates. Specific antibodies against GR, phosphorylated Ser211 GR and β-actin were used to detect protein. The blot is representative of three independent experiments. Statistical analysis was performed using two-way ANOVA with Šídák post-hoc multiple comparisons test comparing the mean of treatment and vehicle rows between each cell line only. (n=3) *P<0.05.*

5.2.1.2 GR induces the transcription of target genes in HL-60 and THP-1 cells

To assess whether the observed Dex-induced activation of GR is functional and capable of producing a transcriptional response, cells were treated with 100nM Dex for 4 hours. Gene expression analysis by RT-qPCR verified an upregulation in the expression of five known GR-regulated genes following acute exposure to Dex: *FKBP5,* encoding an inhibitory chaperone protein component of the complex which holds GR in the cytoplasm; *GILZ,* encoding an inhibitory molecule which facilitates Gc-mediated dampening of pro-inflammatory signalling pathways (302); *PER-1*, encoding a transcriptional repressor involved in the circadian clock; the gene for the phosphatase *DUSP-1*, a negative feedback regulator of the MAP kinase pathway which limits AP-1 activity (303) and *NFKBIA,* encoding the inhibitory molecule responsible for sequestering NF-κB proteins in the cytoplasm (116, 117). **Figure 5.2** shows a consistent, significant upregulation of Gc-inducible genes in response to treatment measured in HL-60 and THP-1 cells. For all genes investigated in the U-937 cells, relatively small fold changes in expression were measured compared to those untreated, none of which reaching statistical significance. This is in line with the lack of measurable ^{P}Ser211 GR phosphorylation (**Figure 5.1**) and suggests that the HL-60 and THP-1 cell lines produce the most robust transcriptional response post-Dex treatment.

5.2.1.3 GR nuclear translocation can be visualised in THP-1 Cells

Given that the measurement of the nuclear shuttling dynamics of GR at a single cell level is important for future investigation of cell morphology, the subcellular localisation of GR was analysed. Suspension cells were seeded onto poly-L-lysine coated coverslips overnight in steroid depleted medium before being treated with 100nM Dex for 1 hour. The HL-60 cells had poor adherence to the coverslips resulting in very low cell numbers for imaging and analysis. Weak staining of F-actin also resulted in poor quality images which suggested these cells would be unsuitable for subsequent imaging studies. U-937 cells displayed staining of GR and F-actin with some evident nuclear localisation of GR in Dex treated cells (data not shown). However, variability was noted between cells in experimental repeats. The most consistent staining was observed in THP-1 cells. In comparison to the other cell lines investigated, the translocation of GR to the nucleus was the most evident, with bright GR staining in the nucleus (**Figure 5.3**). This shows that GR cytoplasmic-nuclear compartmentalization can be visualised in THP-1 cells and that these cells were the most suitable for further assessment by microscopy.
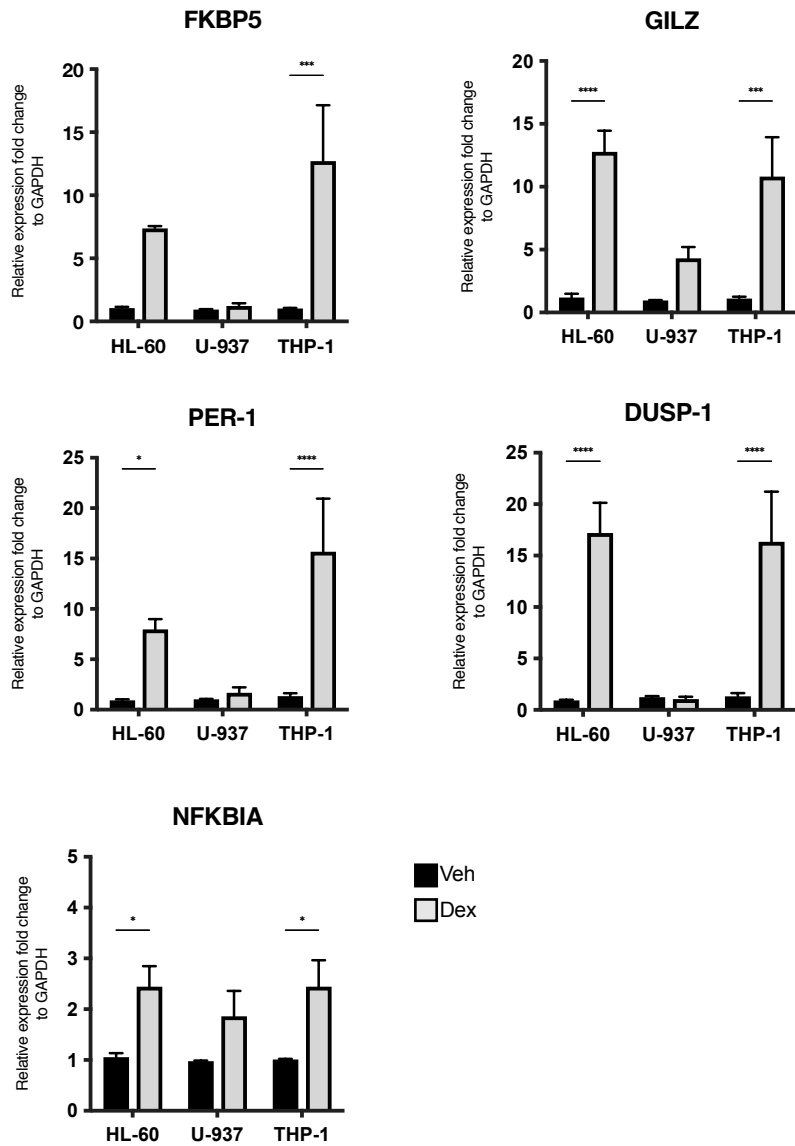
Figure 5.2 Assessment of Dexamethasone responsive gene expression

HL-60, U-937 and THP-1 were treated with 100nM Dexamethasone (Dex) for 4 hours. Cells were lysed and gene expression was assessed by Taqman qPCR. Fold changes were calculated relative to vehicle treated control and normalised to GAPDH housekeeping gene. Data is presented as the mean fold change and standard error of the mean (SEM) of three independent experiments each performed in triplicate. Statistical analysis was performed using two-way ANOVA with Šídák post-hoc multiple comparisons test comparing the mean of treatment and vehicle rows between each cell line only. (n=3) *P<0.05,***P<0.001,****P<0.0001.

5.2.2 Nuclear: Cytoplasmic ratio as a measure of GR and p65 localisation

An initial priority was to establish an image analysis method to measure the nuclear-cytoplasmic ratio of GR and p65 in order to quantify changes in subcellular localisation under different conditions. Building on the work of previous studies quantifying the translocation of the NF-κB subunit p65 (304) and identification of cell phenotypes (305), Cell Profiler image analysis software was used to create a high throughput pipeline (164). The pixel staining intensities of transcription factors from both the cytoplasmic and nuclear compartments were combined to produce a ratio (nuclear: cytoplasmic ratio) as a measure of translocation.

THP-1 cells were plated as before and treated with either: vehicle, 10ng/ml TNF-α for 3 hours, 100nM Dex for 1 hour or a combination. **Figure 5.3** shows that the transcription factor localisation is apparent and can be quantified to determine treatment effects on the cellular distribution of GR and p65. The nature of the cells having a high nuclear to cytoplasmic area ratio however, may limit ability to evaluate compartmentalisation. In the samples treated with Dex, GR staining is evidently more nuclear in comparison to the vehicle which is indicative of translocation in response to ligand. In the samples treated with both TNF-α and Dex the nuclear: cytoplasmic (N:C) ratio of GR is also significantly increased. However, only TNF-α treatment alone resulted in an increase in p65 nuclear localisation.
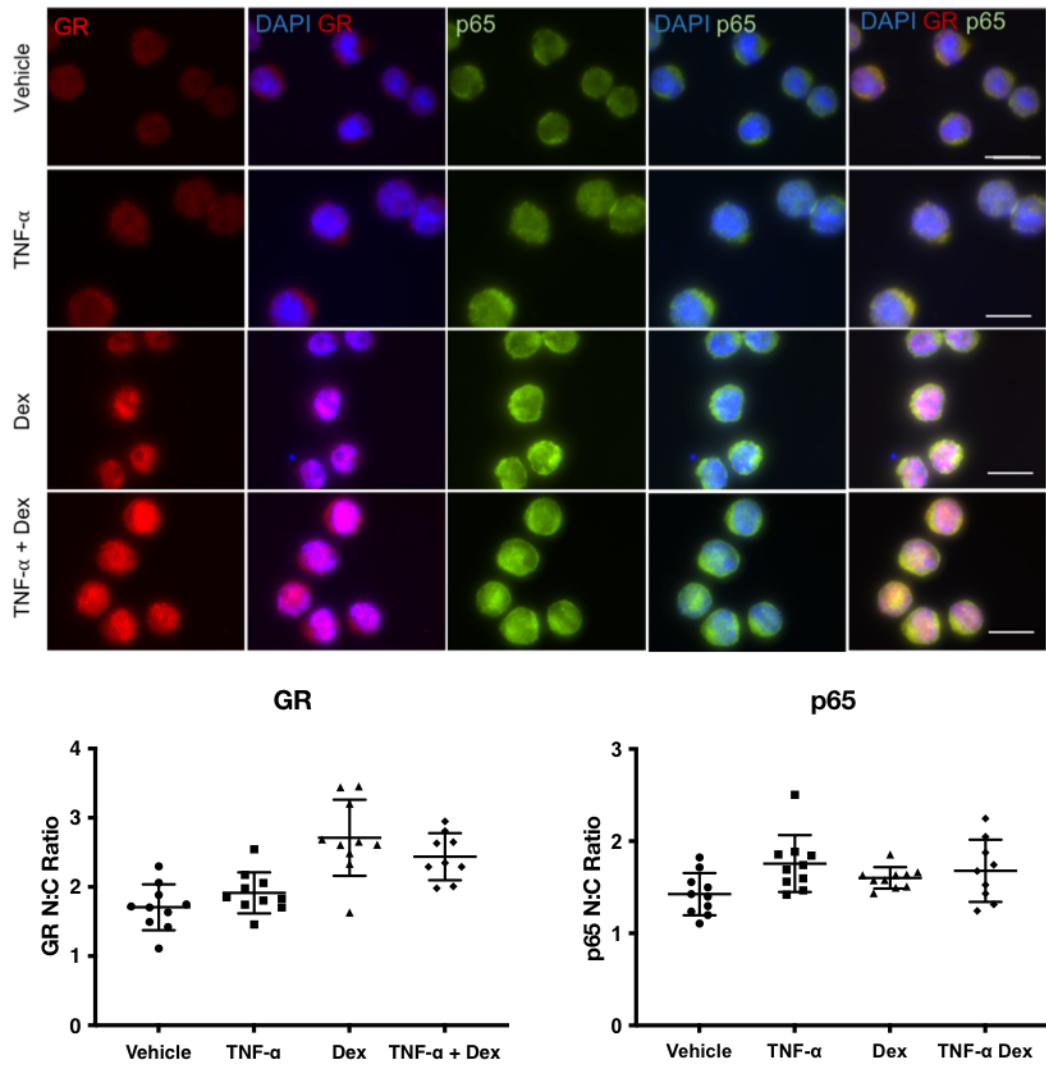
Figure 5.3 Quantification of GR and p65 translocation in THP-1 cells

THP-1 cells seeded on poly-L-lysine-coated coverslips and treated with either: vehicle, 10ng/ml TNF-α (3 hours),100nM Dex (1 hour) or combination. Cells were fixed permeabilised and stained for GR (red) and p65 (green), counterstained with Hoechst 33342 (blue). Representative immunofluorescent images of two independent experiments performed in duplicate, images captured X100 magnification. Quantification of nuclear:cytoplasmic ratio of GR and p65. Data is presented as the mean ratio of pixel intensity in nuclear and cytoplasmic compartments per field of view with the standard deviation for two independent experiments analysed using Cell Profiler. Scale bar: 20μm

5.2.2.1 Nuclear translocation of GR and p65 is evident by 10 minutes

To measure the nuclear-translocation dynamics of the transcription factors and validate the analysis pipeline, A549 cells were treated with 100nM Dex over a time-course of up-to 60 minutes. GR localisation was visualised by immunostaining at each timepoint. This characteristic shift in localisation from cytoplasmic to predominantly nuclear is clearly visible by immunofluorescence in these cells (**Figure 5.4**). A significant increase in the GR N:C ratio is quantifiable by 5 minutes and remains at peak levels between 10-60 minutes post-exposure. Similar time-course experiments were also performed by treating A549 cells with 10ng/ml TNF-α and measuring p65 localisation. This revealed significant increase in p65 nuclear translocation is measurable by 10 minutes, with the greatest N:C ratio peaking at 30 minutes and is sustained at 60 minutes post treatment (**Figure 5.5**). To assess localisation of GR in response to Dex in the context of inflammation, cells were treated with Dex for 60 minutes following 2-hour pre-treatment with TNF-α (**Figure 5.6**). The GR N:C ratio was significantly increased by Dex however, with TNF-α pre-treatment, the extent of translocation quantified by N:C ratio was lower than that of Dex alone but still increased in comparison to untreated cells. Likewise, p65 was significantly increased by TNF-α which was not altered by the presence of 100nm Dex. This demonstrates functional translocation of GR and p65 in response to activating stimuli in A549 cells and ligand-induced translocation of GR is affected in the presence of the inflammatory cytokine TNF-α.
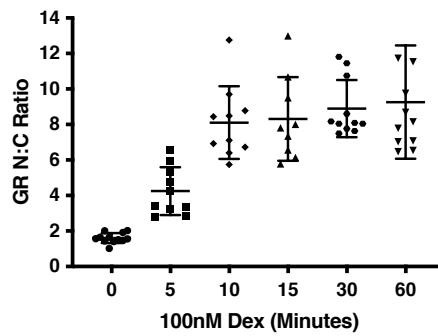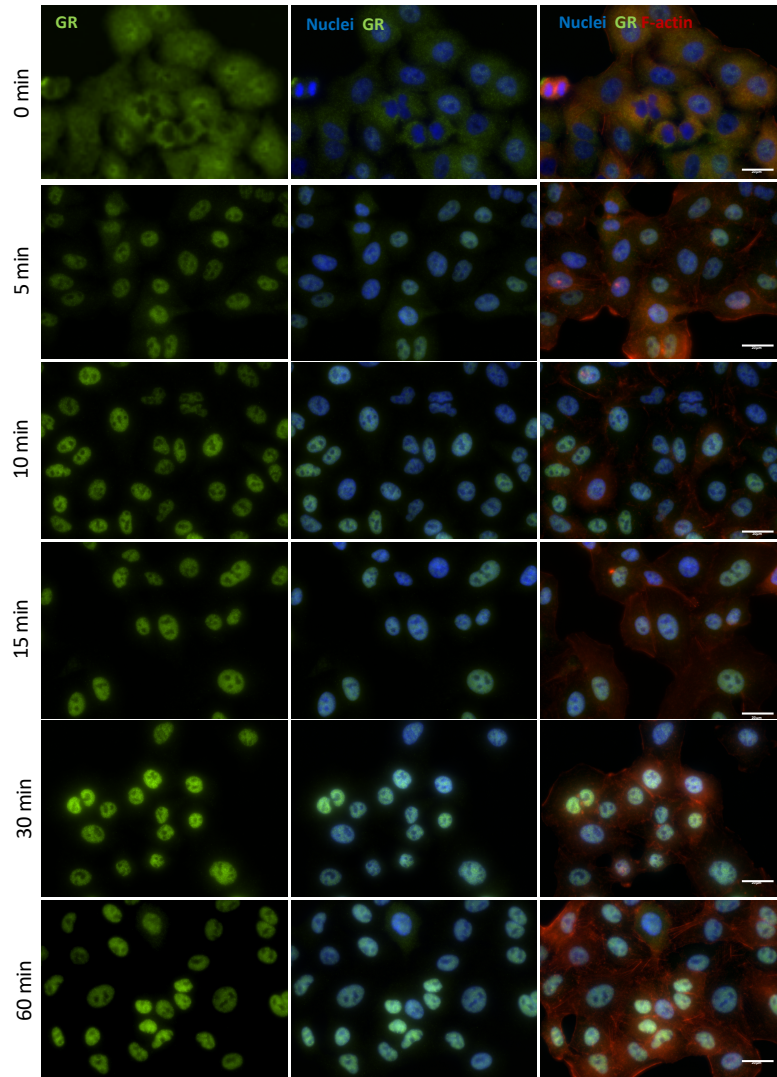
Figure 5.4 Nuclear translocation of GR response to Dexamethasone

A549 cells were seeded onto coverslips and treated with 100nM Dexamethasone over a time course range 5min-60 minutes. Cells were fixed, permeabilised and stained for GR (green), F-actin (red) and counterstained with Hoechst 33342 (blue). Representative immunofluorescent images of two independent experiments captured on Widefield microscope x60 magnification. Scale bar: 20μm. Quantification of nuclear:cytoplasmic (N:C) ratio of GR. Using F-actin staining to determine whole cell area for cytoplasmic region of interest. Data is presented as the mean N:C ratio per field of view and standard deviation for two independent experiments (n=2).
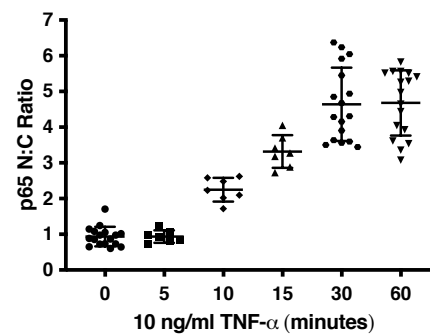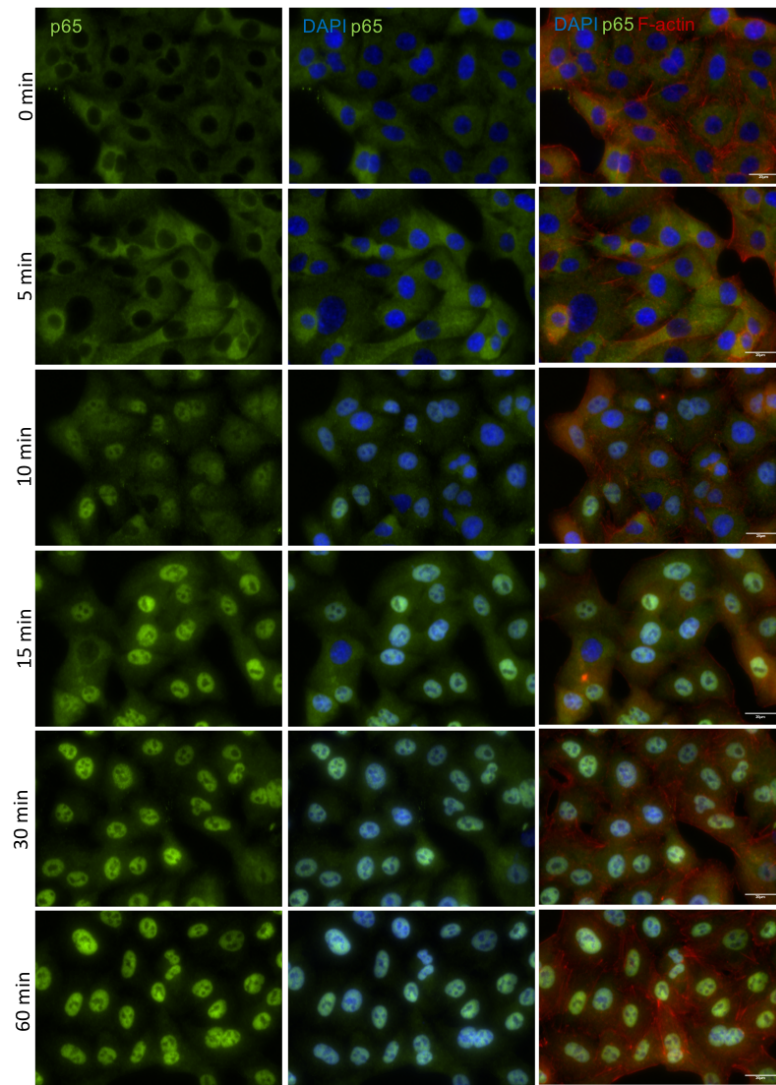
Figure 5.5 Nuclear translocation of p65 in response to TNF-α

A549 cells were seeded onto coverslips and treated with 10ng/ml TNF-α over a time course range 5min-60 minutes. Cells were fixed, permeabilised and stained for p65 (green), F-actin (red) and counterstained with Hoechst 33342 (blue). Representative immunofluorescent images of two independent experiments captured on Widefield microscope x60 magnification. Scale bar: 20µm. Quantification of nuclear:cytoplasmic (N:C) ratio of p65. Using F-actin staining to determine whole cell area for cytoplasmic region of interest. Data is presented as the mean N:C ratio per field of view and standard deviation for two independent experiments. (n=2)
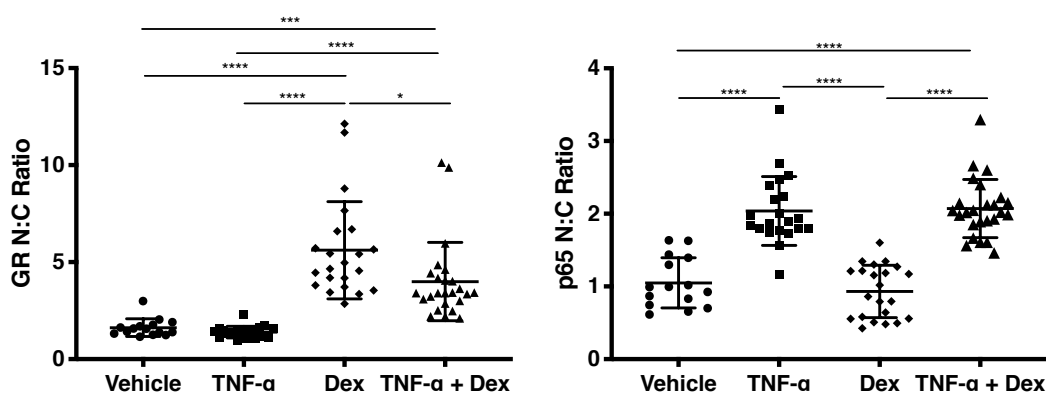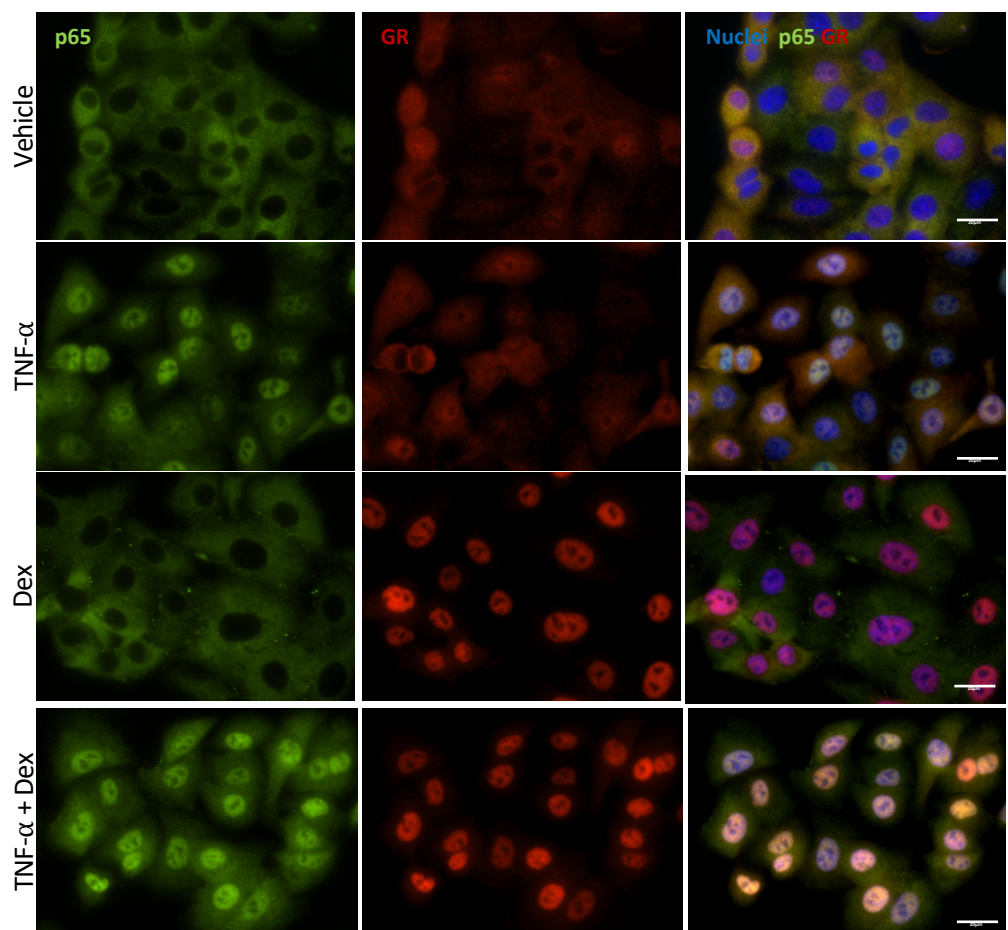
Figure 5.6 GR translocation in the presence of inflammation

*A549 cells were seeded onto coverslips and treated with 10ng/ml TNF-α for 3 hours and/or 100nM Dexamethasone for 1 hour. Cells were fixed, permeabilised and stained for p65 (green), GR (red) and counterstained with Hoechst 33342 (blue). Representative immunofluorescent images of three independent experiments captured on Widefield microscope x60 magnification. Scale bar: 20μm. Quantification of nuclear:cytoplasmic (N:C) ratio of p65 and GR. Using p65 staining to determine whole cell area for cytoplasmic region of interest. Data is presented as the mean N:C ratio per field of view and standard deviation for three independent experiments. Statistical analysis was performed using one-way ANOVA with Tukey's post-hoc multiple comparisons test comparing the mean of treatment with the mean of every other. *P<0.05, ***P<0.001, ****P<0.0001. (n=3)*

5.2.3 PMA induced differentiation

5.2.3.1 THP-1 cells acquire macrophage morphology

The differentiation of the three selected cell lines to a macrophage-like phenotype following treatment with PMA is a well-documented process (163, 306-308). However, the concentration and time period to achieve differentiation varies significantly between studies. Higher concentrations used in early studies are now considered to induce aberrant upregulation of certain genes which mask any experimentally induced pro-inflammatory signals (163). Also, considering more-recent classification of the signals inducing the spectrum of macrophage phenotypes (309), it was necessary to devise an optimised methodology.

Each cell line was treated with 5-100 ng/ml PMA for 48 hours and allowed to rest in PMA free medium for a further 48 hours. This was previously reported as necessary to allow for further upregulation of macrophage markers and allow PMA induced signals to diminish (306). Macrophage differentiation is associated with morphologic changes. Most notably the adherence of the suspension cells to culture plates and an increase in cell size and spreading which were assessed as an initial measure of differentiation (163).

The morphology of human monocyte-derived macrophages is shown for each concentration of PMA (**Figure 5.7A-C**). The images shown were taken at 48 hours and by this time point cell adherence was evident for all cell lines at all concentrations, yet to a lesser extent in the U-937s. HL-60s adhere in clumps (**Figure 5.7A**) with some protruding appendages from the groups of cells. Similarly, the U-937 (**Figure 5.7B**) also form clusters with increasing PMA concentrations and only a small percentage of cells display notable changes in morphology. In contrast the THP-1 cells exhibit characteristic spreading and ameboid morphology with no distinct observable differences between treatment concentration (**Figure 5.7C**).

Following a 48-hour rest period the extent of differentiation was measured by counting the proportion of cells which had adhered to the culture plate compared to those left in suspension, in conjunction with assessing cell viability. There is no clear dose-dependent increase in cell adhesion for any of the cell lines when treated with PMA, which supports the suggestion that lower concentrations are adequate to stably differentiate cells. Adherence of between approximately 70-80% was shown for HL-60 cells (**Figure 5.7A**) and a gradual decline in viability with treatment concentration, yet did not fall lower than 75% viability. The percentage of adherent U-937 cells was variable and cells were easily detached with washing, this is not likely due to cell death from PMA treatment as cells retained high viability. Since U-937 displayed minimal changes in morphology and poor GR responses during characterisation it was decided these cells were an unsuitable model of Gc responses in macrophages.

Around 75% of THP-1 cells differentiated with lower PMA concentrations (5-10 ng/ml). In terms of highest adhesion, **Figure 5.7C** indicates that 25 ng/ml PMA treatment induces the most stable differentiation. Despite a slight dip in viability at this concentration, viability is not compromised at higher concentrations, therefore it seems unlikely treatment causes cell toxicity. Overall, considering the responsiveness to Gcs, immunofluorescent imaging capabilities, and evidence of differentiation the THP-1 cells were selected for subsequent study as the most suitable model.
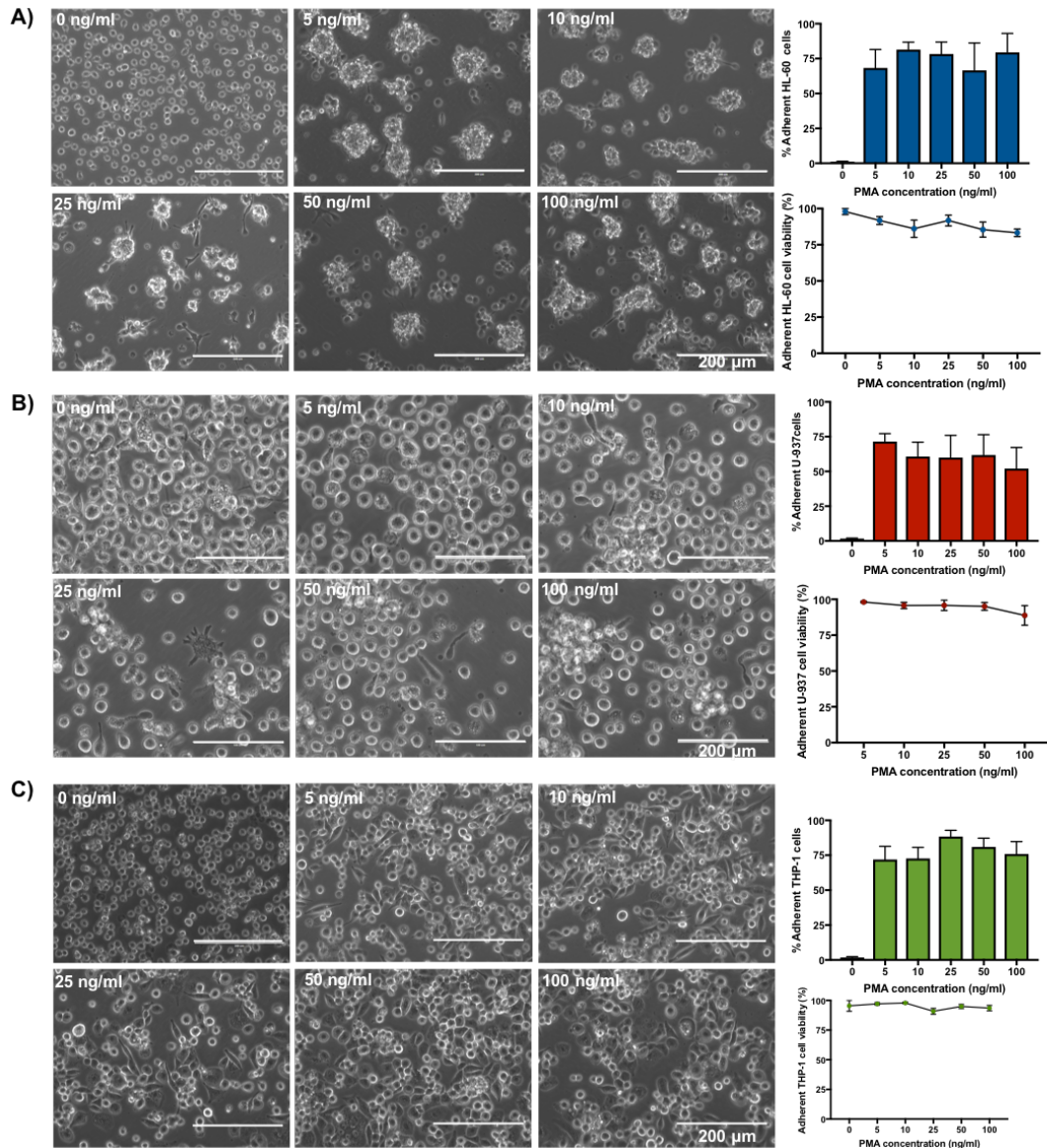
Figure 5.7 Assessment of PMA induced differentiation of monocytic cell lines

HL-60 (A), U-937 (B) and THP-1 (C) cells were treated with varying (0-100 ng/ml) concentrations of PMA for 48 hours, cells were washed and cultured for a further 48 hours in PMA-free media. Representative brightfield images are shown to assess the morphological changes following 48 hours culture with PMA. X20 magnification. Scale bar represents 200µm. Bar graphs showing cell adherence expressed as percentage of total cells measured by cell counts. Cell viability, was assessed by trypan blue exclusion - counts taken 48 hours post media change of three independent experiments. (n=3)

5.2.3.2 Cytokines to further induce M1/M2-like phenotype

The differentiation procedure was expanded further to incorporate the skewing of macrophage phenotypes with cytokines for 48 hours (**outlined in schematic Figure 5.8**). Classically activated macrophages are induced by IFN-ɣ stimulation, with ligation of TLR4 by bacterial LPS and characterised by pro-inflammatory secretion. Exposure to IL-4 or IL-13 generates alternatively activated macrophages which preferentially secrete anti-inflammatory cytokines (307). Cells were differentiated with 25 ng/ml PMA for 48 hours, the media changed and rested for 72 hours prior to treatment for a further 48 hours with either IFN-γ and LPS (M1-like) or IL-4 (M2-like).

Previous nomenclature has focused on the linear range of macrophage phenotypes described as: M1- pro-inflammatory and M2- promote wound healing. However, for experimental reporting this has recently been reconsidered to reflect range of activating stimuli leading to a spectrum of polarised states eg: M(IFN-γ) and M(IL-4) (309, 310). Chronic exposure to Gc in experimental models also generates a glucocorticoid-mediated programme of differentiation in monocytes and macrophages (123, 310). This generates a stable immunosuppressive phenotype, M(Gc), with increased phagocytic capacity, capable of suppressing adaptive inflammation in *in vitro* disease models, both directly and via the induction of regulatory T cells at inflammatory sites (311) (125, 312). Therefore, only acute Gc treatments (<6 hours) to assess immediate GR responses were investigated.

Immunoblotting confirms that differentiation does not affect Gc activation, as measured by an increased level of GR phosphorylated at position ^{P}Ser211 upon Dex exposure (**Figure 5.9A**). The secretory profile of the differentiated cells was evaluated by ELISA. TNF-α was highest on day 2 following PMA stimulation and reduced all subsequent phenotypes after the rest period. Following the rest and cytokine skewing, the 'M1-like' M(IFNγ,LPS) cells had the highest secreted levels TNF-α which was followed by the M0 phenotype which had not been exposed to cytokines (**Figure 5.9B**). The 'M2-like' M(IL-4) displayed the lowest levels of secreted TNF-α and higher levels of IL-10 in comparison to the skewed 'M1-like' phenotype, which reflects the desired characteristics (**Figure 5.9C**).
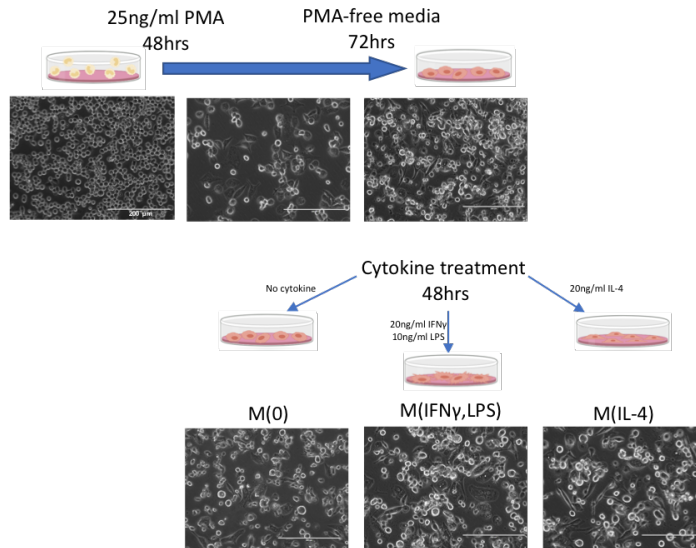
Figure 5.8 Schematic of THP-1 differentiation into macrophage-like phenotype

THP-1 cells were treated with 25ng/ml PMA for 48 hours and cultured for 72 hours in PMA free media before treatment with cytokines: M1 phenotype - 10ng/ml LPS, 20ng/ml IFN-γ or M2 phenotype - 20ng/ml IL-4 for a further 48 hours. Schematic of protocol, brightfield images captured at each time point x20 magnification. Scale bar: 200μm.

A)
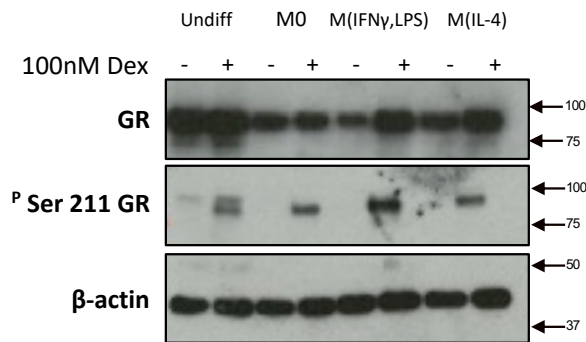
B)
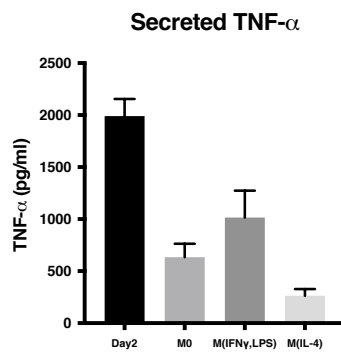
C)
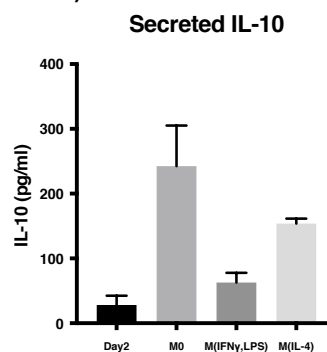
Figure 5.9 Assessment of differentiated THP-1 functional responses

Differentiated cells treated with 100nM Dex for 1hour to measure total level of GR protein and response to ligand post-differentiation. Protein expression was analysed by immunoblot (A). Specific antibodies against GR, phosphorylated Ser211 GR and β-actin were used to detect protein. Representative blots from three independent experiments. (n=3). ELISA quantification of TNF-a (B) and IL-10 (C) secreted in by THP-1 cells following differentiation (n=3).

5.2.3.3 Murine Macrophages

The mouse monocyte/macrophage cell lines RAW264.7 and J774 have the advantageous property in that they are adherent. These cells were included with the aim of using a comparison of adherence with the differentiated THP-1 cells upon the matrix-coated micropattern chips used to manipulate cell geometry. **Figure 5.10A** shows the morphology of the cells under resting conditions, RAW264.7 cells adhere in clusters whereas the J774 cells demonstrate a spread morphology with multiple appendages. The cells were also assessed for their suitability for the model by their capacity to respond to Dex, measured by immunoblot and immunostaining. Both cells express GR protein (**Figure 5.10B**) and both are responsive to Dex treatment, as measured by the increase in phosphorylation of residue Serine 211.

Cytoplasmic shuttling of GR and p65 was evaluated following 2 hr pre-treatment with 10 ng/mL LPS and then 100nM Dex. RAW264.7 cells displayed a measurable increase in GR nuclear translocation for all Dex-treated conditions, including with prior-inflammatory stimulation, while p65 nuclear translocation was significantly increased by LPS (**Figure 5.10C**). J774 cells showed a similar pattern of responsiveness (**Figure 5.10D**), with increased GR nuclear translocation following Dex treatment but this was not affected by the presence of inflammation. p65 translocation was significantly increased only for cells treated with LPS in the presence of Dex. This may be due to the increased resting N:C ratio (>1) GR and p65 in resting cells observed for this cell line which suggests a greater nuclear occupancy under resting conditions and was observable by immunofluorescence.

In summary, I determined that THP-1 cells display a measurable response to Dex, indicative of functional GR activity and differentiation into M1-like or M2-like cells does not alter responsiveness to Dex. The nuclear localisation of GR and p65 can be scored using immunofluorescence microscopy and demonstrate that Dex-induced nuclear localisation is reduced under pro-inflammatory (TNF-α) conditions. These experiment show that THP-1 are suitable to study the effects of cell geometry on GR and p65 cross-talk.
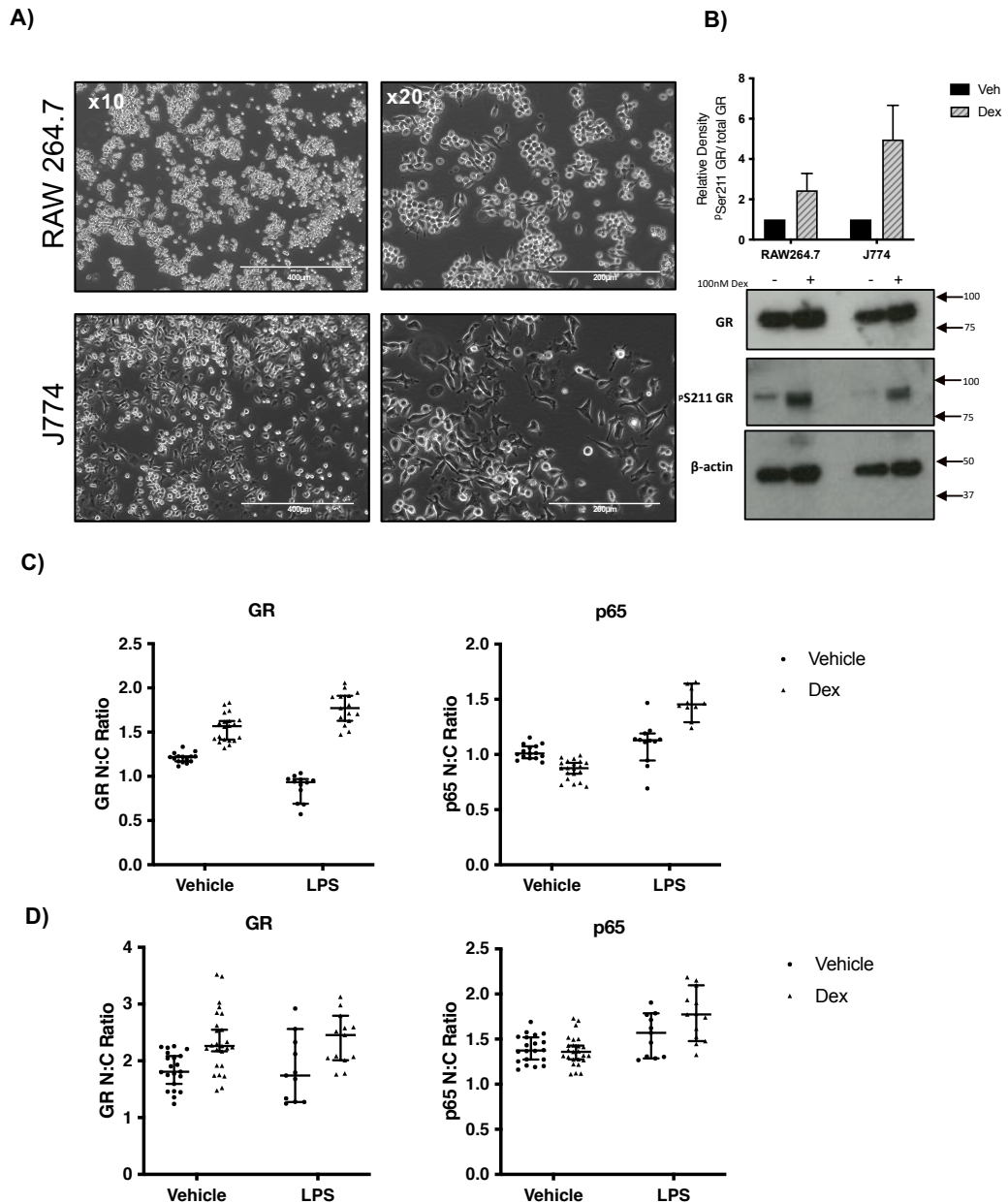
Figure 5.10 Characterisation of murine cell line responsiveness to Dexamethasone

A) Brightfield images RAW264.7 and J774 murine macrophage cell lines in culture captured on EVOS microscope x10 and x20 magnification scale bar 400μm and 200μm respectively. B) Cells were treated with 10 ng/ml LPS prior to 100nM Dex for 1 hour. Protein expression was analysed by immunoblot using 5μg protein lysates. Specific antibodies against GR, phosphorylated Ser211 GR and β-actin were used to detect protein. Representative blots from three independent experiments. (n=3). For the assessment of GR and p65 translocation RAW264.7 (C) and J774 cells (D) were treated with 10ng/ml LPS (3 hours) followed by 100nM Dex (1 hour). Cells were fixed permeabilised and stained for GR (red) and p65 (green), counterstained with Hoechst 33342 (blue). Representative immunofluorescent images of two or three independent experiments respectively. Images captured X60 magnification. Data is presented as the mean ratio of pixel intensity in nuclear and cytoplasmic compartments per field of view analysed using Cell Profiler. RAW264.7 (n=2) J774 (n=3). Scale bar: 20μm

5.2.4 Manipulation of Cell Geometry

5.2.4.1 CYTOOchip^{TM} Micropatterns Force Cell Geometry

Cell shape can direct internal cytoskeletal organisation and nuclear architecture - which in turn regulates gene expression (150). Fibronectin-coated micropatterns attempt to replicate extracellular contacts in the form of adhesive matrix zones, which force cells to spread and adopt an identical morphology (313, 314). This establishment of external cellular contacts is propagated to influence the arrangement of the internal cytoskeleton (314). This method using commercially produced CYTOOchip^{TM} micropatterns permits the controlled study of intracellular cellular signalling events in geometrically altered-cells (size, aspect ratio and shape). This can be utilised to test responses to environmental physical cues (144, 314) and mimic the cell polarity established by cell-cell and cell-ECM interactions.

5.2.4.2 Pattern Optimisation

For initial optimisation of the technique, cells were plated onto micropatterns chips which had been pre-incubated with a fibronectin solution, which selectively coats the 'activated' areas, to which the cells adhere. 'Starter chip A' contains four different shaped patterns, each with three different sizes and were used to determine the most appropriate and reproducible condition for analysis. Cells must attach to the fibronectin region, which occurs as quickly as 20 minutes, but the time taken for cells to spread and adopt the shape can vary. This spreading was observed at hourly intervals to determine the optimal spreading time using the epithelial cell line A549. The brightfield image in **Figure 5.11A** illustrates the grid-like organisation of single cells with unpatterned fibronectin borders around each section for cells to spread without constraint (referred to as 'unpatterned cells'), depicted in the chip-layout diagram in **Figure 5.11B.** At 1-hour post seeding, cells are shown to have adhered to the chip yet a limited number of cells have spread (white arrow) which was evident by 5 hours when the chips were fixed.
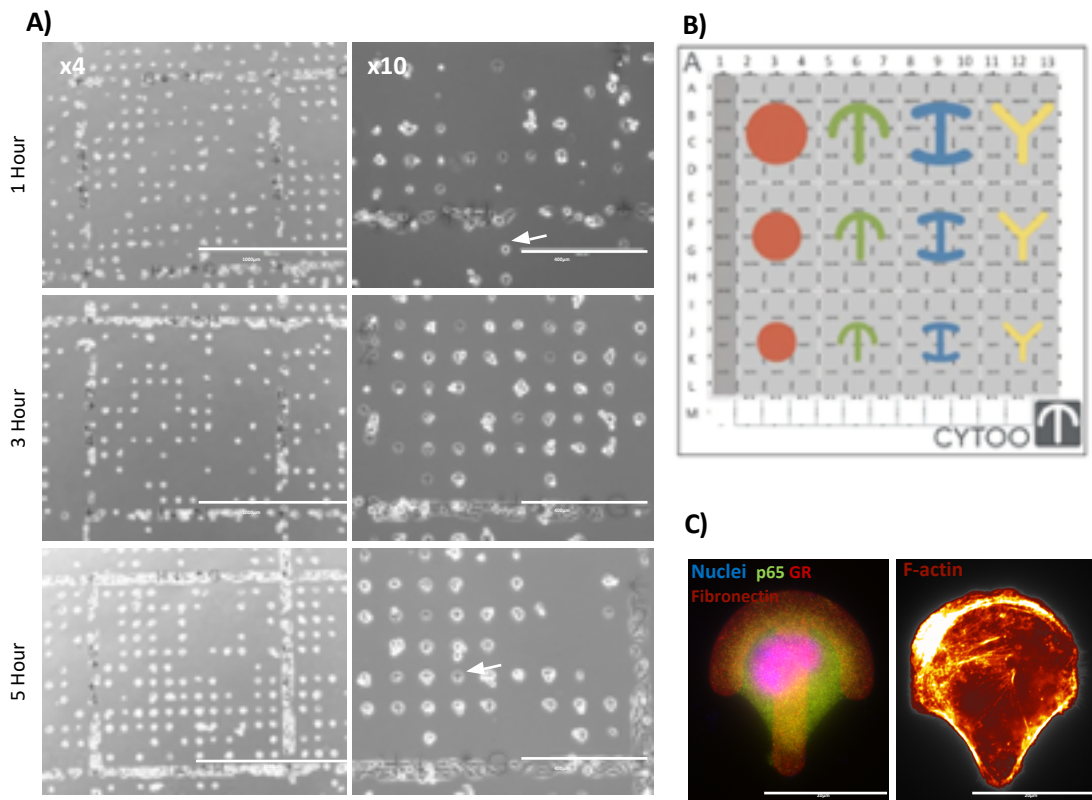
Figure 5.11 Characterisation of A549 on CYTOOchip™ Starter A micropattern chip

*A549 cells were seeded onto Starter A micropattern chips pre-coated with fibronectin. **A)** Brightfield images of A549 cells to observe cell spreading at specified time points: 1,3 and 5 hours at x4 and x10 magnification. White arrow showing adhered but not spread cell (top right panel) and cell spread to adopt cross bow shape (bottom right panel). Scale bars represent 400μm and 1000μm respectively. **B)** Schematic of starter A chip layout taken from CYTOOchip website (https://cytoo.com/micropattern-products/chips/cytoochips™-starters-x18) demonstrating the 4 different cell morphologies and 3 different spreading sizes. **C)** Representative image of A549 cells spread over crossbow micropattern. Left: stained for p65 GR, nuclei stained with Hoechst 33342 and 650nm fluorescent fibronectin pattern in red. Right: Pixel intensity staining of F-actin.*

5.2.4.3 Cell Features

Figure 5.11C shows the shape of the medium crossbow pattern (fibronectin coating stained red) and cells which have fully spread to adopt the external cell geometry with an off-centred nucleus orientating towards the 'contractile' non-adhesive edge, demonstrating how the method forces the polarity of internal organisation of the cell (314). High intensity staining of F-actin is evident with regions of high density fibres around the cell periphery. A549 cells seeded on the starter A pattern are displayed in **Figure 5.12** for all sizes and shapes. Cells were stained for α-tubulin and F-actin to observe internal cytoskeletal features. For cells forced to adopt the shape of the adhesive pattern, the actin network becomes polarised and polymerises at adhesive edges, while the formation of stress fibres and microtubule growth is directed along non-adhesive zones. This contributes to the positioning of the nucleus which is often seen to be off-set from the centre of the cell (314).

The mean cell area was quantified based on the staining of F-actin to define cell edges (**Figure 5.12**). This was found to be greater for cells constrained on micropatterns in comparison to those on the unpatterned fibronectin surface indicating the micropatterns induce a spread morphology larger than the natural phenotype. Generally, the measured cell area increased between small and medium sized patterns - this was most evident for the crossbow and 'H' shape. Inefficient spreading of the cells meant there was an insufficient number of cells on large patterns to perform measurements or for further analysis.

The nuclear area was measured and defined by Hoechst 33342 staining. The nuclear area was proportional to the spreading area by which, the nuclear area was larger for cells spread on micropatterns compared to cells in their natural conformation upon fibronectin (**Figure 5.12**). To some extent, the mean nuclear area is increased, between small and medium size patterns for each shape. These results show that these commercial plates can be used to manipulate the cell morphology and cytoskeleton, although the number of cells adopting the desired morphology was very low; this makes statistical analysis of data difficult.
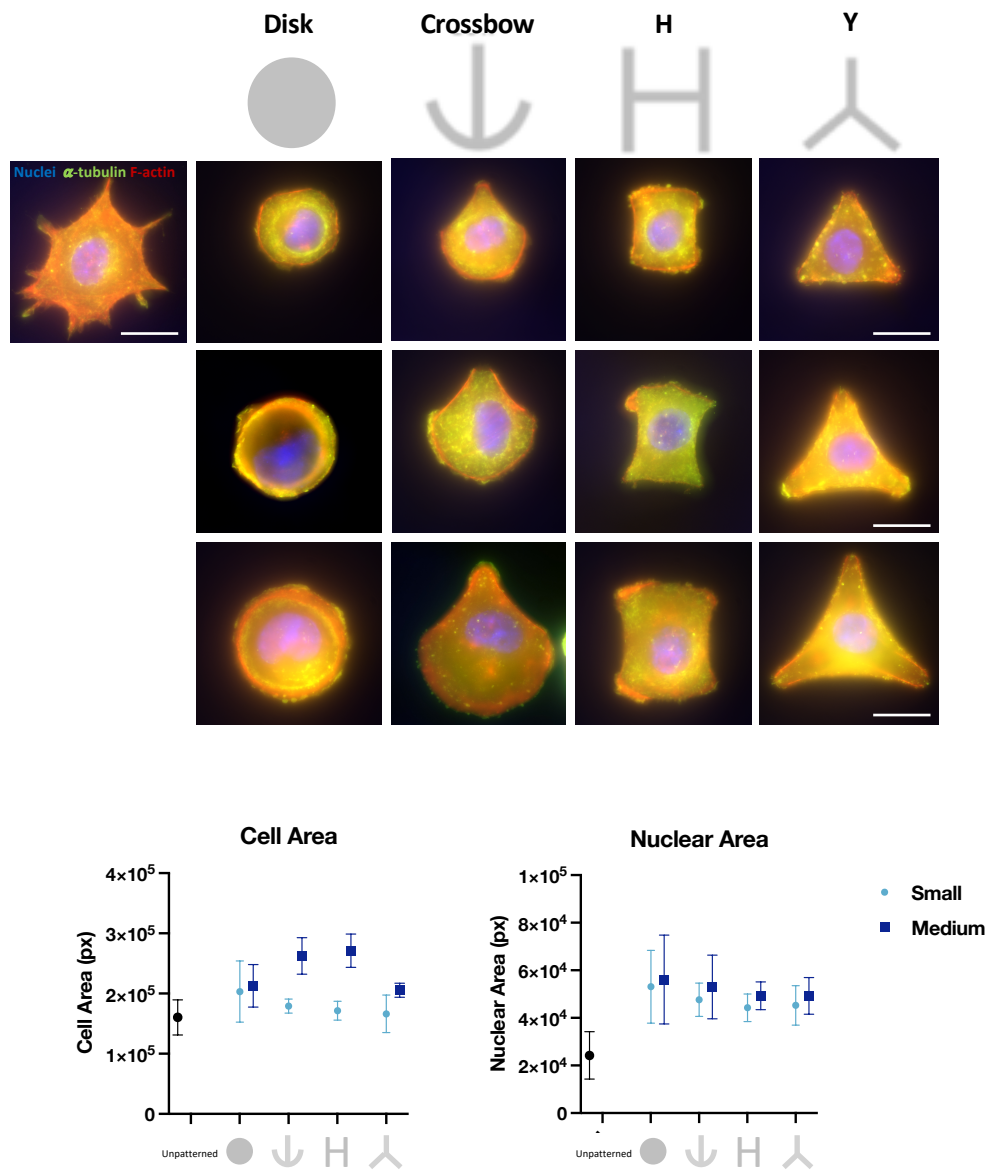
Figure 5.12 A549 cellular morphology on CYTOOchip™ Starter A micropattern chip

A549 cells were seeded onto Starter A micropattern chips which had been pre-coated with fibronectin and allowed to adhere and spread over patterns for 5 hours. Cells were fixed, permeabilized and stained for F-actin (red) and α-tubulin (green), counterstained with Hoechst 33342 (blue). Shown representative immunofluorescent images of cells on disk, crossbow, H and Y patterns taken at x100 magnification. Cell profiler was used for the measurement of cell features. Scale bar: 20μm.

Next, THP-1 cells, differentiated (with PMA) then rested as previously described (without cytokine skewing), were collected and seeded onto the chips. In a preliminary experiment allowing 5 hours spreading, cells failed to adopt any recognisable shape and complete spreading of singlet cells is required for reproducible analysis (data not shown). For proliferating cells, it is vital to fix cells as quickly as possible to avoid singlet-adhered cells dividing on the pattern. However, PMA induces growth arrest and differentiated THP-1 cells were incubated for 5 and 24 hrs to determine whether a longer incubation permitted cells adopting the designated shape. **Figure 5.13** shows the best examples of cells resembling the pattern shape and demonstrates heterogeneity in conditions designed to force the cells to assume uniformity. The cells shown are on the pattern with the smallest surface area ($700\mu m^2$) which is further limited by patterns with doublet cells. This shows that neither micropattern shape – independent of adhesive surface area, or the length of time post plating, influenced the efficiency of cell spreading across the adhesive area. From the data shown, the most apparent determinant of THP-1 cell adopting the appropriate shape was the size of the pattern which are deemed too large to achieve full spreading. Subsequent experiments sought to increase the efficiency of cell plating by utilising smaller patterns, to permit the more reproducible analysis of greater cell numbers. However, following further attempts to increase efficiency, the THP-1 cells were deemed unsuitable for further experiments.
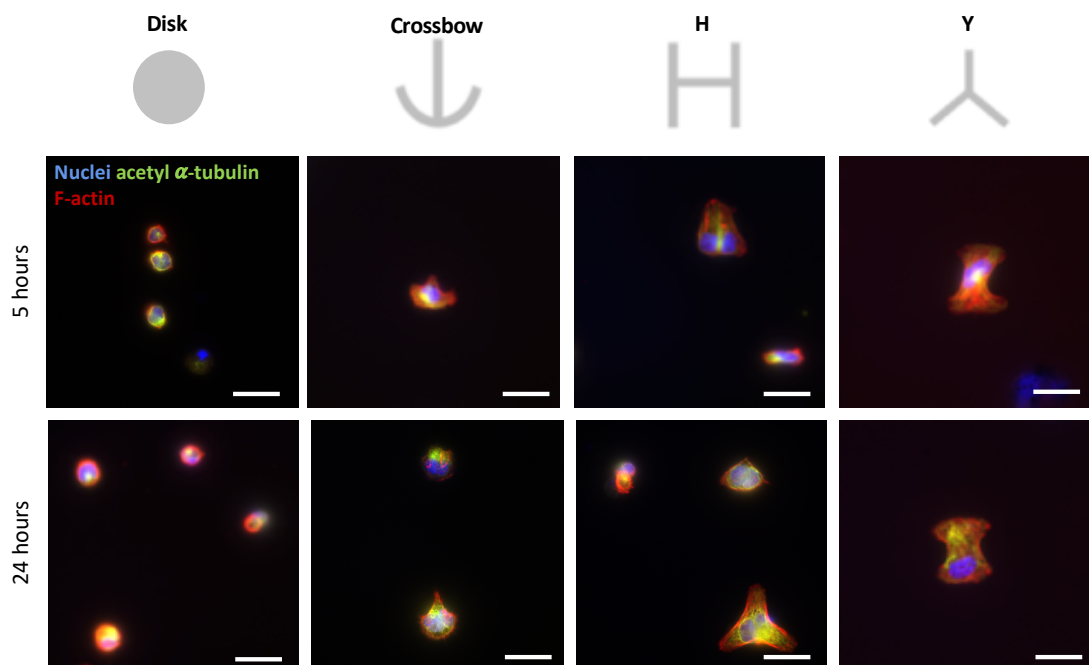
Figure 5.13 CYTOOchip manipulation of THP-1 cell geometry

THP-1 cells differentiated with 25ng/ml PMA for 48 hours and rested for 72 hours, were plated onto CYTOOchip starter A layout and allowed to adhere and spread over patterns for 5 and 24 hours. Cells were fixed, permeabilized and stained for F-actin (red) and α-tubulin (green), counterstained with Hoechst 33342 (blue). Shown are the best representative immunofluorescent images of cells on disk, crossbow, Y and H patterns from one experiment. Scale bar: 20μm

5.2.4.4 Crossbow geometry increases Dex-responsive GR nuclear occupancy

The principal aim of this work was to investigate whether transcription factor dynamics are altered by cell geometry, ideally in a macrophage-like cell (THP-1) thereby modelling an inflammatory reaction. However, as described above, THP-1 cells did not adhere well to the plates and adoption of the desired conformations was inefficient. For this reason, THP-1 cells were replaced with A549 cells; Gc responses in A549 cells with forced geometry were assessed following TNF-α pre-treatment and 100nM Dex as previously described (**Figure 5.14**).

Comparing the N:C ratio in unpatterned cells demonstrates a measurable increase in the GR N:C ratio between conditions treated with Dex and vehicle (**Figure 5.14B** and see **Figure A.3** in the Appendix), consistent with previous measurements. For cells with an altered geometry, plated on the small and medium size crossbow pattern, GR is not fully excluded from the nucleus in the vehicle condition and is diffusely located throughout the whole cell. This is reflected by the slight increase in the GR N:C ratio between unpatterned and cells cultured on micropatterns for vehicle conditions. Nevertheless, Dex significantly increases the GR nuclear occupancy, evident by staining predominantly co-localised in the nucleus. Similarly, there is an increase in GR N:C ratio in response to Dex for cells pre-treated with TNF-α in comparison to TNF-α alone. This was shown for cells seeded onto the crossbow pattern and unpatterned surface (**Figure A.3A,C,E**).

The p65 N:C ratio was increased in response to TNF-α irrespective of Dex treatment (**Figure 5.14C and Figure A.3B,D,F**). This reflects what was previously measured for A549 cells although, no significant difference between the Dex translocation with inflammatory pre-treatment was quantified of GR.

The effect of cell morphology upon transcription factor shuttling were compared across treatment groups. Compared to unpatterned cells, there is further increase in nuclear occupancy of GR in Dex-treated cells plated on small micropatterns, which is even greater for medium micropatterns (**Figure 5.14B**). This increase in GR N:C ratio is reflected by cells pre-treated with TNF-α followed by Dex although, there is no significant difference between the cells on small and medium sized patterns. Cells spread onto small crossbow micropatterns also showed an increase in GR N:C ratio in response Dex treatment, both in presence and absence of TNF-α. While the p65 N:C ratio was increased in response to TNF-α, the level of translocation was greater for cells treated with TNF-α and Dex (**FigureA.3D**). This effect was not seen for cells upon the medium pattern and demonstrated similar trends in translocation dynamics to that seen with unpatterned cells (**Figure A.3B and F**).

The translocation of p65 also demonstrates shape-induced differences between treatment conditions (**Figure 5.14C**). A greater N:C ratio for vehicle treated cells was measured between

the unpatterned and small cross-bow condition yet, was not increased for medium patterns - this was also the case for cells treated with Dex. Whereas, for cells treated with TNF-α only, the level of translocation was only significantly increased between unpatterned and cells spread on medium crossbow patterns. The N:C ratio was significantly higher in both the small and medium crossbow pattern cells when compared to unconstrained cells, in the presence of TNF-α and Dex. Overall this suggests plating cells on cross-bow micropatterns can affect the extent of transcription factor nuclear translocation in response to stimuli.
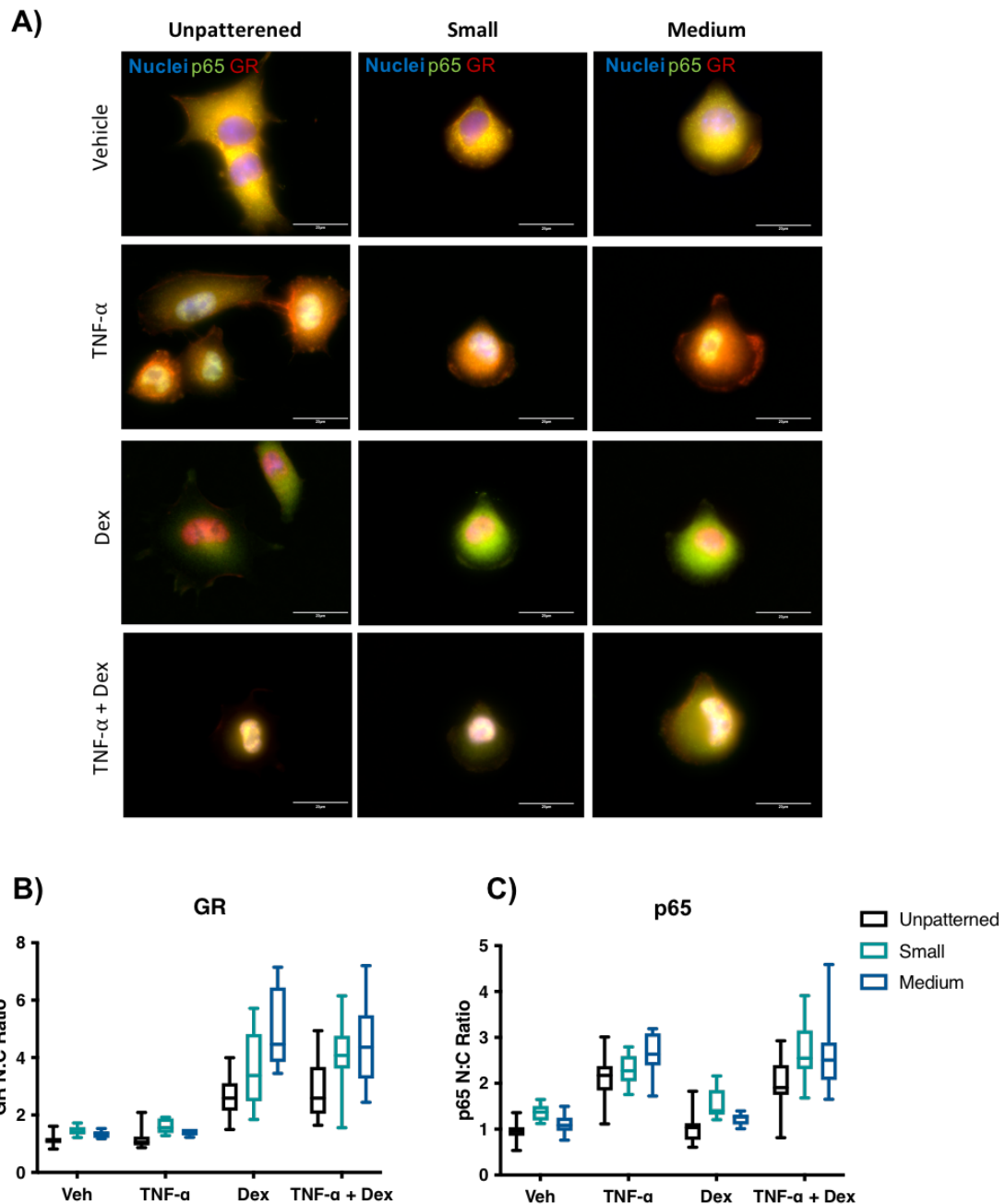
Figure 5.14 Comparison of nucelar:cytoplasmic ratio and micropattern size

*A549 cells plated onto unpatterned substrate, small or medium crossbow micropatterned surface and treated with vehicle, 10ng/ml TNF-α for 3 hours and 100nM Dex for 1 hour. Cells were fixed permeabilised and stained for GR (red) and p65 (green), counterstained with Hoechst 33342 (blue) **(A)**. Quantification of GR and p65 localisation was performed using Cell Profiler software, presented as the nuclear: cytoplasmic ratio of measured pixel intensity. Box plots shows minimum to maximum measurements per condition for GR **(B)** and p65 **(C)**. A549 cells plated on unpatterned substrate, small or medium crossbow micropatterned surface.*

5.2.5 Custom patterns vary cell aspect ratio

Custom micropatterns were used to compare the effect of aspect ratio for the same cellular spreading area. **Figure 5.15A** describes the pattern size and aspect ratio included on the micropattern chip. The spreading time was again observed for A549 cells, which were fixed 5 hours post-plating. To evaluate effect of aspect ratio on ligand-induced GR translocation, cells were treated with 100nM Dex for 1 hour prior to fixing the cells. The N:C ratio of GR and p65 was captured by immunofluorescent staining for small and medium size patterns across all aspect ratios **(Figure 5.15B).**

A Dex-induced increase in GR translocation was quantified for all conditions irrespective of pattern spreading size or aspect ratio (**Figure 5.16A&B**). In contrast to previous observations on the cross-bow patterns, the N:C ratio of Dex-treated cells was significantly greater on the unpatterned substrate in comparison to all cells with confined geometry. Despite the lack of inflammatory stimulus, there were some significant changes in the localisation of p65 with varied aspect ratio (**Figure 5.16C&D**). For the small size pattern, the 1:1 and 1:3 aspect ratios, displayed reduced nuclear localisation of p65 by Dex, in comparison to the vehicle. This effect was significantly lower than the N:C ratio in unpatterned cells. Although, this was not reflected by the cells plated on medium patterns, whereby the only significant differences were a lower level of translocation between vehicle treated cells spread on 1:1 pattern compared to unpatterned.

When comparing the effect of pattern size and aspect ratio for the same treatment group, there were no observed differences in GR translocation between vehicle-treated cells on unpatterned regions and those confined to micropatterns (**Figure 5.17A&B**). The N:C ratio was >1 in all cases suggesting high resting levels nuclear GR. Upon Dex-addition, no size-dependent differences were observed for the same aspect ratio. Rather in comparison to unpatterned cells, the N:C ratio was significantly reduced. This was most evident for aspect ratios inducing the greatest level of stretch, 1:6 and 1:10. regardless by the level of cell stretch induced by different aspect ratios. This suggests that for stretched cells the Dex-induced nuclear translocation of GR is reduced.

No measurable differences in translocation were shown for p65, between cells on patterned or unpatterned regions treated with vehicle (**Figure 5.17C&D**). However, in the presence of Dex a number of significant differences were observed. Namely, the small 1:1 and 1:3 aspect ratio had significantly lower nuclear p65 compared to unpatterned. For 1:1 difference was seen between small and medium sizes. A significantly lower level of translocation cells on small 1:3 patterns in comparison to 1:6 and 1:8. These findings suggest that cell geometry in the context of GR-activation can alter the nuclear localisation of p65.
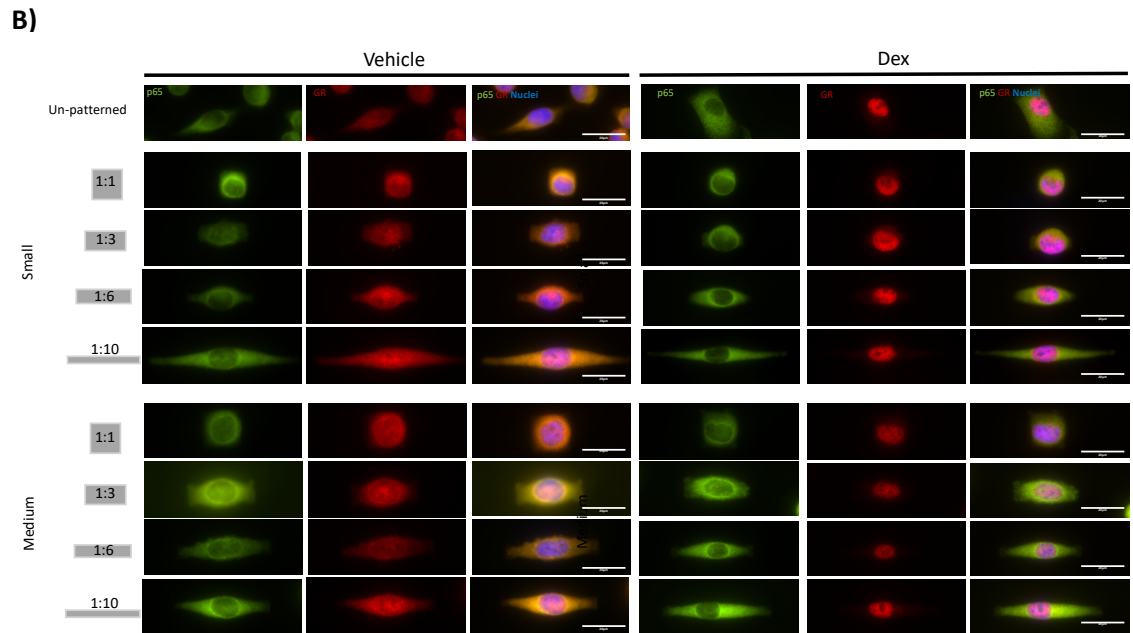
Figure 5.15 Transcription factor localisation in A549 cells with differing aspect ratios

A) Schematic of the "HUMEN' chip layout taken from CYTOOchip product sheet. B) A549 cells plated onto custom HUMEN micropatterns, cells were allowed to spread for 5 hours and were treated with vehicle or 100nM Dex for 1 hour. Cells were fixed permeabilised and stained for GR (red) and p65 (green), counterstained with Hoechst 33342 (blue). Representative images shown for cells on each size and aspect ratio as indicated. Images taken on widefield microscope at X100 magnification. Scale bar represents 20μm.
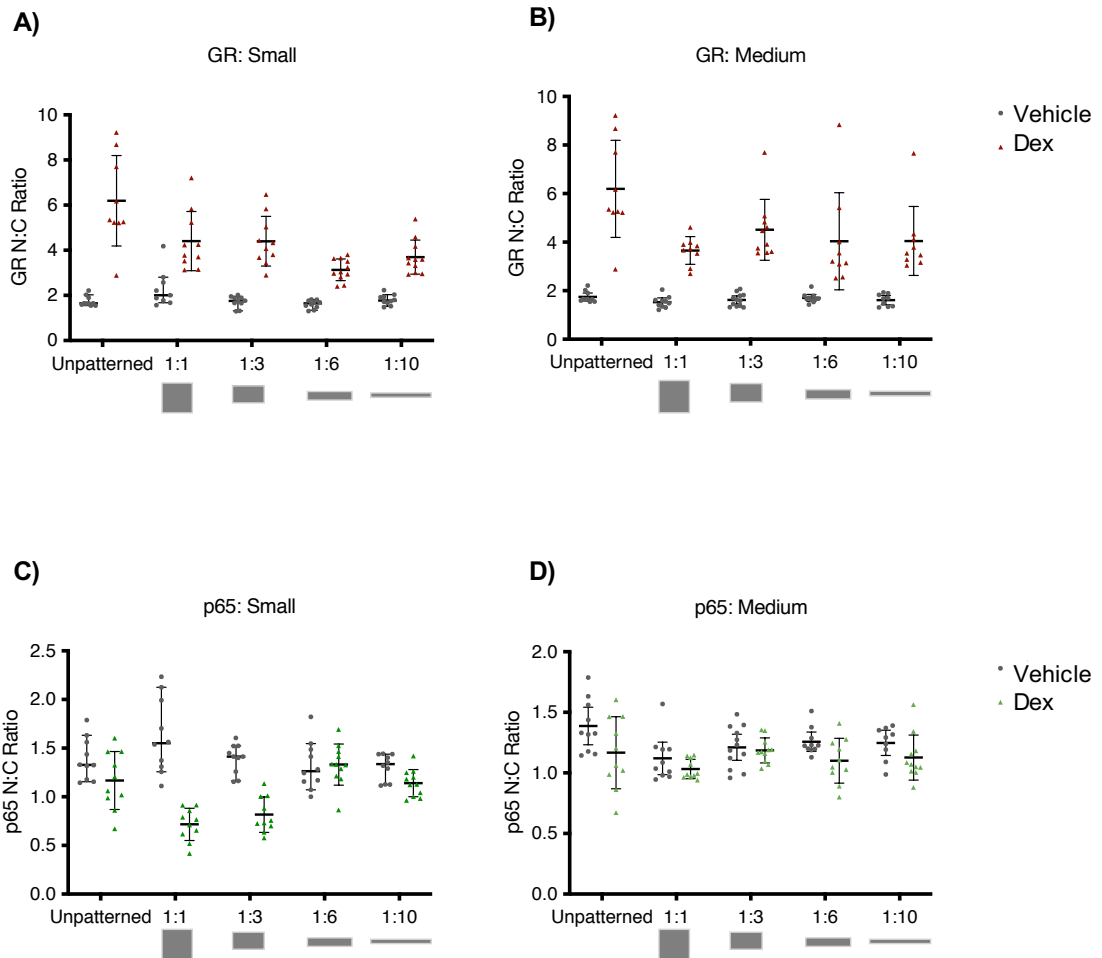
Figure 5.16 The effect of micropattern aspect ratio upon Dexamethasone responsiveness in A549 cells

A549 cells plated onto custom HUMEN micropatterns allowed to spread for 5 hours and were treated with vehicle, or 100nM Dex for 1 hour. The nuclear:cytoplasmic ratio pixel intensity per cell of GR (A&B) and p65 (C&D) on small and medium size patterns, were quantified using cell profiler software using the peri-nuclear measurements pipeline. Each point represents a measurement from a single cell with mean value and standard deviation shown.
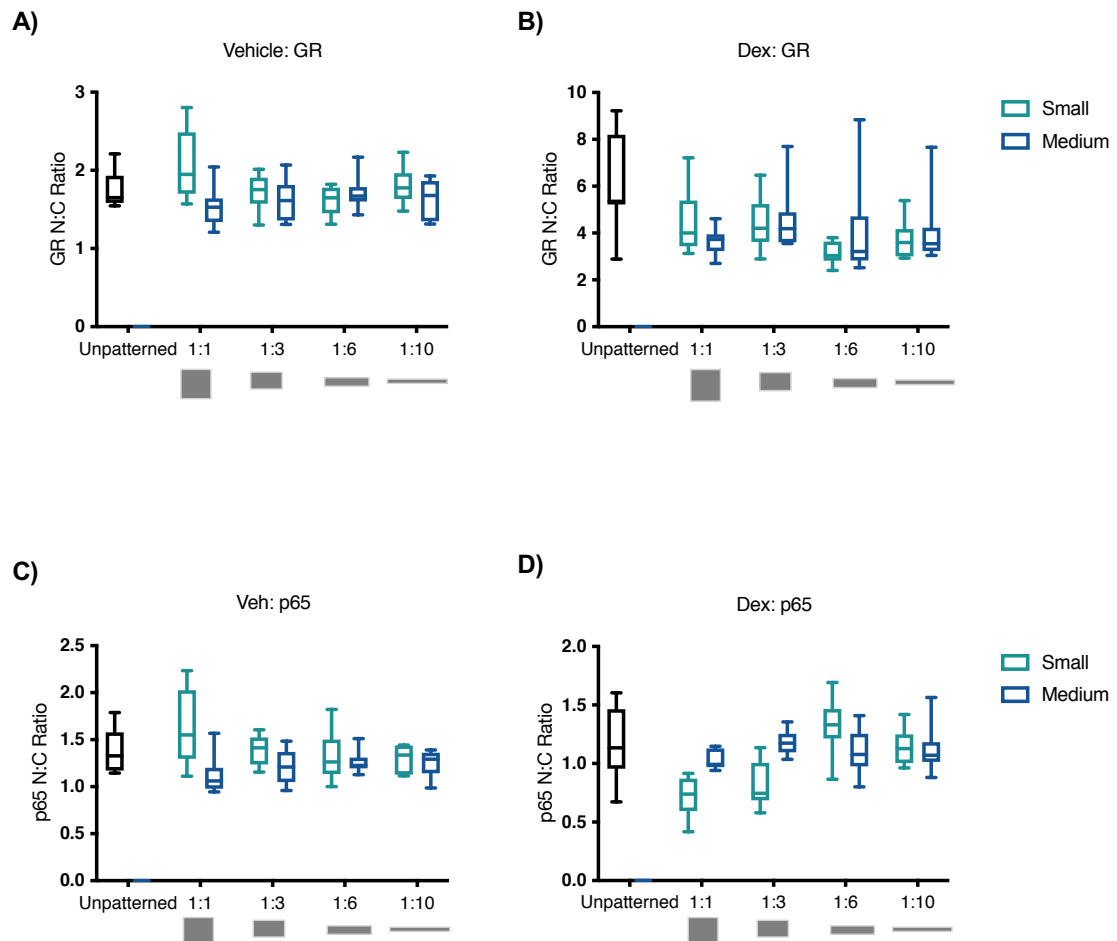
Figure 5.17 The effect of micropattern aspect ratio and size upon Dexamethasone responsiveness in A549 cells

A549 cells plated onto custom HUMEN micropatterns allowed to spread for 5 hours and were treated with vehicle, or 100nM Dex for 1 hour. The nuclear:cytoplasmic ratio pixel intensity per cell of GR (A&B) and p65 (C&D) treated with vehicle or 100nM Dex, were quantified using cell profiler software using the peri-nuclear measurements pipeline. Each point represents a measurement from a single cell with mean value and standard deviation shown. Box plots shows minimum to maximum measurements per condition.

5.2.5.1 Stretched cells have higher nuclear GR

The custom patterns were then used with the mouse macrophage cell lines, since THP-1 cells had failed to reproducibly adhere and spread upon the micropatterns. The spreading efficiency of RAW264.7 and J774 cells was first compared. It was found that the RAW264.7 cells often clumped on the adhesive area as multiple cells and did not sufficiently spread to fill the area, resulting in irregular shaped cells (**Figure 5.18A**). The spreading of J774's was much more complete and uniform across different sizes and aspect ratio, by comparison to RAW264 cells; (as shown in **Figure 5.18B**), and were used for subsequent experiments.

Quantification of the cell area confirms an increase between small and medium patterns (**Figure 5.18C**) Due to the large area range observed for unpatterned cells, there were no measurable differences to those plated on the patterns. Yet across both small and medium sizes the cell area appears to increase slightly with aspect ratio – despite the spreading area being equal. However, there is no change in the nuclear area across aspect ratio and pattern size (**Figure 5.18D**). F-actin staining was high intensity around cell edges. For cells on a 1:1 aspect ratio (square patterns), actin is evenly distributed around the cell perimeter and as the aspect ratio increases, cells show regions of higher intensity at each end of the cell. In line with this, the nucleus becomes more oblong along the plane of stretch. Demonstrating that the geometry of the cell can influence the underlying nuclear morphology.

A) RAW264.7

B) J774

C) Cell area

D) Nuclear area

- Small
- Medium
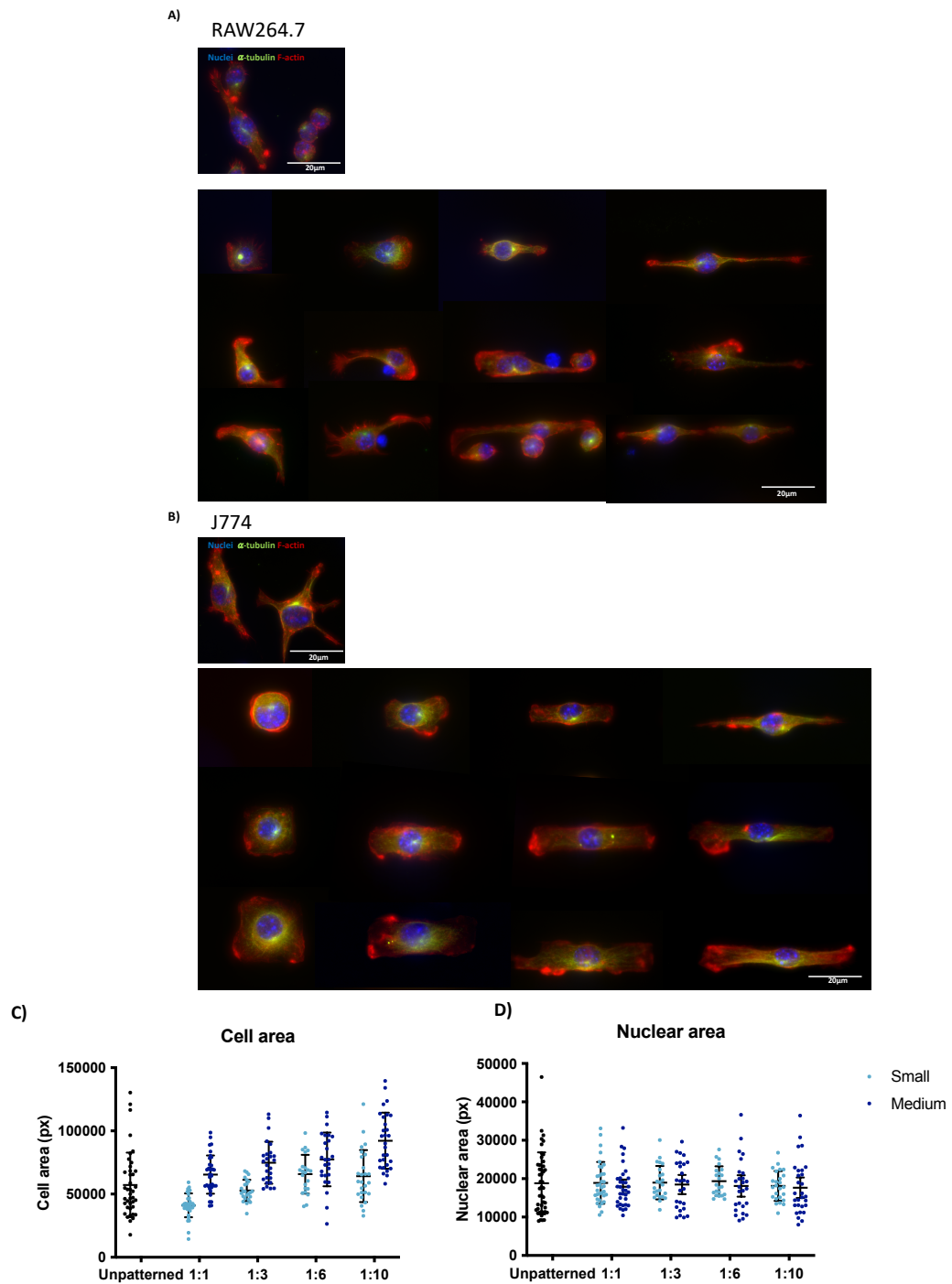
Figure 5.18 Comparison of RAW264.7 and J774 cell morphology on custom micropatterns

*Murine macrophage cells were plated onto 'HUMEN' custom micropatterns coated with fibronectin. RAW264.7 **(A)** and J774**(B)** cells were allowed to spread for 5 hours and were then fixed and permeablilised and stained for F-actin (red) and α-tubulin (green), counterstained with Hoechst 33342 (blue). Shown are the best representative immunofluorescent images of cells across all aspect ratios and sizes. Images captured on widefield microscope x100 objective. Scale bar = 20μm. Measurements of J774 cell **(C)** and nucleus **(D)** pixel area quantified using cell profiler. Each point represents a single cell. Line and bars represent mean +95% CI*

The localisation of GR and p65 was assessed in J774 cells following 100nM Dex treatment for 1 hour (**Figure 5.19**). Again, the treatment and geometry effect were quantified. The localisation of GR on small patterns, revealed a significant increase in N:C ratio only between vehicle and Dex treated cells plated on unpatterned GR substrate and the most stretched morphology- 1:10 aspect ratio (**Figure 5.19B**). However, Dex-dependent increase in GR translocation was measurable for cells upon all aspect ratios for medium patterns (**Figure 5.19C**). Again, the cells with the 1:10 aspect ratio displayed a significant increase of N:C ratio compared to unpatterned cells. Which also may support a possible trend towards increase in GR nuclear localisation with increased aspect ratio.

No significant changes in the N:C ratio of p65 were measured for cells on both small and medium patterns, neither between Dex treatment or aspect ratio (**Figure 5.19D&E**). Although, a potential trend towards decreased levels of nuclear p65 were observed with Dex treatment, for unpatterned cells and with increasing aspect ratio.

In absence of Dex, the levels of nuclear GR are increased with increasing aspect ratio for both small and medium patterns. However, with the addition of Dex only cells with the most stretched morphology show a significant increase in the extent of translocation in comparison to unpatterned cells. In the case of p65, no significant changes of cellular distribution were measured for either treatment condition. Despite what was seen with A549 cells, the localisation of p65 in macrophages is not affected by geometry in the absence of activating stimuli. Further investigation would need to establish what the effect of TNF-α or LPS would have in the context cell geometry and altered aspect ratio.

In summary, the use of micropatterns which influence cell morphology demonstrates that the nuclear localisation of GR and p65 is indeed influenced by morphology and the underlying cytoskeleton. However, this technique is currently limited by the inefficiency of the plating process as described above and current results are preliminary and descriptive. Despite this, these results do show that the responses of cells to inflammatory (TNF) and anti-inflammatory stimuli (Dex) in a densely packed tissue are likely to be influenced by cell morphology.
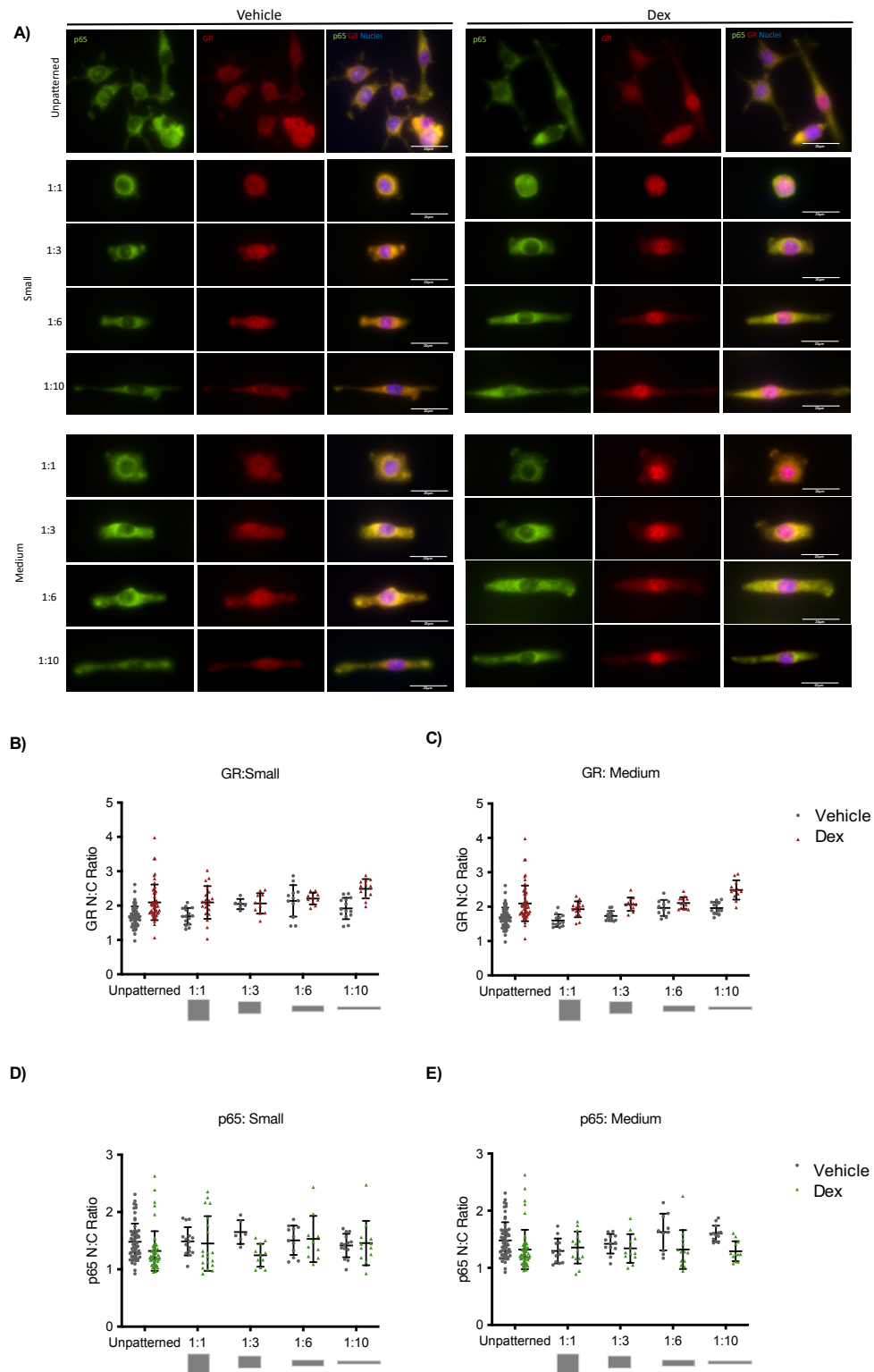
Figure 5.19 The effect of micropattern aspect ratio upon Dex responsiveness in J774 cells

J774 cells plated onto custom HUMEN micropatterns, cells were allowed to spread for 5 hours and were treated with vehicle or 100nM Dex for 1 hour. Cells were fixed permeabilised and stained using GR (red) and p65 (green)- specific antibodies, counterstained with Hoechst 33342 (blue). Representative images shown for cells on each size and aspect ratio as indicated (A). Images taken on widefield microscope at X100 magnification. Scale bar represents 20µm. The nuclear:cytoplasmic ratio of GR (B&C) and p65 (D&E) on small and medium size patterns, were quantified using cell profiler software using the peri-nuclear measurements pipeline.

5.3 Discussion

It is now emerging that Gc signalling can be modified by the microenvironment, and the integration of external signals can fine-tune Gc effects (5, 46). Cell geometry is proposed to regulate transcription factor shuttling, chromatin architecture and transcriptional outcomes (134, 144, 150). However, to date no studies have investigated the role of cell geometry in regulating Gc action. I assessed the effect of cell morphology upon Gc-responsive cell types, the lung epithelium and macrophages which are both relevant targets of therapeutic glucocorticoids. Understanding if and how cell geometry affects GR function will better inform how Gc act *in vivo* and help to understand how this may be perturbed in disease states.

5.3.1 Gc Sensitivity

Macrophages are major Gc targets in inflammatory disease, and for this reason they were chosen as the initial model. Three commonly used cell lines - HL-60, U-937 and THP-1 can be differentiated into macrophage-like cells (161, 163, 315). As the primary measure for this project is Gc sensitivity, the responsiveness of the cell lines was evaluated. Overall, THP-1 cells showed high levels of GR expression, induction of Ser211 phosphorylation, translocation and transcriptional responses and were therefore the most suitable model to study Gc sensitivity. The GR-ligand responsiveness of THP-1 cells was also evaluated post-differentiation, to ensure that GR activity is maintained. Levels of phosphorylated GR at position ^{P}Ser211 was increased following Dex exposure for each condition. GR expression was maintained although varied levels of protein were observed despite no major differences in β-actin levels. However, given the major morphological changes (including a dramatic increase in cell size), levels of cytoskeleton protein β-actin could potentially be altered and would not serve as the most appropriate loading control. Although, one study determined the genes ACTB (encoding β-actin) and RPL37A (encoding ribosomal protein L37a) are the most stable reference genes for qPCR normalisation during THP1 differentiation (316). For further confirmation, expression should be assessed in parallel by another housekeeping protein less likely to be affected by major changes in cytoskeleton composition or metabolic activity such as HDAC1 or TATA-binding protein. Had the model been utilised further in the study, gene expression profiles of key GR target genes should also be assessed to ensure GR-ligand responses are maintained.

5.3.2 Macrophage differentiation

Macrophages are subject to dynamic cytoskeleton rearrangements in comparison to epithelial cells *in vivo*, as they undergo cytoskeleton remodelling and nuclear distortion as they migrate and infiltrate tissues. (317, 318). The mRNA expression and secretory profile of macrophages has been previously shown to be altered by plating on polymer-coated substrates with varied

morphologies (319), which made them an attractive target cell for investigation. I aimed to develop a physiologically relevant model using differentiated macrophages. It is difficult to truly replicate an *in vivo* setting using cell lines, but have advantages over using PMBCs due to their faster doubling time providing abundant yield, in addition to a homogenous genetic background and are therefore not confounded by inter-donor variability (162). The process of differentiation permits comparison of macrophages skewed towards different phenotypes, and also had the added advantage that cells adhere and spread which was required for imaging endpoints.

The myeloblast HL-60 cell line is the least mature and has multipotency towards either neutrophilic or monocytic lineages depending on the stimulating agent (161) which have been used to model proliferation and differentiation of myeloid cells (308). THP-1 cells have been used previously to study nuclear receptors and U-937 to study the effects of Gc (315). U-937 cells have tissue origins and were derived from a patient with histiocytic lymphoma therefore, are more mature than THP-1 cells, which were derived from the blood of a patient with acute monocytic leukaemia (162).

Studies comparing THP-1 monocytes to those isolated from human PBMCs show PMA-differentiated THP-1 cells are more functionally similar to primary monocyte-derived macrophages compared to U-937s (306, 320). These findings are consistent with other studies which preferentially use THP-1 cells as a macrophage model (162, 307).

Numerous publications describe different methodologies for the differentiation to macrophage like cells each differing in stimuli ($1\alpha,25(OH)_2D_3$ or PMA) concentration (5-100ng/ml), culture period (24-96 hours), inclusion of a rest period (48-72 hours) and whether cytokine cocktails are used to polarise to M1 or M2-like phenotypes. $1\alpha,25(OH)_2D_3$ is widely used as a differentiating agent however, as it reportedly drives a less mature macrophage phenotype compared to PMA, it was not tested in this study (321). The average period of exposure to PMA is 48 hours and was replicated for this study – comparing multiple doses of PMA (5-100ng/ml). Introducing a rest period in PMA-free media is reported to result in cells which resemble the primary monocyte-derived monocyte phenotype to a greater extent, but including this rest period means that higher doses of PMA are required for the initial treatment. (306). For example, Chanput *et.al (162)* show that a minimum of 100ng/ml PMA is required with 48 hours with rest, for THP-1 differentiation. Conversely Park *et.al (163)* concluded 5 ng/ml was sufficient to increase adherence and increased CD14 expression but did not include a rest period prior to experimental treatment. The study by *Park* et.al does raise the important consideration that high stimulating conditions induce notable induction of pro-inflammatory genes and can reduce responses to subsequent experimental stimuli – including cytokine cocktails that drive an M2 like phenotype. I also measured a similar effect as levels of secreted TNF-α were the greatest prior to the rest period. By using an intermediate concentration of PMA for the initial treatment and a rest in

PMA free media activation of pro-inflammatory signalling pathways such as NF-κB will be minimised (304, 322).

Recently, more extensive protocols have been developed to include polarising cytokines to better mimic the spectrum of macrophage phenotypes encountered *in vivo*. Similar to protocols used for differentiation of primary human and mouse monocytes, M(IFN-γ & LPS) are polarised to emulate 'classical' pro-inflammatory M1 macrophages and M(IL-4) alternatively activated anti-inflammatory M2 macrophages. This procedure has already been well characterised in THP-1 cells and is reported to induce characteristic cytokine and surface marker expression (307, 323). Subsequent characterisation is required to fully evaluate the model however, due to parallel complications in using the micropatterns the developed model was not characterised any further.

5.3.2.1 Murine Macrophages

Following technical difficulties in differentiated THP-1 cell detachment and spreading on micropatterns, murine macrophage cell lines were instead included in the model. The steroid responsiveness of these cells was again confirmed by increased detection of phosphorylated Ser211 GR in response to Dex treatment. Immunofluorescent imaging of the J774 and RAW264.7 cells reveals the larger spreading size of J774 cells in comparison to RAW264.7 cells, which may account for the superior capacity of J774 cells to spread on the micropatterns.

5.3.3 Cell Geometry

5.3.3.1 Technical challenges

Initial attempts to model cell geometry in THP-1 cells resulted in variable morphology and insufficient spreading, potentially due to either technical issues in detachment and plating, or because the patterns were too large for the cells. Despite attempts using custom patterns with a smaller surface area, differentiated THP-1 cells were too variable to reliably obtain sufficient data and were not used further during the study. Exploration into the expression of surface adhesion molecules may also provide answers to the defects of using the cells in the model. Similarly, RAW264 cells plated on the patterns clumped together in a similar morphology to that observed under routine culture and were not chosen for further evaluation. Using A549 lung epithelial cells I validated the principle of the method and were able to optimise the procedure.

5.3.3.2 Cell features

Adhesive fibronectin regions of the micropatterns induce internal re-organisation of the cytoskeleton (314). The off-centre nucleus signifying micropattern-induced cell polarity was

particularly evident in A549, but less so for J774 cells plated on crossbow patterns. Differences in the organisation of actin structures were observable between the two cell types with A549s best displaying high intensity regions of F-actin staining at non-adhesive edges in contrast to central regions of disordered actin structures in J774 cells. These observations suggest re-arrangement of actin structures forced by geometry directed the orientation of the nucleus in A549s. Macrophages plated on micropatterns have been shown to have altered organisation of F-actin structures in comparison to adhesive cells (324). Changes in actin-cytoskeleton dynamics can modulate nuclear morphology through direct physical connections to the nuclear matrix (136, 137). I found that the nuclear area for both cell types appears to be affected more by cell shape rather than pattern size, which was larger in comparison to unpatterned cells plated on fibronectin. However, no differences in the nuclear area were measured using the patterns which varied the aspect ratio.

The patterns with varied aspect ratios display regions of greater F-actin staining at cell extremities, and resulted in oblong nuclear morphology orientated along the long axis of the cell. This reflects what has been shown for endothelial cells, whereby increased stretch increases the frequency and distribution of mature focal adhesions at the edge of the cell. In turn, the lateral compressive force of F-actin has been shown to elongate nuclear morphology. (139). The published study also reported a corresponding reduction in nuclear volume and increased chromatin compaction. The disparity may be due to increased plating time of cells as they were allowed to adhere for 24 hours rather than the 5 hours used in this study. Alternatively, the compared pattern sizes were much larger and not equally matched 1:1 500µm vs 1:5 1800µm; which is larger than small and medium custom patterns (300 µm and 600 µm) as evaluated during this study.

5.3.3.3 Transcription factor translocation

The nuclear occupancy of transcription factors is often used as a measure of pathway activation and cell morphology may account for heterogeneous responses observed between cells (134, 304, 325). Steady-state variability in both the intensity and duration of NF-κB nuclear occupancy have been observed in breast epithelial and tumour cells (150). Moreover, numerous mechano-sensitive and cytoskeleton-associated mechanisms have been reported to affect p65 nuclear translocation (142, 144, 150, 151). Subsequent differential p65 activation and resultant gene expression profiles have been reported in stretched compared to spherical cells following treatment with TNF-α (134, 153). Transcription factor localisation alone cannot predict functional outcomes such as transcriptional output, which depends on affinity for DNA, chromatin architecture (and accessibility of the target gene/regulatory region) and activity of co-modulators. However, a shift in compartmentalisation of any transcription factor increases the probability of transcriptional changes and was used as a preliminary measure of activity.

The GR and p65 localisation were successfully quantified by the N:C ratio and demonstrated the typical change from predominantly cytoplasmic to nuclear in response to activating stimuli. I compared both the effect of altered cell-geometry and the Dex-treatment and discovered differing transcription factor localisation between cell type, micropattern shape, aspect ratio and size.

Plating A549 cells on crossbow patterns increased the extent of the nuclear localisation of both GR and p65 in response to stimuli. This effect upon GR shuttling was significantly greater for cells plated on micropatterns in a size-dependent manner. This suggests cell morphology is positively affecting the rate of ligand-activated translocation dynamics in this particular geometric state. GR has been shown to regulate the expression of actin genes, the finding of greater GR nuclear occupancy in larger cells could be a mechanosensitive mechanism to fulfil the requirement to produce more actin protein (327). In contrast, Dex-induced GR translocation is reduced in cells with varied aspect ratios in comparison to unpatterned cells. The extent of Dex-induced GR translocation was reduced in comparison to the unpatterned substrate, across all levels of stretch for both small and medium size micropatterns.

J774 cells adopting the greatest levels of substrate-induced stretch were also found to display higher levels of GR nuclear occupancy. This effect was evident in vehicle and Dex treated cells for both pattern sizes. As vehicle-treated stretched cells display higher resting GR N:C ratios, in comparison to unpatterned cells, this may explain the lack of Dex-stimulated differences on small patterns. If cells with increasing aspect ratios have increased nuclear GR prior to Dex stimulation ligand induced changes will be less prominent.

In absence of activating inflammatory stimuli, p65 remained predominately cytoplasmic for all conditions. The resting p65 nuclear occupancy was somewhat increased between unpatterned and small crossbow patterned cells although, not to as great an extent of cells treated with TNF-α. Therefore, activating-stimuli remains the primary determinant of transcription factor localisation but geometry may however induce a degree of heterogenicity in cellular responsiveness.

Nuclear occupancy of p65 is highly indicative of transcriptional activation (126, 326). The p65:p50 complex is capable of binding DNA once released following the degradation of inhibitory protein IκBα. Therefore, increased p65 nuclear localisation would be expected to reflect positive regaultion of target genes thus a more pro-inflammatory phenotype. In the cases whereby GR nuclear entry is hindered by geometry, cells would be less able to elicit transcriptional effects to act against pro-inflammatory signals. The result would be more resistant cells which, in cases of un-resolving inflammation could underlie disease development.

Further investigation would be required to determine the functional state of GR whilst in the nucleus - whether nuclear GR remains in complex with chaperone proteins or is capable of eliciting transcriptional outcomes. Given current understanding of GR-biology it is unlikely that cell geometry would be sufficient to permit GR-transcriptional activity in absence of ligand. ChIP sequencing has shown that basal binding of GR to chromatin, in absence of activating ligand, occurs but is minimal (76) . Nevertheless, greater levels of liganded-GR protein in the nucleus may increase the responsiveness to ligands when present.

The effect of micropattern size was less evident for the TNFα-mediated increase in the p65 N:C ratio on crossbow patterns, in comparison to that seen for GR. However, stimulus-dependent translocation was greater in comparison to unpatterned cells and it appeared that Dex-treatment in the presence of TNF-α further increased the extent of p65 translocation. I also found that for cells with varied aspect ratios, Dex reduced the degree of nuclear p65 particularly on small patterns with less stretched morphology. These findings indicate potential geometry-dependent changes on p65 shuttling which may be affected by Dex. Whereas, in the case of macrophages, no geometry-induced changes upon p65 translocation dynamics were observed although this was only tested in absence of stimuli. In physiological contexts this potential cell-type specificity may be relevant. As epithelial cells are less likely to be subject to morphological changes under homeostatic conditions, they need to be responsive to pathologic changes. This is in contrast to macrophages, which require sensitive perception of microenvironment and any overactivation in response to minor cues could be detrimental and potentially lead to pathologic inflammation. Likewise, the implications of Dex-effect upon p65 translocation requires further investigation to understand the impact of geometry upon their interaction and functional outcome. The overall biological impact of cell geometry would be modulation of the responsiveness to activating ligands.

The nuclear translocation of the NF-κB (p50:p65) complex can occur by two distinct mechanisms. Firstly, nuclear translocation follows the stimulus-initiated degradation of the inhibitory molecule IκB. This reveals the NLS of NF-κB and enables p65 to bind to importins for active transport to the nucleus along microtubules, via dynein molecular motors. The second diffusion-mediated mechanism occurs independent of stimulus and is potentiated by dynactin disruption. Active transport to the nucleus and subsequent NFκB-dependent gene expression is sensitive to dynein inhibition whereas, passive shuttling is not affected and occurs whilst bound to IκB (326). Comparable to p65, the GR-ligand complex relies on the microtubule-cytoskeleton for transport into the nucleus and transition across the nuclear envelope by importins (33). Alternatively, GR can also enter by a diffusion-based mechanism when the cytoskeleton is disrupted (328). The overall cellular localisation of GR depends on the balance between the rates of nuclear import

and export signals. Ligand-induced activation, conformational change and NLS exposure is the predominant factor to skew GR towards nuclear localisation, however ligand-independent translocation has been reported in response to physiological conditions, albeit at slower rates. (31).

p65 is closely associated with the actin-cytoskeleton and can co-localise with actin filaments on stress fibres in membrane ruffles in cells adhered to fibronectin (329). A number of mechanisms have been proposed to underlie morphology-responsive changes in p65 nuclear shuttling. Namely those involving alternate modulators which lead to the degradation of IκB, allowing p65 to be actively transported into the nucleus. TNF-α can induce actin depolymerisation which degrades IκB. Chemical inhibition of actin polymerisation enhances the expression of the NF-κB target gene IL8 in response to inflammatory stimuli in HL-60 cells. Chemical cytoskeletal disruption increases p65 nuclear translocation, subsequent recruitment of RNA pol II to NF-κB promoters and stabilisation of IL8 mRNA post-transcription (152).

In contrast, GR activation and translocation is regulated by different mechanism requiring direct binding of ligand to the receptor rather than convergence of downstream phosphorylation signals. The principle chaperone molecule Hsp-90 interacts with many other proteins and shuttles with GR into the nucleus (29, 30, 32, 328). Therefore, GR may not be subject to the same geometry-regulated process as p65.

To date, no studies have investigated the effect of cellular geometry in controlling transcriptional Gc responses, including GR crosstalk with other transcription factors. To further expand on these observations, future work first needs to establish whether geometry-induced changes manifest as functional changes in cell behaviour and transcriptional output, as previously described for other studies. Subsequently, whether the greater occupancy of GR in the nucleus would effectively modulate p65 function, remains to be determined.

In order to fully understand the differing mechanisms behind the observed differences, the characterisation of other features need to be analysed such as the number and distribution of focal adhesions, quantification of stress fibre formation, markers of chromatin compaction and the localisation of other mechano-sensitive factors. Further investigation of transcription factor translocation dynamics in the presence of chemical cytoskeletal disruptors would also shed light upon Gc activity and understand GR's association with the cytoskeleton.

Further analysis should aim to understand what cellular factors may be responsible for geometry-responsive phenotypes including mechanosensitive transcription factors YAP and TAZ which respond to substrate stiffness and have higher nuclear occupancy in cells with anisotropic geometry, actin stress fibres and high nuclear tension (138). Dex treatment of trabecular

meshwork cells, increases YAP and TAZ expression which subsequently mediate Dex-associated cytoskeletal reorganisation and altered expression of ECM components, during glaucoma progression (330). The transcription factor MRTF-A is responsive to cytoplasmic ratios of F/G-actin corresponding to the extent of actin-polymerisation and localises to the nucleus in response to cell stretching and mechanicals stress. MRTF-A then couples with SRF to regulate expression of cytoskeletal components and immediate early genes (134). Recent evidence demonstrates that LPS induces MRTF-A nuclear accumulation to potentiate iNOS induction (331) and expression of pro-inflammatory cytokines, which is hindered by confined geometry to reduce the inflammatory responsiveness of macrophages (142). This implicates MRTF-A as another candidate worthy of investigation to aid the understanding of these results.

Overall, questions remain regarding whether cell geometry affects GR transcriptional cross-talk with these other mechanosensitive transcription factors or simply that the changes in cytoskeletal architecture affects the capacity of GR to translocate into the nucleus; this remains to be determined. Furthermore, given the rapid non-genomic effects of Gc upon a number of cytoskeletal components (as described in Chapter 3), defining what this effect is and how this may affect cell processes such as cell migration shall also shed light on GR functional activity.

5.3.4 Physiological relevance of Cell geometry

Within the same microenvironment, heterogeneity can exist between the same cells responding to the same chemical signals (134, 153, 332) and geometric differences in cell features may account for this disparity. Understanding this occurrence in normal physiology and how geometry is involved in the maintenance of cellular homeostasis and response to biochemical signals is an important consideration for further research.

This understanding can also be applied to how disease states may perturb cell geometry. For example, in contexts such as fibrosis and solid tumours, whereby the ECM composition is altered and tissue architecture is restructured. Investigation into how cells subsequently respond to the change in microenvironment and whether this transpires to alteration in tissue-level responsiveness to biochemical signals. Under normal physiological contexts, the modulation of GR and p65 transcription factor activity by geometry may provide a mechanism to fine-tune cellular sensitivity to Gc and inflammatory stimuli. This would have implications for the activation and phenotype of responsive cell types.

Normal epithelial architecture requires cell attachment to basement membrane and the establishment and maintenance of correct cell polarity. The lung epithelium displays apical-basolateral polarity which maintains the spatial organisation of cellular components and signalling pathways which is required for correct functioning and development (333). Under

normal conditions cells maintain geometry and mechanical homeostasis, as epithelial cell turnover is limited, the role of cellular geometry would be restricted in this context. Airway remodelling is a characteristic feature of airway diseases such as asthma and COPD which are both treated with Gc. Chronic inflammation combined with aberrant repair can lead to tissue remodelling and fibrosis. EMT occurs when a polarised epithelium differentiates into fibroblast type mesenchymal cells and requires disassembly of cell contacts and cells can acquire migratory activity (334). These processes result in major changes to cell phenotype, in addition aberrant ECM deposition which affects the spatial orientation of neighbouring cells. The effect of reduced GR nuclear translocation may reduce transcriptional programmes required for the therapeutic efficacy and could instil a resistant phenotype.

Loss of apical-basal polarity is a feature of epithelial cancers and can occur as an early event. Misorientation of the mitotic spindle results in symmetric and disorientated cell division leading to tissue disorganisation and overgrowth (335). GR has a crucial role in mitotic progression and localises to the mitotic spindle. Spindle defects occur with loss of GR resulting in chromosome misalignment (231) therefore, if GR nuclear translocation is compromised by geometry, this may result in further genomic instability.

Spatial heterogeneity is a common feature of solid tumours due to the modified internal environment which generates selective pressures upon cell survival. EMT is associated with metastatic progression, as cells acquire a migratory phenotype and invade surrounding tissue(334). In absence of TNF-α, breast cancer cells with a mesenchymal-like morphology have been shown to have higher nuclear NF-κB compared to cells with epithelial-like morphology. Suggesting the geometrical state can reinforce the induction of the EMT phenotype (150). Breast cancer responsiveness to Gc is highly variable between single cells resulting in variable genomic responses. Using scRNAseq, it was established that chromatin landscapes are heterogeneous across cell populations.(332) However, the tumour was dissociated prior to sequencing so spatial and geometric features are lost. Spatial transcriptomics and IHC approach would be one method of investigating this effect to determine whether the heterogeneity in chromatin architecture is affected by the spatial context of the tumour and is responsible for variability in Gc responsiveness.

Similarly, stromal fibroblasts become activated in response to TGF-β secreted from neighbouring cancer cells. Subpopulations of cells which are more responsive to TGF-β in a cancer spheroid co-culture system have been defined. These so-called "primed" cells differed based on their geometric features (140) which again demonstrates a role for cellular geometry for affecting how cells perceive and respond to microenvironmental signals.

Immune cells migrate as a result of forces generated by the re-organisation and cross talk between the actin and microtubule networks. Propulsive force from the actin cytoskeleton and generation of focal adhesions enables directional movement. Gc can inhibit cell motility and migration (186, 327) which is thought to underlie negative effects of Gc upon wound healing and immune cell recruitment. Leukocytes have low expression of lamin A/C (154, 336) which consequently makes their nucleus highly deformable to facilitate their passage into the tissues. The distortion of nuclear architecture occurs by differing mechanisms between immune cell types (154) (337). Although, the transient deformation of the nucleus during trans-epithelial migration is perhaps less-relevant for geometry-dependent modulation of macrophage phenotypes as the process is short lived. Nevertheless, altered geometry can downregulate lamin expression with effects upon epigenetic status and genome integrity (136). Natural deformability of the nucleus of immune cells making them more susceptible to this modulation in pathological contexts of un-resolving, chronic inflammation characterised by high cellular infiltrates. Likewise, pathological overexpression of Lamin A/C in macrophages is associated with pro-inflammatory behaviour (151) and further promotion of the transcription of pro-inflammatory factors would be detrimental.

This study has primarily focussed on single cell responses during initial model development. The next important stages would be to complement this by investigating the effect of geometry of in more physiologically relevant multi-cellular 3D models. Inclusion of different matrix components, and a cell co-culture system could be utilised to understand how biophysical signals can affect cell-fate, particularly in the contexts of inflammation and cancer.

5.3.5 Study Limitations

The study was severely limited by the nature of the experimental setup, which involved analysis at a single cell level which was hindered by limited by cell numbers. Ideally data would be generated regarding the transcription factor localisation for more shapes and treatment conditions. However, to achieve this in a reproducible manner requires a high throughput imaging system. Further to this, confocal rather than widefield microscopy would be superior to measure the volume of cell and nucleus rather than the area. This would also provide better spatial clarity within the Z-plane, to measure cytoskeletal features and the cellular location of and transcription factors.

Chapter 6: Discussion

6.1 Overview of Key findings

The aims of this thesis were to assess factors which modify the cellular response to Gc and consequent activity of the GR. I demonstrate that the signalling action of Gc induces both rapid and long-lasting cellular effects and that rapid non-genomic Gc-activity are important for subsequent genomic action. This indicates synergistic activity between the two mechanisms which had previously been considered to be independent from each other.

Global phosphoproteomics using three pharmacologically distinct GR ligands, reveals that the rapid activation of GR induces the phosphorylation of a spectrum of common protein targets. This was unexpected given the differences in translocation dynamics and transcriptional outputs between the investigated GR ligands and indicates that GR modulators rapidly induce a phosphorylation of common target proteins following GR activation. Gc were found to generally reduce the level of phosphorylation upon the identified protein targets. These shared, regulated phosphoproteins were located throughout the cell and were predicted to perform diverse functions including organisation of internal cellular components, cell-cycle regulation as well as roles in chromatin organisation and splicing. Identified targets included three adhesion GPCRs, which could potentially be responsible for relaying membrane initiated Gc-signals. This was supported by the identification of GPCR Kinase I and downstream effector kinases (MAPKs, PKA, PKC) as implicated regulating kinases via motif analysis. Although, the full functional response of GPR123, GPR126 and CD97 to Gc could not be validated, I explored methodologies which can be used to define the relevance of these receptors in Gc biology.

The differential regulation of a large set of nuclear proteins indicates that rapid signals initiated following GR-ligand engagement are required for subsequent genomic activity. Of these targets, transcriptional CDKs were identified with an association with the regulation of RNA polymerase II. This study is the first to implicate the action of CDK12-cyclin K and CDK13-cyclin K complexes in the transcription of Gc modulated genes, the combination of which, may have implications for the regulation of inflammatory and stress responsive pathways as previously demonstrated for CDK9 and GR-cofactor GRIP1 (69). I show that the phosphorylation status of RNA polymerase II is influenced by Dex, resulting in an acute signature suggestive of a favouring of transcription elongation. Furthermore, the expression of a subset Dex-regulated genes are affected by specific inhibition of CDK12 and CDK13 and appears to largely affect genes regulated by direct binding of GR to DNA rather than tethering through trans-repression.

Using transcriptomics, gene groups that are regulated by Dex and affected by CDK12 and CDK13 inhibition were defined. Subsequent promoter analysis of these gene sets facilitated the identification of a number of candidate transcription factors potentially involved in the expression pattern of the DEGs. The findings indicate a regulatory shift in GR cross-talk with other transcription factors, as a result of inhibition of CDK12 and CDK13 activity. For example, the FOXA1 binding is closely associated with genes upregulated by Dex and not affected by inhibition of CDK12 and CDK13. Whilst, for genes which are affected by inhibition, the association is shifted towards gene groups whose expression is downregulated by Dex with FOXA1 binding motifs found to be enriched within promoter regions of these gene groups. AP-1 factors were differentially expressed and implicated as regulatory factors for the affected gene groups, evident by differential expression of early response genes. The precise effect of CDK12 and CDK13 upon the cross-talk of transcriptional regulators and GR remains to be determined. Nevertheless, such altered actions have implications for the control of stress response, proliferation and differentiation programmes relevant to disease states.

Both phosphoproteomic and RNA sequencing approaches implicated GR in the regulation of cytoskeleton organisation and associated factors. I investigated the effect of cell geometry upon transcription factor localisation and stimulus-dependent shuttling to show that induced cell polarity A549 cells increases Dex-stimulated nuclear occupancy of GR. This effect was also observed for macrophages subject to increased stretch. This corroborates what has been shown in literature and shows that cellular geometric changes influence the underlying nuclear morphology and transcriptomic activity (134). These observations may be important for understanding heterogenic responses within cell populations, particularly in the context of cancer and inflammatory disease.

6.2 Knowledge gaps

This study provides new insight into the relatively uncharacterised field of rapid, non-genomic Gc signalling activity. The hypothesis-generating phosphoproteomic approach lead to the identification of a number of Gc-regulated phosphoproteins, however the precise functionality of Gc upon the protein's activity and downstream pathways remains to be determined. The presence of a phospho-residue does not necessarily equate to increased activation (or vice versa) and the presence of other modified sites on the protein may also influence functionality. A number of proteins which were differentially phosphorylated by Gc were also gene targets identified as being differentially expressed by Dex by RNA sequencing. One example would be the protein AHANK which also contained the greatest number of regulated phospho-motifs. This multi-level of regulation implicates a close functional relationship between rapid changes in

phosphorylation status and expression of Gc target proteins but the cellular functionality and consequences of many of these processes require further evaluation.

A number of questions remain regarding the proposed integration of genomic and non-genomic signalling, including how the two processes operate in concert and modulate cell behaviour. Additional key proteins of interest would be the factors involved in the regulation of the chromatin landscape. In order to answer whether the Gc-induced changes in phosphorylation rapidly results in remodelling of chromatin architecture it is possible to perform Assay for Transposase-Accessible Chromatin using sequencing (ATAC-seq) which identifies active loci, particularly cis-regulatory elements, based on regions of open chromatin. The accessibility of chromatin is known be altered following GR activation which directs the remodelling of chromatin via interactions with co-factors and chromatin remodelling proteins (59, 61, 68). A number of such proteins were identified as differentially phosphorylated in the phosphoproteomics demonstrating that Gc initiates the remodelling of chromatin within 10 minutes of ligand binding to GR. Epigenetic modifying enzymes and co-factors were identified as differentially phosphorylated including components of the SWI/SNF chromatin remodelling complex, which is known to assemble at GR-regulated promoters (338). This rapid Gc-induced modification may contribute to modify the chromatin architecture which imparts the context specificity of GR action (338).

This study also provides the first evidence that CDK12 and CDK13 are involved in the expression of specific subsets of GR-regulated genes. Although the precise mechanistic involvement in addition to how CDK12 and CDK13 become differentially phosphorylated by Dex remains to be determined. Initial investigation suggests that CDK12 and CDK13 are important for the activation (rather than trans-repression) of GR target genes bound by GR at GREs and corresponds to what had been demonstrated for CDK9 (69).

6.2.1 Future Work

To further progress these findings in this work, focus should be applied to the GR mechanism involving CDK12 and CDK13 genomic interaction. In addition to, deciphering the full relevance of the non-genomic signals and the apparent to feed-forward to the nucleus. The functional validation of the findings of key regulated gene targets from the RNA-seq could be performed by qPCR. Then, to generate a clearer view of GR and CDK12 and CDK13 genomic occupancy, ChIP-sequencing could be employed for samples treated in the presence of Dex, using THZ531, and with TNF-α to mimic inflammatory contexts and upregulation of genes to which GR-tethers to. This procedure would also validate predictions of interacting transcription factors generated using motif analysis.

As CDK12 and CDK13 have known active involvement in splicing activities (217), other high-throughput techniques such as ribosome profiling should be used to elucidate the role of GR and CDK12 and CDK13 on active translation and to identify alternatively spliced transcripts as a result of Dex treatment in the presence of CDK12and CDK13 inhibition.

Using temporal phophoproteomics, it would be interesting to perform a time-course analysis from ligand addition to GR- nuclear entry. This would build a clearer view of the dynamic signalling activity initiated following ligand addition (192). The potential successive identification of proteins would help to determine both the activated or repressed signalling pathways and their resultant cellular outcome. Parallel investigation using different ligands would also answer some unanswered questions including BSA-Dex to investigate signals initiated from the cell membrane and using GR-antagonist RU486 to explore the effect of a ligand which induces nuclear translocation and DNA binding but no transcriptional outputs.

A number of approaches could be used to validate the identified phosphotargets and their participation in non-genomic GR activity. These may include site-directed mutagenesis of target residues as well as knock-down and over-expression experiments. These would potentially require the generation of custom antibodies and knowledge of putative functions to measure resultant perturbations. Additional investigation into characterising the identified GPCRs and response to Gc would help to fully elucidate the implications of the receptors. In the short term, the TANGO assay could be developed with cells stably expressing each of the GPCR-constructs which would reduce the inter-experimental variability. This would also allow for the expansion to test a more diverse range of stimuli including specific GPER agonist (G-1) alongside the use of β-oestradiaol. A panel of steroidal ligands in addition to BSA-conjugated-Dex, to GR antagonist RU486 could also be tested in the presence or absence of inflammation. Further to this, the receptors could be tested upon different matrix components – given their designation as

adhesion GPCRs and reported interaction of GPR126 and CD97 with ECM. Such effects upon cell migration and proliferation could be analysed to understand potential pathogenic activity in cancers (239, 247). Once modulators of the GPCRs activity have been identified further work to delineate the downstream signalling activities and engaged pathways shall be easier to dissect. This should also be performed in more physiologically relevant cell type associated with target tissues known to express the receptors.

The data from the phosphoproteomics and RNA-sequencing of cells treated with Dex could be used to identify rapidly phosphorylated cytoskeletal proteins and differentially regulated genes associated with ontology terms such as cell-adhesion molecule binding. The localisation and activation status of these proteins could be assessed by immunofluorescent imaging of cells plated upon micropatterns. Further functional analysis by RNA-fluorescence *in situ* hybridisation (FiSH) could be used to look at gene expression changes at a single cell level.

6.3 Concluding remarks

Overall, the work presented in this thesis sheds light onto relatively uncharacterised aspects of Gc signalling; an understanding of which is crucial, both for the design of selective therapeutics to limit the occurrence of detrimental side-effects and for understanding how GR may contribute to the pathogenic progression of diseases such as cancer. These findings provide a foundation to develop a further understanding of Gc-biology *in vitro,* though the identification of targets for subsequent exploration and pave the way for future studies to apply this knowledge investigating potential clinical benefit.

6.4 Schematic Overview of Findings
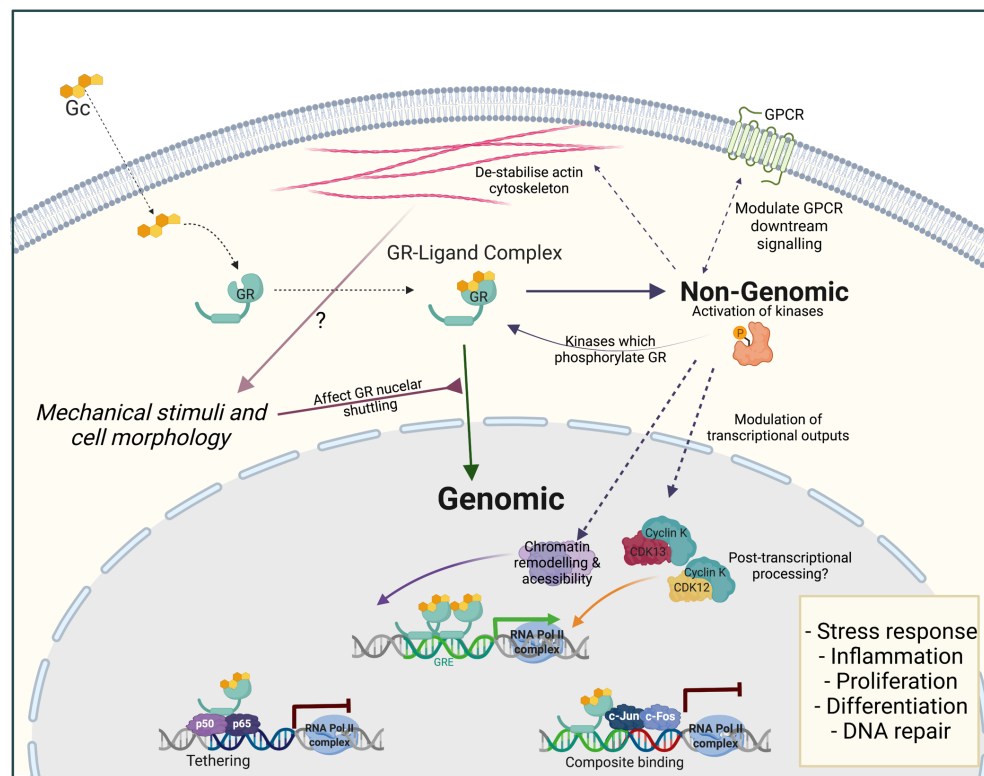
Figure 6.1 Investigated factors involved in mediating GR signalling

An overview of some of the factors investigated by this study, which influence the outcomes of Gc signalling. Within 10 minutes of Gc addition, a number of kinases are activated to mediate non-genomic cellular effects. However, this work shows that these processes feed-forward to affect the activity of nuclear proteins with implications on transcription.

Gc have an inhibitory effect upon the signalling pathways which are engaged downstream of GPCRs. It is yet unknown whether differential phosphorylation of GPR123, GPR126 and CD97 is due to Gc acting as a ligand for the receptors or GR-ligand complex associating at the membrane, most likely in-complex within lipid rafts, to modulate the magnitude of the relayed signals.

Gc also rapidly de-stabilise the actin cytoskeleton via cofilin-1 phosphorylation. In addition, mechanical stimuli and cell morphology are associated with changes in internal cytoskeleton structures which were shown to affect the translocation dynamics of both GR and p65. Further investigation to define whether these two mechanisms are connected and the effect on transcriptional outputs via direct and tethered binding.

Multiple identified kinases responsible for mediating non-genomic signalling are capable of phosphorylating GR protein. This could indicate a positive feedback mechanism to fine-tune specific GR responses.

Phosphorylation of nuclear proteins involved in chromatin remodelling indicates rapid changes genomic accessibility in preparation for GR binding and nuclear occupancy.

Gc rapidly induce measurable changes in the phosphorylation pattern of RNA Polymerase II concomitant to productive elongation. Changes in the phosphorylation signature of CDKs including CDK12, CDK13 and partner cyclin K are in part responsible for the regulation of subsets of GR target genes including transcription factors which are involved in GR-cross talk. Inhibition of CDK12 and CDK13 suggests that their activity modulates the composition of transcription factors co-operating / or opposing GR activity. Absence of pioneer transcription factors, altered combinations of binding partners, loss of tethered binding sites and differential activity of co-factor proteins or chromatin remodelling complexes, are all putative scenarios which may refine GR transcriptomic outputs.

GR-CDK12 / -CDK13 interactions may also affect post-transcriptional processing of mRNA transcripts as another level of regulation and requires further validation

Appendix

Table A. 1 List of identified Gc-regulated phosphoproteins

*Gene and protein names for all proteins differentially phosphorylated by Dexamethasone. *indicates proteins featured in schematic diagram (**Figure 3.5**). In the last three columns, a tick indicates the protein was detected as being differentially phosphorylated by the ligands GRT7 or 086X.*

	Gene	Protein names	Type	Dex	GRT7	086X
*	AAAS	Aladin	Nuclear pore complex	✓	✓	✓
*	AAK1	AP2-associated protein kinase 1	SNF1 family Kinase (ser/thr)	✓	✓	✓
*	AATF	Protein AATF	Transcription factor	✓	✓	✓
*	ABCF1	ATP-binding cassette sub-family F member 1	Transporter GCN20 subfamily	✓	✓	✓
*	ABI1	Abl interactor 1	Adapter	✓	✓	✓
*	ABLIM1	Actin-binding LIM protein 1	Adapter/ LIM protein family	✓	✓	✓
*	ACACA	Acetyl-CoA carboxylase 1;Biotin carboxylase	Enzyme	✓	✓	✓
*	ACIN1	Apoptotic chromatin condensation inducer in the nucleus	Adapter	✓	✓	✓
*	ACLY	ATP-citrate synthase	Enzyme	✓	✓	✓
*	ADAM9	Disintegrin and metalloproteinase domain-containing protein 9	Disintegrin/Metalloprotease	✓	✓	
*	ADD1	Alpha-adducin	Adapter	✓	✓	✓
*	ADD3	Gamma-adducin	Adapter	✓		✓
*	ADD2	Beta-adducin	Adapter	✓	✓	✓
*	ADGB	Androglobin	Adapter	✓	✓	✓
*	ADNP	Activity-dependent neuroprotector homeobox protein	Transcription factor	✓		✓
*	AEBP2	Zinc finger protein AEBP2	Transcriptional repressor	✓	✓	✓
*	AFAP1	Actin filament-associated protein 1	Adapter	✓	✓	
*	AFF4	AF4/FMR2 family member 4	SEC complex	✓	✓	✓
	AGFG1	Arf-GAP domain and FG repeat-containing protein 1	RNA binding	✓	✓	✓
*	AGGF1	Angiogenic factor with G patch and FHA domains 1		✓	✓	✓
*	AHNAK	Neuroblast differentiation-associated protein AHNAK	Adapter	✓	✓	✓
*	AHNAK2	Protein AHNAK2	Adapter	✓	✓	✓
*	AKAP1	A-kinase anchor protein 1, mitochondrial	Adapter	✓		
*	AKAP12	A-kinase anchor protein 12	Adapter	✓	✓	
*	AKAP13	A-kinase anchor protein 13	Adapter	✓	✓	✓
*	AKAP2	A-kinase anchor protein 2	Adapter	✓	✓	✓
*	AKT1S1	Proline-rich AKT1 substrate 1	TORC complex	✓	✓	✓
*	ALKBH5	RNA demethylase ALKBH5	RNA demethylase	✓		✓
*	ANK2	Ankyrin-2	Adapter	✓	✓	✓
*	ANKHD1	Ankyrin repeat and KH domain-containing protein 1		✓	✓	
*	ANKRD17	Ankyrin repeat domain-containing protein 17		✓	✓	✓
*	ANKRD34C	Ankyrin repeat domain-containing protein 34C		✓	✓	
*	ANLN	Actin-binding protein anillin		✓	✓	✓
*	ANX2L2	Putative annexin A2-like protein		✓	✓	
*	ANXA2	Annexin A2		✓	✓	
*	AP1M1	Adaptor-Related Protein complex 1, subunit mu 1	AP-1 complex	✓	✓	✓
*	AP2B1	Adaptor-Related Protein complex 1, complex subunit beta 1	AP2 complex	✓	✓	✓
*	API5	Apoptosis inhibitor 5		✓		✓
*	ARFGEF2	Brefeldin A-inhibited guanine nucleotide-exchange protein 2		✓	✓	✓
*	ARGLU1	Arginine and glutamate-rich protein 1	MED1 complex	✓	✓	✓
*	ARHGEF11	Rho guanine nucleotide exchange factor 11		✓	✓	✓
*	ARHGEF6	Rho guanine nucleotide exchange factor 6		✓	✓	✓
*	ARHGEF7	Rho guanine nucleotide exchange factor 7		✓	✓	✓
*	ARID1A	AT-rich interactive domain-containing protein 1A	Helicase, SWI/SNF family	✓	✓	✓
*	ARID3A	AT-rich interactive domain-containing protein 3A	Transcription factor	✓	✓	✓
*	ARID4B	AT-rich interactive domain-containing protein 4B		✓	✓	✓
*	ARL6IP4	ADP-ribosylation factor-like protein 6-interacting protein 4		✓	✓	✓
*	ASAP1	Arf-GAP with SH3 domain, ANK repeat and PH domain-containing protein 1		✓	✓	✓
*	ASH2L	Set1/Ash2 histone methyltransferase complex subunit ASH2	Methyltransferase	✓	✓	✓
*	ATF7	Cyclic AMP-dependent transcription factor ATF-7	Transcription factor	✓	✓	✓
*	ATN1	Atrophin-1	Transcriptional repressor	✓	✓	
*	ATP2A2	Sarcoplasmic/endoplasmic reticulum calcium ATPase 2	ATPase	✓	✓	✓
*	ATP2B1	Plasma membrane calcium-transporting ATPase 1	ATPase	✓	✓	✓
*	ATP7A	Copper-transporting ATPase 1	ATPase	✓	✓	✓
*	ATRX	Transcriptional regulator ATRX	Helicase, SWI/SNF family	✓	✓	✓
	ATXN2L	Ataxin-2-like protein		✓	✓	
	B4GALT1	Beta-1,4-galactosyltransferase 1	Enzyme	✓	✓	
*	BABAM1	BRISC and BRCA1-A complex member 1		✓	✓	✓
	BAG3	BAG family molecular chaperone regulator 3		✓	✓	✓
	BAG6	Large proline-rich protein BAG6		✓	✓	✓
	BAIAP2L1	Brain-specific angiogenesis inhibitor 1-associated protein 2-like protein 1	Adapter	✓	✓	✓
	BAP18	Chromatin complexes subunit BAP18		✓	✓	✓
	BASP1	Brain acid soluble protein 1		✓	✓	✓
	BAZ2A	Bromodomain adjacent to zinc finger domain protein 2A		✓	✓	
	BCL7B	B-cell CLL/lymphoma 7 protein family member B		✓	✓	
	BCL7C	B-cell CLL/lymphoma 7 protein family member C		✓		✓
*	BCL9L	B-cell CLL/lymphoma 9-like protein	Transcriptional activator	✓	✓	✓
*	BCLAF1	Bcl-2-associated transcription factor 1	Transcription factor	✓	✓	✓
	BICC1	Protein bicaudal C homolog 1		✓	✓	

	Gene	Protein	Class			
	BICD2	Protein bicaudal D homolog 2		✓	✓	
	BLOC1S3	Biogenesis of lysosome-related organelles complex 1 subunit 3		✓	✓	✓
	BMS1	Ribosome biogenesis protein BMS1 homolog		✓	✓	
	BOD1L1	Biorientation of chromosomes in cell division protein 1-like 1		✓	✓	✓
*	BRD2	Bromodomain-containing protein 2	Kinase, BET family	✓	✓	✓
*	BRD3	Bromodomain-containing protein 3	Kinase, BET family	✓	✓	✓
*	BRWD3	Bromodomain and WD repeat-containing protein 3	Chromatin modifier	✓	✓	✓
	BUD13	BUD13 homolog		✓	✓	✓
	BYSL	Bystin		✓	✓	✓
	C11orf84	Uncharacterized protein C11orf84		✓	✓	✓
	C12orf43	Uncharacterized protein C12orf43		✓	✓	
	C2CD5	C2 domain-containing protein 5		✓	✓	✓
	C2orf49	Ashwin		✓	✓	✓
	C7orf50	Uncharacterized protein C7orf50		✓	✓	✓
	CAAP1	Caspase activity and apoptosis inhibitor 1		✓	✓	✓
*	CANX	Calnexin	Chaperone	✓	✓	✓
*	CAP1	Adenylyl cyclase-associated protein 1	Adapter	✓	✓	✓
*	CARHSP1	Calcium-regulated heat stable protein 1	Adapter	✓	✓	✓
	CASC3	Protein CASC3	Adapter	✓		✓
*	CAV1	Caveolin-1	Adapter	✓		✓
	CBY3	Protein chibby homolog 3		✓	✓	✓
	CCAR2	Cell cycle and apoptosis regulator protein 2	Adapter	✓	✓	✓
	CCDC61	Coiled-coil domain-containing protein 61		✓	✓	✓
	CCDC86	Coiled-coil domain-containing protein 86	Adapter	✓	✓	✓
	CCM2	Cerebral cavernous malformations 2 protein	Adapter	✓	✓	✓
*	CCNK	Cyclin-K	Cyclin	✓	✓	✓
*	CCNL1	Cyclin-L1	Cyclin	✓	✓	✓
*	CCNY	Cyclin-Y	Cyclin	✓	✓	✓
	CCNYL1	Cyclin-Y-like protein 1	Cyclin	✓	✓	✓
	CD2BP2	CD2 antigen cytoplasmic tail-binding protein 2	Adapter	✓	✓	✓
*	CD97	CD97 antigen	GPCR	✓		✓
*	CDC23	Cell division cycle protein 23 homolog	E3-ligase	✓	✓	✓
*	CDC42EP4	Cdc42 effector protein 4	Adapter	✓	✓	✓
*	CDC5L	Cell division cycle 5-like protein	DNA binding	✓	✓	✓
*	CDK1	Cyclin-dependent kinase 1	Kinase	✓	✓	✓
*	CDK2	Cyclin-dependent kinase 2	Kinase	✓	✓	✓
*	CDK3	Cyclin-dependent kinase 3	Kinase	✓	✓	✓
*	CDK11B	Cyclin-dependent kinase 11B	Kinase	✓	✓	✓
*	CDK12	Cyclin-dependent kinase 12	Kinase	✓	✓	✓
*	CDK13	Cyclin-dependent kinase 13	Kinase	✓	✓	✓
*	CDS2	Phosphatidate cytidylyltransferase 2	Enzyme	✓	✓	
*	CENPB	Major centromere autoantigen B	Adapter	✓	✓	✓
*	CENPC	Centromere protein C	Adapter	✓	✓	✓
*	CEP170	Centrosomal protein of 170 kDa	Adapter	✓	✓	✓
*	CFL1	Cofilin-1	Adapter	✓	✓	✓
*	CGN	Cingulin	Adapter	✓	✓	✓
*	CHAF1B	Chromatin assembly factor 1 subunit B	Adapter	✓	✓	✓
*	CHAMP1	Chromosome alignment-maintaining phosphoprotein 1	Adapter	✓	✓	✓
*	CHD3	Chromodomain-helicase-DNA-binding protein 3	Helicase	✓	✓	✓
*	CHD8	Chromodomain-helicase-DNA-binding protein 8	Helicase	✓		✓
*	CHD9	Chromodomain-helicase-DNA-binding protein 9	Helicase	✓	✓	✓
*	CHERP	Calcium homeostasis endoplasmic reticulum protein	Adapter	✓	✓	✓
*	CHMP2B	Charged multivesicular body protein 2b	Adapter	✓	✓	✓
*	CIC	Protein capicua homolog	Corepressor	✓	✓	✓
*	CIR1	Corepressor interacting with RBPJ 1	Corepressor	✓	✓	
*	CLASP1	CLIP-associating protein 1	Adapter	✓	✓	✓
*	CLIP1	CAP-Gly domain-containing linker protein 1	Adapter	✓	✓	✓
	CLN3	Battenin	SLC transporters	✓		✓
*	CNNM4	Metal transporter CNNM4	Transporter	✓	✓	✓
*	CNOT2	CCR4-NOT transcription complex subunit 2	Adapter	✓	✓	✓
	COIL	Coilin	Adapter	✓		✓
*	COPB2	Coatomer subunit beta'	Adapter	✓		✓
	CPD	Carboxypeptidase D	Enzyme	✓	✓	
*	CPSF7	Cleavage and polyadenylation specificity factor subunit 7	Adapter	✓		✓
*	CSTF3	Cleavage stimulation factor subunit 3	Adapter	✓	✓	
*	CTAGE5	cTAGE family member 5	Adapter	✓	✓	
*	CYB5B	Cytochrome b5 type B	Electron carrier	✓	✓	✓
*	EIF4EBP1	Eukaryotic translation initiation factor 4E-binding protein 1	Translation repressor	✓	✓	✓
*	EIF4ENIF1	Eukaryotic translation initiation factor 4E transporter	Adapter	✓	✓	
*	GPR123	Probable G-protein coupled receptor 123	GPCR	✓	✓	✓
*	GPR126	G-protein coupled receptor 126	GPCR	✓	✓	✓
*	HSPD1	60 kDa heat shock protein, mitochondrial	Chaperone	✓	✓	✓
*	LRRC16A	Leucine-rich repeat-containing protein 16A	Adapter	✓		✓
*	MLLT10	Protein AF-10	Transcription factor	✓	✓	

*	MLLT4	Afadin, Adherens junction Formation factor	Adapter	✓	✓	✓
*	NCAPH2	Condensin-2 complex subunit H2		✓		✓
*	PRKCDBP	Protein kinase C delta-binding protein	Adapter	✓	✓	✓
*	PTRF	Polymerase I and transcript release factor	Adapter	✓		✓
*	RNF20	E3 ubiquitin-protein ligase BRE1A	E3-ligase	✓	✓	✓
*	SDPR	Serum deprivation-response protein	Adapter	✓	✓	✓
*	SLC1A5	Neutral amino acid transporter B(0)	Transporter	✓	✓	✓
*	STUB1	E3 ubiquitin-protein ligase CHIP	Adapter	✓	✓	✓
*	TRIP10	Cdc42-interacting protein 4	Adapter	✓	✓	✓
	ZFYVE19	Abscission/NoCut checkpoint regulator	Adapter	✓	✓	✓
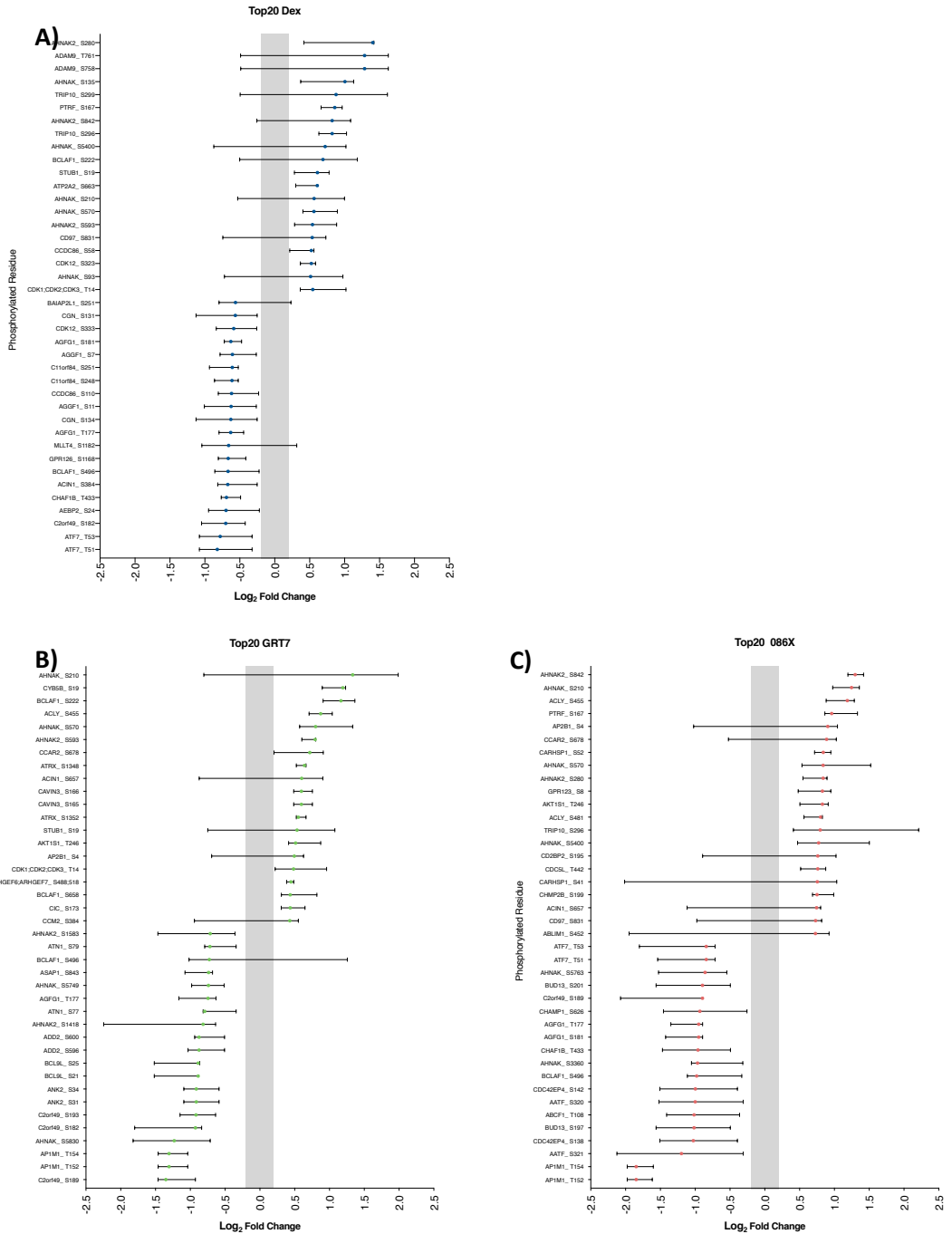
Figure A.1 Top 20 differentially regulated phospho-residues by GR ligand.

The top 20 up- and down regulated phosphorylated residues, in comparison to the vehicle control. Induced by **A)** Dexamethasone, **B)** GRT7 and **C)** 086X. The median fold change plotted and 95% confidence for a minimum of 3 measurements.

Table A.2 Differential phosphorylation of AHNAK and AHNAK2 by Gc ligands and the predicted regulating kinases

The differentially phosphorylated residues for AHNAK **(A)** *and AHNAK2* **(B)** *and predicted phosphorylating kinase. Generated using NetworKIN using 1.5 as minimum score cut off. Numbers correspond to the score of the kinase for that residue.*

A)

AHNAK	Ser135	Ser177	Ser210	Ser216	Ser511	Ser5110	Ser5400	Ser5762	Ser5782	Ser5790	Thr5794
CaMKIIα	1.90		1.90								
MCPH1		1.58			1.58	1.58	1.58				
BRCA1		1.58			1.58	1.58	1.58				
PTIP					1.58	1.58	1.58				
MDC1					1.58	1.58	1.58				
BARD1					1.58	1.58	1.58				
14-3-3 family (αβΘHζεY)	1.66							1.66	1.66	1.66	
MAPK3 (ERK1)				1.76							1.76
MAPK1 (ERK2)				1.90							1.90
PKCβ							2.49				
PKCα							1.63		9.33	5.70	

B)

AHNAK 2	Ser280	Ser765	Ser842	Ser1418	Ser1563	Ser4477
CaMKIIα	1.70				1.79	
MCPH1			1.58	1.58		
BRCA1			1.58	1.58		
PTIP			1.58	1.58		
MDC1			1.58	1.58		
BARD1			1.58	1.58		
14-3-3 family (αβΘHζεY)	1.66					
MAPK3 (ERK1)						1.76
MAPK1 (ERK2)						1.66
PKCβ		2.50	2.50	2.50	2.50	
PKCα		3.05		3.05	3.05	
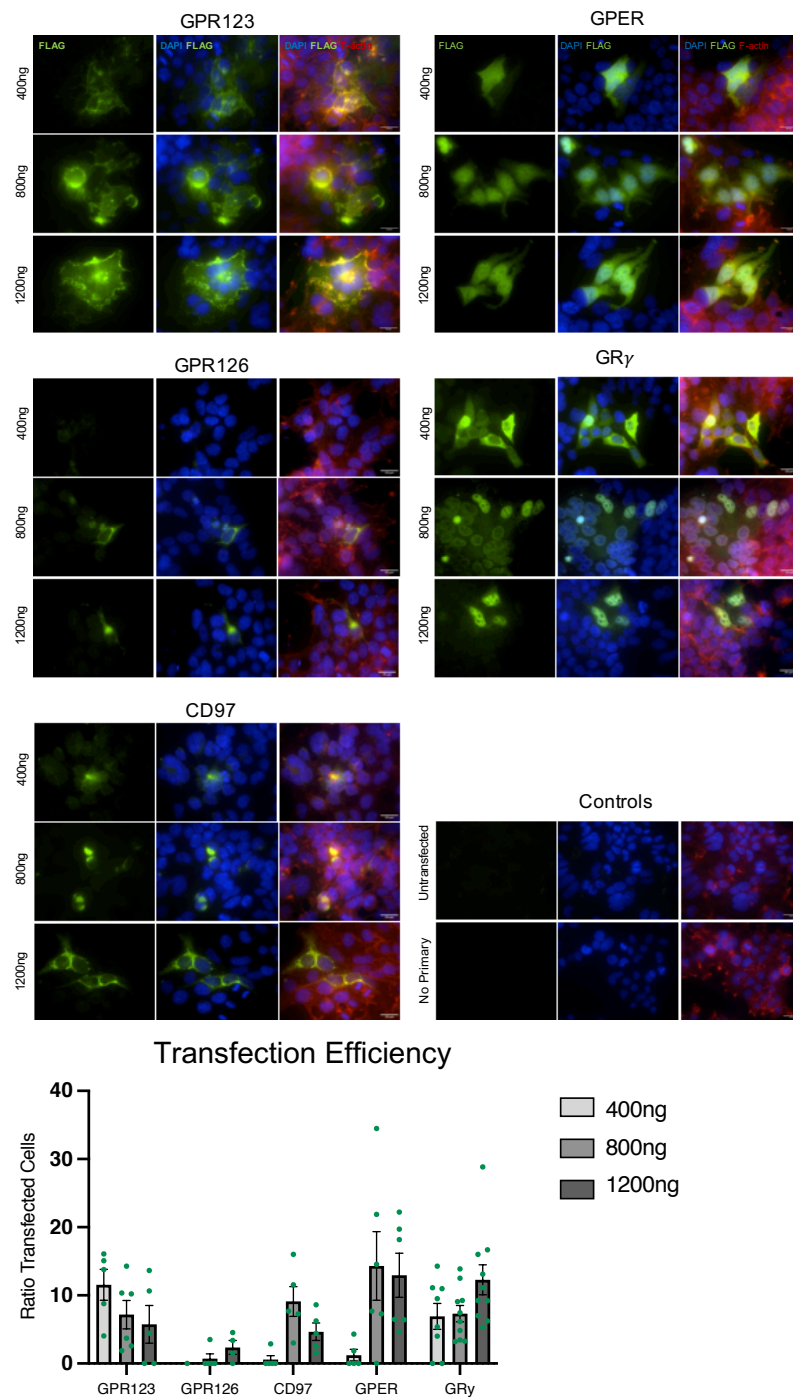
Figure A.2. G-protein coupled receptor transfection efficiency.

HTLA HEK293 cells were transfected with plasmids containing GPR123, GPR126, CD97, GPER or GRγ using fugene 6 reagent and with 3 different concentrations of pDNA to determine the best efficiency. Cells were transfected for 48 hours then media changed. Cells were fixed on day 4 (post transfection), permeabilised and stained to detect expression of the expressed protein using an anti-FLAG antibody (green), F-actin (red) and counterstained with Hoechst 33342 (blue) Images were obtained on widefield microscope using x60 objective. Representative images are shown for each concentration of transfected pDNA on Day 5. Scale bar :20µm Images were processed using image J using a macro to quantify the number of positively transfected cells taken as a proportion of the total number of cells per field of view.
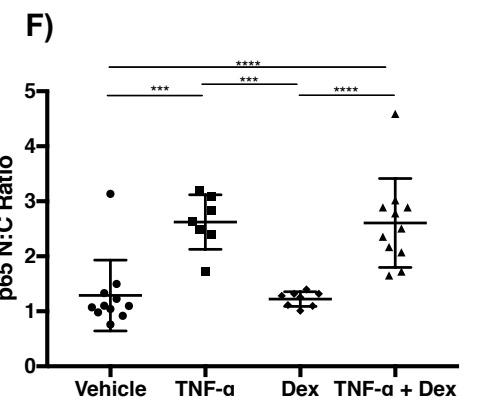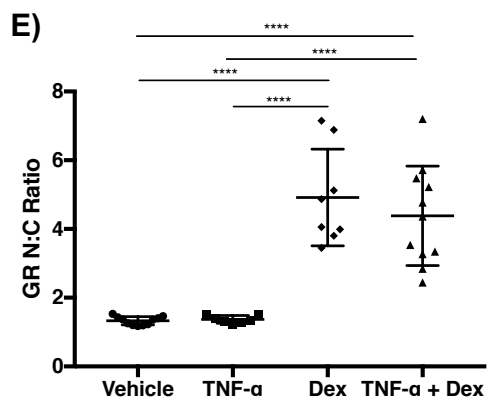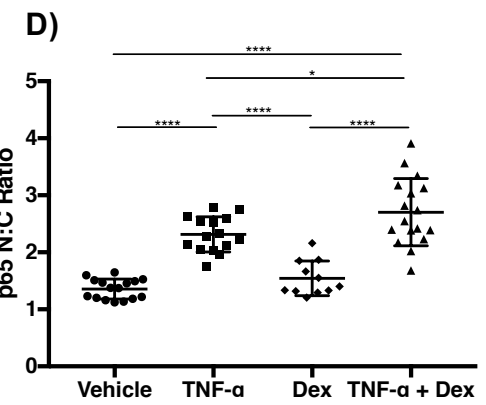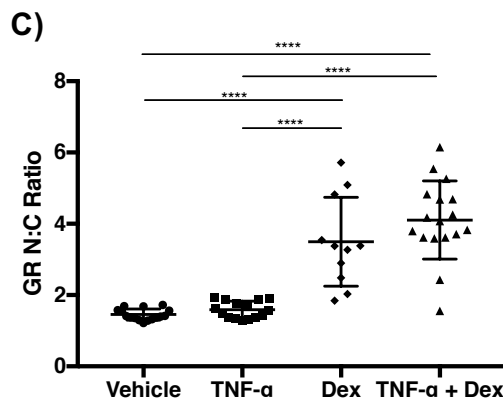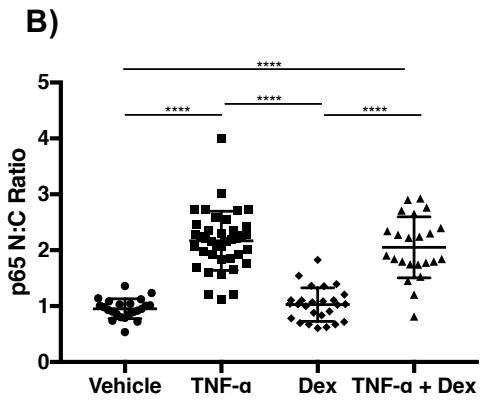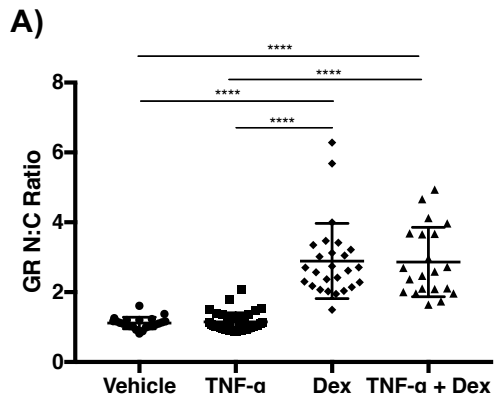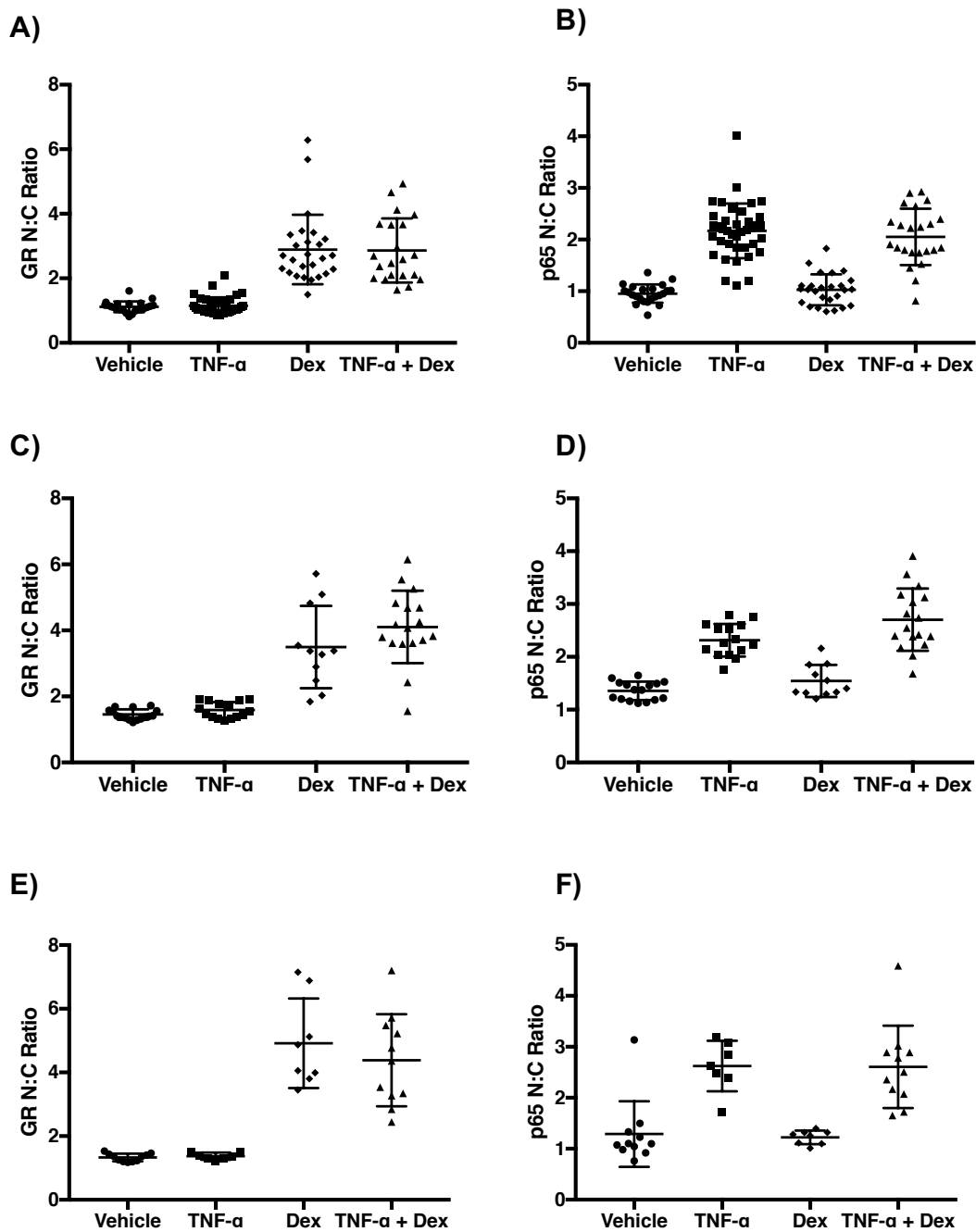
Figure A.3 Comparison of the N:C ratio between treatment types for A549 cells on crossbow micropatterns

A549 cells plated onto starter A micropatterns and treated with vehicle, 10ng/ml TNF-α for 3 hours and 100nM Dex for 1 hour. Cells were fixed permeabilised and stained for GR, p65 and counterstained with Hoechst 33342 33342. Quantification of protein localization of GR (A,C,E) and p65 (B,D,F) seeded on to unpatterned fibronectin-coated surface (A&B), small (C&D) or medium (E&F) size crossbow micropattern. Quantification using Cell Profiler software and the peri-nuclear measurements pipeline, presented as the nuclear: cytoplasmic ratio measured pixel intensity per cell with mean and standard deviation. Each point represents a single cell.

References

1.   Ramamoorthy S, Cidlowski JA. Corticosteroids: Mechanisms of Action in Health and Disease. Rheumatic diseases clinics of North America. 2016;42(1):15-31, vii.
2.   Kadmiel M, Cidlowski JA. Glucocorticoid receptor signaling in health and disease. Trends in Pharmacological Sciences. 2013;34(9):518-30.
3.   Murphy KE, Hannah ME, Willan AR, Hewson SA, Ohlsson A, Kelly EN, et al. Multiple courses of antenatal corticosteroids for preterm birth (MACS): a randomised controlled trial. The Lancet. 2008;372(9656):2143-51.
4.   Rose AJ, Vegiopoulos A, Herzig S. Role of glucocorticoids and the glucocorticoid receptor in metabolism: insights from genetic manipulations. The Journal of steroid biochemistry and molecular biology. 2010;122(1-3):10-20.
5.   Cain DW, Cidlowski JA. Immune regulation by glucocorticoids. Nature reviews Immunology. 2017;17(4):233-47.
6.   van Staa TP, Leufkens HGM, Abenhaim L, Begaud B, Zhang B, Cooper C. Use of oral corticosteroids in the United Kingdom. QJM: An International Journal of Medicine. 2000;93(2):105-11.
7.   Fardet L, Petersen I, Nazareth I. Prevalence of long-term oral glucocorticoid prescriptions in the UK over the past 20 years. Rheumatology. 2011;50(11):1982-90.
8.   Vandewalle J, Luypaert A, De Bosscher K, Libert C. Therapeutic Mechanisms of Glucocorticoids. Trends in Endocrinology & Metabolism. 2018;29(1):42-54.
9.   Rhen T, Cidlowski JA. Antiinflammatory action of glucocorticoids--new mechanisms for old drugs. The New England journal of medicine. 2005;353(16):1711-23.
10.   Du J, Li M, Zhang D, Zhu X, Zhang W, Gu W, et al. Flow cytometry analysis of glucocorticoid receptor expression and binding in steroid-sensitive and steroid-resistant patients with systemic lupus erythematosus. Arthritis Research & Therapy. 2009;11(4):R108.
11.   Lauten M, Cario G, Asgedom G, Welte K, Schrappe M. Protein expression of the glucocorticoid receptor in childhood acute lymphoblastic leukemia. Haematologica. 2003;88(11):1253-8.
12.   Irusen E, Matthews JG, Takahashi A, Barnes PJ, Chung KF, Adcock IM. p38 Mitogen-activated protein kinase-induced glucocorticoid receptor phosphorylation reduces its activity: role in steroid-insensitive asthma. The Journal of allergy and clinical immunology. 2002;109(4):649-57.
13.   Kobayashi Y, Mercado N, Barnes PJ, Ito K. Defects of Protein Phosphatase 2A Causes Corticosteroid Insensitivity in Severe Asthma. PLoS ONE. 2011;6(12):e27627.
14.   Habib T, Sadoun A, Nader N, Suzuki S, Liu W, Jithesh PV, et al. AKT1 has dual actions on the glucocorticoid receptor by cooperating with 14-3-3. Molecular and cellular endocrinology. 2017;439:431-43.
15.   Vukelic S, Stojadinovic O, Pastar I, Rabach M, Krzyzanowska A, Lebrun E, et al. Cortisol synthesis in epidermis is induced by IL-1 and tissue injury. The Journal of biological chemistry. 2011;286(12):10265-75.
16.   Talabér G, Jondal M, Okret S. Extra-adrenal glucocorticoid synthesis: Immune regulation and aspects on local organ homeostasis. Molecular and cellular endocrinology. 2013;380(1):89-98.
17.   Cameron A, Henley D, Carrell R, Zhou A, Clarke A, Lightman S. Temperature-responsive release of cortisol from its binding globulin: a protein thermocouple. The Journal of clinical endocrinology and metabolism. 2010;95(10):4689-95.
18.   Cain DW, Cidlowski JA. Specificity and sensitivity of glucocorticoid signaling in health and disease. Best Practice & Research Clinical Endocrinology & Metabolism. 2015;29(4):545-56.
19.   Chapman K, Holmes M, Seckl J. 11β-hydroxysteroid dehydrogenases: intracellular gate-keepers of tissue glucocorticoid action. Physiol Rev. 2013;93(3):1139-206.

20.   Gilmour JS, Coutinho AE, Cailhier JF, Man TY, Clay M, Thomas G, et al. Local amplification of glucocorticoids by 11 beta-hydroxysteroid dehydrogenase type 1 promotes macrophage phagocytosis of apoptotic leukocytes. Journal of immunology (Baltimore, Md : 1950). 2006;176(12):7605-11.

21.   Diederich S, Eigendorff E, Burkhardt P, Quinkler M, Bumke-Vogt C, Rochel M, et al. 11beta-hydroxysteroid dehydrogenase types 1 and 2: an important pharmacokinetic determinant for the activity of synthetic mineralo- and glucocorticoids. The Journal of clinical endocrinology and metabolism. 2002;87(12):5695-701.

22.   Hunzeker JT, Elftman MD, Mellinger JC, Princiotta MF, Bonneau RH, Truckenmiller ME, et al. A Marked Reduction in Priming of Cytotoxic CD8(+) T Cells Mediated by Stress-Induced Glucocorticoids Involves Multiple Deficiencies in Cross-Presentation by Dendritic Cells. Journal of immunology (Baltimore, Md : 1950). 2011;186(1):183-94.

23.   Dahlman-Wright K, Wright A, Gustafsson JA, Carlstedt-Duke J. Interaction of the glucocorticoid receptor DNA-binding domain with DNA as a dimer is mediated by a short segment of five amino acids. The Journal of biological chemistry. 1991;266(5):3107-12.

24.   Hache RJ, Tse R, Reich T, Savory JG, Lefebvre YA. Nucleocytoplasmic trafficking of steroid-free glucocorticoid receptor. The Journal of biological chemistry. 1999;274(3):1432-9.

25.   Lu NZ, Cidlowski JA. Translational Regulatory Mechanisms Generate N-Terminal Glucocorticoid Receptor Isoforms with Unique Transcriptional Target Genes. Molecular Cell. 2005;18(3):331-42.

26.   Morgan DJ, Poolman TM, Williamson AJK, Wang Z, Clark NR, Ma'ayan A, et al. Glucocorticoid receptor isoforms direct distinct mitochondrial programs to regulate ATP production. Scientific Reports. 2016;6(1):26419.

27.   Quax RA, Manenschijn L, Koper JW, Hazes JM, Lamberts SW, van Rossum EF, et al. Glucocorticoid sensitivity in health and disease. Nature reviews Endocrinology. 2013;9(11):670-86.

28.   Ito K, Chung KF, Adcock IM. Update on glucocorticoid action and resistance. Journal of Allergy and Clinical Immunology. 2006;117(3):522-43.

29.   Echeverria PC, Picard D. Molecular chaperones, essential partners of steroid hormone receptors for activity and mobility. Biochimica et Biophysica Acta (BBA) - Molecular Cell Research. 2010;1803(6):641-9.

30.   Echeverria PC, Mazaira G, Erlejman A, Gomez-Sanchez C, Piwien Pilipuk G, Galigniana MD. Nuclear import of the glucocorticoid receptor-hsp90 complex through the nuclear pore complex is mediated by its interaction with Nup62 and importin beta. Mol Cell Biol. 2009;29(17):4788-97.

31.   Vandevyver S, Dejager L, Libert C. On the trail of the glucocorticoid receptor: into the nucleus and back. Traffic (Copenhagen, Denmark). 2012;13(3):364-74.

32.   Ebong I-o, Beilsten-Edmands V, Patel NA, Morgner N, Robinson CV. The interchange of immunophilins leads to parallel pathways and different intermediates in the assembly of Hsp90 glucocorticoid receptor complexes. Cell Discovery. 2016;2:16002.

33.   Galigniana MD, Radanyi C, Renoir J-M, Housley PR, Pratt WB. Evidence That the Peptidylprolyl Isomerase Domain of the hsp90-binding Immunophilin FKBP52 Is Involved in Both Dynein Interaction and Glucocorticoid Receptor Movement to the Nucleus. Journal of Biological Chemistry. 2001;276(18):14884-9.

34.   Matthews JG, Ito K, Barnes PJ, Adcock IM. Defective glucocorticoid receptor nuclear translocation and altered histone acetylation patterns in glucocorticoid-resistant patients. The Journal of allergy and clinical immunology. 2004;113(6):1100-8.

35.   Khan SH, McLaughlin WA, Kumar R. Site-specific phosphorylation regulates the structure and function of an intrinsically disordered domain of the glucocorticoid receptor. Scientific Reports. 2017;7(1):15440.

36.   Galliher-Beckley AJ, Cidlowski JA. Emerging roles of glucocorticoid receptor phosphorylation in modulating glucocorticoid hormone action in health and disease. IUBMB Life. 2009;61(10):979-86.

37.   Kino T. GR-regulating Serine/Threonine Kinases: New Physiologic and Pathologic Implications. Trends in Endocrinology & Metabolism. 2018;29(4):260-70.

38.   Wang Z, Frederick J, Garabedian MJ. Deciphering the phosphorylation "code" of the glucocorticoid receptor in vivo. The Journal of biological chemistry. 2002;277(29):26573-80.

39.   Blind RD, Garabedian MJ. Differential recruitment of glucocorticoid receptor phospho-isoforms to glucocorticoid-induced genes. The Journal of steroid biochemistry and molecular biology. 2008;109(1-2):150-7.

40.   Miller AL, Webb MS, Copik AJ, Wang Y, Johnson BH, Kumar R, et al. p38 Mitogen-Activated Protein Kinase (MAPK) Is a Key Mediator in Glucocorticoid-Induced Apoptosis of Lymphoid Cells: Correlation between p38 MAPK Activation and Site-Specific Phosphorylation of the Human Glucocorticoid Receptor at Serine 211. Molecular Endocrinology. 2005;19(6):1569-83.

41.   Nader N, Ng SSM, Lambrou GI, Pervanidou P, Wang Y, Chrousos GP, et al. AMPK Regulates Metabolic Actions of Glucocorticoids by Phosphorylating the Glucocorticoid Receptor through p38 MAPK. Molecular Endocrinology. 2010;24(9):1748-64.

42.   Itoh M, Adachi M, Yasui H, Takekawa M, Tanaka H, Imai K. Nuclear Export of Glucocorticoid Receptor is Enhanced by c-Jun N-Terminal Kinase-Mediated Phosphorylation. Molecular Endocrinology. 2002;16(10):2382-92.

43.   Galliher-Beckley AJ, Williams JG, Collins JB, Cidlowski JA. Glycogen synthase kinase 3beta-mediated serine phosphorylation of the human glucocorticoid receptor redirects gene expression profiles. Mol Cell Biol. 2008;28(24):7309-22.

44.   Galliher-Beckley AJ, Williams JG, Cidlowski JA. Ligand-independent phosphorylation of the glucocorticoid receptor integrates cellular stress pathways with nuclear receptor signaling. Mol Cell Biol. 2011;31(23):4663-75.

45.   Piovan E, Yu J, Tosello V, Herranz D, Ambesi-Impiombato A, Da Silva AC, et al. Direct reversal of glucocorticoid resistance by AKT inhibition in acute lymphoblastic leukemia. Cancer Cell. 2013;24(6):766-76.

46.   Oakley RH, Cidlowski JA. The biology of the glucocorticoid receptor: new signaling mechanisms in health and disease. The Journal of allergy and clinical immunology. 2013;132(5):1033-44.

47.   Paakinaho V, Kaikkonen S, Makkonen H, Benes V, Palvimo JJ. SUMOylation regulates the chromatin occupancy and anti-proliferative gene programs of glucocorticoid receptor. Nucleic Acids Res. 2014;42(3):1575-92.

48.   Hua G, Ganti KP, Chambon P. Glucocorticoid-induced tethered transrepression requires SUMOylation of GR and formation of a SUMO-SMRT/NCoR1-HDAC3 repressing complex. Proc Natl Acad Sci U S A. 2016;113(5):E635-43.

49.   Charmandari E, Chrousos GP, Lambrou GI, Pavlaki A, Koide H, Ng SSM, et al. Peripheral CLOCK Regulates Target-Tissue Glucocorticoid Receptor Transcriptional Activity in a Circadian Fashion in Man. PLOS ONE. 2011;6(9):e25612.

50.   Ito K, Yamamura S, Essilfie-Quaye S, Cosio B, Ito M, Barnes PJ, et al. Histone deacetylase 2-mediated deacetylation of the glucocorticoid receptor enables NF-kappaB suppression. The Journal of experimental medicine. 2006;203(1):7-13.

51.   Russcher H, Smit P, van den Akker ELT, van Rossum EFC, Brinkmann AO, de Jong FH, et al. Two Polymorphisms in the Glucocorticoid Receptor Gene Directly Affect Glucocorticoid-Regulated Gene Expression. The Journal of Clinical Endocrinology & Metabolism. 2005;90(10):5804-10.

52.   Molnár Á, Patócs A, Likó I, Nyírő G, Rácz K, Tóth M, et al. An unexpected, mild phenotype of glucocorticoid resistance associated with glucocorticoid receptor gene mutation case report and review of the literature. BMC Medical Genetics. 2018;19:37.

53.   Deng Q, Waxse B, Riquelme D, Zhang J, Aguilera G. Helix 8 of the ligand binding domain of the glucocorticoid receptor (GR) is essential for ligand binding. Molecular and cellular endocrinology. 2015;408:23-32.

54.   Hsin J-P, Manley JL. The RNA polymerase II CTD coordinates transcription and RNA processing. Genes Dev. 2012;26(19):2119-37.

55.   Chen FX, Smith ER, Shilatifard A. Born to run: control of transcription elongation by RNA polymerase II. Nature Reviews Molecular Cell Biology. 2018;19(7):464-78.

56.   Harlen KM, Trotta KL, Smith EE, Mosaheb MM, Fuchs SM, Churchman LS. Comprehensive RNA Polymerase II Interactomes Reveal Distinct and Varied Roles for Each Phospho-CTD Residue. Cell Rep. 2016;15(10):2147-58.

57.   Vockley CM, D'Ippolito AM, McDowell IC, Majoros WH, Safi A, Song L, et al. Direct GR Binding Sites Potentiate Clusters of TF Binding across the Human Genome. Cell. 2016;166(5):1269-81.e19.

58.   Meijsing SH, Pufall MA, So AY, Bates DL, Chen L, Yamamoto KR. DNA binding site sequence directs glucocorticoid receptor structure and activity. Science (New York, NY). 2009;324(5925):407-10.

59.   Weikum ER, Knuesel MT, Ortlund EA, Yamamoto KR. Glucocorticoid receptor control of transcription: precision and plasticity via allostery. Nature Reviews Molecular Cell Biology. 2017;18(3):159-74.

60.   Sacta MA, Chinenov Y, Rogatsky I. Glucocorticoid Signaling: An Update from a Genomic Perspective. Annual review of physiology. 2016;78:155-80.

61.   Escoter-Torres L, Caratti G, Mechtidou A, Tuckermann J, Uhlenhaut NH, Vettorazzi S. Fighting the Fire: Mechanisms of Inflammatory Gene Regulation by the Glucocorticoid Receptor. Front Immunol. 2019;10:1859.

62.   Surjit M, Ganti KP, Mukherji A, Ye T, Hua G, Metzger D, et al. Widespread negative response elements mediate direct repression by agonist-liganded glucocorticoid receptor. Cell. 2011;145(2):224-41.

63.   Hudson WH, Youn C, Ortlund EA. The structural basis of direct glucocorticoid-mediated transrepression. Nature structural & molecular biology. 2013;20(1):53-8.

64.   Burd CJ, Archer TK. Chromatin Architecture Defines the Glucocorticoid Response. Molecular and cellular endocrinology. 2013;380(0):25-31.

65.   Jenkins BD, Pullen CB, Darimont BD. Novel glucocorticoid receptor coactivator effector mechanisms. Trends Endocrinol Metab. 2001;12(3):122-6.

66.   Surjit M, Ganti Krishna P, Mukherji A, Ye T, Hua G, Metzger D, et al. Widespread Negative Response Elements Mediate Direct Repression by Agonist- Liganded Glucocorticoid Receptor. Cell. 2011;145(2):224-41.

67.   Wu D-Y, Ou C-Y, Chodankar R, Siegmund KD, Stallcup MR. Distinct, Genome-Wide, Gene-Specific Selectivity Patterns of Four Glucocorticoid Receptor Coregulators. Nuclear receptor signaling. 2014;12(1):nrs.12002.

68.   Monczor F, Chatzopoulou A, Zappia CD, Houtman R, Meijer OC, Fitzsimons CP. A Model of Glucocorticoid Receptor Interaction With Coregulators Predicts Transcriptional Regulation of Target Genes. Front Pharmacol. 2019;10:214-.

69.   Rollins DA, Kharlyngdoh JB, Coppo M, Tharmalingam B, Mimouna S, Guo Z, et al. Glucocorticoid-induced phosphorylation by CDK9 modulates the coactivator functions of transcriptional cofactor GRIP1 in macrophages. Nature Communications. 2017;8(1):1739.

70.   Caratti G, Matthews L, Poolman T, Kershaw S, Baxter M, Ray D. Glucocorticoid receptor function in health and disease. Clinical endocrinology. 2015;83(4):441-8.

71.   De Bosscher K, Vanden Berghe W, Vermeulen L, Plaisance S, Boone E, Haegeman G. Glucocorticoids repress NF-kappaB-driven genes by disturbing the interaction of p65 with the basal transcription machinery, irrespective of coactivator levels in the cell. Proc Natl Acad Sci U S A. 2000;97(8):3919-24.

72.   Uhlenhaut NH, Barish GD, Yu RT, Downes M, Karunasiri M, Liddle C, et al. Insights into negative regulation by the glucocorticoid receptor from genome-wide profiling of inflammatory cistromes. Mol Cell. 2013;49(1):158-71.

73.   Rao NAS, McCalman MT, Moulos P, Francoijs K-J, Chatziioannou A, Kolisis FN, et al. Coactivation of GR and NFKB alters the repertoire of their binding sites and target genes. Genome Research. 2011;21(9):1404-16.

74.   Petta I, Dejager L, Ballegeer M, Lievens S, Tavernier J, De Bosscher K, et al. The Interactome of the Glucocorticoid Receptor and Its Influence on the Actions of Glucocorticoids

in Combatting Inflammatory and Infectious Diseases. Microbiology and Molecular Biology Reviews : MMBR. 2016;80(2):495-522.

75. Escoter-Torres L, Greulich F, Quagliarini F, Wierer M, Uhlenhaut NH. Anti-inflammatory functions of the glucocorticoid receptor require DNA binding. Nucleic Acids Res. 2020;48(15):8393-407.

76. Reddy TE, Pauli F, Sprouse RO, Neff NF, Newberry KM, Garabedian MJ, et al. Genomic determination of the glucocorticoid response reveals unexpected mechanisms of gene regulation. Genome research. 2009;19(12):2163-71.

77. Franco LM, Gadkari M, Howe KN, Sun J, Kardava L, Kumar P, et al. Immune regulation by glucocorticoids can be linked to cell type-dependent transcriptional responses. The Journal of experimental medicine. 2019;216(2):384-406.

78. Gertz J, Savic D, Varley KE, Partridge EC, Safi A, Jain P, et al. Distinct properties of cell-type-specific and shared transcription factor binding sites. Molecular cell. 2013;52(1):25-36.

79. Oh KS, Patel H, Gottschalk RA, Lee WS, Baek S, Fraser IDC, et al. Anti-Inflammatory Chromatinscape Suggests Alternative Mechanisms of Glucocorticoid Receptor Action. Immunity. 2017;47(2):298-309.e5.

80. Watson LC, Kuchenbecker KM, Schiller BJ, Gross JD, Pufall MA, Yamamoto KR. The glucocorticoid receptor dimer interface allosterically transmits sequence-specific DNA signals. Nature Structural & Molecular Biology. 2013;20(7):876-83.

81. Van Looveren K, Van Boxelaere M, Callaerts-Vegh Z, Libert C. Cognitive dysfunction in mice lacking proper glucocorticoid receptor dimerization. PLoS One. 2019;14(12):e0226753.

82. Ballegeer M, Van Looveren K, Timmermans S, Eggermont M, Vandevyver S, Thery F, et al. Glucocorticoid receptor dimers control intestinal STAT1 and TNF-induced inflammation in mice. The Journal of clinical investigation. 2018;128(8):3265-79.

83. Lim HW, Uhlenhaut NH, Rauch A, Weiner J, Hübner S, Hübner N, et al. Genomic redistribution of GR monomers and dimers mediates transcriptional response to exogenous glucocorticoid in vivo. Genome research. 2015;25(6):836-44.

84. Presman DM, Ogara MF, Stortz M, Alvarez LD, Pooley JR, Schiltz RL, et al. Live cell imaging unveils multiple domain requirements for in vivo dimerization of the glucocorticoid receptor. PLoS Biol. 2014;12(3):e1001813-e.

85. Presman DM, Ganguly S, Schiltz RL, Johnson TA, Karpova TS, Hager GL. DNA binding triggers tetramerization of the glucocorticoid receptor in live cells. Proceedings of the National Academy of Sciences. 2016;113(29):8236-41.

86. Johnson TA, Paakinaho V, Kim S, Hager GL, Presman DM. Genome-wide binding potential and regulatory activity of the glucocorticoid receptor's monomeric and dimeric forms. Nature Communications. 2021;12(1):1987.

87. Nuñez FJ, Johnstone TB, Corpuz ML, Kazarian AG, Mohajer NN, Tliba O, et al. Glucocorticoids rapidly activate cAMP production via G(αs) to initiate non-genomic signaling that contributes to one-third of their canonical genomic effects. FASEB journal : official publication of the Federation of American Societies for Experimental Biology. 2020;34(2):2882-95.

88. Panettieri RA, Schaafsma D, Amrani Y, Koziol-White C, Ostrom R, Tliba O. Non-genomic Effects of Glucocorticoids: An Updated View. Trends in Pharmacological Sciences. 2019;40(1):38-49.

89. Hynes D, Harvey BJ. Dexamethasone reduces airway epithelial Cl(-) secretion by rapid non-genomic inhibition of KCNQ1, KCNN4 and KATP K(+) channels. Steroids. 2019;151:108459.

90. Prenek L, Boldizsár F, Kugyelka R, Ugor E, Berta G, Németh P, et al. The regulation of the mitochondrial apoptotic pathway by glucocorticoid receptor in collaboration with Bcl-2 family proteins in developing T cells. Apoptosis. 2017;22(2):239-53.

91. Strehl C, Gaber T, Löwenberg M, Hommes DW, Verhaar AP, Schellmann S, et al. Origin and functional activity of the membrane-bound glucocorticoid receptor. Arthritis & Rheumatism. 2011;63(12):3779-88.

92.   Bruna A, Nicolàs M, Muñoz A, Kyriakis JM, Caelles C. Glucocorticoid receptor-JNK interaction mediates inhibition of the JNK pathway by glucocorticoids. The EMBO journal. 2003;22(22):6035-44.

93.   Matthews L, Berry A, Ohanian V, Ohanian J, Garside H, Ray D. Caveolin mediates rapid glucocorticoid effects and couples glucocorticoid action to the antiproliferative program. Molecular endocrinology (Baltimore, Md). 2008;22(6):1320-30.

94.   Jozic I, Vukelic S, Stojadinovic O, Liang L, Ramirez HA, Pastar I, et al. Stress Signals, Mediated by Membranous Glucocorticoid Receptor, Activate PLC/PKC/GSK-3β/β-catenin Pathway to Inhibit Wound Closure. The Journal of investigative dermatology. 2017;137(5):1144-54.

95.   Croxtall JD, Choudhury Q, Flower RJ. Glucocorticoids act within minutes to inhibit recruitment of signalling factors to activated EGF receptors through a receptor-dependent, transcription-independent mechanism. Br J Pharmacol. 2000;130(2):289-98.

96.   Flaherty RL, Owen M, Fagan-Murphy A, Intabli H, Healy D, Patel A, et al. Glucocorticoids induce production of reactive oxygen species/reactive nitrogen species and DNA damage through an iNOS mediated pathway in breast cancer. Breast Cancer Res. 2017;19(1):35-.

97.   Rainville JR, Weiss GL, Evanson N, Herman JP, Vasudevan N, Tasker JG. Membrane-initiated nuclear trafficking of the glucocorticoid receptor in hypothalamic neurons. Steroids. 2019;142:55-64.

98.   Nahar J, Rainville JR, Dohanich GP, Tasker JG. Further evidence for a membrane receptor that binds glucocorticoids in the rodent hypothalamus. Steroids. 2016;114:33-40.

99.   Vernocchi S, Battello N, Schmitz S, Revets D, Billing AM, Turner JD, et al. Membrane glucocorticoid receptor activation induces proteomic changes aligning with classical glucocorticoid effects. Mol Cell Proteomics. 2013;12(7):1764-79.

100.   Yamagata S, Tomita K, Sano H, Itoh Y, Fukai Y, Okimoto N, et al. Non-genomic inhibitory effect of glucocorticoids on activated peripheral blood basophils through suppression of lipid raft formation. Clin Exp Immunol. 2012;170(1):86-93.

101.   Bartholome B, Spies CM, Gaber T, Schuchmann S, Berki T, Kunkel D, et al. Membrane glucocorticoid receptors (mGCR) are expressed in normal human peripheral blood mononuclear cells and up-regulated after in vitro stimulation and in patients with rheumatoid arthritis. FASEB journal : official publication of the Federation of American Societies for Experimental Biology. 2004;18(1):70-80.

102.   Spies CM, Schaumann DH, Berki T, Mayer K, Jakstadt M, Huscher D, et al. Membrane glucocorticoid receptors are down regulated by glucocorticoids in patients with systemic lupus erythematosus and use a caveolin-1-independent expression pathway. Annals of the rheumatic diseases. 2006;65(9):1139-46.

103.   Samarasinghe RA, Di Maio R, Volonte D, Galbiati F, Lewis M, Romero G, et al. Nongenomic glucocorticoid receptor action regulates gap junction intercellular communication and neural progenitor cell proliferation. Proceedings of the National Academy of Sciences of the United States of America. 2011;108(40):16657-62.

104.   Pedram A, Razandi M, Sainson RC, Kim JK, Hughes CC, Levin ER. A conserved mechanism for steroid receptor translocation to the plasma membrane. The Journal of biological chemistry. 2007;282(31):22278-88.

105.   Schlegel A, Wang C, Katzenellenbogen BS, Pestell RG, Lisanti MP. Caveolin-1 potentiates estrogen receptor alpha (ERalpha) signaling. caveolin-1 drives ligand-independent nuclear translocation and activation of ERalpha. The Journal of biological chemistry. 1999;274(47):33551-6.

106.   Nicolaides NC, Kino T, Roberts ML, Katsantoni E, Sertedaki A, Moutsatsou P, et al. The Role of S-Palmitoylation of the Human Glucocorticoid Receptor (hGR) in Mediating the Nongenomic Glucocorticoid Actions. J Mol Biochem. 2017;6(1):3-12.

107.   Hauser AS, Attwood MM, Rask-Andersen M, Schiöth HB, Gloriam DE. Trends in GPCR drug discovery: new agents, targets and indications. Nature Reviews Drug Discovery. 2017;16(12):829-42.

108.   Bar-Shavit R, Maoz M, Kancharla A, Nag JK, Agranovich D, Grisaru-Granovsky S, et al. G Protein-Coupled Receptors in Cancer. Int J Mol Sci. 2016;17(8):1320.

109.   Kroeze WK, Sassano MF, Huang X-P, Lansu K, McCorvy JD, Giguère PM, et al. PRESTO-Tango as an open-source resource for interrogation of the druggable human GPCRome. Nature structural & molecular biology. 2015;22(5):362-9.

110.   Wang C, Liu Y, Cao J-M. G protein-coupled receptors: extranuclear mediators for the non-genomic actions of steroids. Int J Mol Sci. 2014;15(9):15412-25.

111.   Kaddah S, Khreich N, Kaddah F, Khrouz L, Charcosset C, Greige-Gerges H. Corticoids modulate liposome membrane fluidity and permeability depending on membrane composition and experimental protocol design. Biochimie. 2018;153:33-45.

112.   Buttgereit F, Brand MD, Burmester G-R. Equivalent doses and relative drug potencies for non-genomic glucocorticoid effects: a novel glucocorticoid hierarchy. Biochemical Pharmacology. 1999;58(2):363-8.

113.   Wang D, Müller N, McPherson KG, Reichardt HM. Glucocorticoids engage different signal transduction pathways to induce apoptosis in thymocytes and mature T cells. Journal of immunology (Baltimore, Md : 1950). 2006;176(3):1695-702.

114.   Lim H-Y, Müller N, Herold MJ, van den Brandt J, Reichardt HM. Glucocorticoids exert opposing effects on macrophage function dependent on their concentration. Immunology. 2007;122(1):47-53.

115.   Reily MM, Pantoja C, Hu X, Chinenov Y, Rogatsky I. The GRIP1:IRF3 interaction as a target for glucocorticoid receptor-mediated immunosuppression. The EMBO journal. 2006;25(1):108-17.

116.   Auphan N, DiDonato JA, Rosette C, Helmberg A, Karin M. Immunosuppression by glucocorticoids: inhibition of NF-kappa B activity through induction of I kappa B synthesis. Science. 1995;270(5234):286-90.

117.   Jacobs MD, Harrison SC. Structure of an IκBα/NF-κB Complex. Cell. 1998;95(6):749-58.

118.   Berrebi D, Bruscoli S, Cohen N, Foussat A, Migliorati G, Bouchet-Delbos L, et al. Synthesis of glucocorticoid-induced leucine zipper (GILZ) by macrophages: an anti-inflammatory and immunosuppressive mechanism shared by glucocorticoids and IL-10. Blood. 2003;101(2):729-38.

119.   Abraham SM, Lawrence T, Kleiman A, Warden P, Medghalchi M, Tuckermann J, et al. Antiinflammatory effects of dexamethasone are partly dependent on induction of dual specificity phosphatase 1. The Journal of experimental medicine. 2006;203(8):1883-9.

120.   Kim S-W, Rhee HJ, Ko J, Kim YJ, Kim HG, Yang JM, et al. Inhibition of Cytosolic Phospholipase A2 by Annexin I: SPECIFIC INTERACTION MODEL AND MAPPING OF THE INTERACTION SITE. Journal of Biological Chemistry. 2001;276(19):15712-9.

121.   Perretti M, Dalli J. Exploiting the Annexin A1 pathway for the development of novel anti-inflammatory therapeutics. Br J Pharmacol. 2009;158(4):936-46.

122.   GALON J, FRANCHIMONT D, HIROI N, FREY G, BOETTNER A, EHRHART-BORNSTEIN M, et al. Gene profiling reveals unknown enhancing and suppressive actions of glucocorticoids on immune cells. The FASEB Journal. 2002;16(1):61-71.

123.   Ehrchen J, Steinmüller L, Barczyk K, Tenbrock K, Nacken W, Eisenacher M, et al. Glucocorticoids induce differentiation of a specifically activated, anti-inflammatory subtype of human monocytes. Blood. 2007;109(3):1265-74.

124.   Smoak K, Cidlowski JA. Glucocorticoids regulate tristetraprolin synthesis and posttranscriptionally regulate tumor necrosis factor alpha inflammatory signaling. Mol Cell Biol. 2006;26(23):9126-35.

125.   Giles KM, Ross K, Rossi AG, Hotchin NA, Haslett C, Dransfield I. Glucocorticoid augmentation of macrophage capacity for phagocytosis of apoptotic cells is associated with reduced p130Cas expression, loss of paxillin/pyk2 phosphorylation, and high levels of active Rac. Journal of immunology (Baltimore, Md : 1950). 2001;167(2):976-86.

126.   Chen FE, Huang D-B, Chen Y-Q, Ghosh G. Crystal structure of p50/p65 heterodimer of transcription factor NF-[kappa]B bound to DNA. Nature. 1998;391(6665):410-3.

127.   Busillo JM, Cidlowski JA. The five Rs of glucocorticoid action during inflammation: ready, reinforce, repress, resolve, and restore. Trends in endocrinology and metabolism: TEM. 2013;24(3):109-19.

128.   Scheidereit C. IkappaB kinase complexes: gateways to NF-kappaB activation and transcription. Oncogene. 2006;25(51):6685-705.

129.   Ray A, Prefontaine KE. Physical association and functional antagonism between the p65 subunit of transcription factor NF-kappa B and the glucocorticoid receptor. Proceedings of the National Academy of Sciences of the United States of America. 1994;91(2):752-6.

130.   Tanaka T, Narazaki M, Kishimoto T. IL-6 in Inflammation, Immunity, and Disease. Cold Spring Harbor Perspectives in Biology. 2014;6(10):a016295.

131.   Bettelli E, Carrier Y, Gao W, Korn T, Strom TB, Oukka M, et al. Reciprocal developmental pathways for the generation of pathogenic effector TH17 and regulatory T cells. Nature. 2006;441(7090):235-8.

132.   Reddy TE, Pauli F, Sprouse RO, Neff NF, Newberry KM, Garabedian MJ, et al. Genomic determination of the glucocorticoid response reveals unexpected mechanisms of gene regulation. Genome Research. 2009;19(12):2163-71.

133.   Damodaran K, Venkatachalapathy S, Alisafaei F, Radhakrishnan AV, Sharma Jokhun D, Shenoy VB, et al. Compressive force induces reversible chromatin condensation and cell geometry-dependent transcriptional response. Mol Biol Cell. 2018;29(25):3039-51.

134.   Mitra A, Venkatachalapathy S, Ratna P, Wang Y, Jokhun DS, Shivashankar GV. Cell geometry dictates TNFα-induced genome response. Proceedings of the National Academy of Sciences. 2017;114(20):E3882-E91.

135.   Roy B, Venkatachalapathy S, Ratna P, Wang Y, Jokhun DS, Nagarajan M, et al. Laterally confined growth of cells induces nuclear reprogramming in the absence of exogenous biochemical factors. Proc Natl Acad Sci U S A. 2018;115(21):E4741-e50.

136.   Makhija E, Jokhun DS, Shivashankar GV. Nuclear deformability and telomere dynamics are regulated by cell geometric constraints. Proc Natl Acad Sci U S A. 2016;113(1):E32-40.

137.   Alisafaei F, Jokhun DS, Shivashankar GV, Shenoy VB. Regulation of nuclear architecture, mechanics, and nucleocytoplasmic shuttling of epigenetic factors by cell geometric constraints. Proceedings of the National Academy of Sciences. 2019;116(27):13200-9.

138.   Bao M, Xie J, Piruska A, Huck WTS. 3D microniches reveal the importance of cell size and shape. Nature Communications. 2017;8(1):1962.

139.   Versaevel M, Grevesse T, Gabriele S. Spatial coordination between cell and nuclear shape within micropatterned endothelial cells. Nature Communications. 2012;3:671.

140.   Venkatachalapathy S, Jokhun DS, Shivashankar GV. Multivariate analysis reveals activation-primed fibroblast geometric states in engineered 3D tumor microenvironments. Mol Biol Cell. 2020;31(8):803-12.

141.   Vergani L, Grattarola M, Nicolini C. Modifications of chromatin structure and gene expression following induced alterations of cellular shape. The International Journal of Biochemistry & Cell Biology. 2004;36(8):1447-61.

142.   Jain N, Vogel V. Spatial confinement downsizes the inflammatory response of macrophages. Nature Materials. 2018;17(12):1134-44.

143.   Wang Y, Nagarajan M, Uhler C, Shivashankar GV. Orientation and repositioning of chromosomes correlate with cell geometry-dependent gene expression. Mol Biol Cell. 2017;28(14):1997-2009.

144.   Jain N, Iyer KV, Kumar A, Shivashankar GV. Cell geometric constraints induce modular gene-expression patterns via redistribution of HDAC3 regulated by actomyosin contractility. Proceedings of the National Academy of Sciences of the United States of America. 2013;110(28):11349-54.

145.   Dupont S, Morsut L, Aragona M, Enzo E, Giulitti S, Cordenonsi M, et al. Role of YAP/TAZ in mechanotransduction. Nature. 2011;474(7350):179-83.

146.   Le Beyec J, Xu R, Lee S-Y, Nelson CM, Rizki A, Alcaraz J, et al. Cell shape regulates global histone acetylation in human mammary epithelial cells. Experimental cell research. 2007;313(14):3066-75.
147.   Chen X, Barozzi I, Termanini A, Prosperini E, Recchiuti A, Dalli J, et al. Requirement for the histone deacetylase Hdac3 for the inflammatory gene expression program in macrophages. Proc Natl Acad Sci U S A. 2012;109(42):E2865-74.
148.   Mullican SE, Gaddis CA, Alenghat T, Nair MG, Giacomin PR, Everett LJ, et al. Histone deacetylase 3 is an epigenomic brake in macrophage alternative activation. Genes Dev. 2011;25(23):2480-8.
149.   Gao Z, He Q, Peng B, Chiao PJ, Ye J. Regulation of nuclear translocation of HDAC3 by IkappaBalpha is required for tumor necrosis factor inhibition of peroxisome proliferator-activated receptor gamma function. The Journal of biological chemistry. 2006;281(7):4540-7.
150.   Sero JE, Sailem HZ, Ardy RC, Almuttaqi H, Zhang T, Bakal C. Cell shape and the microenvironment regulate nuclear translocation of NF-κB in breast epithelial and tumor cells. Molecular Systems Biology. 2015;11(3):0790.
151.   Kim Y, Bayona PW, Kim M, Chang J, Hong S, Park Y, et al. Macrophage Lamin A/C Regulates Inflammation and the Development of Obesity-Induced Insulin Resistance. Frontiers in Immunology. 2018;9(696).
152.   Kustermans G, El Mjiyad N, Horion J, Jacobs N, Piette J, Legrand-Poels S. Actin cytoskeleton differentially modulates NF-κB-mediated IL-8 expression in myelomonocytic cells. Biochemical Pharmacology. 2008;76(10):1214-28.
153.   McWhorter FY, Wang T, Nguyen P, Chung T, Liu WF. Modulation of macrophage phenotype by cell shape. Proceedings of the National Academy of Sciences. 2013;110(43):17253-8.
154.   Barzilai S, Yadav SK, Morrell S, Roncato F, Klein E, Stoler-Barak L, et al. Leukocytes Breach Endothelial Barriers by Insertion of Nuclear Lobes and Disassembly of Endothelial Actin Filaments. Cell Rep. 2017;18(3):685-99.
155.   Burkhardt JK, Carrizosa E, Shaffer MH. The Actin Cytoskeleton in T Cell Activation. Annual Review of Immunology. 2008;26(1):233-59.
156.   Issaq HJ, Veenstra TD. Two-dimensional polyacrylamide gel electrophoresis (2D-PAGE): advances and perspectives. BioTechniques. 2008;44(5):697-700.
157.   Zhang Z, Wu S, Stenoien DL, Paša-Tolić L. High-Throughput Proteomics. Annual Review of Analytical Chemistry. 2014;7(1):427-54.
158.   O'Connell JD, Paulo JA, O'Brien JJ, Gygi SP. Proteome-Wide Evaluation of Two Common Protein Quantification Methods. J Proteome Res. 2018;17(5):1934-42.
159.   Lowe R, Shirley N, Bleackley M, Dolan S, Shafee T. Transcriptomics technologies. PLOS Computational Biology. 2017;13(5):e1005457.
160.   Oshlack A, Wakefield MJ. Transcript length bias in RNA-seq data confounds systems biology. Biology Direct. 2009;4(1):14.
161.   Gupta D, Shah HP, Malu K, Berliner N, Gaines P. Differentiation and Characterization of Myeloid Cells. Current protocols in immunology / edited by John E Coligan [et al]. 2014;104:Unit-22F.5.
162.   Chanput W, Mes JJ, Wichers HJ. THP-1 cell line: an in vitro cell model for immune modulation approach. International immunopharmacology. 2014;23(1):37-45.
163.   Park EK, Jung HS, Yang HI, Yoo MC, Kim C, Kim KS. Optimized THP-1 differentiation is required for the detection of responses to weak stimuli. Inflammation research : official journal of the European Histamine Research Society [et al]. 2007;56(1):45-50.
164.   Carpenter AE, Jones TR, Lamprecht MR, Clarke C, Kang IH, Friman O, et al. CellProfiler: image analysis software for identifying and quantifying cell phenotypes. Genome Biology. 2006;7(10):R100.
165.   Kershaw S. Investigating the non-genomic actions of the glucocorticoid receptor: University of Manchester; 2018.
166.   Chen X, Wei S, Ji Y, Guo X, Yang F. Quantitative proteomics using SILAC: Principles, applications, and developments. Proteomics. 2015;15(18):3175-92.

167.	Shannon P, Markiel A, Ozier O, Baliga NS, Wang JT, Ramage D, et al. Cytoscape: A Software Environment for Integrated Models of Biomolecular Interaction Networks. Genome research. 2003;13(11):2498-504.

168.	Doncheva NT, Morris JH, Gorodkin J, Jensen LJ. Cytoscape StringApp: Network Analysis and Visualization of Proteomics Data. J Proteome Res. 2019;18(2):623-32.

169.	Kuleshov MV, Jones MR, Rouillard AD, Fernandez NF, Duan Q, Wang Z, et al. Enrichr: a comprehensive gene set enrichment analysis web server 2016 update. Nucleic Acids Res. 2016;44(W1):W90-7.

170.	Horn H, Schoof EM, Kim J, Robin X, Miller ML, Diella F, et al. KinomeXplorer: an integrated platform for kinome biology studies. Nature Methods. 2014;11(6):603-4.

171.	Mortazavi A, Williams BA, McCue K, Schaeffer L, Wold B. Mapping and quantifying mammalian transcriptomes by RNA-Seq. Nature Methods. 2008;5(7):621-8.

172.	Dobin A, Davis CA, Schlesinger F, Drenkow J, Zaleski C, Jha S, et al. STAR: ultrafast universal RNA-seq aligner. Bioinformatics (Oxford, England). 2013;29(1):15-21.

173.	Anders S, Huber W. Differential expression analysis for sequence count data. Genome Biology. 2010;11(10):R106.

174.	Kanehisa M, Goto S. KEGG: kyoto encyclopedia of genes and genomes. Nucleic Acids Res. 2000;28(1):27-30.

175.	Wu G, Feng X, Stein L. A human functional protein interaction network and its application to cancer data analysis. Genome Biol. 2010;11(5):R53.

176.	Périer RC, Praz V, Junier T, Bonnard C, Bucher P. The Eukaryotic Promoter Database (EPD). Nucleic Acids Res. 2000;28(1):302-3.

177.	McLeay RC, Bailey TL. Motif Enrichment Analysis: a unified framework and an evaluation on ChIP data. BMC Bioinformatics. 2010;11(1):165.

178.	Janky R, Verfaillie A, Imrichová H, Van de Sande B, Standaert L, Christiaens V, et al. iRegulon: from a gene list to a gene regulatory network using large motif and track collections. PLoS Comput Biol. 2014;10(7):e1003731.

179.	Qin Q, Fan J, Zheng R, Wan C, Mei S, Wu Q, et al. Lisa: inferring transcriptional regulators through integrative modeling of public chromatin accessibility and ChIP-seq data. Genome Biology. 2020;21(1):32.

180.	Urbach V, Walsh DE, Mainprice B, Bousquet J, Harvey BJ. Rapid non-genomic inhibition of ATP-induced Cl– secretion by dexamethasone in human bronchial epithelium. J Physiol. 2002;545(3):869-78.

181.	Vockley CM, D'Ippolito AM, McDowell IC, Majoros WH, Safi A, Song L, et al. Direct GR Binding Sites Potentiate Clusters of TF Binding across the Human Genome. Cell. 2016;166(5):1269-81.e19.

182.	Stahn C, Buttgereit F. Genomic and nongenomic effects of glucocorticoids. Nature Clinical Practice Rheumatology. 2008;4(10):525-33.

183.	Leaker BR, O'Connor B, Singh D, Barnes PJ. The novel inhaled glucocorticoid receptor agonist GW870086X protects against adenosine-induced bronchoconstriction in asthma. The Journal of allergy and clinical immunology. 2015;136(2):501-2.e6.

184.	Uings IJ, Needham D, Matthews J, Haase M, Austin R, Angell D, et al. Discovery of GW870086: a potent anti-inflammatory steroid with a unique pharmacological profile. Br J Pharmacol. 2013;169(6):1389-403.

185.	Biggadike K, Bledsoe RK, Coe DM, Cooper TW, House D, Iannone MA, et al. Design and x-ray crystal structures of high-potency nonsteroidal glucocorticoid agonists exploiting a novel binding site on the receptor. Proc Natl Acad Sci U S A. 2009;106(43):18114-9.

186.	Kershaw S, Morgan DJ, Boyd J, Spiller DG, Kitchen G, Zindy E, et al. Glucocorticoids rapidly inhibit cell migration through a novel, non-transcriptional HDAC6 pathway. J Cell Sci. 2020;133(11).

187.	Trebble PJ, Woolven JM, Saunders KA, Simpson KD, Farrow SN, Matthews LC, et al. A ligand-specific kinetic switch regulates glucocorticoid receptor trafficking and function. J Cell Sci. 2013;126(14):3159-69.

188.   D'Ippolito AM, McDowell IC, Barrera A, Hong LK, Leichter SM, Bartelt LC, et al. Pre-established Chromatin Interactions Mediate the Genomic Response to Glucocorticoids. Cell systems. 2018;7(2):146-60.e7.

189.   McDowell IC, Barrera A, D'Ippolito AM, Vockley CM, Hong LK, Leichter SM, et al. Glucocorticoid receptor recruits to enhancers and drives activation by motif-directed binding. Genome research. 2018;28(9):1272-84.

190.   Seo J, Koçak DD, Bartelt LC, Williams CA, Barrera A, Gersbach CA, et al. AP-1 subunits converge promiscuously at enhancers to potentiate transcription. Genome research. 2021;31(4):538-50.

191.   Prekovic S, Schuurman K, Mayayo-Peralta I, Manjón AG, Buijs M, Yavuz S, et al. Glucocorticoid receptor triggers a reversible drug-tolerant dormancy state with acquired therapeutic vulnerabilities in lung cancer. Nature Communications. 2021;12(1):4360.

192.   Francavilla C, Hekmat O, Blagoev B, Olsen JV. SILAC-Based Temporal Phosphoproteomics. In: Warscheid B, editor. Stable Isotope Labeling by Amino Acids in Cell Culture (SILAC): Methods and Protocols. New York, NY: Springer New York; 2014. p. 125-48.

193.   Boncompagni S, Arthurton L, Akujuru E, Pearson T, Steverding D, Protasi F, et al. Membrane glucocorticoid receptors are localised in the extracellular matrix and signal through the MAPK pathway in mammalian skeletal muscle fibres. J Physiol. 2015;593(12):2679-92.

194.   Caratti G, Poolman T, Hurst RJ, Ince L, Knight A, Krakowiak K, et al. Caveolin1 interacts with the glucocorticoid receptor in the lung but is dispensable for its anti-inflammatory actions in lung inflammation and Trichuris Muris infection. Scientific Reports. 2019;9(1):8581.

195.   Weiss GL, Rainville JR, Zhao Q, Tasker JG. Purity and stability of the membrane-limited glucocorticoid receptor agonist dexamethasone-BSA. Steroids. 2019;142:2-5.

196.   Mu R, Wang YB, Wu M, Yang Y, Song W, Li T, et al. Depletion of pre-mRNA splicing factor Cdc5L inhibits mitotic progression and triggers mitotic catastrophe. Cell Death Dis. 2014;5(3):e1151.

197.   Davis TA, Loos B, Engelbrecht AM. AHNAK: the giant jack of all trades. Cellular signalling. 2014;26(12):2683-93.

198.   Chen B, Wang J, Dai D, Zhou Q, Guo X, Tian Z, et al. AHNAK suppresses tumour proliferation and invasion by targeting multiple pathways in triple-negative breast cancer. Journal of Experimental & Clinical Cancer Research. 2017;36(1):65.

199.   Park JW, Kim IY, Choi JW, Lim HJ, Shin JH, Kim YN, et al. AHNAK Loss in Mice Promotes Type II Pneumocyte Hyperplasia and Lung Tumor Development. Molecular cancer research : MCR. 2018;16(8):1287-98.

200.   Chen Z, Lan X, Wu D, Sunkel B, Ye Z, Huang J, et al. Ligand-dependent genomic function of glucocorticoid receptor in triple-negative breast cancer. Nature Communications. 2015;6(1):8323.

201.   Linding R, Jensen LJ, Pasculescu A, Olhovsky M, Colwill K, Bork P, et al. NetworKIN: a resource for exploring cellular phosphorylation networks. Nucleic Acids Res. 2008;36(Database issue):D695-D9.

202.   Hayes MJ, Shao D, Bailly M, Moss SE. Regulation of actin dynamics by annexin 2. The EMBO journal. 2006;25(9):1816-26.

203.   Kuhlman PA, Hughes CA, Bennett V, Fowler VM. A new function for adducin. Calcium/calmodulin-regulated capping of the barbed ends of actin filaments. The Journal of biological chemistry. 1996;271(14):7986-91.

204.   Zhou G-L, Zhang H, Wu H, Ghai P, Field J. Phosphorylation of the cytoskeletal protein CAP1 controls its association with cofilin and actin. J Cell Sci. 2014;127(Pt 23):5052-65.

205.   Moriyama K, Iida K, Yahara I. Phosphorylation of Ser-3 of cofilin regulates its essential function on actin. Genes to cells : devoted to molecular & cellular mechanisms. 1996;1(1):73-86.

206.   Lachmann A, Ma'ayan A. KEA: kinase enrichment analysis. Bioinformatics (Oxford, England). 2009;25(5):684-6.

207. Araç D, Boucard AA, Bolliger MF, Nguyen J, Soltis SM, Südhof TC, et al. A novel evolutionarily conserved domain of cell-adhesion GPCRs mediates autoproteolysis. The EMBO journal. 2012;31(6):1364-78.

208. Lagerstrom MC, Rabe N, Haitina T, Kalnina I, Hellstrom AR, Klovins J, et al. The evolutionary history and tissue mapping of GPR123: specific CNS expression pattern predominantly in thalamic nuclei and regions containing large pyramidal cells. J Neurochem. 2007;100(4):1129-42.

209. Uhlén M, Fagerberg L, Hallström BM, Lindskog C, Oksvold P, Mardinoglu A, et al. Proteomics. Tissue-based map of the human proteome. Science. 2015;347(6220):1260419.

210. Wang T, Ward Y, Tian L, Lake R, Guedez L, Stetler-Stevenson WG, et al. CD97, an adhesion receptor on inflammatory cells, stimulates angiogenesis through binding integrin counterreceptors on endothelial cells. Blood. 2005;105(7):2836-44.

211. Barnea G, Strapps W, Herrada G, Berman Y, Ong J, Kloss B, et al. The genetic design of signaling cascades to record receptor activation. Proceedings of the National Academy of Sciences. 2008;105(1):64.

212. Sandén C, Broselid S, Cornmark L, Andersson K, Daszkiewicz-Nilsson J, Mårtensson UE, et al. G protein-coupled estrogen receptor 1/G protein-coupled receptor 30 localizes in the plasma membrane and traffics intracellularly on cytokeratin intermediate filaments. Molecular pharmacology. 2011;79(3):400-10.

213. Greifenberg AK, Honig D, Pilarova K, Duster R, Bartholomeeusen K, Bosken CA, et al. Structural and Functional Analysis of the Cdk13/Cyclin K Complex. Cell Rep. 2016;14(2):320-31.

214. Gajdušková P, Ruiz de Los Mozos I, Rájecký M, Hluchý M, Ule J, Blazek D. CDK11 is required for transcription of replication-dependent histone genes. Nat Struct Mol Biol. 2020;27(5):500-10.

215. Loyer P, Trembley JH, Grenet JA, Busson A, Corlu A, Zhao W, et al. Characterization of Cyclin L1 and L2 Interactions with CDK11 and Splicing Factors: INFLUENCE OF CYCLIN L ISOFORMS ON SPLICE SITE SELECTION *. Journal of Biological Chemistry. 2008;283(12):7721-32.

216. Li S, Song W, Jiang M, Zeng L, Zhu X, Chen J. Phosphorylation of cyclin Y by CDK14 induces its ubiquitination and degradation. FEBS Letters. 2014;588(11):1989-96.

217. Fan Z, Devlin JR, Hogg SJ, Doyle MA, Harrison PF, Todorovski I, et al. CDK13 cooperates with CDK12 to control global RNA polymerase II processivity. Science Advances. 2020;6(18):eaaz5041.

218. Bartkowiak B, Greenleaf AL. Expression, purification, and identification of associated proteins of the full-length hCDK12/CyclinK complex. The Journal of biological chemistry. 2015;290(3):1786-95.

219. Carson MW, Luz JG, Suen C, Montrose C, Zink R, Ruan X, et al. Glucocorticoid Receptor Modulators Informed by Crystallography Lead to a New Rationale for Receptor Selectivity, Function, and Implications for Structure-Based Design. Journal of Medicinal Chemistry. 2014;57(3):849-60.

220. Chen W, Dang T, Blind RD, Wang Z, Cavasotto CN, Hittelman AB, et al. Glucocorticoid receptor phosphorylation differentially affects target gene expression. Molecular endocrinology (Baltimore, Md). 2008;22(8):1754-66.

221. Patt M, Gysi J, Faresse N, Cidlowski JA, Odermatt A. Protein phosphatase 1 alpha enhances glucocorticoid receptor activity by a mechanism involving phosphorylation of serine-211. Molecular and cellular endocrinology. 2020;518:110873-.

222. Stournaras C, Gravanis A, Margioris AN, Lang F. The actin cytoskeleton in rapid steroid hormone actions. Cytoskeleton. 2014;71(5):285-93.

223. Sundararaj S, Ravindran A, Casarotto MG. AHNAK: The quiet giant in calcium homeostasis. Cell calcium. 2021;96:102403.

224. Stiff T, Shtivelman E, Jeggo P, Kysela B. AHNAK interacts with the DNA ligase IV–XRCC4 complex and stimulates DNA ligase IV-mediated double-stranded ligation. DNA Repair. 2004;3(3):245-56.

225.   Hohaus A, Person V, Behlke J, Schaper J, Morano I, Haase H. The carboxyl-terminal region of ahnak provides a link between cardiac L-type Ca2+ channels and the actinbased cytoskeleton. The FASEB Journal. 2002;16(10):1205-16.

226.   Benaud C, Gentil BtJ, Assard N, Court M, Garin J, Delphin C, et al. AHNAK interaction with the annexin 2/S100A10 complex regulates cell membrane cytoarchitecture. Journal of Cell Biology. 2003;164(1):133-44.

227.   Lekmine F, Sassano A, Uddin S, Smith J, Majchrzak B, Brachmann SM, et al. Interferon-γ engages the p70 S6 kinase to regulate phosphorylation of the 40S S6 ribosomal protein. Experimental Cell Research. 2004;295(1):173-82.

228.   Kino T, Ichijo T, Amin ND, Kesavapany S, Wang Y, Kim N, et al. Cyclin-dependent kinase 5 differentially regulates the transcriptional activity of the glucocorticoid receptor through phosphorylation: clinical implications for the nervous system response to glucocorticoids and stress. Molecular endocrinology (Baltimore, Md). 2007;21(7):1552-68.

229.   Pfänder P, Fidan M, Burret U, Lipinski L, Vettorazzi S. Cdk5 Deletion Enhances the Anti-inflammatory Potential of GC-Mediated GR Activation During Inflammation. Front Immunol. 2019;10:1554.

230.   Choi SH, Martinez TF, Kim S, Donaldson C, Shokhirev MN, Saghatelian A, et al. CDK12 phosphorylates 4E-BP1 to enable mTORC1-dependent translation and mitotic genome stability. Genes Dev. 2019;33(7-8):418-35.

231.   Matthews LC, Berry AA, Morgan DJ, Poolman TM, Bauer K, Kramer F, et al. Glucocorticoid receptor regulates accurate chromosome segregation and is associated with malignancy. Proceedings of the National Academy of Sciences. 2015;112(17):5479.

232.   Yang S, Roselli F, Patchev AV, Yu S, Almeida OFX. Non-receptor-tyrosine kinases integrate fast glucocorticoid signaling in hippocampal neurons. The Journal of biological chemistry. 2013;288(33):23725-39.

233.   Harris C, Weiss GL, Di S, Tasker JG. Cell signaling dependence of rapid glucocorticoid-induced endocannabinoid synthesis in hypothalamic neuroendocrine cells. Neurobiol Stress. 2019;10:100158-.

234.   Caratti G, Poolman T, Hurst RJ, Ince L, Knight A, Krakowiak K, et al. Caveolin1 interacts with the glucocorticoid receptor in the lung but is dispensable for its anti-inflammatory actions in lung inflammation and Trichuris Muris infection. Sci Rep. 2019;9(1):8581.

235.   Peffer ME, Chandran UR, Luthra S, Volonte D, Galbiati F, Garabedian MJ, et al. Caveolin-1 regulates genomic action of the glucocorticoid receptor in neural stem cells. Mol Cell Biol. 2014;34(14):2611-23.

236.   Xu S, Yu S, Dong D, Lee LTO. G Protein-Coupled Estrogen Receptor: A Potential Therapeutic Target in Cancer. Frontiers in Endocrinology. 2019;10(725).

237.   Lagerström MC, Rabe N, Haitina T, Kalnina I, Hellström AR, Klovins J, et al. The evolutionary history and tissue mapping of GPR123: specific CNS expression pattern predominantly in thalamic nuclei and regions containing large pyramidal cells. Journal of Neurochemistry. 2007;100(4):1129-42.

238.   Consortium IMP. Adhesion G protein-coupled receptor A1 mousephoentype.org [Available from: https://www.mousephenotype.org/data/genes/MGI:1277167#phenotypesTab.

239.   Leon K, Cunningham RL, Riback JA, Feldman E, Li J, Sosnick TR, et al. Structural basis for adhesion G protein-coupled receptor Gpr126 function. Nature Communications. 2020;11(1):194.

240.   Monk KR, Naylor SG, Glenn TD, Mercurio S, Perlin JR, Dominguez C, et al. A G Protein–Coupled Receptor Is Essential for Schwann Cells to Initiate Myelination. Science. 2009;325(5946):1402-5.

241.   Monk KR, Oshima K, Jörs S, Heller S, Talbot WS. Gpr126 is essential for peripheral nerve development and myelination in mammals. Development. 2011;138(13):2673-80.

242.   Cui H, Wang Y, Huang H, Yu W, Bai M, Zhang L, et al. GPR126 Protein Regulates Developmental and Pathological Angiogenesis through Modulation of VEGFR2 Receptor Signaling. Journal of Biological Chemistry. 2014;289(50):34871-85.

243.   Qian, Haino, Kelly, Song. Structural characterization of mouse CD97 and study of its specific interaction with the murine decay-accelerating factor (DAF, CD55). Immunology. 1999;98(2):303-11.

244.   Stacey M, Chang G-W, Davies JQ, Kwakkenbos MJ, Sanderson RD, Hamann Jr, et al. The epidermal growth factor–like domains of the human EMR2 receptor mediate cell attachment through chondroitin sulfate glycosaminoglycans. Blood. 2003;102(8):2916-24.

245.   Gad AA, Balenga N. The Emerging Role of Adhesion GPCRs in Cancer. ACS pharmacology & translational science. 2020;3(1):29-42.

246.   Wang S, Sun Z, Zhao W, Wang Z, Wu M, Pan Y, et al. CD97/ADGRE5 Inhibits LPS Induced NF-*κ*B Activation through PPAR-*γ* Upregulation in Macrophages. Mediators of Inflammation. 2016;2016:1605948.

247.   Safaee M, Clark AJ, Ivan ME, Oh MC, Bloch O, Sun MZ, et al. CD97 is a multifunctional leukocyte receptor with distinct roles in human cancers (Review). Int J Oncol. 2013;43(5):1343-50.

248.   Wei W, Chen ZJ, Zhang KS, Yang XL, Wu YM, Chen XH, et al. The activation of G protein-coupled receptor 30 (GPR30) inhibits proliferation of estrogen receptor-negative breast cancer cells in vitro and in vivo. Cell Death & Disease. 2014;5(10):e1428-e.

249.   Seyedabadi M, Gharghabi M, Gurevich EV, Gurevich VV. Receptor-Arrestin Interactions: The GPCR Perspective. Biomolecules. 2021;11(2):218.

250.   Petrillo MG, Oakley RH, Cidlowski JA. β-Arrestin-1 inhibits glucocorticoid receptor turnover and alters glucocorticoid signaling. The Journal of biological chemistry. 2019;294(29):11225-39.

251.   Alver BH, Kim KH, Lu P, Wang X, Manchester HE, Wang W, et al. The SWI/SNF chromatin remodelling complex is required for maintenance of lineage specific enhancers. Nature Communications. 2017;8(1):14648.

252.   Kolodkin AN, Bruggeman FJ, Plant N, Moné MJ, Bakker BM, Campbell MJ, et al. Design principles of nuclear receptor signaling: how complex networking improves signal transduction. Molecular Systems Biology. 2010;6(1):446.

253.   Bortolozzi R, Mattiuzzo E, Trentin L, Accordi B, Basso G, Viola G. Ribociclib, a Cdk4/Cdk6 kinase inhibitor, enhances glucocorticoid sensitivity in B-acute lymphoblastic leukemia (B-All). Biochemical Pharmacology. 2018;153:230-41.

254.   Liang K, Gao X, Gilmore JM, Florens L, Washburn MP, Smith E, et al. Characterization of Human Cyclin-Dependent Kinase 12 (CDK12) and CDK13 Complexes in C-Terminal Domain Phosphorylation, Gene Transcription, and RNA Processing. Mol Cell Biol. 2015;35(6):928.

255.   Chao S-H, Price DH. Flavopiridol Inactivates P-TEFb and Blocks Most RNA Polymerase II Transcription in Vivo*. Journal of Biological Chemistry. 2001;276(34):31793-9.

256.   Zhang T, Kwiatkowski N, Olson CM, Dixon-Clarke SE, Abraham BJ, Greifenberg AK, et al. Covalent targeting of remote cysteine residues to develop CDK12 and CDK13 inhibitors. Nat Chem Biol. 2016;12(10):876-84.

257.   Bösken CA, Farnung L, Hintermair C, Merzel Schachter M, Vogel-Bachmayr K, Blazek D, et al. The structure and substrate specificity of human Cdk12/Cyclin K. Nat Commun. 2014;5:3505.

258.   Tellier M, Zaborowska J, Caizzi L, Mohammad E, Velychko T, Schwalb B, et al. CDK12 globally stimulates RNA polymerase II transcription elongation and carboxyl-terminal domain phosphorylation. Nucleic Acids Res. 2020;48(14):7712-27.

259.   Zhang T, Kwiatkowski N, Olson CM, Dixon-Clarke SE, Abraham BJ, Greifenberg AK, et al. Covalent targeting of remote cysteine residues to develop CDK12 and CDK13 inhibitors. Nat Chem Biol. 2016;12:876.

260.   Chen S, Wang J, Yu G, Liu W, Pearce D. Androgen and glucocorticoid receptor heterodimer formation. A possible mechanism for mutual inhibition of transcriptional activity. The Journal of biological chemistry. 1997;272(22):14087-92.

261.   Krajewska M, Dries R, Grassetti AV, Dust S, Gao Y, Huang H, et al. CDK12 loss in cancer cells affects DNA damage response genes through premature cleavage and polyadenylation. Nature Communications. 2019;10(1):1757.

262.   Citri A, Yarden Y. EGF–ERBB signalling: towards the systems level. Nature Reviews Molecular Cell Biology. 2006;7(7):505-16.

263.   Chotiyarnwong P, McCloskey EV. Pathogenesis of glucocorticoid-induced osteoporosis and options for treatment. Nature reviews Endocrinology. 2020;16(8):437-47.

264.   Greenleaf AL. Human CDK12 and CDK13, multi-tasking CTD kinases for the new millenium. Transcription. 2019;10(2):91-110.

265.   Zhu R, Yang G, Cao Z, Shen K, Zheng L, Xiao J, et al. The prospect of serum and glucocorticoid-inducible kinase 1 (SGK1) in cancer therapy: a rising star. Ther Adv Med Oncol. 2020;12:1758835920940946-.

266.   Wu G, Haw R. Functional Interaction Network Construction and Analysis for Disease Discovery. Methods in molecular biology (Clifton, NJ). 2017;1558:235-53.

267.   Biddie Simon C, John S, Sabo Pete J, Thurman Robert E, Johnson Thomas A, Schiltz RL, et al. Transcription Factor AP1 Potentiates Chromatin Accessibility and Glucocorticoid Receptor Binding. Molecular Cell. 2011;43(1):145-55.

268.   Cheng H, Zhang N, Pati D. Cohesin subunit RAD21: From biology to disease. Gene. 2020;758:144966.

269.   Hsin J-P, Xiang K, Manley JL. Function and control of RNA polymerase II C-terminal domain phosphorylation in vertebrate transcription and RNA processing. Mol Cell Biol. 2014;34(13):2488-98.

270.   Egloff S, O'Reilly D, Chapman RD, Taylor A, Tanzhaus K, Pitts L, et al. Serine-7 of the RNA Polymerase II CTD Is Specifically Required for snRNA Gene Expression. Science. 2007;318(5857):1777-9.

271.   Becker M, Baumann C, John S, Walker DA, Vigneron M, McNally JG, et al. Dynamic behavior of transcription factors on a natural promoter in living cells. EMBO Rep. 2002;3(12):1188-94.

272.   Czudnochowski N, Bösken CA, Geyer M. Serine-7 but not serine-5 phosphorylation primes RNA polymerase II CTD for P-TEFb recognition. Nature Communications. 2012;3(1):842.

273.   Ma Y, Chen L, Wright GM, Pillai SR, Chellappan SP, Cress WD. CDKN1C negatively regulates RNA polymerase II C-terminal domain phosphorylation in an E2F1-dependent manner. The Journal of biological chemistry. 2010;285(13):9813-22.

274.   Wong KH, Jin Y, Struhl K. TFIIH phosphorylation of the Pol II CTD stimulates mediator dissociation from the preinitiation complex and promoter escape. Molecular cell. 2014;54(4):601-12.

275.   Yu M, Yang W, Ni T, Tang Z, Nakadai T, Zhu J, et al. RNA polymerase II-associated factor 1 regulates the release and phosphorylation of paused RNA polymerase II. Science. 2015;350(6266):1383-6.

276.   Rimel JK, Poss ZC, Erickson B, Maas ZL, Ebmeier CC, Johnson JL, et al. Selective inhibition of CDK7 reveals high-confidence targets and new models for TFIIH function in transcription. Genes Dev. 2020.

277.   Nieto Moreno N, Villafañez F, Giono LE, Cuenca C, Soria G, Muñoz MJ, et al. GSK-3 is an RNA polymerase II phospho-CTD kinase. Nucleic Acids Res. 2020;48(11):6068-80.

278.   Devaiah BN, Lewis BA, Cherman N, Hewitt MC, Albrecht BK, Robey PG, et al. BRD4 is an atypical kinase that phosphorylates serine2 of the RNA polymerase II carboxy-terminal domain. Proceedings of the National Academy of Sciences of the United States of America. 2012;109(18):6927-32.

279.   Uppal S, Gegonne A, Chen Q, Thompson PS, Cheng D, Mu J, et al. The Bromodomain Protein 4 Contributes to the Regulation of Alternative Splicing. Cell Rep. 2019;29(8):2450-60.e5.

280.   Luecke HF, Yamamoto KR. The glucocorticoid receptor blocks P-TEFb recruitment by NFκB to effect promoter-specific transcriptional repression. Genes Dev. 2005;19(9):1116-27.

281.   Martinez-Fabregas J, Wang L, Pohler E, Cozzani A, Wilmes S, Kazemian M, et al. CDK8 Fine-Tunes IL-6 Transcriptional Activities by Limiting STAT3 Resident Time at the Gene Loci. Cell Rep. 2020;33(12):108545.

282.	Vilasco M, Communal L, Hugon-Rodin J, Penault-Llorca F, Mourra N, Wu Z, et al. Loss of glucocorticoid receptor activation is a hallmark of BRCA1-mutated breast tissue. Breast cancer research and treatment. 2013;142(2):283-96.

283.	Li X, Chatterjee N, Spirohn K, Boutros M, Bohmann D. Cdk12 Is A Gene-Selective RNA Polymerase II Kinase That Regulates a Subset of the Transcriptome, Including Nrf2 Target Genes. Sci Rep. 2016;6:21455.

284.	Iñiguez-Lluhí JA, Lou DY, Yamamoto KR. Three Amino Acid Substitutions Selectively Disrupt the Activation but Not the Repression Function of the Glucocorticoid Receptor N Terminus *. Journal of Biological Chemistry. 1997;272(7):4149-56.

285.	Juan HC, Lin Y, Chen HR, Fann MJ. Cdk12 is essential for embryonic development and the maintenance of genomic stability. Cell death and differentiation. 2016;23(6):1038-48.

286.	Dubbury SJ, Boutz PL, Sharp PA. CDK12 regulates DNA repair genes by suppressing intronic polyadenylation. Nature. 2018;564(7734):141-5.

287.	Illumina I. Considerations for RNA-Seq read length and coverage [updated 13.04.2021. Available from: https://emea.support.illumina.com/bulletins/2017/04/considerations-for-rna-seq-read-length-and-coverage-.html.

288.	Greifenberg AK, Hönig D, Pilarova K, Düster R, Bartholomeeusen K, Bösken CA, et al. Structural and Functional Analysis of the Cdk13/Cyclin K Complex. Cell Rep. 2016;14(2):320-31.

289.	Eifler TT, Shao W, Bartholomeeusen K, Fujinaga K, Jäger S, Johnson JR, et al. Cyclin-dependent kinase 12 increases 3' end processing of growth factor-induced c-FOS transcripts. Mol Cell Biol. 2015;35(2):468-78.

290.	Yu L, Zhang B, Deochand D, Sacta MA, Coppo M, Shang Y, et al. Negative elongation factor complex enables macrophage inflammatory responses by controlling anti-inflammatory gene expression. Nature Communications. 2020;11(1):2286.

291.	Pong Ng H, Kim GD, Ricky Chan E, Dunwoodie SL, Mahabeleshwar GH. CITED2 limits pathogenic inflammatory gene programs in myeloid cells. FASEB journal : official publication of the Federation of American Societies for Experimental Biology. 2020;34(9):12100-13.

292.	Kim GD, Das R, Rao X, Zhong J, Deiuliis JA, Ramirez-Bergeron DL, et al. CITED2 Restrains Proinflammatory Macrophage Activation and Response. Mol Cell Biol. 2018;38(5).

293.	Hoffman JA, Trotter KW, Ward JM, Archer TK. BRG1 governs glucocorticoid receptor interactions with chromatin and pioneer factors across the genome. eLife. 2018;7.

294.	Swinstead Erin E, Miranda Tina B, Paakinaho V, Baek S, Goldstein I, Hawkins M, et al. Steroid Receptors Reprogram FoxA1 Occupancy through Dynamic Chromatin Transitions. Cell. 2016;165(3):593-605.

295.	Cohen H, Ben-Hamo R, Gidoni M, Yitzhaki I, Kozol R, Zilberberg A, et al. Shift in GATA3 functions, and GATA3 mutations, control progression and clinical presentation in breast cancer. Breast Cancer Research. 2014;16(6):464.

296.	Kim S, Yu N-K, Kaang B-K. CTCF as a multifunctional protein in genome regulation and gene expression. Experimental & Molecular Medicine. 2015;47(6):e166-e.

297.	Paranjapye A, Mutolo MJ, Ebron JS, Leir S-H, Harris A. The FOXA1 transcriptional network coordinates key functions of primary human airway epithelial cells. American Journal of Physiology-Lung Cellular and Molecular Physiology. 2020;319(1):L126-L36.

298.	Starick SR, Ibn-Salem J, Jurk M, Hernandez C, Love MI, Chung HR, et al. ChIP-exo signal associated with DNA-binding motifs provides insight into the genomic binding of the glucocorticoid receptor and cooperating transcription factors. Genome research. 2015;25(6):825-35.

299.	Eguchi T, Prince T, Wegiel B, Calderwood SK. Role and Regulation of Myeloid Zinc Finger Protein 1 in Cancer. J Cell Biochem. 2015;116(10):2146-54.

300.	Ko H, Kim S, Yang K, Kim K. Phosphorylation-dependent stabilization of MZF1 upregulates N-cadherin expression during protein kinase CK2-mediated epithelial-mesenchymal transition. Oncogenesis. 2018;7(3):27.

301.	Lawrence T, Natoli G. Transcriptional regulation of macrophage polarization: enabling diversity with identity. Nature Reviews Immunology. 2011;11:750.

302.   Marco BD, Massetti M, Bruscoli S, Macchiarulo A, Virgilio RD, Velardi E, et al. Glucocorticoid-induced leucine zipper (GILZ)/NF-κB interaction: role of GILZ homo-dimerization and C-terminal domain. Nucleic Acids Res. 2007;35(2):517-28.

303.   Oh K-S, Patel H, Gottschalk RA, Lee WS, Baek S, Fraser IDC, et al. Anti-Inflammatory Chromatinscape Suggests Alternative Mechanisms of Glucocorticoid Receptor Action. Immunity. 2017;47(2):298-309.e5.

304.   Noursadeghi M, Tsang J, Haustein T, Miller RF, Chain BM, Katz DR. Quantitative imaging assay for NF-kappaB nuclear translocation in primary human macrophages. Journal of immunological methods. 2008;329(1-2):194-200.

305.   Rostam HM, Reynolds PM, Alexander MR, Gadegaard N, Ghaemmaghami AM. Image based Machine Learning for identification of macrophage subsets. Scientific Reports. 2017;7(1):3521.

306.   Daigneault M, Preston JA, Marriott HM, Whyte MKB, Dockrell DH. The Identification of Markers of Macrophage Differentiation in PMA-Stimulated THP-1 Cells and Monocyte-Derived Macrophages. PLOS ONE. 2010;5(1):e8668.

307.   Genin M, Clement F, Fattaccioli A, Raes M, Michiels C. M1 and M2 macrophages derived from THP-1 cells differentially modulate the response of cancer cells to etoposide. BMC Cancer. 2015;15:577.

308.   Xu YZ, Thuraisingam T, de Lima Morais DA, Rola-Pleszczynski M, Radzioch D. Nuclear Translocation of β-Actin Is Involved in Transcriptional Regulation during Macrophage Differentiation of HL-60 Cells. Molecular Biology of the Cell. 2010;21(5):811-20.

309.   Murray PJ, Allen JE, Biswas SK, Fisher EA, Gilroy DW, Goerdt S, et al. Macrophage activation and polarization: nomenclature and experimental guidelines. Immunity. 2014;41(1):14-20.

310.   Sudan B, Wacker MA, Wilson ME, Graff JW. A Systematic Approach to Identify Markers of Distinctly Activated Human Macrophages. Frontiers in Immunology. 2015;6(253).

311.   Varga G, Ehrchen J, Brockhausen A, Weinhage T, Nippe N, Belz M, et al. Immune Suppression via Glucocorticoid-Stimulated Monocytes: A Novel Mechanism To Cope with Inflammation. The Journal of Immunology. 2014.

312.   Martinez FO, Sica A, Mantovani A, Locati M. Macrophage activation and polarization. Frontiers in bioscience : a journal and virtual library. 2008;13:453-61.

313.   Albert PJ, Schwarz US. Dynamics of Cell Ensembles on Adhesive Micropatterns: Bridging the Gap between Single Cell Spreading and Collective Cell Migration. PLoS Computational Biology. 2016;12(4):e1004863.

314.   Thery M, Racine V, Piel M, Pepin A, Dimitrov A, Chen Y, et al. Anisotropy of cell adhesive microenvironment governs cell internal organization and orientation of polarity. Proc Natl Acad Sci U S A. 2006;103(52):19771-6.

315.   Koehler L, Hass R, Goppelt-Struebe M, Kaever V, Resch K. Differential effect of dexamethasone on the regulation of phospholipase A2 and prostanoid synthesis in undifferentiated and phorbolester-differentiated U937 cells. Journal of cellular biochemistry. 1989;40(3):397-406.

316.   Maess MB, Sendelbach S, Lorkowski S. Selection of reliable reference genes during THP-1 monocyte differentiation into macrophages. BMC molecular biology. 2010;11:90.

317.   Huse M. Mechanical forces in the immune system. Nature Reviews Immunology. 2017;17:679.

318.   Sorokin L. The impact of the extracellular matrix on inflammation. Nature reviews Immunology. 2010;10(10):712-23.

319.   Bartneck M, Schulte VA, Paul NE, Diez M, Lensen MC, Zwadlo-Klarwasser G. Induction of specific macrophage subtypes by defined micro-patterned structures. Acta Biomaterialia. 2010;6(10):3864-72.

320.   Riddy DM, Goy E, Delerive P, Summers RJ, Sexton PM, Langmead CJ. Comparative genotypic and phenotypic analysis of human peripheral blood monocytes and surrogate monocyte-like cell lines commonly used in metabolic disease research. PLoS ONE. 2018;13(5):e0197177.

321.	Schwende H, Fitzke E, Ambs P, Dieter P. Differences in the state of differentiation of THP-1 cells induced by phorbol ester and 1,25-dihydroxyvitamin D3. Journal of leukocyte biology. 1996;59(4):555-61.

322.	Starr T, Bauler TJ, Malik-Kale P, Steele-Mortimer O. The phorbol 12-myristate-13-acetate differentiation protocol is critical to the interaction of THP-1 macrophages with Salmonella Typhimurium. PLOS ONE. 2018;13(3):e0193601.

323.	Chanput W, Mes JJ, Savelkoul HF, Wichers HJ. Characterization of polarized THP-1 macrophages and polarizing ability of LPS and food compounds. Food & function. 2013;4(2):266-76.

324.	Trescos Y, Tessier E, Rougeaux C, Goossens PL, Tournier JN. Micropatterned macrophage analysis reveals global cytoskeleton constraints induced by Bacillus anthracis edema toxin. Infection and immunity. 2015;83(8):3114-25.

325.	Lee RE, Walker SR, Savery K, Frank DA, Gaudet S. Fold change of nuclear NF-kappaB determines TNF-induced transcription in single cells. Molecular cell. 2014;53(6):867-79.

326.	Shrum CK, DeFrancisco D, Meffert MK. Stimulated nuclear translocation of NF-κB and shuttling differentially depend on dynein and the dynactin complex. Proceedings of the National Academy of Sciences. 2009:pnas.0806677106.

327.	Mayanagi T, Morita T, Hayashi Ki, Fukumoto K, Sobue K. Glucocorticoid receptor-mediated expression of caldesmon regulates cell migration via the reorganization of the actin cytoskeleton. The Journal of biological chemistry. 2008;283(45):31183-96.

328.	Galigniana MD, Scruggs JL, Herrington J, Welsh MJ, Carter-Su C, Housley PR, et al. Heat shock protein 90-dependent (geldanamycin-inhibited) movement of the glucocorticoid receptor through the cytoplasm to the nucleus requires intact cytoskeleton. Molecular endocrinology (Baltimore, Md). 1998;12(12):1903-13.

329.	Bolshakova A, Magnusson K-E, Pinaev G, Petukhova O. EGF-induced dynamics of NF-κB and F-actin in A431 cells spread on fibronectin. Histochemistry and Cell Biology. 2015;144(3):223-35.

330.	Peng J, Wang H, Wang X, Sun M, Deng S, Wang Y. YAP and TAZ mediate steroid-induced alterations in the trabecular meshwork cytoskeleton in human trabecular meshwork cells. Int J Mol Med. 2018;41(1):164-72.

331.	Lin L, Zhang Q, Fan H, Zhao H, Yang Y. Myocardin-Related Transcription Factor A Mediates LPS-Induced iNOS Transactivation. Inflammation. 2020;43(4):1351-61.

332.	Hoffman JA, Papas BN, Trotter KW, Archer TK. Single-cell RNA sequencing reveals a heterogeneous response to Glucocorticoids in breast cancer cells. Communications Biology. 2020;3(1):126.

333.	Nakajima Y, Meyer EJ, Kroesen A, McKinney SA, Gibson MC. Epithelial junctions maintain tissue architecture by directing planar spindle orientation. Nature. 2013;500(7462):359-62.

334.	Pain M, Bermudez O, Lacoste P, Royer PJ, Botturi K, Tissot A, et al. Tissue remodelling in chronic bronchial diseases: from the epithelial to mesenchymal phenotype. European respiratory review : an official journal of the European Respiratory Society. 2014;23(131):118-30.

335.	Nakajima Y-i, Meyer EJ, Kroesen A, McKinney SA, Gibson MC. Epithelial junctions maintain tissue architecture by directing planar spindle orientation. Nature. 2013;500(7462):359-62.

336.	Rowat AC, Jaalouk DE, Zwerger M, Ung WL, Eydelnant IA, Olins DE, et al. Nuclear Envelope Composition Determines the Ability of Neutrophil-type Cells to Passage through Micron-scale Constrictions. The Journal of biological chemistry. 2013;288(12):8610-8.

337.	Thiam H-R, Vargas P, Carpi N, Crespo CL, Raab M, Terriac E, et al. Perinuclear Arp2/3-driven actin polymerization enables nuclear deformation to facilitate cell migration through complex environments. Nature Communications. 2016;7:10997.

338.	John S, Sabo PJ, Thurman RE, Sung M-H, Biddie SC, Johnson TA, et al. Chromatin accessibility pre-determines glucocorticoid receptor binding patterns. 2011;43:264.